Metal Mediated Mechanisms of Drug Release

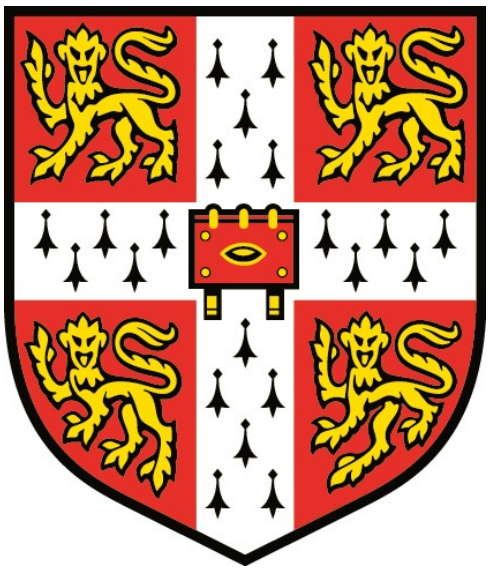

A dissertation presented by

Benjamin James Stenton

Jesus College

This dissertation is submitted for the degree of Doctor of Philosophy

at the

University of Cambridge

April 2018

Metal Mediated Mechanisms of Drug Release

Benjamin J. Stenton

In this thesis will be described research towards the development of bioorthogonal bond-cleavage reactions, and their applications in targeted drug delivery (**Figure 1**). The first project relates to the development of a palladium mediated bond-cleavage or "decaging" reaction which can cause a propargyl carbamate to decompose and release an amine. This was further developed by the incorporation of a protein modification handle which allowed an amine-bearing drug to be covalently ligated to a protein by a palladium-cleavable linker. This chemistry was demonstrated by the conjugation of the anticancer drug doxorubicin to a tumour targeted anti-HER2 nanobody. The drug could then be delivered to cancer cells upon addition of a palladium complex.[1]

The second project relates to the development of a platinum mediated bond-cleavage reaction. This was developed with the aim of using platinum-containing anticancer drugs – such as cisplatin – as a catalyst to cause drug release reactions in tumours. In this reaction an alkyne-containing amide can decompose to release an amine upon addition of platinum complexes, and was applied to the release of prodrugs of the cytotoxins monomethylauristatin E and 5-fluorouracil in cancer cells. A cisplatin-cleavable antibody-drug conjugate was designed and synthesised, and progress towards its biological evaluation will be discussed.

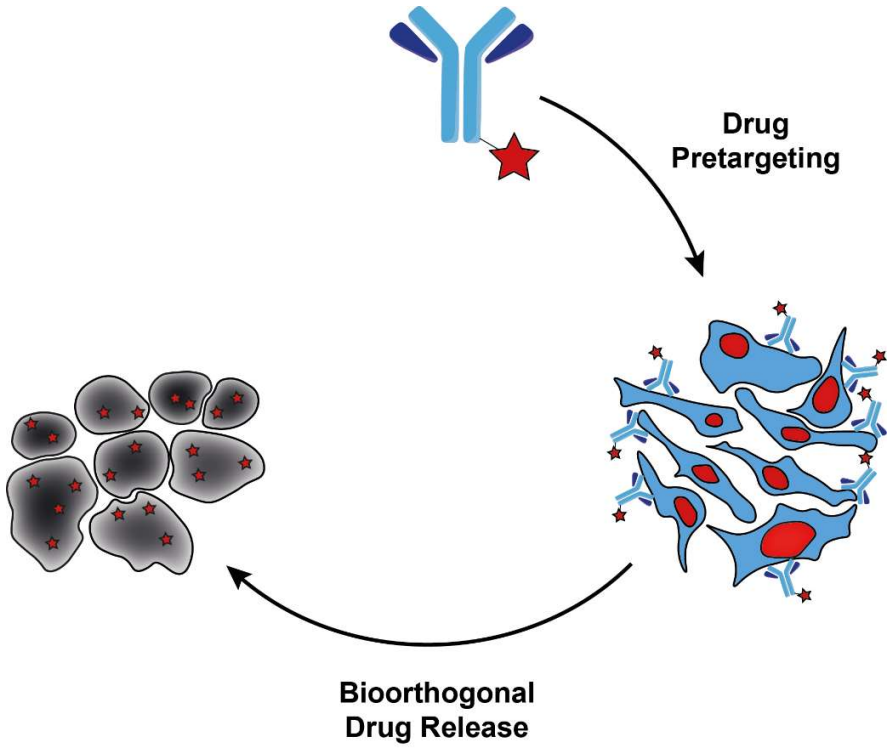

Figure 1: General principle of the subject of this dissertation.

Declaration

This dissertation is submitted in fulfilment of the requirements for the degree of Doctor of Philosophy. Unless specifically indicated in the text, the research described is the result of my own work and not the product of collaboration.

Benjamin James Stenton, April 2018

Statement of Length

This thesis does not exceed the word limit of 60,000 as set by the Degree Committee for the Faculty of Physics and Chemistry.

Acknowledgements

A thesis isn't a thesis without some ramble-y acknowledgements! Feel free to skip to the science if you like.

To Dr Gonçalo Bernardes, thanks for accepting me as one of your first PhD students in Cambridge. In the beginning there were just the two of us: Russell Zijian Guo (the handsome, intelligent one) and myself (the ~~tidy~~ ~~enthusiastic~~ other one) sharing a fumehood. As the group grew, we moved to our own fumehoods and I was glad to be free of Russell's mess (though sad that I had no-one to blame for my own mess). Thanks to Gonçalo's efforts and relentless grant applications, we now have a huge group, lab space and amazing equipment that we wouldn't have believed at the start.

An enormous thank you to a dedicated and marvellously talented team of proof-readers: Dr Barbara "Bada" Bernardim (Chapter Four), Soon-to-be-Dr Padma Akkapeddi (Chapter One), only-two-more-years-till-Dr Sarah Davies (Chapters Two **and** Three) and the rather fabulous Mlle Corentine Marie Cécile Laurin for a more general critique of the thesis, being herself and wonderfully supportive. Now that the reader has their names, they know exactly who to blame should they have any problems with the text. Finally, for actually (probably) reading (skimming) the entire thesis (maybe just the pictures), thank you to Dr Gonçalo Bernardes.

Nic and Naomi thank you for ensuring that the Whiffen Lab was only refurbished immediately *after* I left. I really appreciate that act of kindness and will never truly understand how you pulled it off. Also, thanks for making almost every other aspect of the Chemistry Department actually work! To the Phippsies, thanks for adopting some of us more Thursday-night-nachos-and-drinking inclined of the Bernardes Group and treating us like your own. I feel as though we've developed a lifelong bond that only be fostered by a pervasive solvent smell, dodgy work hours and surprisingly frequent indoor rainfall. To Prof Steve Ley and the Ley-ies… Ley-ites… Ley Group Members past and present: thanks for having us!

“I am old, Gandalf. I don’t look it, but I am beginning to feel it in my heart of hearts. Well-preserved indeed! Why, I feel all thin, sort of stretched, if you know what I mean: like butter that has been over too much bread. I need a change, or something.” – Bilbo Baggins

Abbreviations

°C	Degrees Celsius
δ	Chemical Shift
µ	Micro
λ	Wavelength
3-MPA	3-Mercaptopropionic Acid
Å	Angstrom
Abs	Absorbance
Ac	Acetyl
Ac	Acetate
ADC	Antibody-Drug Conjugate
aq.	Aqueous
Ar	Aryl
ATR	Attenuated Total Reflectance
Bn	Benzyl
Boc	*tert*-Butyloxycarbonyl
Bu	Butyl
CDR	Complimentarity Determining Region
COD	1,5-Cycloctadiene
Cys	Cysteine
d	Deci, day(s) or doublet (NMR spectroscopy)
Da	Daltons
DAR	Drug-to-Antibody Ratio
DAVLB	Desacetylvinblastine
DBU	1,8-Diazabicyclo[5.4.0]undec-7-ene
DCM	Dichloromethane
decomp.	Decomposition
DIPEA	N,N-Diisopropylethylamine
DM	Duocarmycin
DMAP	4-(Dimethylamino)pyridine
DMF	*N,N*-Dimethylformamide
DMP	Dess-Martin Periodinane
DMSO	Dimethylsulfoxide

DNA	Deoxyribonucleic Acid
Dox	Doxorubicin
DSC	*N,N'*-Disuccinimidyl carbonate
DTT	Dithiothreitol
EDC	*N*-(3-Dimethylaminopropyl)-*N*'-ethylcarbodiimide
em	Emission
eq.	Equivalents
ESI	Electrospray Ionisation
Et	Ethyl
et al.	*Et alia*
ex	Excitation
Fab	Antigen binding fragment
Fc	Crystalisable fragment
FcRn	Neonatal Fc Receptor
FDA	United States Food and Drug Administration
FT	Fourier Transform
FU	Fluorouracil
Fv	Variable Fragment
g	Gram
GSH	Glutathione
h	Hours
HATU	1-[Bis(dimethylamino)methylene]-1H-1,2,3-triazolo[4,5-b]pyridinium 3-oxide hexafluorophosphate
hept	Heptet
HPLC	High-performance liquid chromatography
hv	Planck's Constant x Frequency of Light
i	*iso*
IC_{50}	50% Inhibitory Concentration
IgG	Immunoglobulin G
IR	Infrared
k	Kilo
L	Litre(s) or unspecified two-electron neutral ligand
LC	Liquid Chromatography
M	Molar or unspecified metal

m	Metre or milli
m.p.	Melting point
m/z	Mass-to-charge ratio
mAb	Monoclonal Antibody
mc	Maleimido-caprolyl
Me	Methyl
MED	Minimum Effective Dose
MTX	Methotrexate
min	Minutes
MMAE	Monomethylauristatin E
MMAF	Monomethylauristatin F
MS	Mass Spectrometry
MTD	Maximum Tolerated Dose
n	Nano
n	normal
NaPi	Sodium Phosphate Buffer
NBD	Norbornadiene
NMR	Nuclear Magnetic Resonance
Nu	Undefined Nucleophile
o	*ortho*
p	Pico
p	*para*
PAB	*p*-Aminobenzyl
PBD	Pyrrolobenzodiazepine Dimer
PBS	Phosphate-buffered Saline
PEG	Polyethylene Glycol
Ph	Phenyl
ppm	Parts Per Million
q	Quartet (NMR spectroscopy)
R	Undefined Substituent
RNA	Ribonucleic Acid
s	Seconds, or singlet (NMR spectroscopy)
sat.	Saturated
scFv	Single Chain Variable Fragment

sept	Septet (NMR spectroscopy)
SIP	Small Immune Protein
SM	Starting Material
SMCC	*N*-Succinimidyl 4-(*N*-maleimidomethyl)cyclohexane-1-carboxylate
SPDB	*N*-Succinimidyl 4-(pyridin-2-yldisulfanyl)butanoate
t	Triplet (NMR spectroscopy)
t	*tert*
TBAF	Tetrabutylammonium fluoride
TBS	*Tert*-butyldimethylsilyl
TCEP	Tris(2-carboxyethyl)phosphine
TCO	*Trans*-cyclooctene
TCO-OH	*Trans*-cyclooct-2-ene-1-ol
TEA	Triethylamine
TFA	Trifluoroacetic acid
THF	Tetrahydrofuran
TLC	Thin-layer Chromatography
tRNA	Transfer-RNA
Trt	Trityl
Ts	Tosyl
Ub	Ubiquitin K63C
UPLC	Ultra Performance Liquid Chromatography
UV	Ultraviolet
V	Volts
vs	*Versus*
w.r.t.	With Respect To

Contents

Chapter 1:

Antibody-Drug Conjugates for Cancer Therapy

1.1 Cancer and Conventional Chemotherapy

Mortality due to cancer is only expected to rise as the world's population grows and ages, and it already killed as many as 8.2 million in 2012.[2] The current method of treatment is generally the surgical excision of the majority of a tumour mass, followed by a combination of chemotherapy and radiotherapy depending on the particular course followed.

The combination chosen is selected based on myriad factors, but common to all types of cancer treatment is a selection of chemotherapeutics with diverse modes of action. The doses of individual drugs can therefore be lower while maintaining a high enough overall dose of chemotherapeutics to hopefully eradicate the tumours. Common combinations include:

In the treatment of colon cancer, the following drugs are used in various combinations: fluorodeoxyuridine for the inhibition of RNA synthesis, folinic acid for thymidylate synthase inhibition and as a fluorodeoxyuridine adjuvant and oxaliplatin as a DNA cross-linking agent.[3]

In the treatment of lung cancer, a common course is cisplatin for DNA cross-linking perhaps in combination with vinorelbine as a microtubule-formation inhibitor.[4]

In the treatment of breast cancer, one of many courses is epirubicin as a DNA intercalator, cyclophosphamide as a DNA alkylator, fluorodeoxyuridine and docetaxel as a microtubule-formation inhibitor.[5]

These cytotoxins are all slightly selective for tumours and have been shown to be effective treatments in practice. The slight selectivity arises as all these agents inhibit the replication of nucleic acids, something that tumours do at a much higher rate than healthy cells. The high toxicity of these treatments from non-specific cell killing – a dose-limiting factor – therefore determines how effective the treatment can be. Higher selectivity would allow lower effective doses and better survival rates for cancer patients.

Cytotoxic chemotherapeutic agents are usually given at their Maximum Tolerated Dose (MTD) to be effective, and the more selective these drugs are, the lower their Minimum Effective Dose (MED). The issue with very highly cytotoxic drugs (IC_{50} < 1 nM) is that they often reach their MTD before an MED can be achieved. The cytotoxicity of common chemotherapeutics therefore tends to be much lower than possible. The possibility of taking highly cytotoxic drugs and adding a targeting moiety to increase their selectivity is therefore very exciting. These drugs could then be cleaved from the targeting moiety at the desired site of action.

1.2 First Generation ADCs

The concept of the antibody-drug conjugate (ADC) arose from the idea of targeting highly potent toxins that otherwise cannot be chemotherapeutics. Antibodies are immunoglobulin proteins that bind strongly to specific antigens and are therefore a logical choice for a targeting protein. The first report of a cytotoxin conjugated to an antibody was in 1958,[6] when antibodies were generated by implanting hamsters with mouse tumour cells. The hamsters generated antibodies against the tumour and these were isolated as a mixture. Methotrexate was then conjugated to these antibodies by diazotisation with its amine groups, and coupling these diazonium salts with nucleophilic groups on the antibodies (mainly tyrosine). It was shown that when these ADCs were used to treat mouse tumours, the mice survived for longer than when given ADCs with non-specific antibodies. Another classic example was in 1970[7] when diphtheria toxin (a protein) was conjugated to a murine antibody targeted to mumps-virus antigens with toluene diisocyanate. After infecting monkey kidney cells with the mumps-virus, the cells presented mumps-virus antigens on their cell membranes. The conjugates could effectively target and kill the infected cells. This was followed by a flurry of activity in ADC research.

During this period of research some ADCs were shown to be more effective on human tumour xenografts in mice than the free drug.[8,9] Of the ADCs in early human clinical trials, none showed a meaningful therapeutic activity. However, the results were used to further refine aspects of ADCs. These clinical trials showed a high level of immunogenicity of the ADCs, eventually leading to the use of fully human antibodies. Three important areas for research were also highlighted:

The antibody. Good specificity of the antibodies to antigens on the surface of tumour cells in humans was demonstrated by radiolabelling[10] or immunohistochemical staining[11] for early ADCs. This identified the importance of tumour localisation and tissue penetration.

The drug payload. As drug conjugation to the antibody almost always reduced toxicity of the drug,[8,9] more toxic payloads were sought. It was thought that as the number of cancer antigens was low (typically < 10^5 per cell), a highly toxic drug (IC_{50} < 1 nm) would be necessary to kill the cell.

The linker. As non-specific drug release would lead to systemic toxicity, a selective drug-release methodology with acid-sensitive hydrazones was demonstrated by incubation of ADCs at various pH.[8] This highlighted the importance of the linker between antibody and drug, which should be stable in circulation but be able to release the drug to the tumour. These three major factors are discussed here.

1.3 Antibodies for Cancer Treatment

Antibodies are generated by the immune system as a response to a perceived pathogen. The regions of DNA that encode their binding regions have a mutation rate approximately one million times greater than normal DNA,[12] and therefore large numbers of binding region sequences can be assayed by the immune system to find a strongly binding antibody. These antibodies bind strongly to the perceived pathogen and can then elicit a number of responses from the immune system including phagocytosis and endocytosis. Modern antibodies targeted to a specific purified antigen are most commonly generated by phage display, or by taking transgenic mice – with antibody-coding DNA replaced with human DNA – innoculating with the antigen of interest and then using hybridoma technology. There are many antibody subtypes, but the dominant type in human plasma is the IgG format monoclonal antibody (mAb) which is therefore the most widely studied. The format of an IgG antibody derived from X-ray crystal structures is shown in **Figure 2**.

The first human cancer treatment with monoclonal antibodies was in 1980 when a leukaemia patient was treated with murine antibodies targeting AB 89.[13] In the following years, the treatment of cancer with mAbs was further investigated, but a recurring issue in their development was immune responses in the patients. Attempting to circumvent these issues, regions of the murine antibody protein sequence were replaced with those of human antibodies, making the mAbs increasingly human-like and reducing immune response.

At first, the entire constant region of the murine mAb was replaced with that of human mAb to create "chimeric" antibodies. As these still contained much of the murine antibody sequence, antibodies were further engineered to include human variable fragments (Fv) to create fully "humanised" antibodies (**Figure 2**).

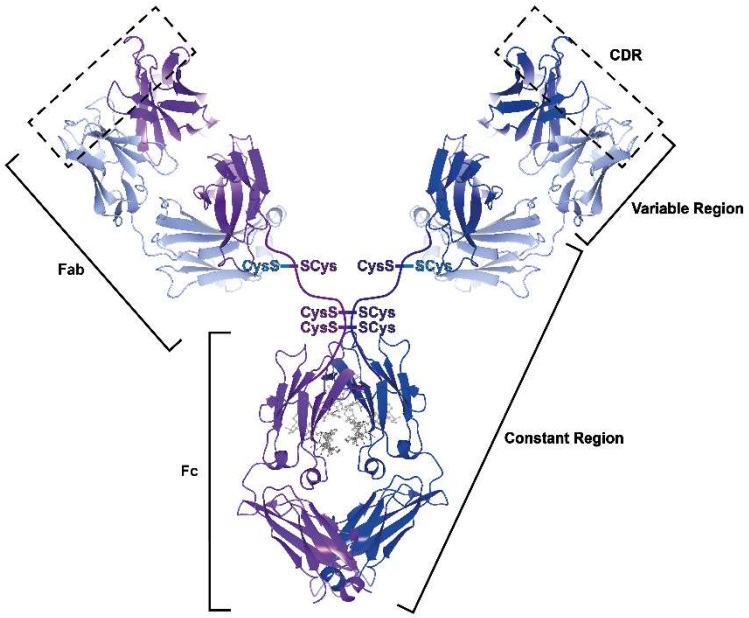

Designation	Region Origin		
	Complimentarity Determining Region (CDR)	Variable Region	Constant Region
Mouse	Mouse	Mouse	Mouse
Chimeric	Mouse	Mouse	Human
Humanised	Mouse	Human	Human
Fully Human	Human	Human	Human

Figure 2: Crystal structure representation of an IgG1 mAb adapted from PDB 5VH5[14] (Crystallisable fragment, Fc) and 4G3Y[15] (Antigen binding fragment, Fab).[15]. Light chains are highlighted in **light blue**, heavy chains in **dark blue** and **purple**, and glycosylation in **grey**. Comparison of mouse to fully human IgG antibodies. CDR: complementarity determining region.[16]

The benefits of these fully "humanised" antibodies are increased circulation time (lower metabolism rate), and lower immunogenicity. The availability of these technologies has led to commercial development of mAbs to treat cancer, a summary of which can be seen in **Table 1**.

Table 1: Commercially available mAbs for the treatment of cancer, adapted from the literature.[17,18]

mAb	Trade name	Target	Type	Indication(s)
Alemtuzumab	Campath	CD52	Humanised IgG1	Chronic lymphocytic leukaemia
Avelumab	Bavencio	PD-L1	Human IgG1	Urothelial carcinoma
Bevacizumab	Avastin	VEGFR	Humanised IgG1	Colorectal, renal, lung, and brain cancer
Catumaxomab	Removab	EpCAM	Rat IgG2b/mouse IgG2a bispecific	Malignant ascites in patients with epCAM+ cancer
Cetuximab	Erbitux	EGFR	Chimeric IgG1	Head/neck and colorectal cancer
Daratumumab	Darzalex	CD38	Human IgG1	Multiple myeloma
Denosumab	Prolia Xgeva	RANKL	Human IgG2	Breast cancer, prostate cancer, and giant cell tumours of the bone
Durvalumab	Imfinzi	PD-1	Human IgG1	Urothelial carcinoma
Ibritumomab	Zevalin	CD20	Murine IgG1	Non-Hodgkin lymphoma
Ipilimumab	Yervoy	CTLA-4	Human IgG1	Melanoma
Nimotuzumab	Nimotuzumab	EGFR	Human IgGh-R3	Head/neck cancer
Nivolumab	Opdivo	PD-1	Human IgG4	Melanoma
Obinutuzumab	Gazyva	CD20	Human IgG1	Chronic lymphocytic leukaemia
Ofatumumab	Arzerra	CD20	Human IgG1	Chronic lymphocytic leukaemia
Olaratumab	Lartruvo	PDGF-Rα	Human IgG1	Soft tissue sarcoma
Panitumomab	Vectibix	EGFR	Human IgG2	Colorectal carcinoma
Pembrolizumab	Keytruda	PD-1	Humanised IgG4	Gastric or gastroesophageal junction adenocarcinoma

Table 1: Continued…

mAb	Trade name	Target	Type	Indication(s)
Pertuzumab	Perjeta	HER2	Humanised IgG1	Breast cancer
Ramucirumab	Cyramza	VEGFR	Humanised IgG1	Gastric or gastroesophageal junction cancer
Rituximab	Rituxan MabThera	CD20	Chimeric IgG1	Chronic lymphocytic leukaemia and non-Hodgkin lymphoma
Siltuximab	Sylvant	IL-6	Chimeric IgG1	Castleman disease, multicentric (in patients who are HIV negative and HHV-8 negative)
Tositumomab	Bexxar	CD20	Murine IgG2a	Non-Hodgkin lymphoma
Trastuzumab	Herceptin	HER2	Humanised IgG1	Breast cancer, gastric or gastroesophageal junction cancer

1.4 Modified Antibodies and their Derivatives

Thanks to the advances in monoclonal antibodies, the list of potential ADC targets has grown ever longer. There are now many chimeric and humanised antibodies in development as ADCs on their own or in combination with other chemotherapeutic agents, as shown in **Table 2**.

Table 2: ADCs currently on the market or in clinical development.[19]

ADC	Drug	Target	Release Mechanism	Indication(s)
		FDA-Approved		
Brentuximab vedotin (Adcetris)	MMAE	CD30	Val-Cit-PAB carbamate cleavage[20]	Hodgkin's lymphoma or anaplastic large cell lymphoma
Gemtuzumab ozogamicin (Mylotarg)	Calichaemicin	CD33	Disulfide reduction and hydrazone hydrolysis[21]	Acute myelogenous leukaemia
Inotuzumab ozogamicin (Besponsa)	Calichaemicin	CD22	Disulfide reduction and hydrazone hydrolysis[21]	Acute lymphoblastic leukaemia
Trastuzumab emtansine (Kadcyla)	DM1	HER2	Retro-Michael and protease cleavage[22]	Breast cancer
		Phase III		
Depatuxizumab mafodotin	MMAF	EGFR	Retro-Michael and protease cleavage[23–25]	Glioblastoma/gliosarcoma
Mirvetuximab soravtansine	DM4	FOLR1	sulfo-SPDB reduction[26]	Ovarian cancer, endometrial cancer, lung adeno-carcinoma
Polatuzumab vedotin	MMAE	CD79b	Val-Cit-PAB carbamate cleavage[20,27]	Lymphoma
Rovalpituzumab tesirine	SG3249 (PBD)	DLL3	Val-Ala-PAB carbamate cleavage[28]	Small-cell lung cancer
Sacituzumab govitecan	SN-38 (campothecin)	TROP-2	Lys-PAB carbonate cleavage[29–31]	Breast cancer
SYD985	seco-DUBA (duocarmycin)	HER2	Val-Cit-PAB cyclisation[32–34]	Locally advanced or Metastatic breast cancer

Table 2: Continued…

Candidate	Drug	Target	Release Mechanism	Indication(s)
		Phase III		
Vadastuximab talirine	SG1882 (PBD)	CD33	Val-Ala cleavage[35,36]	Acute myeloid leukaemia
		Phase II		
AGS-16C3F	MMAF	ENPP3	Retro-Michael and protease cleavage[37]	Renal cell and liver carcinoma, prostate cancer
Anetumab ravtansine	DM4	Mesothelin	SPDB disulfide reduction/cyclisation[38]	Lung adenocarcinoma
CDX-014	MMAE	TIM-1	Val-Cit-PAB carbamate cleavage[39]	Renal cell carcinoma
Coltuximab ravtansine	DM4	CD19	SPDB disulfide reduction/cyclisation[38]	Lymphoma
Denintuzumab mafodotin	MMAF	CD19	Retro-Michael and protease cleavage[23–25]	Leukemia, lymphoma
DS-8201a	DXd	HER2	Gly-Gly-Phe-Gly ether cleavage[40,41]	Breast cancer
Enfortumab vedotin	MMAE	Nectin-4	Val-Cit-PAB carbamate cleavage[20,42]	Urothelial cancer
Glembatumumab Vedotin	MMAE	GPNMB	Val-Cit-PAB carbamate cleavage[20,43]	Osteosarcoma
hLL1-DOX	Doxorubicin	CD74	Hydrazone hydrolysis[44,45]	Leukemia, myeloma, lymphoma
Labetuzumab govitecan	SN-38 (campothecin)	CEACAM5	Phe-Lys-PAB carbonate cleavage[30,46]	Colorectal cancer
Lorvotuzumab mertansine	DM1	CD56	SPDB disulfide reduction/cyclisation[47]	Small-cell lung cancer and neuroendocrine tumours

Table 2: Continued…

Candidate	Drug	Target	Release Mechanism	Indication(s)
			Phase II	
PSMA ADC	SG-3199	PSMA	Val-Ala-PAB carbamate cleavage[48,49]	Prostate cancer
Sacituzumab govitecan	SN-38 (campothecin)	Trop-2	Phe-Lys-PAB carbonate cleavage[30,50]	Breast cancer
SGN15	Doxorubicin	Lewis Y	Hydrazone hydrolysis[9,51]	Leukaemia and carcinoma
Tisotumab vedotin	MMAE	CD142	Val-Cit-PAB carbamate cleavage[20]	Cervical cancer
Vadastuximab talirine	SG1882 (PBD)	CD33	Val-Ala cleavage[35,52]	AML, ulcerative colitis, myelodysplastic syndromes, gastric adenocarcinoma

However, not only the whole IgG monoclonal antibody format has been used in ADCs. It is possible to generate modified fragments of IgG antibodies which can retain binding (**Figure 3**). These can even offer improved properties over IgG monoclonal antibodies such as deeper tumour penetration, and faster maximum localisation at the tumour site (0.5 h for scFv *vs* 48-96 h for IgG).[53] However some of these smaller format antibodies suffer from an increased clearance rate as they can be excreted *via* the kidney due to their smaller size.[54] For example an anti-CD30 diabody-auristatin conjugate was shown to be cleared 25-34 times faster than its corresponding IgG-auristatin conjugate.[55] The Fc region plays a critical role in determining the long half-life of IgG antibodies, and therefore antibody derivatives with a modified or removed Fc region can have shortened half-lives.[56]

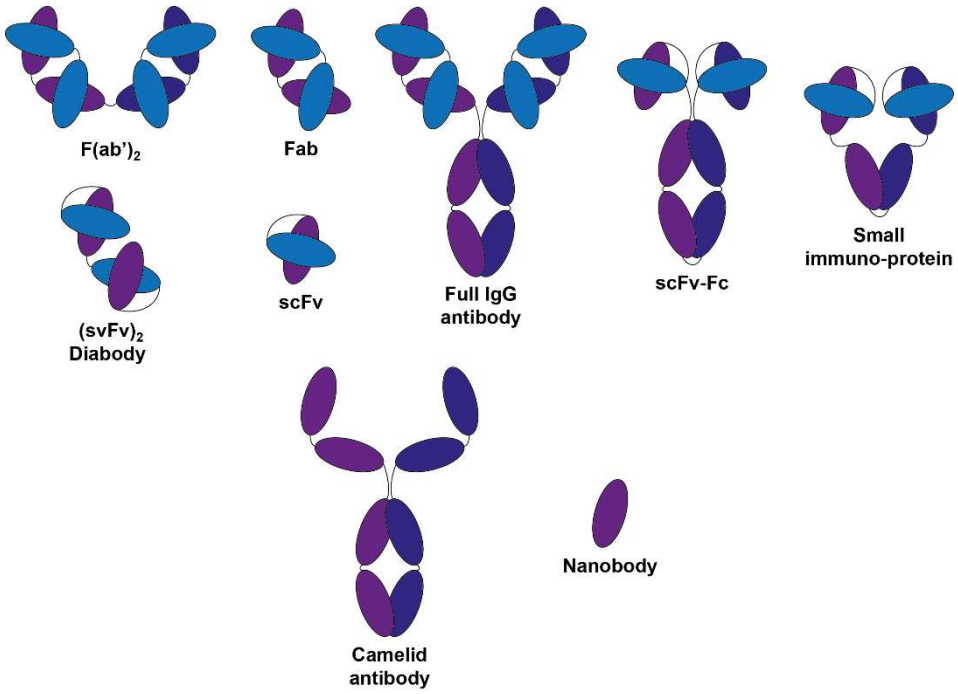

Figure 3: An overview of the most common antibody fragment and derivative types, adapted from the literature.[57] Light chains are highlighted in **light blue**, heavy chains in **dark blue** and **purple**.

Antibody fragments and their derivatives have been approved for the treatment of human disease by the FDA (**Table 3**). The choice of antibody for a particular ADC therapy is not just reliant on a strong binding affinity, and other important factors will be discussed here.

Table 3: Commercially available antibody fragment based therapeutics.[58,59]

Antibody	Trade name	Target	Type	Indication(s)
Abatacept	Orencia	CD80/CD86	CTLA4-Fc fusion	Rheumatoid arthritis
Abciximab	ReoPro	GPIIb/IIIa	Chimeric Fab	Prevention of blood clots in angioplasty
Aflibercept, ziv-aflibercept	EYLEA, ZALTRAP	VEGFA	VEGF-R-Fc fusion	Wet age-related macular degeneration, colorectal cancer
Alefacept	Amevive	CD2	CD58 (LFA-3)-Fc fusion	Psoriasis
Asfotase alfa	Strensiq	Factor substitute	TNSALP-Fc fusion	Hypophosphatasia
Belatacept	Nuloji®	CD80/CD86	CTLA-4 Fc fusion	Organ transplant rejection
Blinatumomab	Blincyto	CD19/CD3	Bispecific diabody	Acute lymphoblastic leukemia
Certolizumab pegol	Cimzia	TNF-α	PEGylated humanised Fab	Moderate to severe Crohn's disease
Dulaglutide	Trulicity	GLP1R	GLP-1-Fc fusion	Type 2 diabetes
Eftrenonacog alfa	Alprolix	Factor substitute	Monomeric Factor IX Fc fusion	Haemophilia B
Etanercept	Enbrel	TNF	P75-TNFR-Fc fusion	Rheumatoid arthritis
Idarucizumab	Praxbind	Dabigatran	Humanized Fab	Anticoagulant
Ranibizumab	Lucentis	VEGF-A	Humanised Fab	Wet age-related macular degeneration
Rilonacept	Arcalyst	IL-1α, IL1β, IL-1RA	IL-1R and IL-1AP Fc fusion	Cropyrin-associated periodic syndrome, Muckle-Wells syndrome
Romiplostim	Nplate	MPL	Fc-peptide fusion	Thrombocytopenia

1.5 Internalisation and Metabolism

An important factor in ADCs is the efficiency of internalisation. Depending on the antibody and antigen, ADCs can be internalised to varying degrees. This is most often thought to happen by receptor mediated clathrin-dependent endocytosis into acidic lysosomes where degradation can occur as ADCs have been shown to collect in lysosomes of tumours.[20,22] However this has been challenged as some internalisation can occur into caveolae.[60] In another case, internalisation was mediated by actin-polymerisation, and the receptor subsequently degraded by ubiquitination.[61]

For many of the ADCs in development, it is thought that drug release upon internalisation is a pre-requisite for selective drug delivery and low off-target toxicity. Therefore, antibodies with efficient internalisation are sought. The factors determining the efficiency of this internalisation are not always clear but in the case of a series of anti-HER2 antibodies, more strongly binding antibodies were found to be more efficiently internalised.[62] In the same study, it was also found that the highest affinity antibodies (0.56 nM) did not penetrate deeply into the tumour whereas those of lowest affinity (270 nm) penetrated the deepest, and that moderate affinity (23 nM) antibodies had the greatest accumulation at the tumour site overall.

Internalisation does not always mean degradation, as internalised antibodies can be removed from the cell by a process of FcRn mediated recycling.[56] The FcRn protein is membrane bound, and can strongly bind the Fc region of an antibody at pH < 6.5, but not at pH 7.4.[63,64] It can therefore mediate the transport of antibodies from acidic lysosomes to the exterior of the cell. Large quantities of proteins in serum are non-specifically internalised by endothelial cells[65] and FcRn recycling can ensure that ADCs do not extensively release their drugs off-target. FcRn recycling can therefore extend the half-life of an ADC. Engineering the Fc region of antibodies to increase binding affinity with FcRn at acidic pH has been successfully employed to increase antibody half-life by 4x *in vivo*.[66]

1.6 Tumour Penetration of ADCs

In order to effectively treat a whole solid tumour, an ADC would have diffuse deep into the tumour. For this to be effective, the ADC has to have efficient extravasation from the blood stream. Fluid pressure in healthy tissue is lower than that of the blood stream, aiding the transport of fluid from blood to tissue which is then directed to the lymph system. In tumours, the abnormal vasculature leads to leaky blood vessels and heterogeneous flow,[67] ultimately meaning a higher pressure in tumours than the blood stream.[68] This means that extravasation into tumours is compromised. Not only that,

but diffusion of drugs or ADCs is also limited by an abnormally dense extracellular matrix of proteoglycans and fibrous proteins such as collagens, fibronectins and laminins.[69] Greater particle size correlates with poorer diffusion through tumours.[70] It is for this reason that smaller antibody fragments are favoured for applications where rapid tumour penetration is crucial, such as imaging.[71] Antibody-cytokine conjugates also frequently employ antibody fragments lacking the Fc region as this limits exposure of Fc receptor bearing cells (such as immune cells) to cytokines.[57]

1.7 Drug Payloads

Another major area of importance in ADCs is the drug for conjugation. An antigen on a cancer cell is considered highly expressed when the copy number of the targeted antigen is > 10^5 per cell.[16] The number of drug molecules that can be delivered to a cancer cell is limited by the number of receptors on its surface. Therefore the drug has to be highly toxic to ensure cell death. In reality, not all antigens will bind ADC and not all binding events will result in drug delivery. However, receptors may be recycled to the cell surface after internalisation and allow further drug to be delivered. Upon cell death, the drug may also be released and go on to kill the surrounding cells which is known as the bystander effect.[20]

Of the disclosed drugs used as payloads in modern ADCs, most are of at least nanomolar IC_{50} potency. A selection of payloads most commonly used in ADCs can be seen in **Table 4**. These more successful ADCs frequently share common characteristics in their drugs: at least nanomolar IC_{50} and functional groups and physicochemical properties that make them amenable to protein modification. In the case of monomethylauristatin F (**MMAF**), it is thought that its intracellular toxicity is much higher than its IC_{50} in standard cellular assays. This is because it bears a carboxylic acid group, and the negative charge inhibits membrane permeation and therefore access to its intracellular target tubulin. When this acid is protected as the methyl ester (**MMAF-OMe**, **1**), the toxicity is increased more than 10^5 times.[24] This drug is used to limit the non-specific toxicity of the drug if it released outside of a cancer cell or by the bystander effect.

Table 4: Examples of drug payloads commonly used in clinical ADCs.

Drug / Class	Structure	Mode of action	IC_{50} / nM	Cell Line
DM1 / Maytansinoid	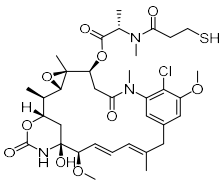	Tubulin binding	1.10 [72]	Various[a]
DM4 / Maytansinoid	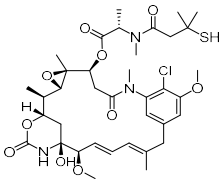	Tubulin binding	0.205 [72]	Various[a]
MMAE / Auristatin	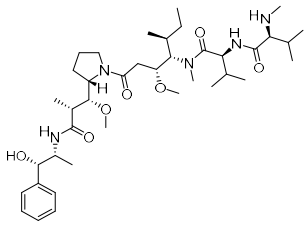	Tubulin binding	0.825 [24]	Various[a]
MMAF[b] / Auristatin	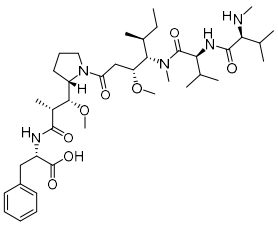	Tubulin binding	170 [24]	Various[a]
Calicheamicin θ_1[c] / Calicheamicin	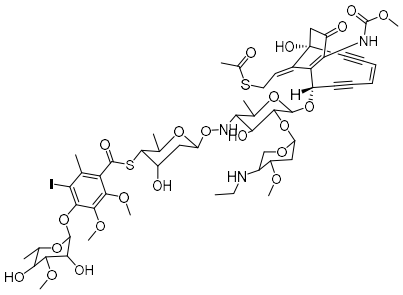	DNA cleavage	< 0.001 [73]	MOLT-4

Table 4: Continued…

Drug / Class	Structure	Mode of action	IC_{50} / nM	Cell Line
SG2285[c] / Pyrrolobenzodiazepine dimer (PBD)	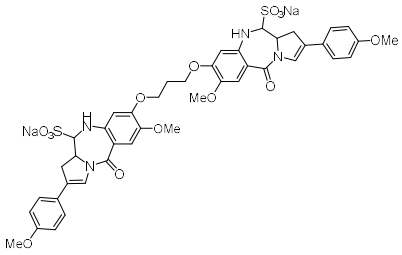	DNA alkylation	0.3 [74]	Various[a]
Duocarmycin Sa[c] / Duocarmycin	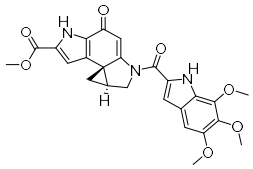	DNA alkylation	0.01 [75]	L1210
SN-38 / Camptothecin	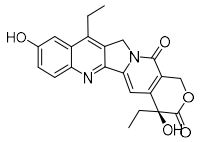	Topo I inhibition	46.8 [76]	Various[a]
Doxorubicin / Anthracycline	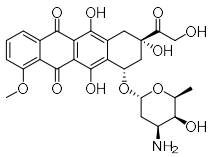	DNA intercalation	77 [77]	Various[a]

a) This value is the mean of various cell lines assayed. b) The free acid causes poor cell penetration, but if the acid is protected as the methyl ester: **MMAF**-OMe **1** IC_{50} < 0.001 nm (Karpas cells).[24] c) In cases where the exact drug is undisclosed, or the drug has no literature known IC_{50}, a closely related analogue has been given.

1.8 Linkers

ADC linkers are thought to play a pivotal role in drug release and have therefore been the focus of much attention. Of utmost importance are the sites of conjugation,[78] drug-to-antibody ratio (DAR),[79] and the choice of drug release mechanism. For ADCs, the convention is that a “cleavable” linker has a designed cleavage mechanism (e.g. enzymatic cleavage, acid hydrolysis or disulfide reduction) whereas a “non-cleavable” linker is designed to be more stable to digestion than the antibody. Typically, ADCs are thought to be internalised and trafficked into lysosomes to undergo metabolism.

1.9 Site-Selective Conjugation

When conjugating drugs to antibodies, the functional groups used for conjugation are highly important. The local protein environment at the site of conjugation is also highly important as it can intimately affect the stability of the conjugate. For maleimide-thiol conjugates it has been shown that highly solvent accessible sites of conjugation lead to increased maleimide-exchange with endogenous thiols – e.g. glutathione (**GSH**) or albumin – and that these processes are slower for less solvent-accessible conjugation sites. In the same study, it was shown that an overall positive charge in a less solvent accessible conjugation site can lead to further increased stability, as it promotes succinimide hydrolysis after maleimide conjugation.[78] Therefore if a cysteine is engineered into an antibody to facilitate site-specific conjugation, the stability of the resulting conjugates must be extensively studied with respect to the choice of conjugation site.[80,81] Hydrolysed succinimides are much less capable of thiol-exchange, which has been used to generate self-hydrolysing succinimides to further increase stability.[82–84]

Selectivity of conjugation is important for many reasons, for example: reproducibility of conjugation, site of conjugation and number of conjugated drugs. Early ADCs largely utilised lysine labelling strategies to introduce their drugs. For example, in the development of anti-A7 ADCs N-hydroxy succinimidyl esters were used to label anti-A7 antibodies and introduce a maleimide functionality.[85] However as lysine is such an abundant amino acid this leads to non-specific labelling across the antibody. Only with careful control of reaction conditions is the DAR kept reasonably constant – in this case DAR = 1-6. Each of these different antibodies in the mixture will have different properties, making studying their effects less reproducible and more complex. This chemistry would later be used in the development of trastuzumab emtansine – now on the market for the treatment of HER2+ breast cancer – with a mean DAR of 3.5. A similarly modified ADC, huN901–**DM1**, was studied by mass spectrometry in combination with protease cleavage to identify modification sites. Despite having a mean DAR between 3 and 4, the studies revealed DAR ranging from 1 to 6, with 40 out of 86 lysines potentially being modified.[86] Remarkably, no modification was detected in the binding regions, and modifications were generally in flexible, solvent accessible regions. Succinimidyl esters have also been shown to react with cysteine and tyrosine to form unstable thioesters and esters which degrade even at neutral pH.[87]

Later ADCs were made by reducing interchain disulfides (in this case with dithiothreitol, **DTT**) and then alkylating the liberated cysteines with maleimide-linker-drug constructs.[88] The issue with this technique is that there are potentially too many reactive cysteines, and not all should be alkylated. This is because reducing all these reactive interchain disulfides and alkylating them leads to a DAR of

8. While this leads to higher *in vitro* potency of the ADCs (due to more drugs being delivered per ADC), the greatly increased hydrophobicity of the ADC can lead to increased aggregation or plasma clearance and therefore lower potency *in vivo*.[79] However this effect has been shown to be alleviated when using highly hydrophilic linkers, leading to high *in vivo* potency ADCs with DAR of 8.[89] While the interchain disulfides are more prone to reduction/alkylation, this chemistry is still not highly specific, and these ADCs require a challenging purification by hydrophobic interaction chromatography.[90] A further possibility is mutating some native cysteines to serines, thereby reducing the number of possible sites for conjugation to cysteine.[91] Another method using mutagenesis is to insert cysteines into the antibody in particularly solvent accessible or reactive sites, thereby allowing selective reduction/alkylation of these cysteines.[78,92] In order to affect the folding of the antibody as little as possible, it is clearly favourable to leave structural intrachain and interchain disulfides intact (**Figure 4**).

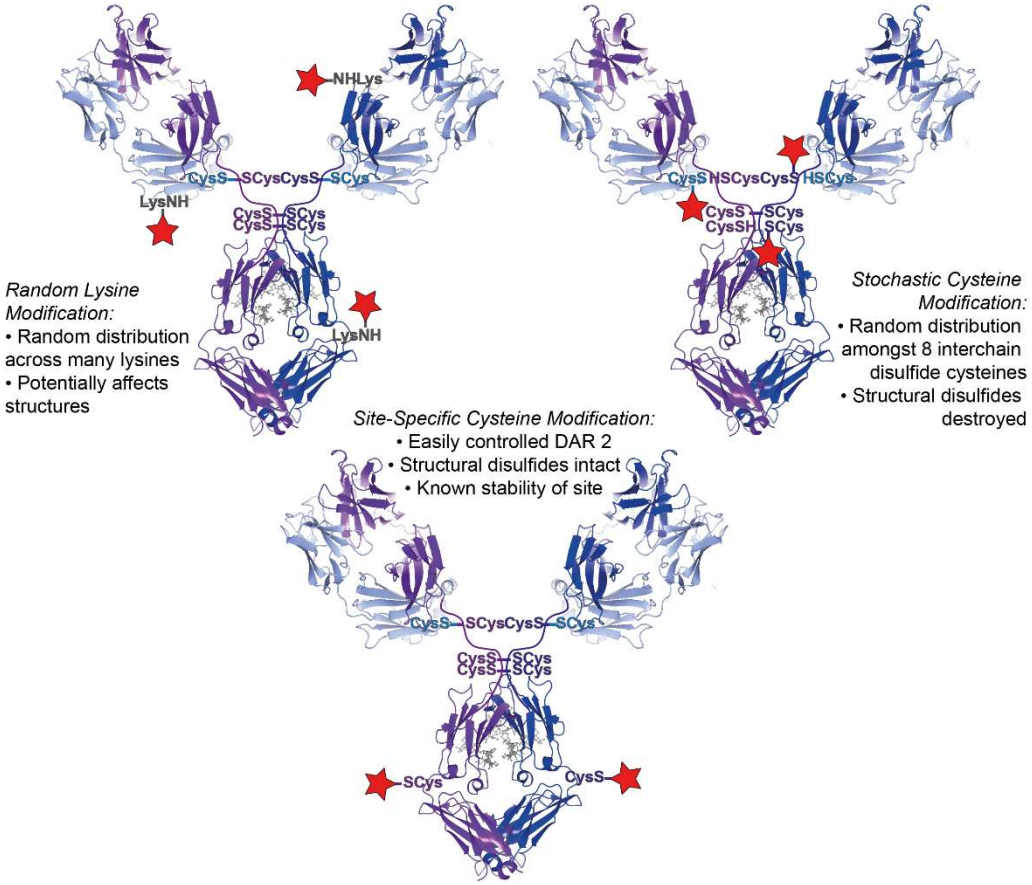

Figure 4: Different methods of antibody conjugation and their distributions of payload.

1.10 Mechanisms of Drug Release

A striking feature of ADCs is the lack of diversity in their mechanisms of drug release, as all those that have progressed beyond Phase I clinical trials rely on degradation by acid, proteases or reduction. Common structural motifs and release mechanisms for ADCs which have made it to clinical trials are discussed here.

AMIDES: KS1/4-**MTX** is the drug methotrexate conjugated to murine antibody KS1/4 *via* an amide and was evaluated in a Phase I trial,[11] and again in Phase I at higher doses.[93] Although the mechanisms of drug release were never studied, a logical step would be amide cleavage catalysed by proteases. There was little therapeutic benefit observed from the ADC, and the majority of patients developed anti-ADC antibodies. More recently, trastuzumab emtansine has been released to the market and amide cleavage has been shown to be responsible for the majority of its drug delivery as Lysine-SMCC-**DM1** (**2**).[22] Vadastuximab talirine bears a Val-Ala motif with an amide bond to an aniline nitrogen.[35,36] There are many proteases in cells, and the specific nature of an amide bond can greatly affect the specificity for a given protease and the rate of cleavage. By optimising the cleavage rate and specificity of peptidic linkers on ADCs it has been shown that *in vivo* efficacy can be improved.[94] This was achieved by screening many different peptidic linkers including non-proteinogenic amino acids. Denintuzumab mafodotin and depatuxizumab mafodotin have achieved Phase II clinical trials with the same linker (maleimido caprolyl, mc) and payload (**MMAF**) but different antibodies. When ADCs with isotopically labelled drugs were studied, the only **MMAF** containing compound that could be detected had resulted from protease cleavage of the antibody – producing Cys-mc-**MMAF** (**3**).[24] The toxicity of this compound was not tested, but the charged ammonium of **MMAE** and **MMAF** is a key interaction in the binding mode their target tubulin (salt bridge with Asp179). As ionic interactions tend to be very strong it is likely that the toxicity of Cys-mc-**MMAF** (**3**) is much less than that of the parent drug.[95,96] AGS-16C3F bears the same linker and payload as denintuzumab mafodotin and depatuxizumab mafodotin and is likely to follow the same drug release mechanism although it has not been studied.[37]

HYDRAZONES: Hydrazones are more stable to hydrolysis than their corresponding Schiff bases, and were used to conjugate desacetylvinblastine hydrazide (**DAVLB**) to KS1/4 murine antibodies to give KS1/4-**DAVLB**. The sugars on the mAb were first oxidised with $NaIO_4$ (which causes cleavage of 1,2 diols to aldehydes) then condensed with desacetylvinblastine hydrazide.[8] These ADCs were tested *in vivo* against a human tumour xenograft in mice,[97] and a Phase I clinical study for immune response.[98] The hydrolysis of hydrazones is slow at neutral pH, but is thought to be highly efficient in the acidic environment of lysosomes. However, no therapeutic benefit could be shown in clinical trials, and the majority of patients developed immune responses. Two marketed ADCs, gemtuzumab ozogamicin and

inotuzumab ozogamicin, both bear hydrazones as well as disulfides in their linkers. The hydrazone is shown to be stable at neutral pH and efficiently hydrolysed in acid.[21] However disulfide reduction has been shown to be key to toxicity of the calicheamicin payloads[99] but the competing rates of hydrazone hydrolysis and disulfide reduction in cancer cells were not studied. ADCs hLL1-**Dox**[44,45] and SGN15[9,51] also bear the payload doxorubicin (**Dox**) *via* a hydrazone linker and have achieved Phase II clinical trials.

ESTERS: In KS1/4-**DAVLB**, desacetylvinblastine was conjugated to KS1/4 murine antibody *via* a short succinic ester linker. This was tested in a Phase I clinical trial for drug efficacy against adenocarcinoma,[10] and a Phase I trial of immune responses.[98] While mechanisms of drug release were not studied, a logical step would be ester hydrolysis catalysed by esterases analogous to that of KS1/4-**MTX**.

DISULFIDES: Disulfides are one of the best studied linkers and are a common linker in ADCs. Reduction of the disulfide is the obvious mechanism of drug release, but this can occur both intra- and extracellularly. To investigate the relative rates of drug release, several analogous disulfide-linked ADCs were synthesised with varying steric constraints about the disulfide (from RCH_2SSCH_2R to $RC(Me)_2SSC(Me)_2R$). Their relative rates of reduction when exposed to **DTT** were then tested. While IC_{50} *in vitro* cell killing stayed similar for all conjugates, the RCH_2SSCH_2R linked ADC showed cleavage rates 22000 faster than that of $RC(Me)_2SSC(Me)_2R$. *In vivo*, this corresponded to a half-life of 15 h *vs* 218 h respectively. This was greater than the corresponding succinimidyl thioether conjugate, which had a half-life of 134 h.[100] Perhaps counterintuitively, the conjugates with the greatest therapeutic effect *in vivo* were not the most or least stable, but those of moderate stability. In another study, a small immune protein (SIP) format disulfide linked ADC was compared to the analogous IgG ADC. The SIP format was found to release drug much faster than the IgG (half-life 3 h and > 48 h respectively), and this was attributed to the close proximity of linking cysteines in the SIP format. This could be because the two linking cysteines in SIP format are capable of forming an intramolecular disulfide after drug cleavage.[101] This effect is similar to **DTT** being a stronger reducing agent than 2-mercaptoethanol, as **DTT** is capable of forming intramolecular disulfides.[102]

In another study, tritium labelled maytansinoids were conjugated to antibodies *via N*-succinimidyl 4-(pyridin-2-yldisulfanyl)butanoate (SPDB) linkers and these ADCs were used to treat mice in a tumour xenograft model. The mouse livers and tumours were then excised, and the metabolites characterised by LC-MS with radioactivity detection.[22] The most major intracellular metabolite for the disulfide-linked ADC was *S*-methyl-**DM4** (**4**) which had an IC_{50} 2 pM against assayed cell lines, followed by a minor Lysine-SPDB-**DM4** (**5**) at early time points which was then quickly degraded. This suggests that both amide cleavage and disulfide reduction play a fundamental role in drug release (**Scheme 1**). When

a lysosome formation inhibitor was added, the formation of these metabolites was massively reduced. The limitation of this study however is that only radioactive metabolites could be detected, and also only those detectable using their LC-MS parameters. Lorvotuzumab mertansine (Phase II),[47] coltuximab ravtansine (Phase II) and anetumab ravtansine (Phase II)[38] all also bear SPDB linkers. Mertansine employs the drug **DM4** which has a gem-dimethyl adjacent to its thiol and ravtansine employs **DM1** which has no methyl groups. Therefore mertansine is expected to reduce more slowly than ravtansine due to increased steric shielding of the disulfide. Mirvetuximab soravtansine (Phase III)[26] bears **DM4** with a sulfo-SPDB linker which is modified with a sulfonate group to increase water solubility. Gemtuzumab ozogamicin and inotuzumab ozogamicin contain a hydrazone and a disulfide in their linkers. The hydrazone is predicted to cleave first[21] however disulfide reduction is still necessary for the calicheamicin to exert toxicity.[99]

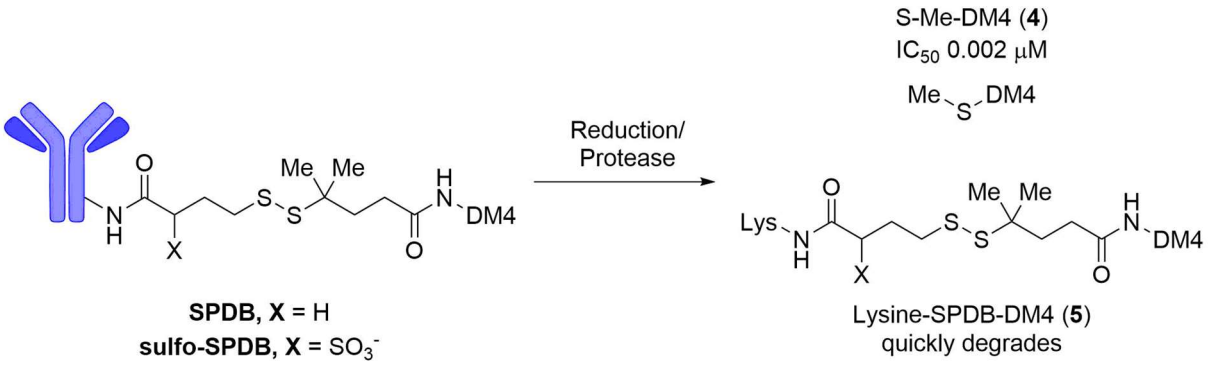

Scheme 1: Lysosomal degradation pathway of disulfide-linked ADCs and structure of different disulfide linkers. Lysines are typically modified *via* the free ε amine but can be modified at the α amine of an N-terminal lysine.

SUCCINIMIDYL THIOETHERS: This is by far the most popular means of conjugating drugs to antibodies, as the reaction of a thiol with maleimide is incredibly fast, and is used in the production of two ADCs currently on the market: trastuzumab emtansine and brentuximab vedotin. These linkers are ubiquitous in ADCs despite the fact they have been shown to slowly undergo thiol exchange.[78,103] In a study of one succinimidyl thioether linked maytansinoid ADC, it was found that lysosomal processing was necessary for release of the drug. A tritium labelled maytansinoid was conjugated to an antibody *via* an *N*-succinimidyl 4-(*N*-maleimidomethyl)cyclohexane-1-carboxylate (SMCC) linker – the same used in trastuzumab emtansine – and the metabolites from a mouse tumour xenograft monitored by LC-MS with radioactivity detection. The only significant metabolite detected was Lysine-SMCC-**DM1** (**2**), which suggests the drug is mainly released by amide cleavage (**Scheme 2**). Lysine-SMCC-**DM1** (**2**) this was found to have an IC_{50} of only 0.1 μM against the assayed cell lines, but the ADC still had high efficacy against tumour cells. It was hypothesised that Lysine-SMCC-**DM1** (**2**) simply had poor cell penetration in the IC_{50} assay, but once released intracellularly could be highly potent.[22] Again, the

limitation of this study is that only radioactive metabolites could be detected, and only those detectable using their LC-MS parameters.

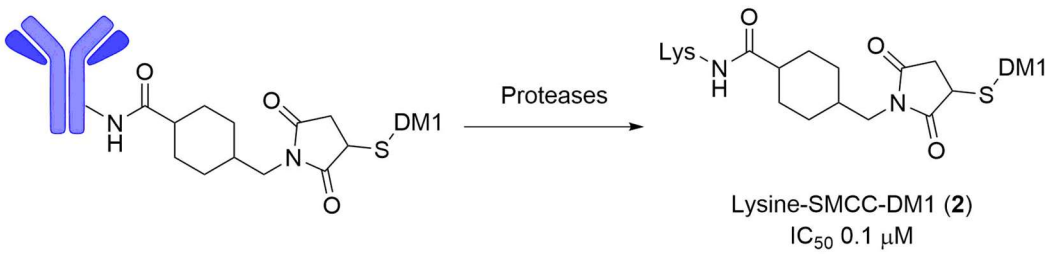

Scheme 2: Lysosomal degradation of SMCC-linked ADCs. Lysines are typically modified *via* the free ε amine but can be modified at the α amine of an N-terminal lysine.

SELF-IMMOLATING PAB: This particular motif has seen success in now marketed brentuximab vedotin, which has a valine-citrulline-*p*-aminobenzyl (Val-Cit-PAB) linker which can undergo 1,6-immolation after the Val-Cit linker is cleaved by proteases (e.g. Cathepsin B). When brentuximab vedotin with ^{14}C labelled **MMAE** was used to treat tumour cells *in vitro*, the only detectable species by LC-MS with radioactivity detection was **MMAE**, showing efficient amide cleavage and 1,6-immolation leading to effective drug release (**Scheme 3**). As well as potent cell killing, these ADCs showed efficient bystander killing in co-cultures of cancer and healthy cells as **MMAE** can freely diffuse out of cells or is still active after release from dead cells.[20] This study is also limited as non-radioactive metabolites of **MMAE** cannot be detected. The study demonstrates the benefit of having linkers which can release a whole drug intact, as opposed to those which release drug-derivatives which may have attenuated toxicity as previously discussed for mc-, SMCC- and SPDB-linked ADCs.

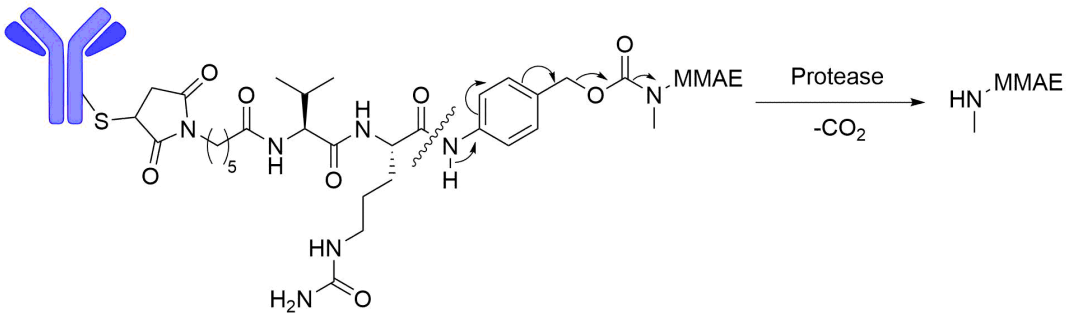

Scheme 3: Lysosomal degradation of a Val-Cit-PAB self-immolating linker.

SELF IMMOLATION FOR RELEASE OF *O*-LINKED DRUGS

Most drug release methodologies from ADCs have focused on the release of amine- and sulfur- linked drugs. However many potent drugs do not have these functional groups or they are not amenable to conjugation. Strategies have been developed for the release of hydroxyl-containing drugs that have been applied in DS-8201a[40,41] for Phase II and SYD985[32,33] for Phase III clinical trials. In the case of DS-8201a, protease cleavage is used to release an aminomethyl ether which can then spontaneously undergo imine formation and hydroxyl release (**Scheme 4**). This mechanism is similar to that employed for rapid DNA sequencing with the Staudinger reduction.[104,105]

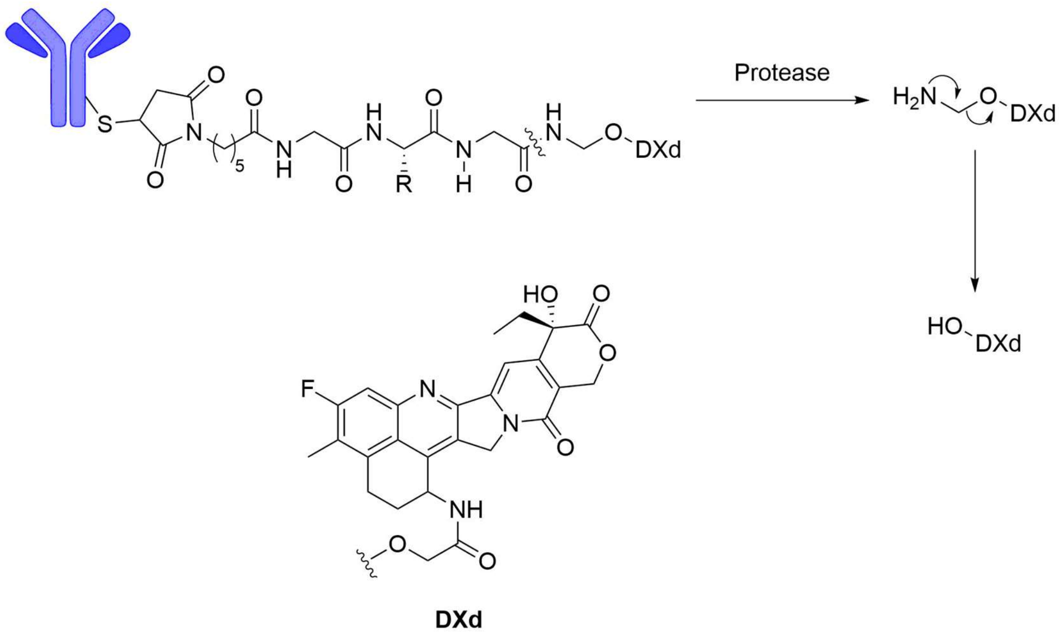

Scheme 4: Degradation pathway of DS-8201a by protease cleavage.

In the case of SYD985, the common amide cleavage followed by PAB elimination is used to release a reactive amine. The reactive amine is then free to act as a nucleophile and attack into the carbonyl of a proximal carbamate. This cyclisation causes the release of hydroxyl bearing drug **seco-DUBA** (**Scheme 5**).

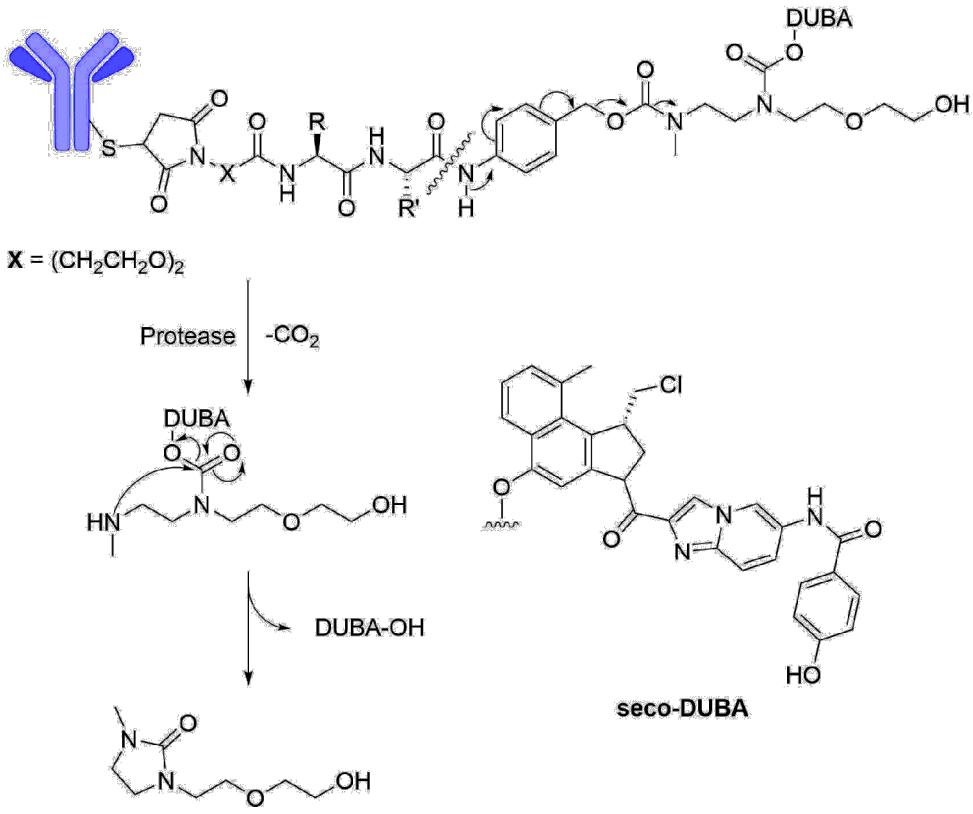

Scheme 5: Protease-triggered drug release mechanism of Phase III ADC SYD985.

NON-INTERNALISING ADC MECHANISMS OF DRUG RELEASE

The vast majority of ADCs in clinical trials have focused on using linkers that should selectively cleave *after* internalisation into cancer cells. Clear outliers in this trend are sacituzumab govitecan (Phase III) and labetuzumab govitecan (Phase II). These are based on the concept that a "moderately stable" linker should be able to release its payload after conventional internalisation and degradation but also after degradation by the lower concentration of extracellular proteases.[29,31] Sacituzumab govitecan has shown promising results in a Phase II clinical trial[50] and has been advanced to Phase III. The linkers of sacituzumab govitecan and labetuzumab govitecan employ a peptide cleavage site and PAB self-immolation followed by decarboxylation of a carbonate for release of campothecin drug **SN-38**. Moderate stability of the linker is attributed to the carbonate linkage being less hydrolytically stable than amides or carbamates. The success of these ADCs highlight the fact that non-internalising ADCs may be a path towards the successful treatment of solid tumours.

Most ADCs in clinical trials contain a peptide drug-release trigger which has been designed to be efficiently cleaved by proteases inside cancer cells. For example the most popular would be the Val-Cit-PAB linker of marketed brentuximab vedotin. The Val-Cit dipeptide was designed to be cleaved by Cathepsin B as this protease is often upregulated in cancers. However, when Cathepsin B expression

was knocked-down in cancer cells, no decrease in toxicity of a Val-Cit-PAB-MMAE ADC was observed.[106] In fact, it was shown that other proteases could also cleave the linker in various places leading to products which could still exert toxicity.

As cleavage by specific proteases was shown to be unnecessary for efficacious ADCs, it also begs the question whether or not internalisation is necessary. The clinical successes of sacituzumab govitecan and labetuzumab govitecan have increased efforts to study non-internalising ADCs based on the fact that sacituzumab is slowly internalised.[107,108] However work was already underway in this field.[109] For example, extracellular matrix proteins such as fibronectin[110] and tenascin-C[111] were already being targeted with a view to developing cancer treatments. Later, antibody fragments targeting aberrantly spliced fibronectin in tumours would be targeted by ADCs of antibody fragments bearing a disulfide linker to a thiol-modified cemadotin.[112] This was demonstrated to be effective in shrinking solid tumour xenografts in mice. The stability of the disulfide linker was shown to be crucial in determining therapeutic efficacy, with the most stable disulfides giving the greatest therapeutic benefit.[113]

These ADCs were later adapted to contain various drug payloads, including a carbamate- and carbonate-linked duocarmycin as well as maytansinoid **DM1**.[114] The carbonate-linked duocarmycin outperformed the carbamate, likely due to a lower linker stability enabling greater drug release in the tumour microenvironment. However, **DM1** was predicted to form the greatest stability conjugates and yet this resulted in curing of solid tumours in mice. This is attributed to the fact that the cancer cell line assayed is highly sensitive to **DM1**. It could also be due to the fact that **DM1** is much more potent than duocarymicin. So despite a lower dose of **DM1** delivered to the tumour than duocarmycin, it can cause more cell killing.

A disulfide linker to a **DM1** payload was later used to compare the efficacy of antibody-fragment SIP ADC with the same linker and payload on an IgG ADC.[101] It was found that the IgG ADC was the most stable but also the least efficacious at treating solid tumour xenografts in mice. This may be because SIP format ADCs are smaller and therefore better able to penetrate solid tumours allowing greater doses of released drug. Extracellular matrix protein tenascin-C has also been developed as a target for cancer treatment[111] including ADCs. Conjugating anti-tenascin-C IgG antibody F16 to a doxorubicin derivative *via* a protease-cleavable Val-Cit-PAB linker led to reasonably efficient solid tumour shrinkage in mouse xenograft models.[115] The drug was then exchanged for **MMAE** or **MMAF**. The F16-**MMAE** ADC led to efficient tumour shrinkage while F16-**MMAF** ADC had no effect whatsoever. This supports a hypothesis of extracellular drug cleavage as **MMAF** is not cell penetrant due to its free carboxylate group, whereas **MMAE** is highly cell penetrant.

Bizarrely, when the F16-**MMAE** IgG ADC was compared to its SIP format analogue, the IgG ADC performed much better in solid tumour mouse xenografts. This is in stark contrast to earlier studies in which the disulfide-linked anti-fibronectin-**DM1** SIP ADC had performed much better than its IgG analogue.[101] This is likely due to the fact that in both cases the IgG is more stable and the time required for drug delivery. In the case of anti-fibronectin-**DM1** SIP ADC, the greatest tumour shrinkage was achieved after ~10 days, whereas for the F16-**MMAE** IgG ADC this required ~30 days. Reduction of unhindered disulfides has been shown to be a faster process than protease cleavage.[22] Therefore the disulfide-linked **DM1**-SIP ADC has time to quickly release its payload before the ADC is removed from circulation. The disulfide-linked **DM1** IgG ADC would not be able to penetrate the tumours enough to release a significant amount of payload within the same time period as the SIP ADC. The **MMAE**-IgG ADC has its payload released by the slower process of protease cleavage, which means that the SIP format ADC is not stable within the mouse for long enough to deliver a significant amount of drug to the tumour. The **MMAE**-IgG ADC can circulate for a long time and slowly release drug to the tumour. This hypothesis is supported by studies into different peptide linkers in the F16-**MMAE** IgG ADC which showed that the specific nature of the peptide can influence the efficacy of the ADC in tumour xenografts.[116]

1.11 Conclusion

ADCs have achieved great pre-clinical and clinical success, but still have far to go before becoming the "magic bullet" as dreamed of by Paul Ehrlich.[117] In fact, while ADCs appear to offer improvements over existing therapies, the increase in survival seems surprisingly low for a "targeted therapy" (**Table 5**). Clearly there is much optimisation left to do in the development of ADCs and much to learn about their efficacy.

Table 5: Summary of clinical results that led to ADCs becoming FDA approved.

	Measure	ADC	Standard treatment
Gemtuzumab ozogamicin[118]	Event free survival	17.3 months	9.5 months
Trastuzumab emtansine[119]	Survival	30.9 months	25.1 months
Brentuximab vedotin[120]	Progression free survival	17 months	4 months
Inotuzumab ozogamicin[121]	Complete remission	35.8% of patients for 8 months	17.4% of patients for 4.9 months

In order to give ADCs the greatest possible chance of improving cancer patients' lives, the largest possible diversity of targets, linkers and drugs should be trialled. The most neglected set of targets seems to be extracellular antigens to give non-internalising ADCs. No extracellular antigen-targeting ADCs have made it thus far to Phase II clinical trials and therefore this appears an important area to focus research. Most ADC linkers have been designed with an internalisation/lysosomal degradation pathway to drug release, so non-internalising ADCs will require new and further optimised linker systems.

To study the roles extracellular-drug release can play in cancer treatment, the field will require chemical biology tools in order to:

- Explore the efficacy of drugs when released into the intercellular space
- Develop novel mechanisms of drug release from ADCs

Therefore in the next chapter, bioorthogonal approaches to the release (decaging) of small molecules and proteins to study and modulate biological systems will be discussed, with a view to developing bioorthogonal decaging reactions to study potential non-internalising ADCs.

Chapter 2:

Bioorthogonal Decaging for Chemical Biology

2.1 Key Elements of Bioorthogonal Decaging Reactions

The objective of bioorthogonal chemistry is to develop reactions which can occur in living systems without affecting any endogenous processes. In reality this is an ideal which is likely unachievable. However, many bioorthogonal reactions have been developed which affect the chosen biological system so little, that they allow the study of key processes in previously inconceivable ways. The criteria for a bioorthogonal reaction can be diverse and depend on the exact system that is to be studied. For example, bioorthogonal reactions can be used to study proteins simply *in vitro*, to more complex systems *in vivo*. Clearly, proteins *in vitro* constitute the least complex system and the requirements of the reactions are therefore less demanding. This chapter will primarily focus on bioorthogonal reactions developed for use in mammalian cells or even *in vivo*. In these cases, the pre-requisites for a useful reaction are:

- **Rapid rate constants.** Typically, biological processes of interest occur on timescales in the order of seconds to days, between room temperature and 37 °C and at relatively low concentration (pM to μM). Reactions that study these processes therefore cannot rely on high temperatures or high concentrations to increase their rates and must have high rate constants.
- **Low toxicity.** Another key factor of the reagents in bioorthogonal reactions is that they be minimally toxic. If the reagents are too toxic, they will affect the organism of study so much that they may mask the processes which they were designed to study.
- **Excellent selectivity.** If the reagents in bioorthogonal reactions cross-react with chemical functionalities endogenous to the organism of study, it will cause a hindrance to their reactivity and may alter the usual functions of the organism. Therefore the reagents involved in the reaction must be highly selective.
- **Synthetic tractability.** The utility of bioorthogonal reagents can be limited by the ease with which they can be synthesised. When the synthesis of the reagents is long, complex, expensive and possesses limited functional group tolerance, the number of applications of these reagents is restricted.

The vast majority of bioorthogonal reactions have focused on ligation – bond forming reactions between two molecules-of-interest. However, recently interest has been growing in the field of bioorthogonal decaging reactions – bond cleavage reactions that liberate molecules-of-interest for gain-of-function studies or drug delivery.

2.2 Light Mediated Decaging

The most widely used bioorthogonal bond cleavage reaction in chemical biology is UV mediated decaging.[122] It has been used extensively in the study of protein[123] and small molecule[124] function in biology and has even seen use *in vivo*.[125,126] The premise of light mediated decaging is that a protecting group on a molecule-of-interest can absorb energy from photons, and its excited state undergoes a series of reactions that cause decomposition. The newly released molecule-of-interest can then perform its function. The most common photoremovable protecting groups are derived from *o*-nitrobenzyl protection of an anionic leaving group (**Scheme 6**).

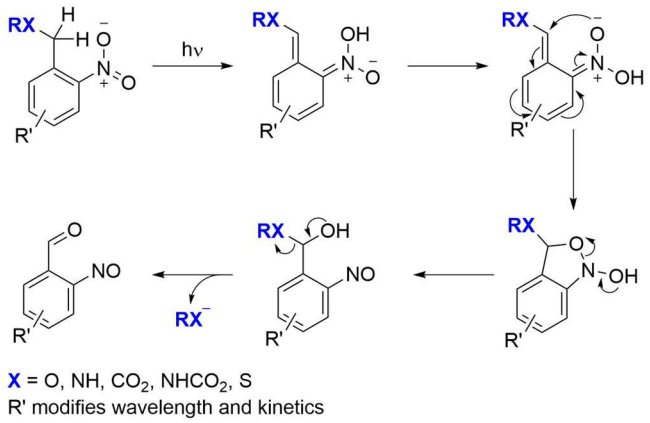

Scheme 6: Mechanism of decaging of *o*-nitrobenzyl caging groups.

The mechanism of this reaction requires the absorption of light, and in the excited state the nitro group behaves as a base, abstracting one proton from the neighbouring benzyl methylene.[127] Subsequently, the nitro group behaves as a nucleophile and the molecule undergoes an intramolecular 1,8-conjugate addition. The cyclised intermediate can then decompose to give nitroso and hydroxyl groups. The newly liberated hydroxyl can push electron density onto its methylene to form an aldehyde and release an anionic leaving group. The nature of the leaving group covers a broad p*K*a range – from carboxylic acids and carbonates to aliphatic alcohols. A range of photoremovable protecting groups have been used in the activation of small molecules for diverse applications (**Table 6**).

Table 6: A selection of reactions used in the photorelease of small molecules.

Reaction	Wavelength	Application
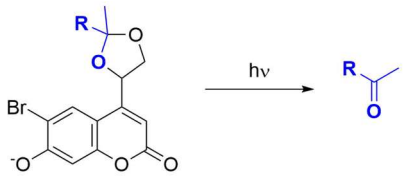	~365 nm	Progesterone decaging in sperm[128]
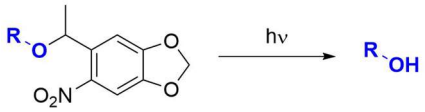	~365 nm	Oligonucleotide decaging in immune cells[129]
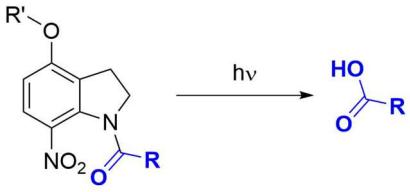 R' = photosensitiser	~350 nm	L-glutamate decaging in neurones[130]
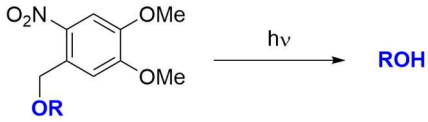	~360 nm	Peptide decaging in mammalian cells[131] Plant hormone decaging in wheat[132] Retinoic acid decaging in Zebrafish[125] Hydroxy-cyclofen decaging in Zebrafish[126]
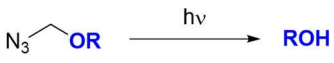	~365 nm	Fluorophore decaging in mammalian cells[133]
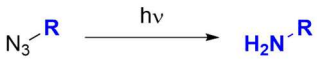	~365 nm	Fluorophore decaging in mammalian cells[134]

Table 6: Continued…

Reaction	Wavelength	Application
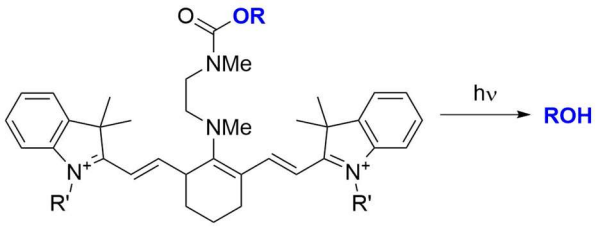	~690 nm	Hydroxy-cyclofen decaging in mammalian cells[135]
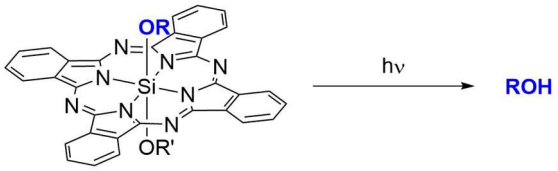	~690 nm	*Z*-CA4 decaging in mammalian cells[136]

The majority of light mediated decaging reactions use high-energy UV light (350-365 nm) with powerful lamps which has problems of poor tissue penetration and cytotoxicity.[136,137] Using lower energy, longer wavelengths of light would offer a solution to this problem. Near-IR cleavable protecting groups for alcohols have been developed with larger chromophores that have lower energy transitions. For example, a cyanine dye was adapted with a linker which would oxidatively decompose and self-immolate to release an alcohol-bearing fluorophore or drug (**Scheme 7**).[135]

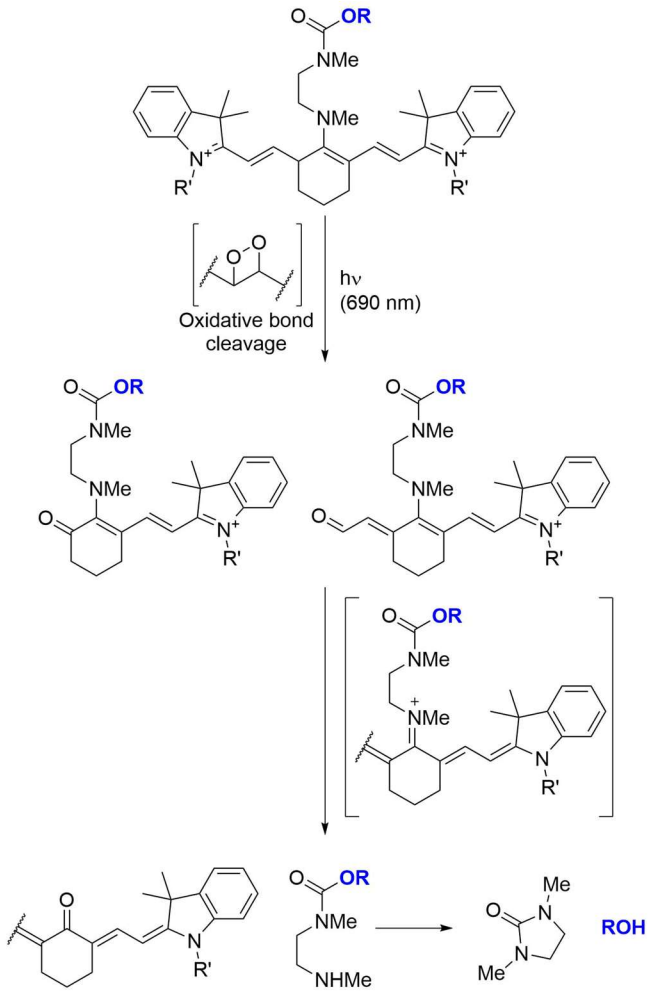

Scheme 7: Release mechanism of a near-IR activated protecting group.

In another example, a silicon phthalocyanine was adapted to contain the alcohol-bearing drug ***Z*-CA4**.[136] When irradiated with near-IR light, the complex reaches an excited singlet state, which then undergoes intersystem crossing to a triplet state. In the presence of reducing agents – such as **GSH** – the triplet is reduced to a radical anion which can release an alcohol.

While near-IR has the benefits of greater tissue penetration and lower toxicity, UV photoremovable protecting groups have seen more widespread use in more demanding applications such as genetically-encoded amino acids. This may be because UV removable protecting groups can be smaller and therefore more easily incorporated as unnatural amino acids. Smaller protecting groups also have less of an effect on the native structure and properties of the molecule-of-interest, which may lead to preferable characteristics such as greater stability or solubility. This has allowed precise probing of the functions of single amino acids in proteins (**Table 7**).

Table 7: Examples of photocaged amino acids successfully genetically incorporated into proteins and their applications.

Amino acid	Transformation	Applications
Cysteine	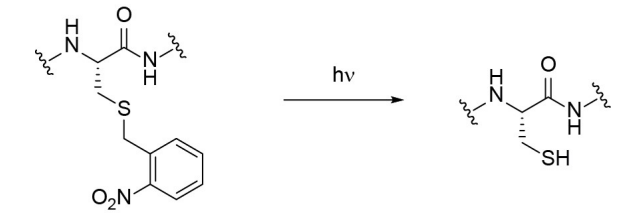	Enzyme activation *in vitro*[138] Enzyme activation in bacteria[139,140] Enzyme activation in mammalian cells[140]
Cysteine sulfenic acid	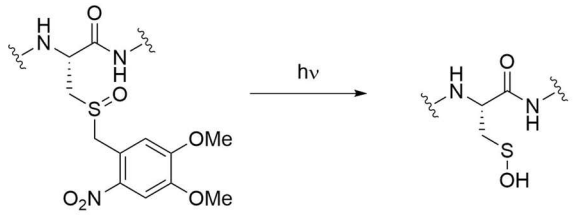	Enzyme activation in bacteria[141]
Tyrosine	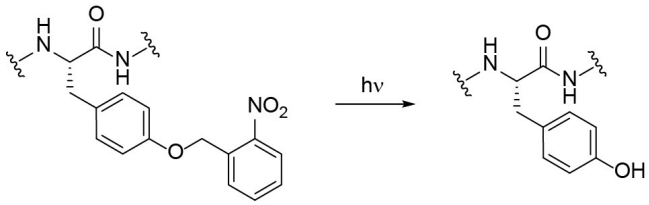	Protein expression[142] Enzyme activation in mammalian cells[143] Signal activation in mammalian cells[144]
Serine	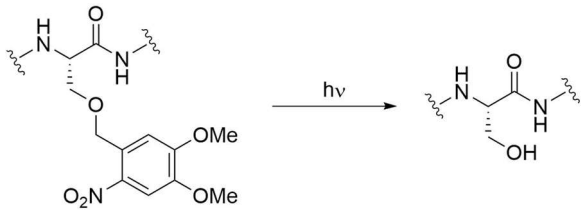	Signal activation in mammalian cells[145]
Selenocysteine	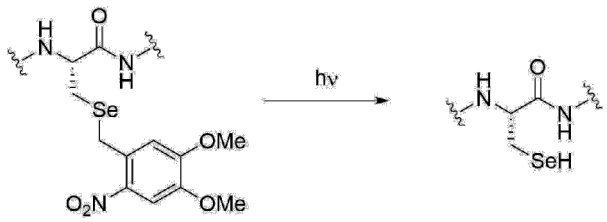	Protein activation in yeast[146]

Table 7: Continued…

Amino acid	Transformation	Application
Lysine	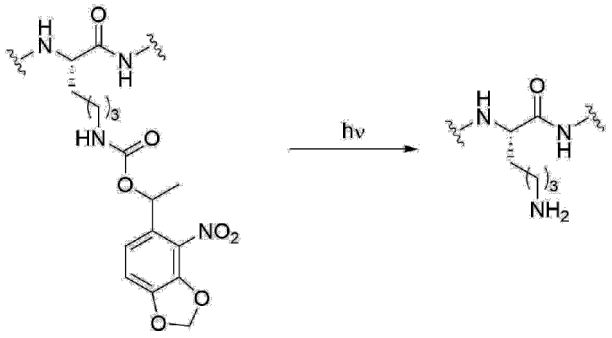	Signal activation in mammalian cells[147]
Threonine	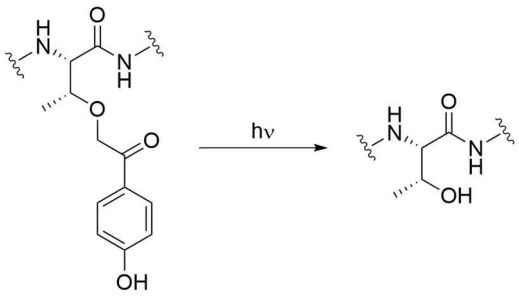	Kinase activation in mammalian cells[148]

2.3 Organic Small Molecule Mediated Decaging

While genetically-encoded UV photoremovable protecting groups have allowed incredible insights into cell biology, they are not capable of progressing to *in vivo* use due to the poor tissue penetration of UV light. Genetically-encoded near-IR or IR photoremovable protecting groups could possibly solve this problem. However, the large size of the groups hinder the design of the necessary tRNA synthetase enzymes which are necessary for successful genetic encoding of non-canonical amino acids. This reason combined with the toxicity of UV light, as well as difficulty in reproducing exact conditions for UV decaging have led research to focus on bioorthogonal reactions of small-molecules. These should allow the release of molecules-of-interest after reaction with a small organic or inorganic reagent. Such reactions with organic molecules have seen tremendous progress in chemical biology and have even been used *in vivo* (**Table 8**).

Table 8: Examples of bioorthogonal decaging reactions with small organic molecules that have been applied in mammalian cells or higher organisms.

Reaction	Applications
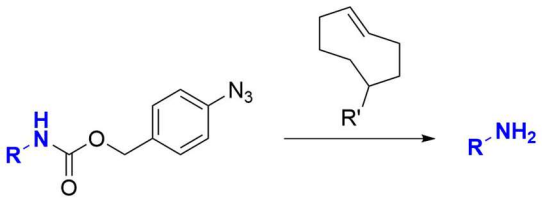	Prodrug activation[149]
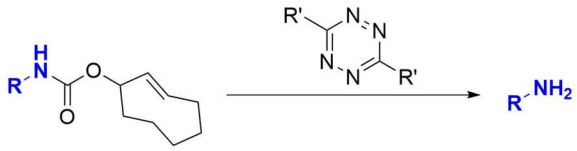	Prodrug activation[150,151] Protein activation[152] ADC drug release[153] Prodrug activation *in vivo*[154]
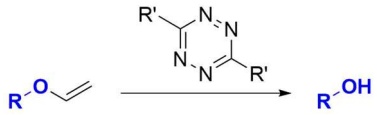	Prodrug activation[155] Fluorophore activation[156]
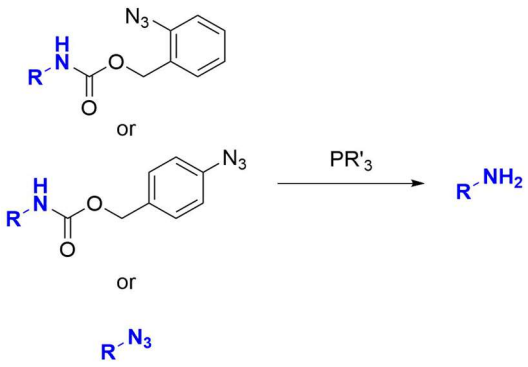	Prodrug activation[157,158] Protein activation[159,160]
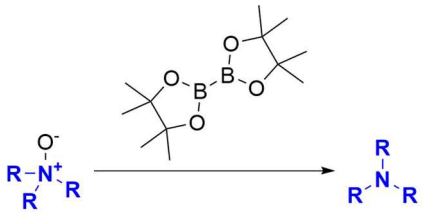	Fluorophore activation[161]
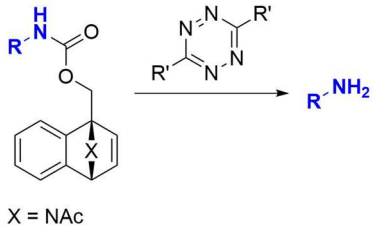	Prodrug activation[162]

Some the most promising reagents in small organic molecule mediated decaging are *trans*-cyclooctenes. Their highly strained structures lead to some interesting and rapid chemistry that has been applied to the release of drugs and fluorophores in mammalian cells and *in vivo*. For example, *trans*-cyclooctene derivatives were used in the release of a caged doxorubicin prodrug. First, a 1,3-dipolar addition reaction with an azide leads to the formation of an unstable triazoline which decomposes to give an imine (**Scheme 8**). The unstable imine is then hydrolysed to release a self-immolating *p*-aminobenzyl linker. This reaction demonstrated a second-order rate constant of 0.027 M^{-1} s^{-1} in 1:1 MeCN:PBS which is of a similar order to slower bioorthogonal ligation reactions such as the Staudinger ligation.[163]

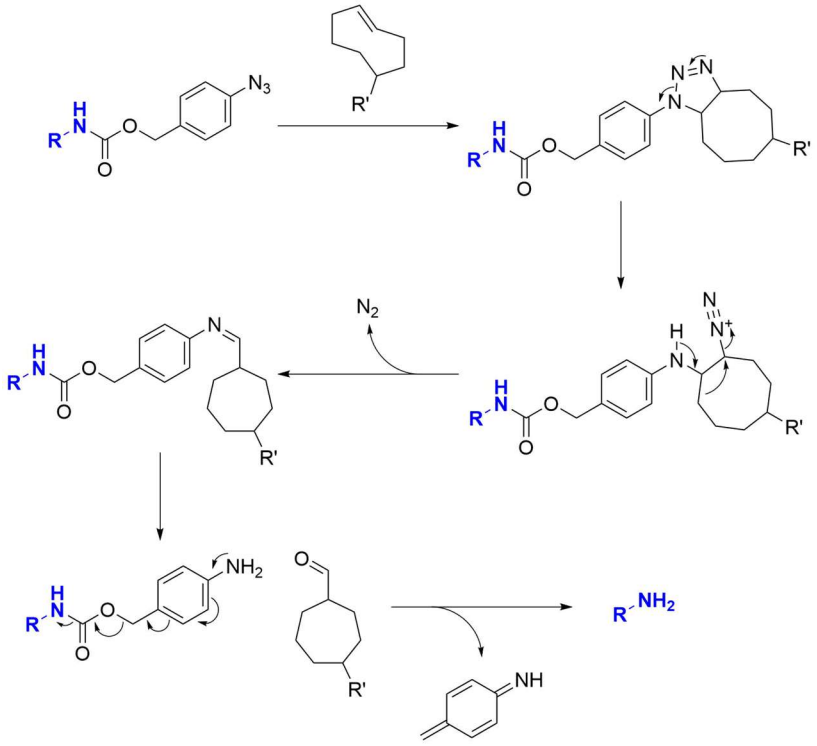

Scheme 8: *Trans*-cyclooctene mediated decaging of an azide-containing carbamate.

In another example, when amines were protected as carbamates of *trans*-cyclooct-2-ene-1-ol (TCO-OH) they could be decaged after an inverse-electron Diels-Alder reaction with tetrazines (**Scheme 9**). First a [4+2] cycloaddtion occurs rapidly with a second order rate constant of 57.7 ± 5.0 M^{-1} s^{-1} in MeCN. Then a tautomerisation allows a 1,4-elimation, decarboxylation and release of an amine.[150,164] This reaction has allowed the delivery of TCO-OH caged prodrugs,[150] decaging of a TCO-OH caged lysine residue on a protein in mammalian cells[152] and even the development of a TCO-OH derived linker for an ADC targeting tumours in mice.[153]

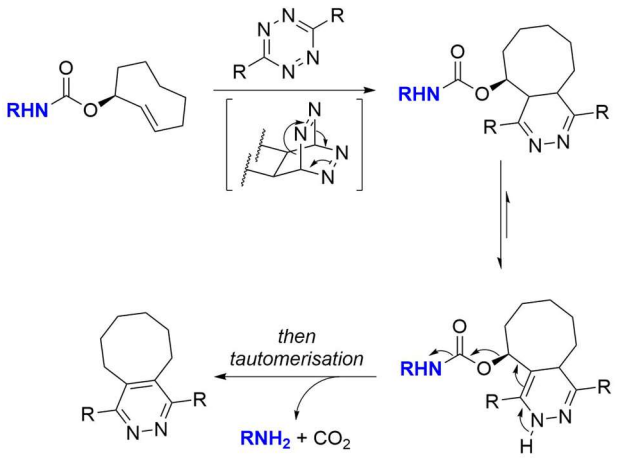

Scheme 9: Tetrazine mediated decaging of a TCO-OH carbamate-caged amine.

This reaction represents the fastest reported bioorthogonal decaging reaction. When compared directly to photorelease of caged lysines in cells, optimised tetrazine derivatives led to greater conversion to the decaged free lysine of TCO-OH carbamates.[165]

2.4 Metal Mediated Decaging

While some organic decaging reactions are fast and highly applicable to living cells and mice, they have been used less frequently than metal mediated bioorthogonal decaging reactions. Metal complexes have proven to be versatile in the release of fluorophores and drugs in mammalian cells, on proteins and even *in vivo* (**Table 9**).

Table 9: Examples of bioorthogonal decaging reactions with metal complexes that have been applied in mammalian cells or higher organisms.

Reaction	Applications
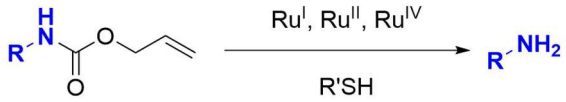	Fluorophore and prodrug activation[166–171]
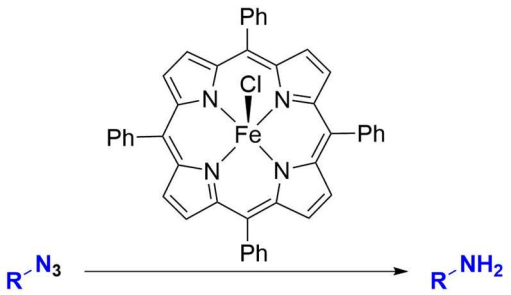	Fluorophore activation[172]
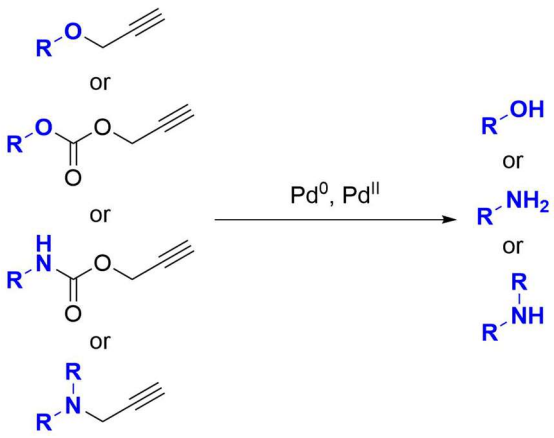	Propargyl ether fluorophore activation in mammalian cells[173–175] and Zebrafish[176] Propargyl carbonate fluorophore activation in mammalian cells[177] Propargyl carbamate fluorophore activation in mammalian cells[171,178,179] Propargyl carbamate decaging for protein activation in mammalian cells[180] Sugar release on mammalian cell surface[181] Propargyl carbamate decaging of prodrugs *in vivo*[182]
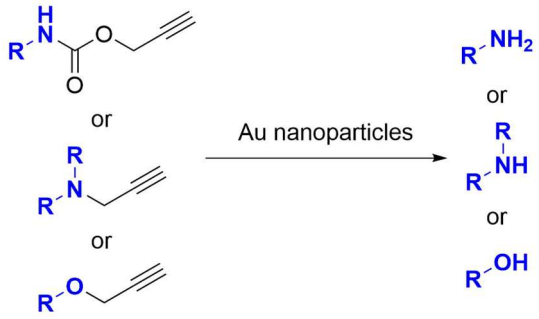	Fluorophore and prodrug activation in Zebrafish[183]
	Tyrosine activation on proteins in mammalian cells[184]

The most successful of these reactions (having been successfully implemented in mice[182]) is palladium mediated decaging of carbamates (**Scheme 10**). Both propargyl and allyl carbamate decaging are mechanistically related to the Tsuji-Trost reaction[185] and have been reported together.[180,182,186] However propargyl groups have been more widely used and shown to possess superior reactivity in mammalian cells.[180] Firstly, a Pd^0 complex forms a binding interaction with the alkyne of a propargyl group. Pd^0 can subsequently behave as a nucleophile, pushing electron density into the alkyne terminus. This causes the formation of an allene, and the elimination of a negatively charged leaving group. This leaving group can be in the form of hydroxyl or amine groups, providing that they have suffiently low pKa. This reaction is therefore typically restricted to the release of aromatic hydroxy groups[173–176] and heteroaromatic amines.[171,187,188] When amines or alcohols with high pKa released (such as alkyl amines or alcohols) then carbamates[171,178–182] or carbonates[177] are employed respectively. After addition of the Pd^0 complex to a propargyl carbamate or carbonate, a carboxylate anion is the leaving group which can then decarboxylate to release the desired amine or alcohol. The release of a gas provides a large entropic driving force for the reaction. The fate of the palladium allenyl species is then unclear. It has been suggested that it is hydrolysed, but the evidence for this relies of LC-MS detection of hydroxyacetone (**Scheme 10**).[189] A catalytic cycle of Pd^{IV} has been suggested,[175,180] however there is little evidence to support this at room temperature.[189–192] Palladium mediated reactions that have Pd^{IV} intermediates often require high temperature, strong oxidizing reagents or facile oxidative addition to aryl iodides.[193]

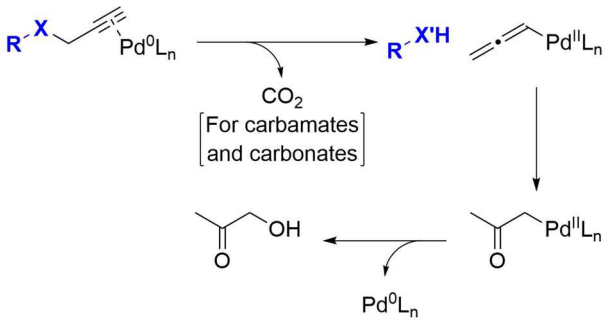

Scheme 10: Palladium mediated decaging of propargyl ethers, amines, carbonates and carbamates.

Metal mediated bioorthogonal decaging reactions have been applied to the delivery of many different prodrugs (**Table 10**). These reactions have employed complexes of ruthenium and palladium, as well as nanoparticles of palladium[182] and gold.[183] Key to all of these reactions is that the metal complexes and nanoparticles can achieve reactive concentrations while being minimally toxic to the organism of

study. The most widely used and studied system is that of palladium mediated decaging, having been used with the most diverse group of prodrugs and applied *in vivo*.[182] Palladium complexes have also been shown to be cell-penetrant and not cause formation of reactive-oxygen species in mammalian cells.[180]

Table 10: Examples of metal mediated decaging reactions for drug delivery.

Transition Metal	Reaction	Released Drug
Ruthenium	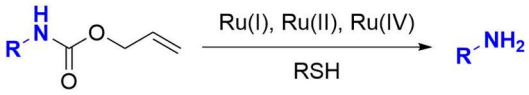	Doxorubicin (**Dox**)[170]
Palladium	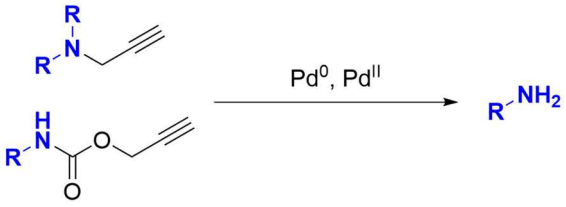	5-Fluorouracil (**5-FU**)[171,187] Gemcitabine[188] Vorinostat[194] Floxuridine[195] Doxorubicin (**Dox**)[182]
Gold	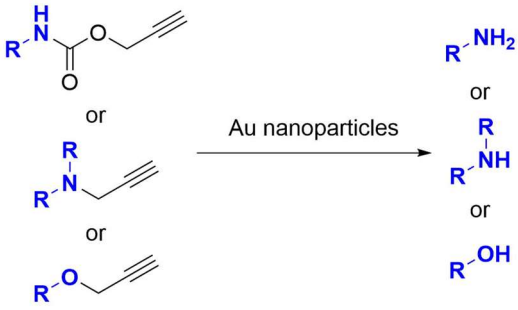	5-Fluorouracil (**5-FU**) Doxorubicin (**Dox**) Vorinostat[183]

2.5 Decaging of Bifunctional Linkers

While bioorthogonal caging groups have been used extensively to protect small molecules and functional groups of proteins, reports of bioorthogonally cleavable bifunctional linkers have been limited. In these cases, two molecules-of-interest have been ligated in such a way that they can be cleaved from one another with a bioorthogonal reaction. This has been most notably used in targeted drug delivery using bioorthogonally cleavable ADCs, whereby an antibody is ligated to a drug *via* a bioorthogonally cleavable linker.[137,153,196–198] After the antibody has targeted cancerous cells, a

bioorthogonal reaction can be used to release the drug payload. In an early example, an antibody drug conjugate was synthesised bearing an anti-transferrin antibody ligated to a toxic ribosome inactivating protein (PAP-S[1]) *via* a UV-cleavable *o*-nitrobenzyl linker. The ADC was shown to be non-toxic until UV irradiation caused release of its payload in mammalian cells (**Scheme 11**).[196]

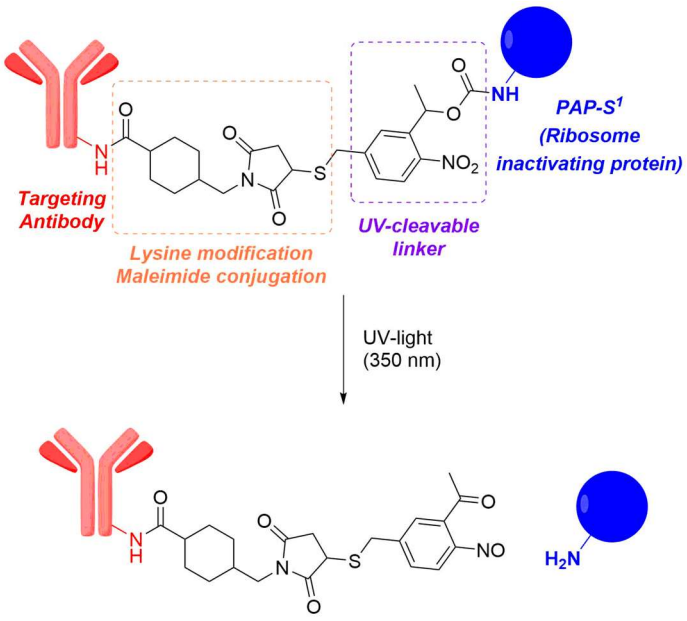

Scheme 11: UV photorelease of a toxic payload from an anti-transferrin, *o*-nitrobenzyl linked ADC.

In another example, tetrazine/TCO-OH decaging was adapted so that the TCO-OH moiety could act as a bifunctional linker. Attachment *via* the alcohol allowed a tetrazine-cleavable carbamate to be installed, and attachment *via* an activated succinimidyl ester allowed antibody conjugation (**Scheme 12**).[153] Despite the conjugation of a hydrophobic drug (doxorubicin) and the TCO linker, the half-life of the ADC was almost identical to the naked antibody. The ADC could reach ~65% decaging in only 2 minutes in PBS, and ~25% in mouse serum after the same time. It was shown that tetrazine-cleavable ADCs would accumulate at a tumour xenograft in mice and that they would react with a radiolabelled tetrazine. If a non-radioactive tetrazine was infused first into the xenografted mice, TCO sites would be consumed and therefore radiolabelled tetrazine did not react with the ADC afterwards. It was however not shown that effective drug release was possible in tumour xenografts from a tetrazine-cleavable ADC, nor that a clinically meaningful tumour shrinkage or increased survival of the mice was possible. The linker for this ADC also required a challenging 11-step synthesis, which requires specialised equipment for UV-irradiation in flow.[153] It also thus far only allows non-selective lysine conjugation which is undesirable in the development of ADCs. These factors limit its applicability for use in other systems.

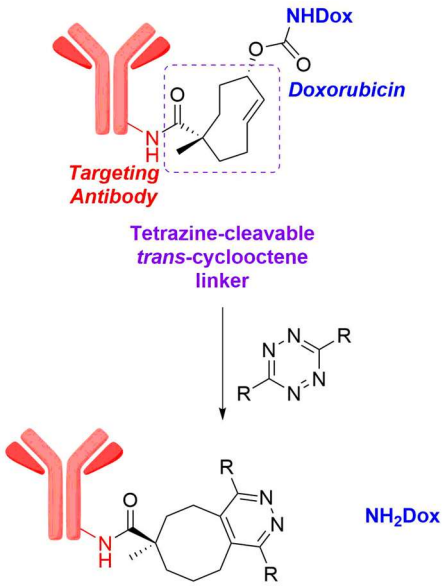

Scheme 12: Tetrazine mediated release of a drug payload from a TCO linked anti-TAG72 ADC.

In another example, a near-IR cleavable cyanine caging group was adapted for conjugation to an antibody (**Scheme 13**).[135,137] The ADC was shown by the inherent fluorescence of the cyanine group to accumulate in tumour xenografts in mice. Upon irradiation with near-IR light, the mechanism that causes drug release also causes decay of the cyanine. Decrease in cyanine fluorescence was shown, however release of the drug in mice, tumour shrinkage or increased mouse survival were not shown. In a second generation ADC, the linker was adapted with a more potent duocarmycin payload and tumour shrinkage and increased survival of the mice could be shown.[197] However the tumours did not shrink to the point of remission. As an adjuvant therapy, the near-IR cleavable ADCs were later combined with antibodies ligated to photosensitizers.[198] These sensitizers absorb near-IR wavelengths of light and cause formation of reactive-oxygen species which can kill tumours. With this combination therapy the tumour shrinkage was far greater and the survival of the mice was significantly longer.

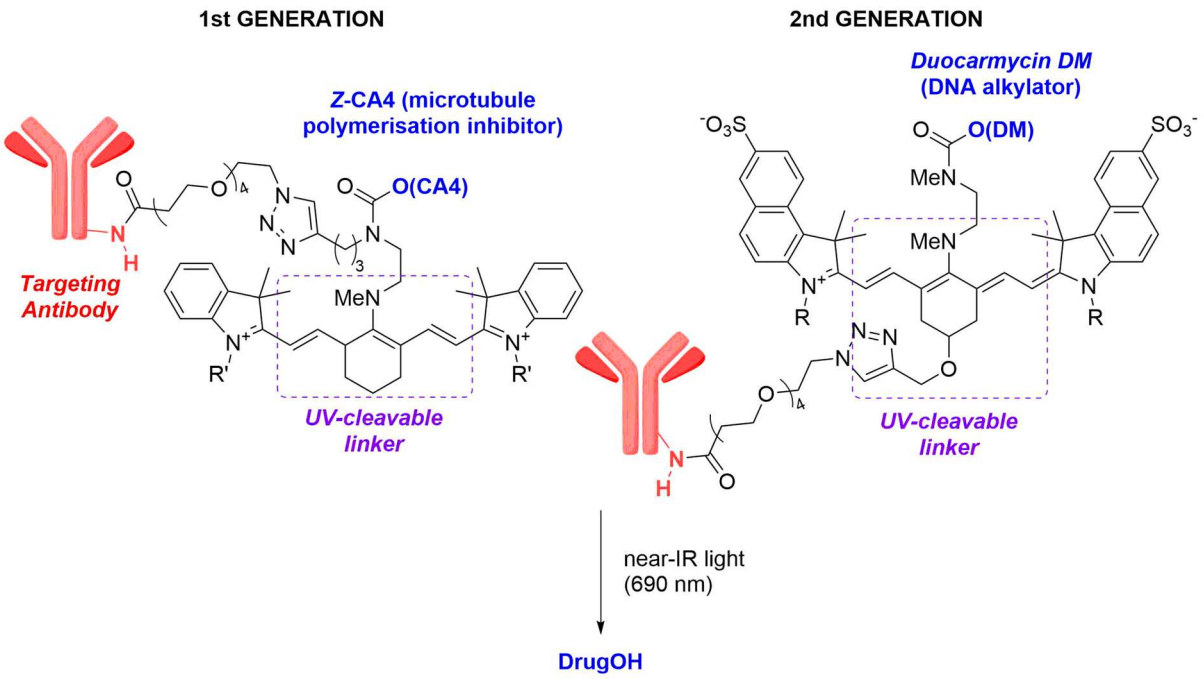

Scheme 13: Near-IR mediated release of a drug payload from a cyanine linked ADC.

Despite the success of palladium mediated decaging reactions in the activation of prodrugs and intracellular protein targets, these reactions have never been adapted to allow drug release from an ADC. However, palladium-cleavable bifunctional linkers have been developed for target pull-down assays (**Scheme 14**).[186] These linkers were used to conjugate kinase inhibitor **BIRB796** to a HaloTag ligand. Once the kinase inhibitor had bound to its targets in cell lysates, the HaloTag ligand was reacted with the HaloTag protein[199] immobilised on magnetic beads. The magnetic beads were then be separated from the cell lysates, and palladium complexes used to cleave the linker. Mass spectrometry could then identify all the proteins in solution, which are the targets of kinase inhibitor **BIRB796**.

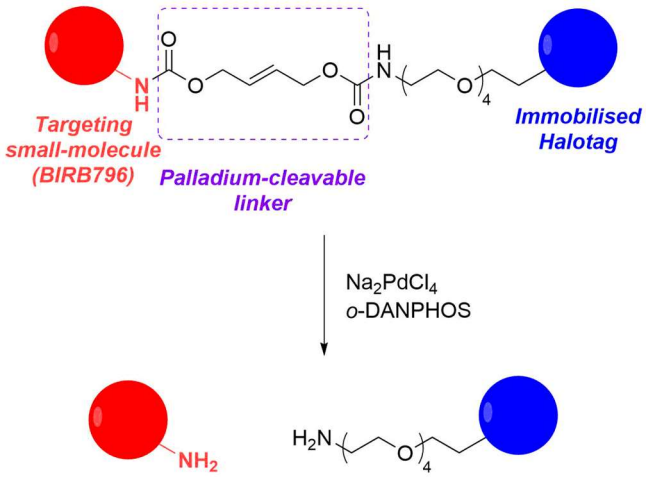

Scheme 14: Palladium mediated release of a drug payload from an allyl carbamate-linked drug-Halotag conjugate for deconvolution of protein targets.

2.6 Conclusion

Bioorthogonal decaging reactions have enabled key insights into biological systems that were previously impossible such as the functions of individual amino acids on proteins and the activation of prodrugs. The use of bifunctional linkers with bioorthogonal cleavage mechanisms however remain scarce. As palladium mediated decaging has shown great promise in chemical biology for prodrug activation and the intracellular activation of proteins, it seems a perfect candidate for the development of bifunctional, bioorthogonally cleavable linkers for the release of bioactive payloads from proteins. These could be used for the study of targeted drug delivery systems.

Chapter 3:

Palladium Mediated Drug Release

3.1 *Aims of the Project*

The purpose of this project was to develop a new linker which would allow bioorthogonal drug or fluorophore release. The linker was designed to be bifunctional, containing a bioorthogonally cleavable site, and contain a handle for facile site-selective cysteine bioconjugation (**Figure 5b**). This could allow bioorthogonally triggered, targeted drug delivery and could be a useful tool for chemical biology. Currently such reactions have been reported for UV decaging,[200] *trans*-cyclooctene-tetrazine decaging[150,153] and near-IR decaging.[137] Palladium mediated decaging has been demonstrated in the literature to be versatile and robust, having found applications in the release of small molecules,[175,180,182,187,188,194,195] proteins,[180,184] (**Figure 5a**) and in target identification.[186] It was hypothesised that palladium mediated decaging would allow for more structurally simple linkers without the need for complex syntheses or equipment to carry out targeted drug delivery experiments.

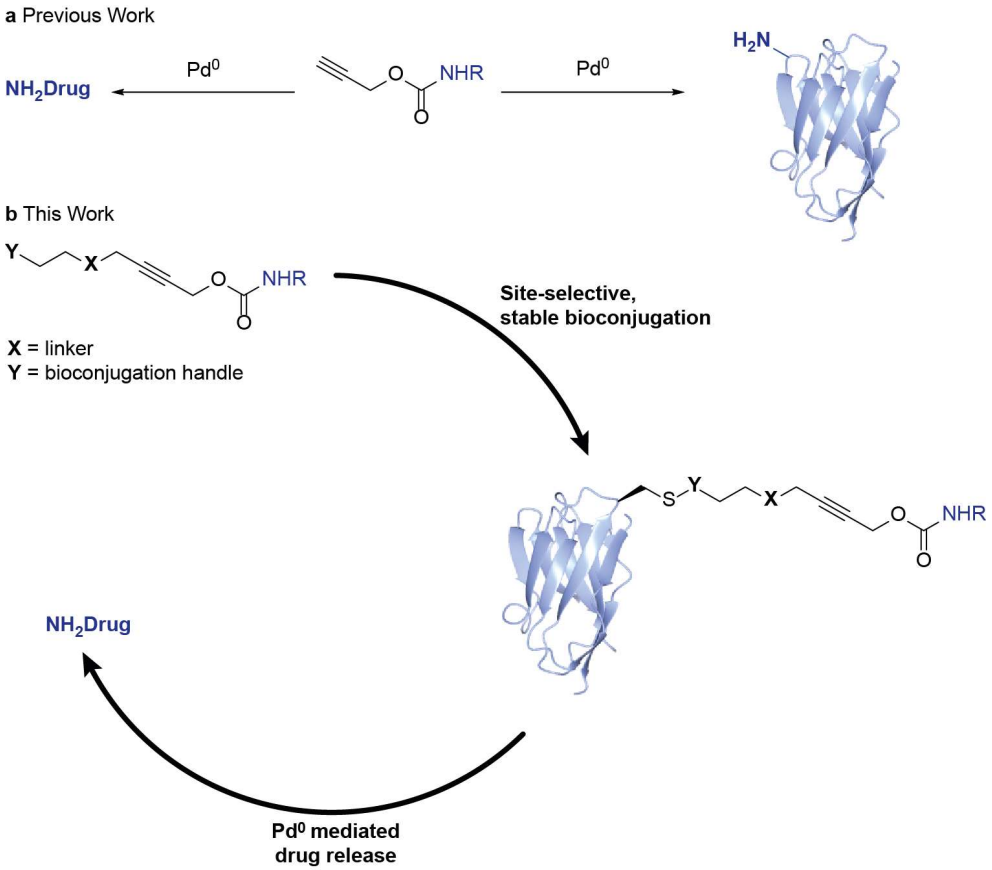

Figure 5: a) Previous work on palladium mediated propargyl carbamate decaging has allowed the release of amine-containing small molecules, or the release of lysines on proteins. **b)** Illustration of palladium mediated decaging of bifunctional linkers for targeted payload delivery.

3.2 Results and Discussion

The most obvious approach would be taking the literature known terminal propargyl carbamates, and extending *via* the alkyne C-H to later incorporate a bioconjugation handle (**Figure 6**). However simply extending the alkyne with methylene units could lead to steric repulsion about the alkyne and diminish reactivity with palladium complexes. Certain functional groups in proximity to the alkyne may be tolerated or even able to promote reactivity

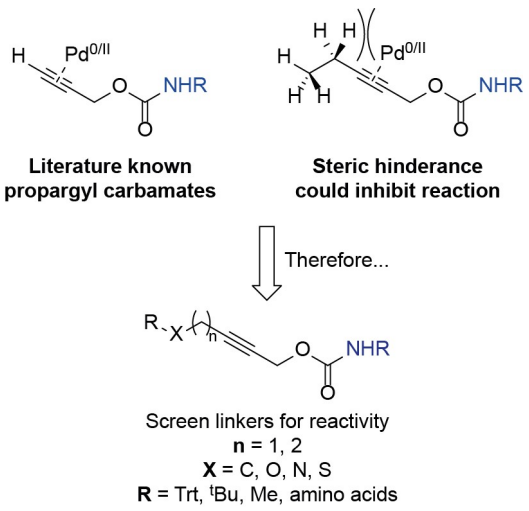

Figure 6: Potential steric inhibition of an alkyne-palladium binding interaction.

In order to test many different carbamates, palladium complexes and conditions, a 96-well plate based format for rapid screening was developed (**Figure 7**). For this, a known decaging procedure of propargyl carbamate protected fluorophore **7** was adapted from the literature.[181] This enabled reactions to be run in triplicate as well as a high throughput of organic compounds and palladium complexes. Terminal propargyl carbamate protected fluorophore **7** was screened against the literature known $allyl_2Pd_2Cl_2$ dimer for decaging. The solvents screened were water miscible, and used both in protein modification and palladium catalysis. Due to the poor water solubility of the 7-amino-4-methylcoumarin fluorophore (**8**) in water, 90% of the solvent had to be organic. The reactions were run in air to ensure air-stability of reagents and at room temperature to be similar to biological systems but not cause excessive evaporation of organic solvents.

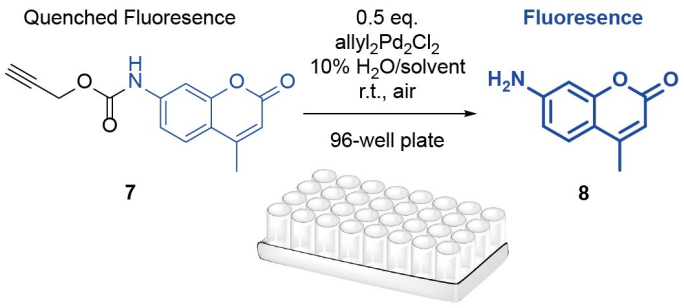

10% H_2O/Solvent	SM is Soluble?	Reaction Progress?	Non-volatile Solvent?
^{i}PrOH, EtOH, MeOH	No	-	-
Dioxane, THF, DME	No	-	-
Acetonitrile	Yes	No	-
DMSO	Yes	No	-
Acetone	Yes	Yes	No
DMF	Yes	Yes	Yes

Figure 7: Solvent screening to establish a high-throughput fluorescence screen for reactivity between the literature known terminal propargyl carbamates and allyl$_2$Pd$_2$Cl$_2$.

Only 10% water was tolerated in these reactions due to the limited aqueous solubility of the coumarin **8**. The fluorophore was also insoluble in the alcohol solvents assayed, as well as the ethers but showed solubility in acetonitrile and DMSO. Unfortunately these solvents did not allow any reaction progress. Some reaction progress was observed in acetone, but acetone was too volatile and not suitable for an open well-plate format over an extended period of time. DMF proved to be the optimum solvent for these reactions and was selected for further fluorescence screening.

The next step was to determine which functional groups would be tolerated in proximity to the alkyne and a range of groups were selected (**Figure 8**). It was found that with 0.5 equivalents of the literature known allyl$_2$Pd$_2$Cl$_2$ (therefore 1 equivalent of palladium), the best reactivity was achieved with a terminal propargyl carbamate. However when increasing to 10 equivalents of allyl$_2$Pd$_2$Cl$_2$, an appended *S*-trityl group **9** gives comparable reactivity. The possibility of sulfur promoting the reaction was exciting as this may facilitate attachment of a cysteine. However, a propargyl carbamate derivative bearing an *N*-Boc protected cysteine methyl ester (**16**) gave no significant reactivity when a range of substituted allyl$_2$Pd$_2$Cl$_2$ were assayed. None of the substituted allyl$_2$Pd$_2$Cl$_2$ derivatives (**17**-**19**) gave increased reactivity when compared to the literature known allyl$_2$Pd$_2$Cl$_2$.

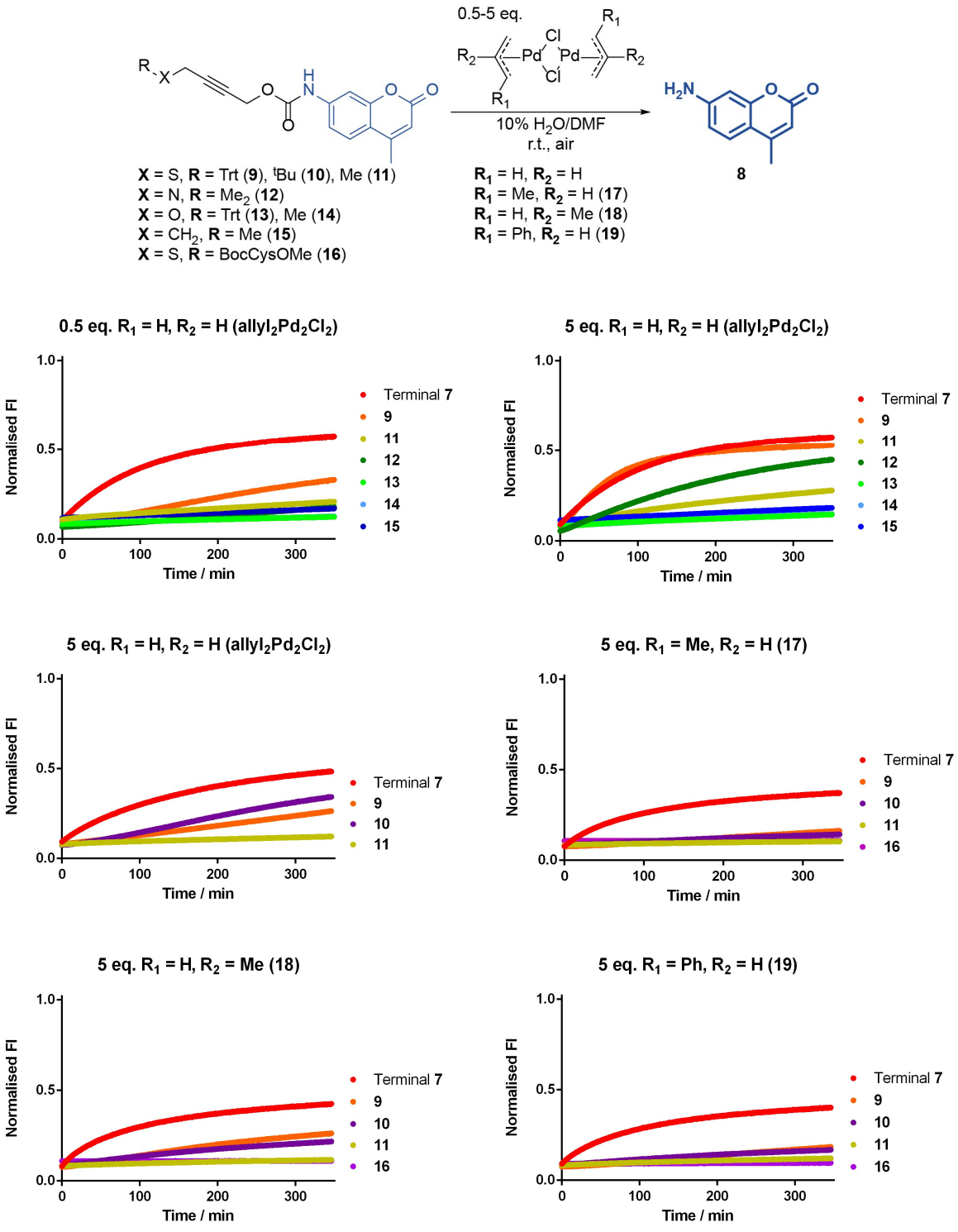

Figure 8: Fluorescence screening of allyl$_2$Pd$_2$Cl$_2$ and substituted analogues to determine functional group tolerance of decaging. 200 µM solutions of caged fluorophore in 10% H_2O/DMF were diluted 1:1 with solutions of palladium complexes at room temperature. Fluorescence intensity (λ_{ex} 352 nm, λ_{em} 415 nm) was normalised to a 100 µM solution of free fluorophore **8** mixed with the appropriate concentration of palladium complex.

Allyl palladium chloride complexes are known to reduce to Pd^0 after attack by nucleophiles (**Scheme 15**).[190] Given the large number of nucleophiles endogenous to biological systems (cysteine thiols, amines) it is likely that $allyl_2Pd_2Cl_2$ is activated this way to react with propargyl carbamates. Therefore, further palladium complexes were sought with similar modes of activation. Complexes of 1,5-cycloctadiene (**COD**) and palladium are known to also have a nucleophilic mode of reduction,[201,202] and $Pd(COD)Cl_2$ was screened against a range of propargyl carbamate derivatives (**Figure 9**). While it did not display considerable reactivity using stoichiometric concentrations, with ten equivalents it showed favourable reactivity and fast reaction kinetics with an *S*-methyl appended derivative **11**. Oddly, it showed very little reactivity with the literature known terminal propargyl carbamate **7**. The complex was then trialled against cysteine-containing propargyl carbamates as it was thought this could serve as a conjugation site to proteins. Reactivity was favourable against compounds bearing an *N*-Boc protected cysteine methyl ester **16** and *N*-Boc acetyl cysteine methyl ester derivatives **20**, showing the flexibility of tolerated groups at this site. Unprotected cysteine methyl ester derivative **21** resulted in complete quenching of reactivity, most likely due to chelation of palladium.

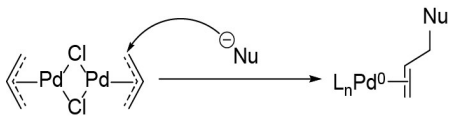

Scheme 15: Nucleophilic mode of reduction of palladium allyl complexes.

As palladium is thiophilic, it seems likely that the explanation of this reactivity is a binding interaction between palladium and the thioether. If **COD** does serve as a reducing agent for the palladium however, the thioether would need to displace a chloride, leaving a complex with an overall positive charge which may not be favourable. A second complex, Pd(COD)MeCl, was trialled as a methyl ligand would be expected to be much less labile than a chloride. If the complex shows diminished reactivity, it may be evidence of a binding interaction *via* the displacement of chlorides. In fact, this complex did exhibit diminished reactivity for all thioether bearing propargyl carbamates but strangely increased reactivity for the terminal propargyl carbamate **7**. This may be because the methyl group offers a reductive elimination mediated palladium reduction mechanism (to release methyl chloride) which is however less efficient than reduction by nucleophilic attack on **COD**. To investigate the effects of strain on the ligands of palladium, norbornadiene (**NBD**) was assayed in complex $Pd(NBD)Cl_2$. The overall decaging conversion for cysteine appended derivatives **16** and **20** was diminished for $Pd(COD)Cl_2$ and $Pd(NBD)Cl_2$, and the rate of decaging was much lower. The steric constraints of **NBD** could lead to a slower nucleophilic addition step or slower β-hydride migration step.

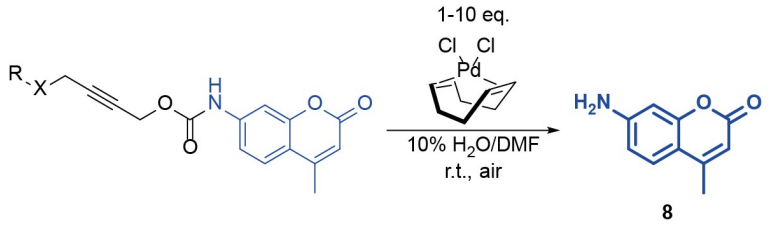

X = S, **R** = Trt (**9**), ^{t}Bu (**10**), Me (**11**)
X = N, **R** = Me_2 (**12**)
X = O, **R** = Trt (**13**), Me (**14**)
X = CH_2, **R** = Me (**15**)
X = S, **R** = BocCysOMe (**16**), AcCysOMe (**20**), CysOMe (**21**)

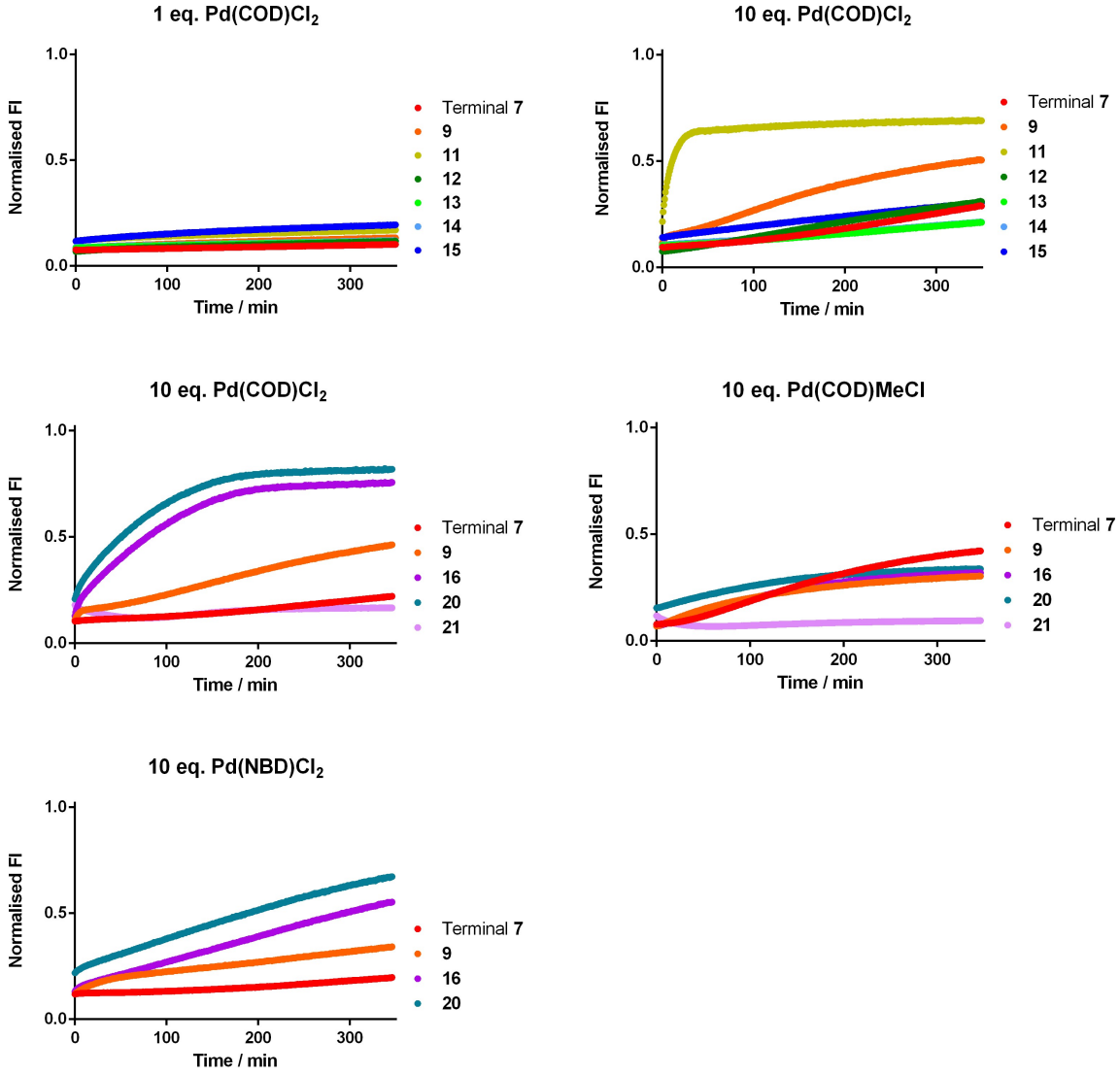

Figure 9: Fluorescence screening with $Pd(COD)Cl_2$, Pd(COD)MeCl and $Pd(NBD)Cl_2$.

Further evidence of a binding interaction is provided by the fact that insertion of an extra methylene between thioether and alkyne still allows reactivity (**Figure 10**). Greatest results for allyl$_2$Pd$_2$Cl$_2$ are still provided by the *S*-trityl derivative **9**. With the addition of an extra methylene spacer, reactivity is slightly diminished. In the case of Pd(COD)Cl$_2$, *S*-methyl derivative **11** still shows the best conversion, and an extra methylene spacer again does not significantly inhibit the reaction.

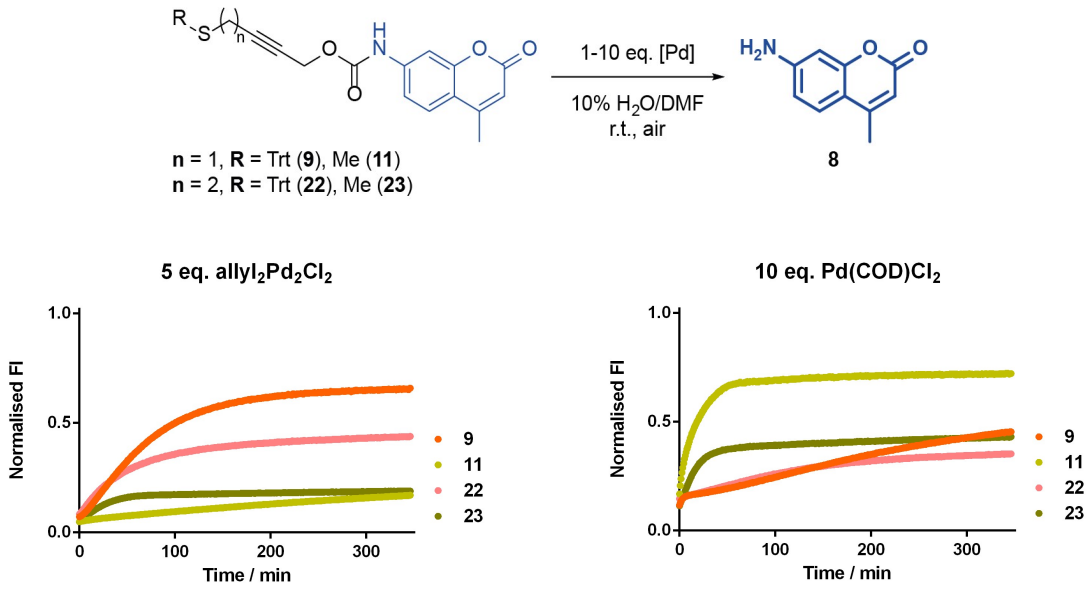

Figure 10: Fluorescence screening to determine effect of extra methylene insertion between thioether and alkyne.

It is clear that thioethers offer the best reactivity for extending the alkyne into a bifunctional linker. With allyl ligands on palladium however, this requires large, bulky groups on the thioether which limits the possibilities of further modification. A group such as trityl would render any linker much less water soluble. With a **COD** ligand on palladium only small groups such as methyl are required on the thioether, and this allowed for further functionalisation of this group – for example with cysteines (**16** and **20**). This shows the flexibility of possible modifications at this site and therefore the methyl thioether **11**-Pd(COD)Cl$_2$ reaction partners were selected for additional study and development. A summary of reactivity data is shown in **Figure 11**.

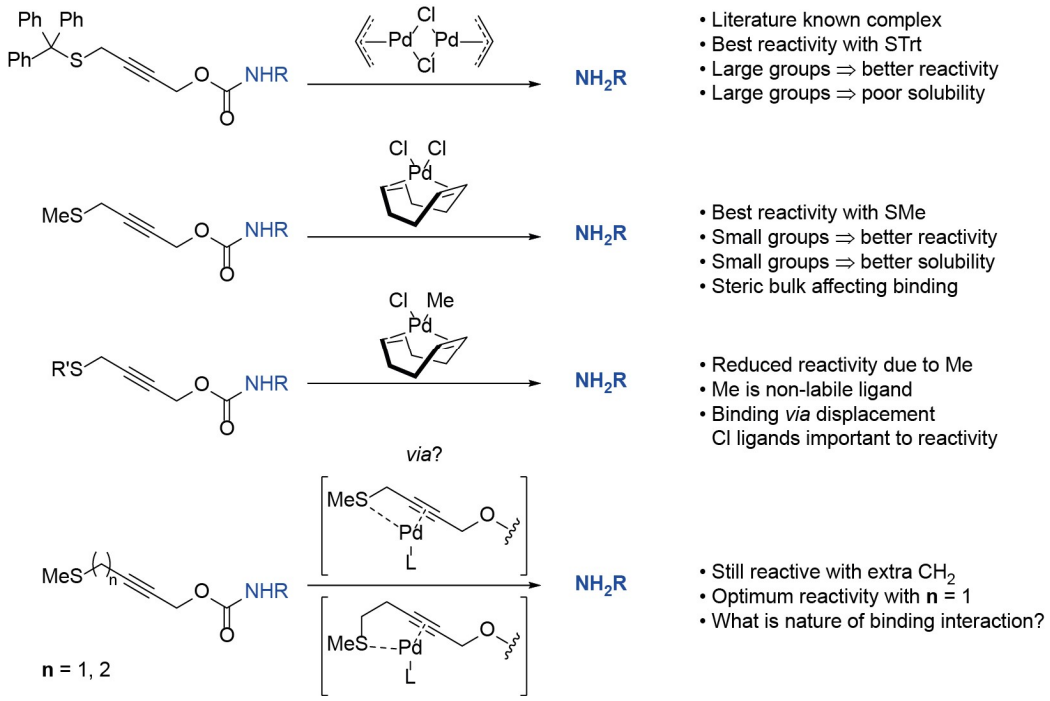

Figure 11: Summary of mechanistic data from fluorescence screening.

In order to seek further confirmation of a thioether mediated binding mechanism, a truncated propargyl thioether **24** was studied by ^{1}H NMR (**Figure 12**). A stoichiometric amount of Pd(COD)Cl_2 was added to propargyl thioether **24**, and only signals from the thioether were observed to shift completely after 10 minutes at room temperature. The alcohol protons were unshifted. This is evidence that the binding is mediated by the alkyne and thioether of these compounds, but not the precise nature of the complexes. In the mixture, there is an approximately 1:1 ratio of free **COD** to Pd(COD)Cl_2 – or peaks with the same chemical shifts – with some minor signals likely from palladium **COD** complexes with displaced chlorides around 3.5-4 ppm. When substituting the thioether for ether **25**, no shifts in signals were observed in either Pd(COD)Cl_2 or the propargyl ether **25**.

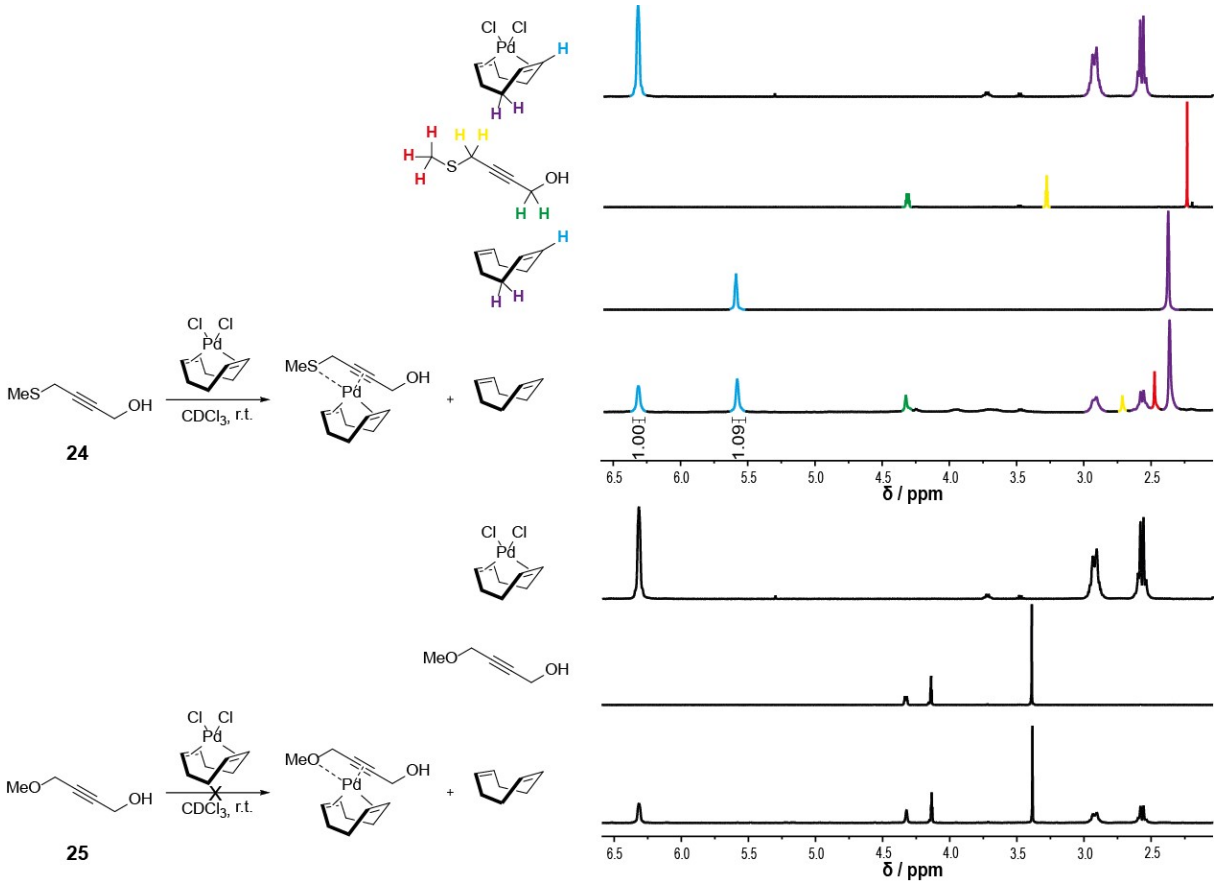

Figure 12: ^{1}H NMR binding experiment of propargyl thioether **24** and propargyl ether **25** with Pd(COD)Cl_2.

A 1:1 ratio of **COD** to Pd(COD)Cl_2 would be consistent with a binding mode of two propargyl thioethers (**24**) per palladium. However, this would not be consistent with a reactive intermediate as there would be no mechanism to reduce Pd^{II} to Pd^{0}. It could however be that the reaction goes *via* minor complexes in solution and that the major complexes are unreactive (**Figure 13**).

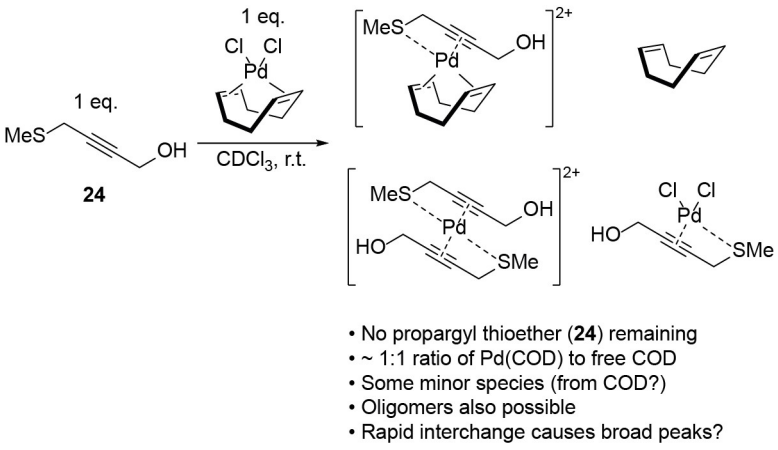

Figure 13: Potential binding modes of Pd(COD)Cl_2 with propargyl thioether **24**.

Based on literature known reactions of palladium **COD** complexes[201,202] a mechanism was devised whereby palladium can bind to the linker between thioether and alkyne. When **COD** is also bound to palladium, **COD** is activated to nucleophilic attack by the electron withdrawing effect of the thioether – enabling nucleophilic attack of water in the fluorescence screen. Evidence that this is not occurring without thioether binding is that $Pd(COD)Cl_2$ does not react with terminal propargyl carbamate **7**. If $Pd(COD)Cl_2$ could be reduced by any other means in solution the Pd^0 species could then go on to react with the terminal propargyl carbamate **7**. After nucleophilic attack of water on **COD**, the alkyl palladium species **27** could then undergo β-hydride migration with a proximal hydrogen from the **COD**-derived ligand. The palladium hydride intermediate could then undergo reductive elimination to give a Pd^0 species. Pd^0 can then nucleophilically add to the propargyl carbamate as per the standard Tsuji-Trost reaction mechanism.[190] A mechanistic proposal is shown in **Scheme 16**. The fate of the palladium allenyl species is then unclear. It has been postulated in the literature that it undergoes hydrolysis to regenerate Pd^0 and hydroxyacetone, but the evidence of this mechanism relies on LC-MS detection of hydroxyacetone.[189] As hydroxyacetone has a high volatility and low mass, it makes it a challenging compound to detect by LC-MS and distinguish from fragments of larger organic compounds.

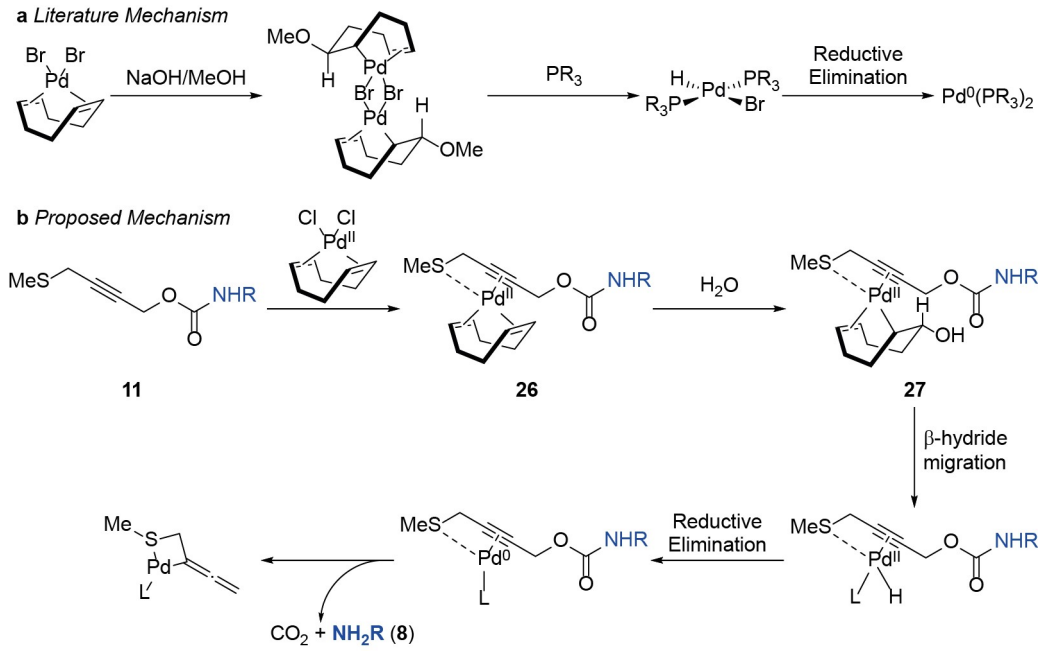

Scheme 16: Mechanistic proposal of $Pd(COD)Cl_2$ mediated decaging of propargyl carbamates. **a)** Literature known mechanism of reduction of $Pd(COD)Br_2$.[201,202] **b)** Proposed mechanism of propargyl carbamate decaging with $Pd(COD)Cl_2$ (charges omitted for clarity).

To verify this mechanism and that the reaction does not go *via* non-specific Pd^{II} mediated hydrolysis, propargyl carbamates were tested against $Pd(OAc)_2$, $Zn(OAc)_2$ and $Cu(OAc)_2$ (**Figure 14**). All compounds tested showed no reactivity with these complexes. Metal acetates were selected as organic soluble

sources of M^{II} where the ligands are generally inert. Pd^{II} is likely still binding to the linker *via* the thioether and alkyne, but no reaction is occurring. This should mean that **COD** is responsible for the reactivity and that any reactive intermediate should involve a bound Pd^{II} ion as well as **COD**.

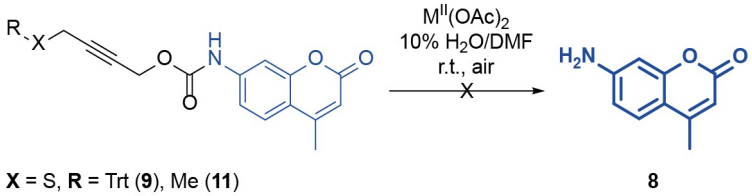

X = S, **R** = Trt (**9**), Me (**11**) **8**

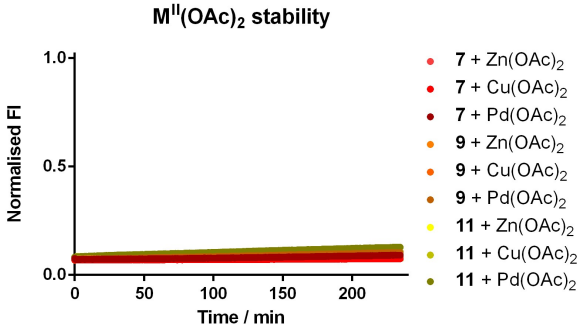

Figure 14: Stability of propargyl carbamates to Pd^{II}, Zn^{II} and Cu^{II} acetate.

As reaction with $Pd(COD)Cl_2$ allows variability of groups that can be attached to the thioether, this complex was chosen to further develop a palladium cleavable linker system. A linker bearing a triethylene glycol thioether was synthesised, as polyethylene glycol (PEG) forms straight chains in water. This would later allow distance between the reactive site of $Pd(COD)Cl_2$ and any functionalities later added to the linker. For example, a protein may interfere with the reaction due to many chelating groups on its surface, and therefore it might be advantageous to have this PEG spacer. A triethylene glycol propargyl carbamate **28** was synthesised and the kinetics of its reaction with $Pd(COD)Cl_2$ studied under pseudo-first order conditions. Reacting with between 10 and 40 equivalents of $Pd(COD)Cl_2$, it was found to have a second order rate constant of 1.136 M^{-1} s^{-1} (**Figure 15**).

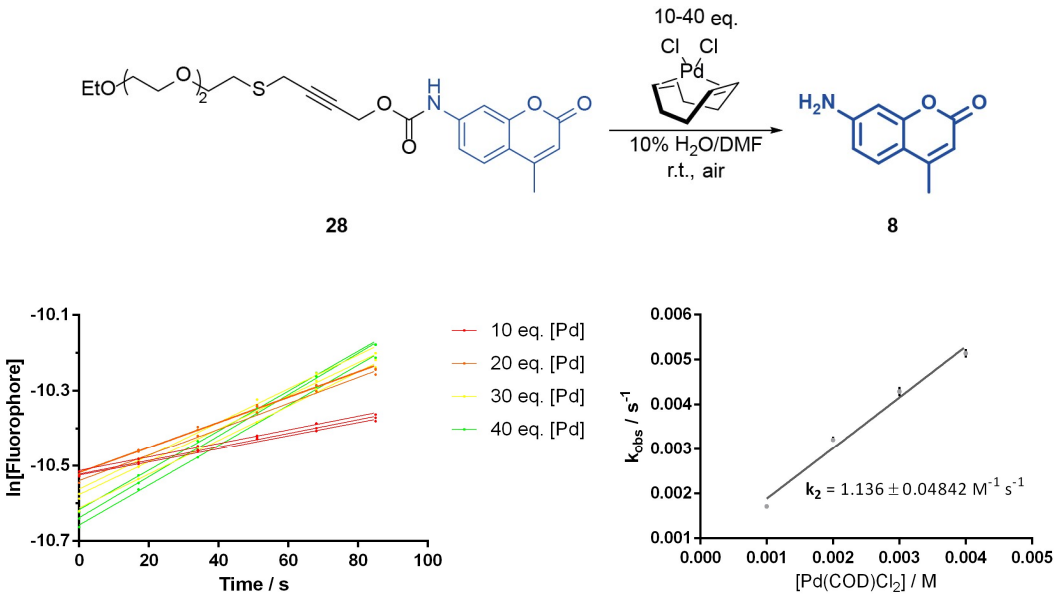

Figure 15: Pseudo-first order kinetics of triethylene glycol propargyl carbamate **28**. 200 µM solutions of caged fluorophore **28** in 10% H_2O/DMF were diluted 1:1 with solutions of palladium complexes at room temperature. Fluorescence intensity (λ_{ex} 352 nm, λ_{em} 415 nm) was normalised to a 100 µM solution of free fluorophore **8** mixed with the appropriate concentration of $Pd(COD)Cl_2$. Concentration of the fluorophore [Fluorophore] was assumed as Normalised FI multiplied by 100 µM fluorophore **8.**

While this rate constant is modest, it is compatible with chemical biology applications and drug release. Following the second order half-life equation, $t_{½} = 1/k[C]_0$, where $[C]_0$ is the initial concentration of reagents (assuming both reagents are at the same concentration) this gives a half-life of approximately 1 day at 10 µM concentrations. Following the first order half-life equation $t_{½} = \ln(2)/k_1 = \ln(2)/(k_2 \cdot [Pd])$ this gives a half-life of approximately 0.7 d at 10 µM concentrations of $Pd(COD)Cl_2$. Of course, only limited comparisons can be drawn between a rate constant determined in mostly organic solvent to the rate of the same reaction in cell culture, but this offers an approximation. Interestingly, when increasing the amount of $Pd(COD)Cl_2$ beyond 40 equivalents, the observed rate constant starts to decrease. This is likely due to $Pd(COD)Cl_2$ reaching such a high concentration that it starts to precipitate or form aggregates (**Figure 16**). The large error could also be significant in that the aggregation is not uniform across all replicates.

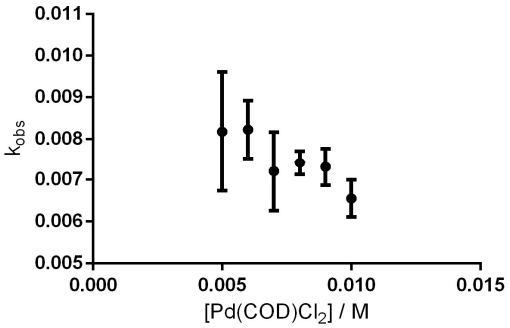

Figure 16: Decaging of triethylene glycol modified propargyl carbamate under pseudo-first order with 50-100 eq. $Pd(COD)Cl_2$.

The pegylated propargyl carbamate of **28** seeming like a good choice of linker, a pegylated doxorubicin prodrug **cDox** (**35**) was synthesised (**Scheme 17**) to verify whether this decaging could function in cell culture. This was achieved in 5 steps from commercially available triethylene glycol monoethyl ether **29**. A monoprotected short PEG **29** was selected as a starting point as the polarity of PEG compounds makes them very challenging to purify. A shorter PEG is easier to purify, and as it is already monoprotected with an ethyl group, this reduces the number of by-products to purify after tosylation to give tosylate **30** in 90% yield. The tosylate **30** could then be displaced by potassium thioacetate to give the thioester protected thiol **31** in 86% yield. Deprotection with sodium methoxide in methanol afforded the thiol which was reacted *in situ* with propargyl chloride **32** to give propargyl thioether **33** in 73% yield over two steps. After reaction with *p*-nitrophenyl chloroformate, an activated carbonate **34** could be isolated in 59% yield. In a final step, doxorubicin hydrochloride could be reacted with activated carbonate **34** to give the target doxorubicin prodrug **cDox** (**35**) in 76% yield. Doxorubicin was selected as a suitable drug, as it is clinically used to treat cancer and bears the required reactive amine in order to convert it to a propargyl carbamate prodrug. Doxorubicin exerts its anti-cancer effects by intercalating with and binding to the rapidly dividing DNA of cancer cells. Its amine is positively charged and forms strong interactions with the negatively charged DNA phosphate backbone (**Scheme 17**). When the amine is protected as a carbamate, the positive charge is lost which leads to a loss in potency.

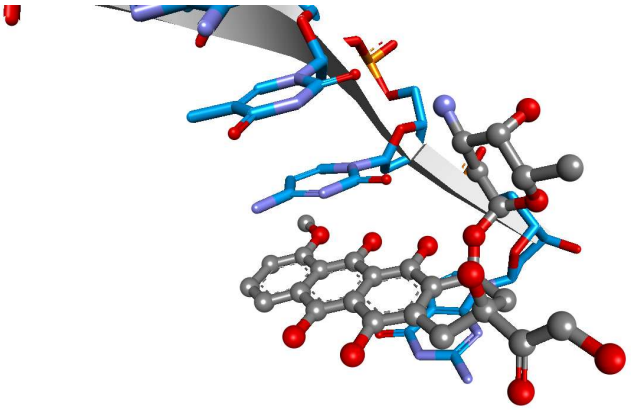

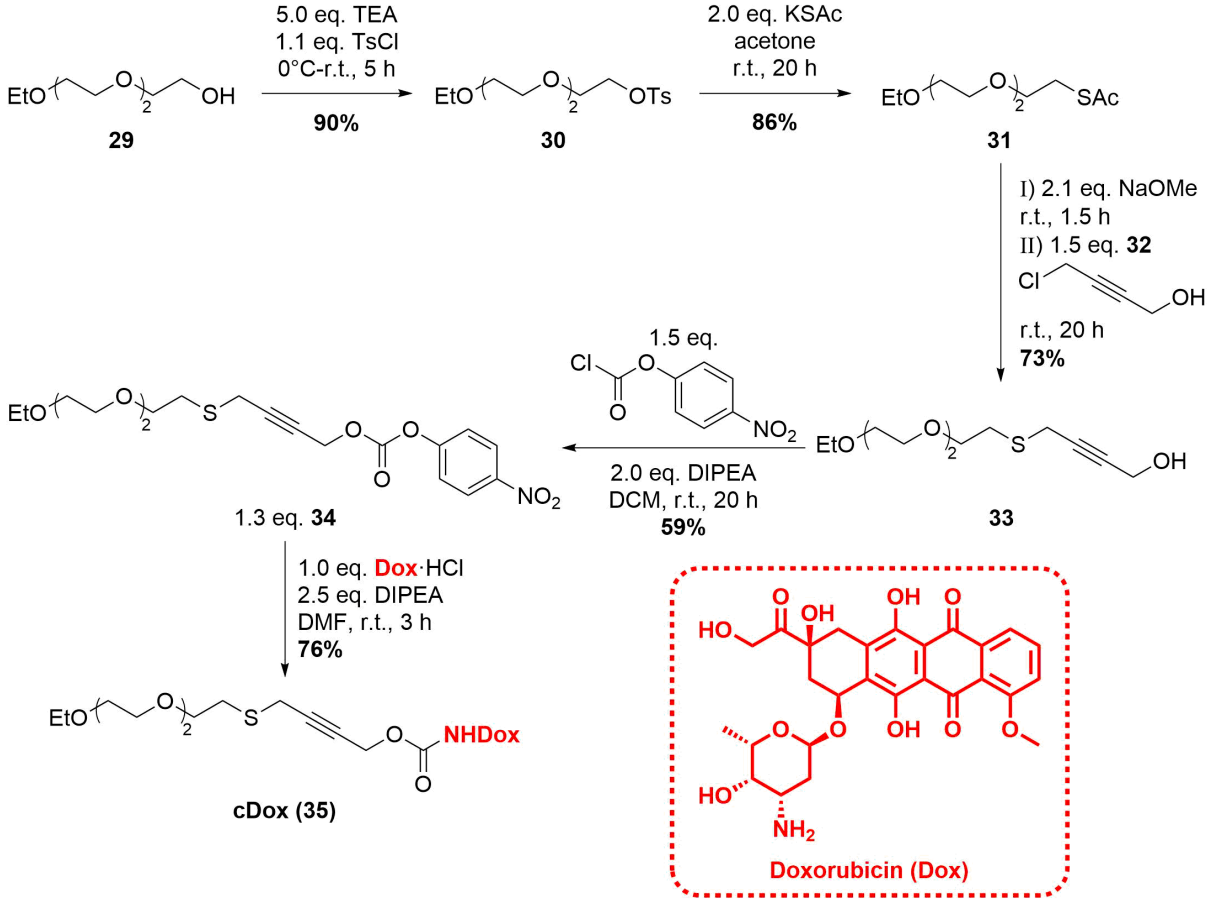

Scheme 17: Crystal structure of doxorubicin in complex with DNA from PDB 1D12[203] and synthesis of PEGylated doxorubicin prodrug **cDox** (**35**). Doxorubcin causes cancer cell death by intercalating its rapidly dividing DNA thereby inhibiting DNA replication. The strong ionic interation between doxorubicin ammonium and DNA backbone phosphate is disrupted when the amine is protected as a carbamate.

With doxorubicin prodrug **cDox** (**35**) in hand, the decaging reaction could be trialled in cell culture. **cDox** (**35**) was found to be significantly less toxic than doxorubicin at the same concentrations. This is

likely due to impaired cell membrane penetration due to the loss of an overall positive charge, and the ammonium of doxorubicin forms a key interaction with the negatively charged DNA phosphate backbone[203] which would be lost in **cDox** (**35**). Given the large number of nucleophiles endogenous to biological systems, $Pd(COD)Cl_2$ is not likely to be very stable. For this reason, it was decided to add $Pd(COD)Cl_2$ daily in order to push the reaction further towards completion. To serve as a control, water soluble palladium salt Na_2PdCl_4 was also trialled at the same concentrations. At 48, 72 and 96 h $Pd(COD)Cl_2$ was found to be more effective than Na_2PdCl_4 (**Figure 17**). This shows that either $Pd(COD)Cl_2$ is more stable or more reactive than Na_2PdCl_4.

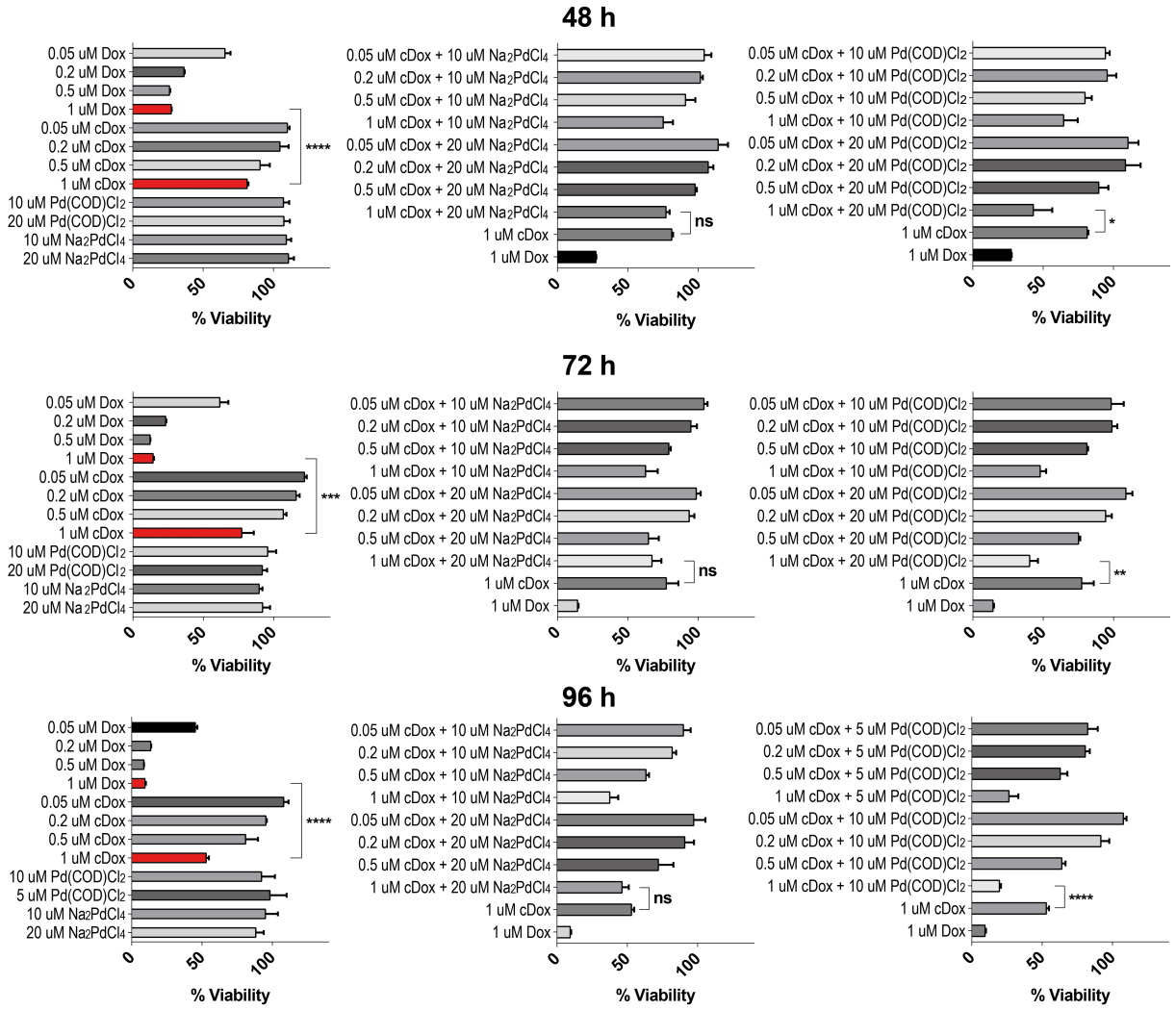

Figure 17: Cell viability studies with doxorubicin prodrug **cDox** (**35**) in HEK cells. Cell viability was determined by AlamarBlue assay, in which viability is directly proportional to the ability of cells to reduce non-fluorescent resazurin to fluorescent resorfurin. Treated cells were normalised to cells cultured with an equal concentration of DMSO which were assumed to be 100% viable. Statistical significance was determined with a two-tailed unpaired t-test. ****p = < 0.0001. ***p = 0.0002. **p = 0.0035. * p = 0.0318. ns = non-significant.

As expected, the effectiveness of the drug release increases with the concentration of reagents. Interestingly, Na_2PdCl_4 still showed some efficacy in the reaction despite the fact $Pd(OAc)_2$ showed no activity in the fluorescence screen (**Figure 14**). Both are sources of Pd^{II} without ligands capable of reducing the metal centre. The reason Na_2PdCl_4 shows efficacy is likely due to the abundance of reducing agents in cell media, for example ascorbic acid. In another study, it was shown that ascorbic acid can increase the rate of palladium decaging *in vitro*.[180] The largest turn-on of toxicity is at 96 h with 10 μM $Pd(COD)Cl_2$ per day. The reason is likely that longer timepoints allow the reaction to progress further, and the released doxorubicin has a longer period in which to exert its toxicity – note that the free doxorubicin becomes more toxic as the incubation time increases. The optimal

concentrations for this decaging in cell culture are presented in **Figure 18**, alongside brightfield microscopy demonstrating the cell killing.

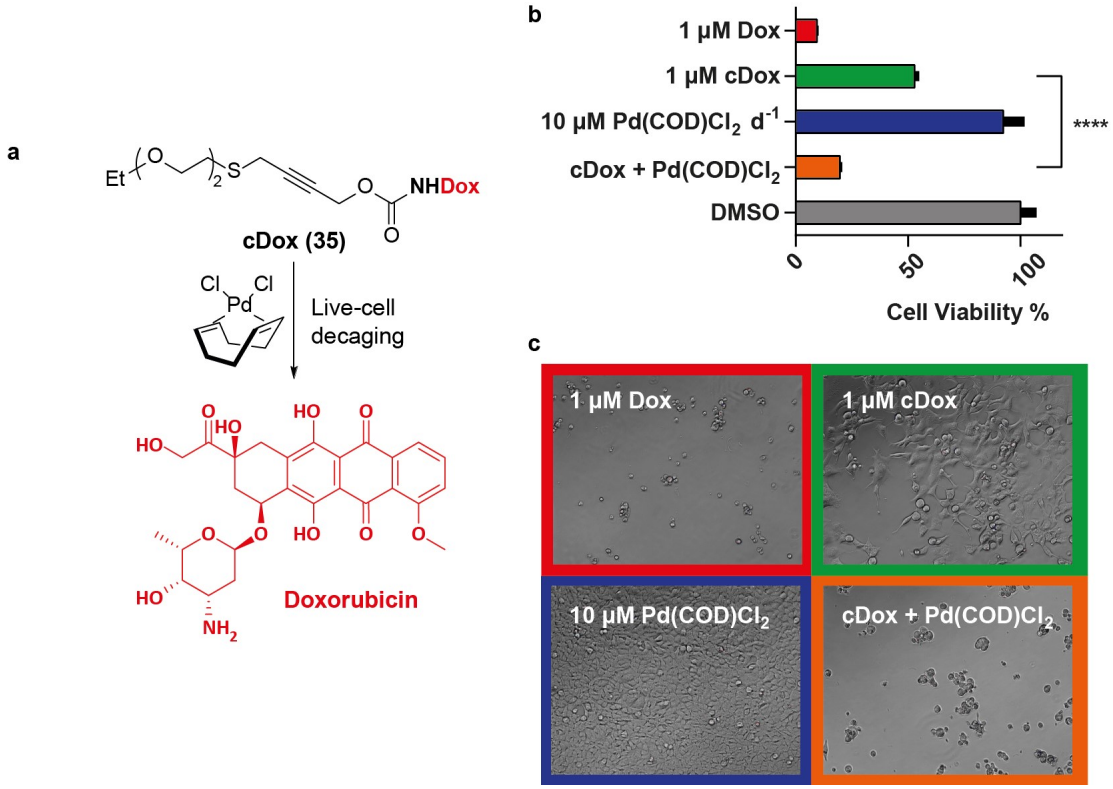

Figure 18: Summary of optimal conditions (96 h) for cellular decaging of doxorubicin prodrug **cDox 35** along with brightfield microscopy of the cells. Statistical significance was determined with a two-tailed unpaired t-test. ****p = < 0.0001.

With evidence that this reaction can work well in cell culture, the linker of **cDox** (**35**) was adapted to contain a cysteine-selective bioconjugation handle previously developed in the group.[204] These acrylamide bioconjugation handles react rapidly and selectively with cysteine – not lysine or any other nucleophilic amino acid – to give a stable bioconjugate. This is a valuable alternative to maleimide cysteine bioconjugation which has been shown to be unstable due to rapid retro-Michael addition. The bioconjugation handle could be introduced in the first step of the synthesis, and doxorubicin in the last step. This is important as it could allow a range of payloads to be introduced to the molecule rapidly in the final step. In this case, doxorubicin was selected as a payload for facile comparison with **cDox** (**35**).

To demonstrate release of a payload from a protein-drug conjugate, a protein with a single reactive cysteine, 2Rb17c, was selected. 2Rb17c is a nanobody which is targeted to the HER2 receptor[205] – the same target as commercially available ADC trastuzumab emtansine. HER2 is overexpressed in certain breast cancers and is known to rapidly internalise upon binding of an antibody.[62,206,207] The cysteine of

2Rb17c is protected as a disulfide with **GSH** or cysteine in the stock solution, so 50 equivalents of tris(2-carboxyethyl)phosphine hydrochloride (**TCEP**) were added to reduce any disulfide bonds. Following this, 50 equivalents of doxorubicin-acrylamide **36** were reacted with the free cysteine of nanobody 2Rb17c (**Figure 19a,b**). The conjugate 2Rb17c-**36** could then be decaged with only 10 equivalents of $Pd(COD)Cl_2$ in 2 h at 37 °C (**Figure 19a,c**). As proteins contain many metal chelating functional groups (amines, thiols, acids etc.), a palladium scavenger is required to ensure that metals are not bound to the protein for MS analysis as this would complicate the spectra.[208–210]

The optimum conditions and concentrations from the **cDox** (**35**) decaging study were used to investigate the toxicity of the conjugate 2Rb17c-**36**. The conjugate 2Rb17c-**36** is much more toxic than **cDox** (**35**) likely due to internalisation of 2Rb17c-**36** after binding with HER2 and subsequent lysosomal trafficking and degradation. However, when reacted with $Pd(COD)Cl_2$, the toxicity is doubled to completely recover the toxicity of free doxorubicin (**Figure 19d**). The $Pd(COD)Cl_2$ was added after 2 h to allow localisation of the conjugate on the HER2 positive cell line MCF-7. The number of copies of HER2 per MCF-7 cell is on the order of 10^3. With 5000 cells in 200 µL per well in the experiment, this leads to a concentration of ~10^{-14} M of the HER2 receptor. There is clearly a large excess of the conjugate 2Rb17c-**36** at 10^{-6} M and therefore much of the decaging and toxicity should arise from extracellular decaging. A control experiment should be performed using a non-targeted protein (e.g. a nanobody with a scrambled binding region sequence) to understand if the turn-on of toxicity upon addition of $Pd(COD)Cl_2$ is similar. Another useful control would be to use a HER2 negative cell line such as HeLa, but the varying toxicities of doxorubicin in each cell line would complicate interpretation of the results.

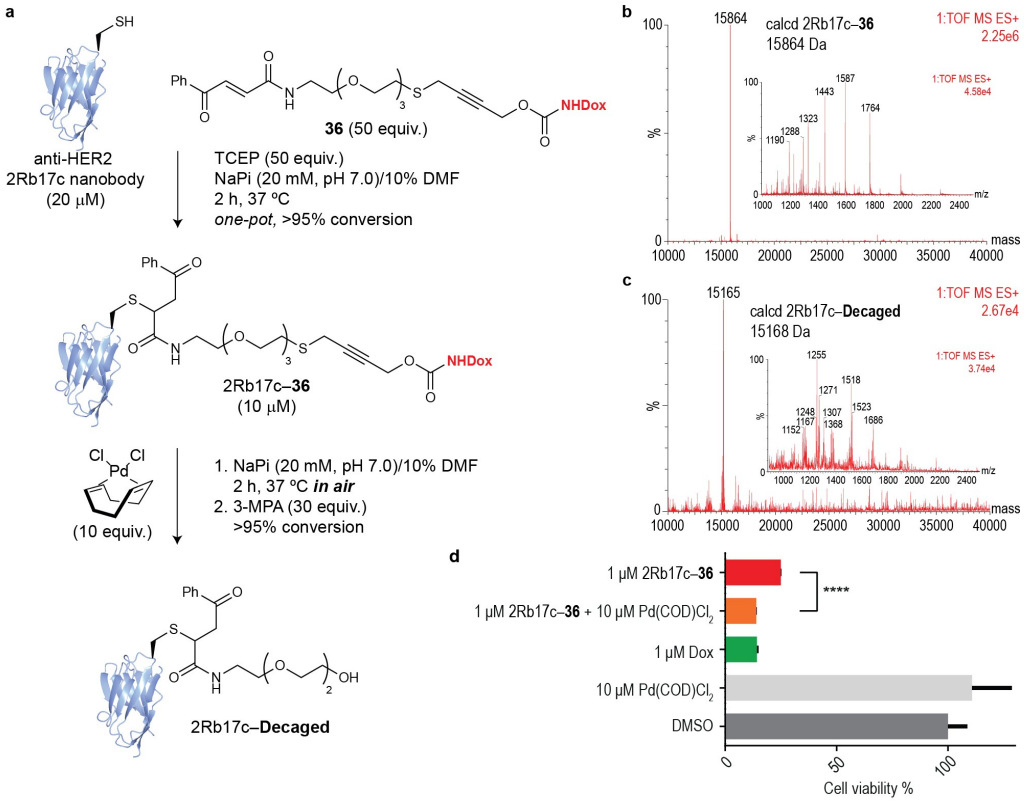

Figure 19: a) Protein bioconjugation and subsequent decaging. Synthesis of protein modification reagent **36** was carried out by Laura Sinatra and the nanobody 2Rb17c kindly provided by the Caveliers group. **b)** MS of modified 2Rb17c-**36**. **c)** MS of decaged 2Rb17c-**36**. **d)** Cell viability of MCF-7 cells after treatment with 2Rb17c-**36** and subsequent decaging. Statistical significance was determined with a two-tailed unpaired t-test. ****p = < 0.0001.

After decaging of the conjugate *in vitro* no remaining starting material 2Rb17c-**36** could be detected by LC-MS, and the major product seemed to result from decaging followed by an elimination or hydrolysis. As this seems to evoke an unexpected mechanism, the conjugate was studied for stability to the palladium scavenger 3-mercaptopropionic acid (**3-MPA**). The conjugate shows complete stability to even 500 equivalents of **3-MPA** (**Figure 20**), and therefore the decaging must be resulting from reaction with the palladium complex as in **Figure 19a,c**. A possible reaction mechanism is proposed in **Scheme 18**.

3. Palladium Mediated Drug Release

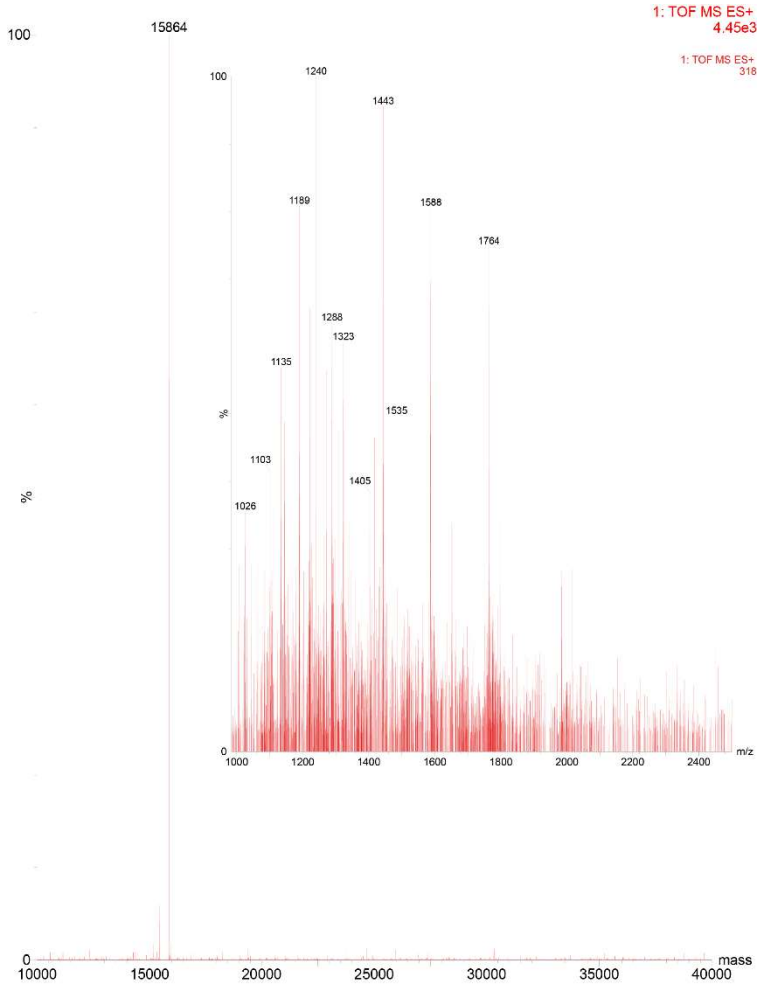

Figure 20: LC-MS showing stability of conjugate 2Rb17c-**36** to the palladium scavenger used after decaging.

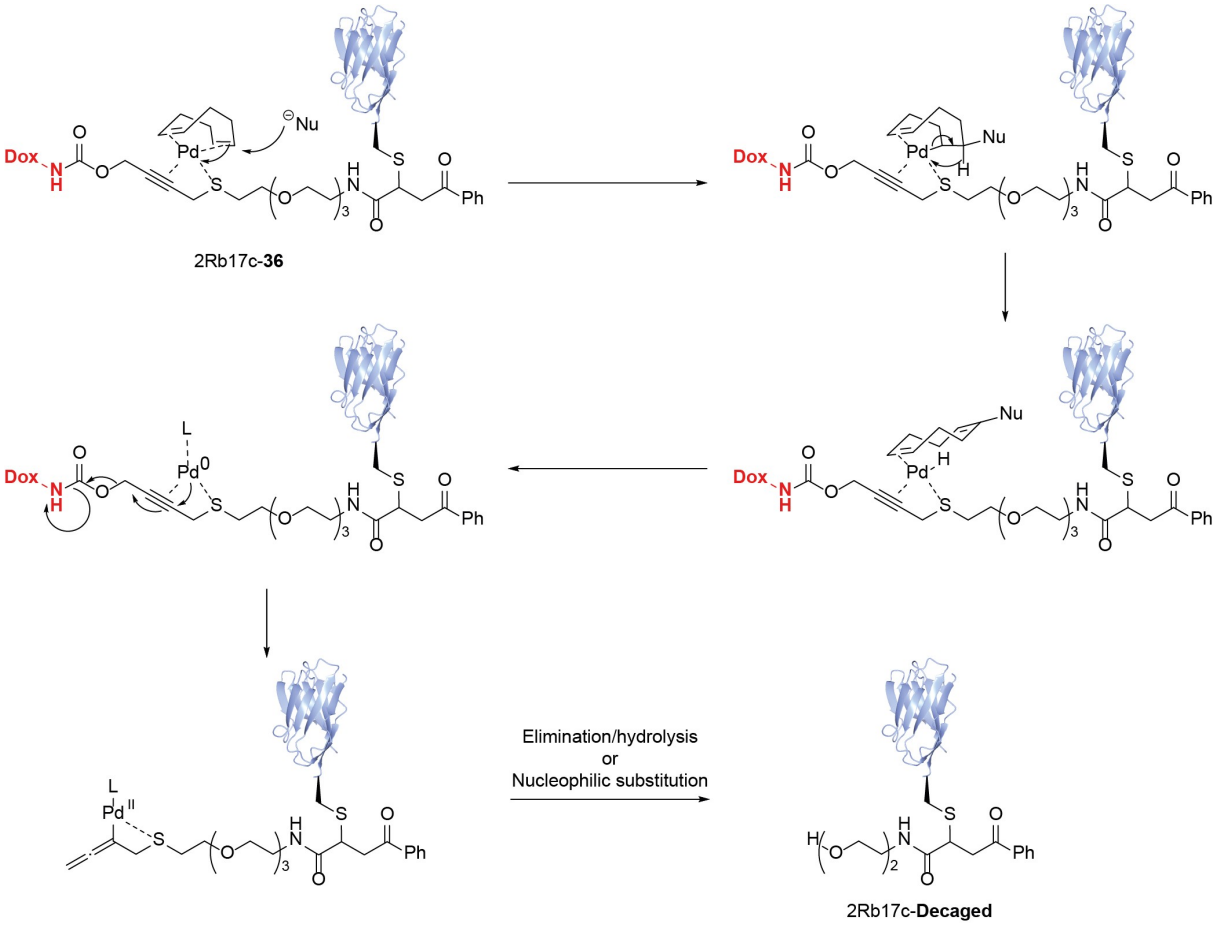

Scheme 18: Proposed mechanism for unusual product observed after decaging of 2Rb17c-**36** by $Pd(COD)Cl_2$.

This chemical biology tool is not the first to enable release of small molecules from a bifunctional linker, however it has some key advantages. A tetrazine/TCO-OH mediated decaging of an antibody drug conjugate[153] required eight steps to synthesise the linker, in a total yield of 7.6%. The synthesis is challenging and the reported starting material is not yet commercially available on a large scale (£38.75/10 mg, Aldrich CPR).[211] In order to make the starting material, literature procedures require 3 steps[212,213] from 1,5-cyclooctadiene and this brings the overall yield to 4.7%. Our synthesis is unoptimised, yet has an overall yield of 4.6% in six steps from a commercially available starting material ($720/10 g, Carbosynth)[214] Another potential advantage of our system is that the PEG linker offers greater polarity than the *trans*-cyclooctene linker. Downsides to our system are the relative instability of palladium complexes in biological media with respect to tetrazines and lower reaction rates.

A palladium cleavable bifunctional linker was reported for conjugating pharmaceutical compounds to HaloTag for verification of drug targets.[186] This was performed in cell lysates whereas our chemistry could be performed in live cell cultures. Also, the tool is only designed to conjugate HaloTag and therefore has a limited scope of potential proteins. In another example, an ADC was prepared which would release its payload in response to near-IR light at 690 nm.[137] This is an exciting application as

near-IR light has to ability to deeply penetrate biological tissues. An advantage of our approach is that the drug can be added in the final step, whereas in the near-IR cleavable linker the drug must be added after three out of five steps. Also, the sulfonated cyanine dye at its core makes purification difficult, and it requires three challenging reverse phase purifications.

3.3 Conclusions and Future Work

In this project we have successfully developed a method of targeted drug delivery using a bioorthogonal decaging reaction. This required the study of literature known palladium-mediated propargyl carbamate decaging in order to move this chemistry from simple cleavable protecting groups that enable prodrug synthesis, to complex linkers that allow protein bioconjugation and targeted drug release. The mechanism of this reaction relies on the unexpected favourable interaction of a palladium complex with a thioether in proximity to the propargyl carbamate. While many palladium catalysts can be poisoned by thioethers and sulfur-containing compounds, this reaction relies on thioethers to function. However, the mechanism of this reaction is not fully understood and future studies should focus on understanding the fate of the propargyl carbamate caging group and palladium species after cleavage, both mechanistically and biologically. These studies should include NMR and LC-MS monitoring of intermediates and products in the reaction, as well as the isolation and purification of these products to test in cell culture for toxicity.

The potential of extracellular drug decaging is that it could deliver drugs to cancerous cells that have been targeted to antigens in their extracellular matrix. ADCs have had limited success in treating solid tumours, and many cancers express mutated or alternatively spliced extracellular matrix proteins. The ability to target ADCs to the extracellular matrix and then release their payloads with a bioorthogonal reaction would increase the number of antigens available for targeting and eliminate the need for an internalising antigen on the cell surface. While palladium complexes are unlikely to make it to the clinic due to their poor stability, a palladium cleavable ADC could at least elucidate whether or not a bioorthogonally activated, tumour extracellular matrix targeted ADC could be a viable therapeutic option.

An interesting aspect of this to examine would be if a payload will still selectively accumulate in a cancer cell when only released in proximity to it. A palladium cleavable ADC could be synthesised which targets extracellular matrix proteins[109] such a fibronectin[112,215] or tenascin[115,116] that has a fluorescent payload. These ADCs could then be used to treat a co-culture normal healthy cells and cancer cells expressing these aberrant proteins. The same ADCs could also be applied to tumour spheroids or patient-derived tumour samples. If the fluorophore selectively accumulates in cancerous cells as

opposed to healthy cells, then this could be a therapeutic avenue for future research. Also interesting to study would be the concentration of payload at increasing distances from a tumour (**Figure 21**), as certain ADCs attempt to increase "bystander killing". This is when the drug once released can diffuse away from its target antigen and kill other cancerous cells which do not bear that antigen. It would be valuable to study whether bystander killing can be increased by extracellular drug release as opposed to intracellular drug release.

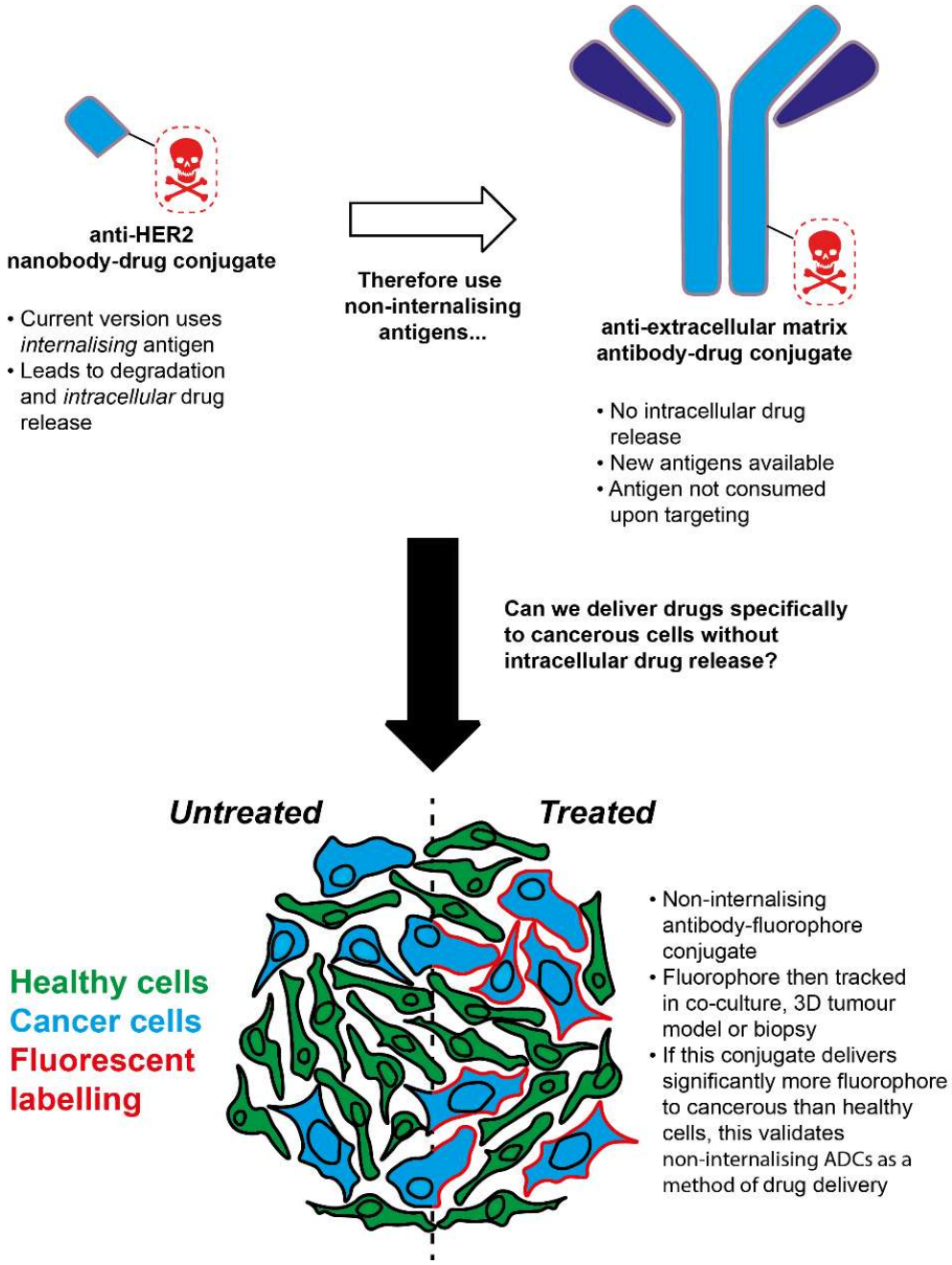

Figure 21: Future applications of palladium cleavable, targeted antibody-fluorophore conjugates.

Chapter 4:

Platinum Mediated Drug Release

4.1 Aims of the Project

Bioorthogonal decaging chemistry has focused on developing reagent pairs that individually affect biological systems in the smallest way possible. The purpose of this project was to find a reactive compound which is already used in cancer therapy in human patients, and use it as a reagent to cause decaging on a non-internalising ADC. A decaging reaction of this type would have several advantages:

- The toxicity and metabolism of any compound which is regularly used to treat cancer patients is generally very well known. Developing *novel* reagents for bioorthogonal chemistry would require careful studies of the toxicity and metabolism.
- If a reagent is already being used to treat a patient, an ADC that is cleaved by this reagent then becomes an adjuvant therapy. The non-internalising ADC would be a supplementary, combination therapy that still allows the first reagent to exert its effects as a drug in its own right.
- Many marketed compounds used in the clinic are often commercially available, and as they are made on a large scale they could be more affordable and applicable when compared to, for example, *trans*-cyclooctenes and cyclooctynes.

A key factor in the development of many marketed compounds for the treatment of cancer patients is metabolic stability, and therefore most chemotherapeutics are reasonably chemically inert. A selection of the most commonly used anti-cancer chemotherapeutics, their activity and reactivity[216] are given in **Figure 22**. When looking at the reactivity of these compounds, it is clear that many of them will be chemically inert – especially those with long half-lives in circulation. Outliers in the reactivity of common chemotherapeutic drugs are the platinum DNA crosslinking agents. Cisplatin in particular has a very short half-life in humans (20-30 minutes),[217] which is indicative of its high reactivity.

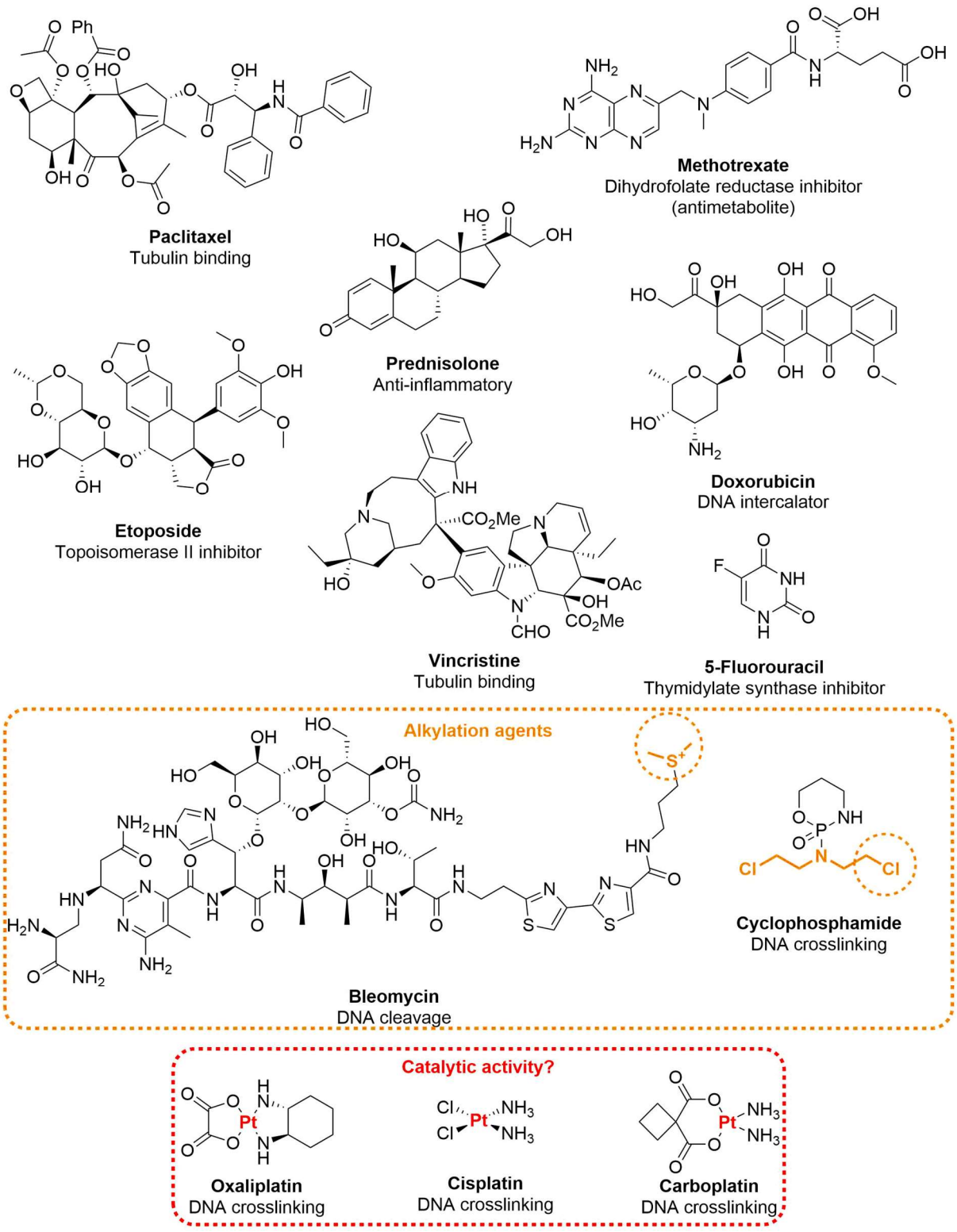

Figure 22: Structures, activities and reactivity of chemotherapy drugs from the most common treatment regimens. Moderately reactive compounds are highlighted in **orange** and reactive compounds in **red**.

Platinum-based chemotherapy drugs are frequently used to treat cancer patients and are clearly reactive compounds which leads to their low half-lives. Therefore, a targeted drug delivery strategy was devised whereby a cancer patient could be treated with a non-internalising platinum-cleavable

ADC. When the ADC reaches its maximum accumulation in the tumour, cisplatin or another platinum-based drug would be infused to cause drug release from the ADC (**Figure 23**).

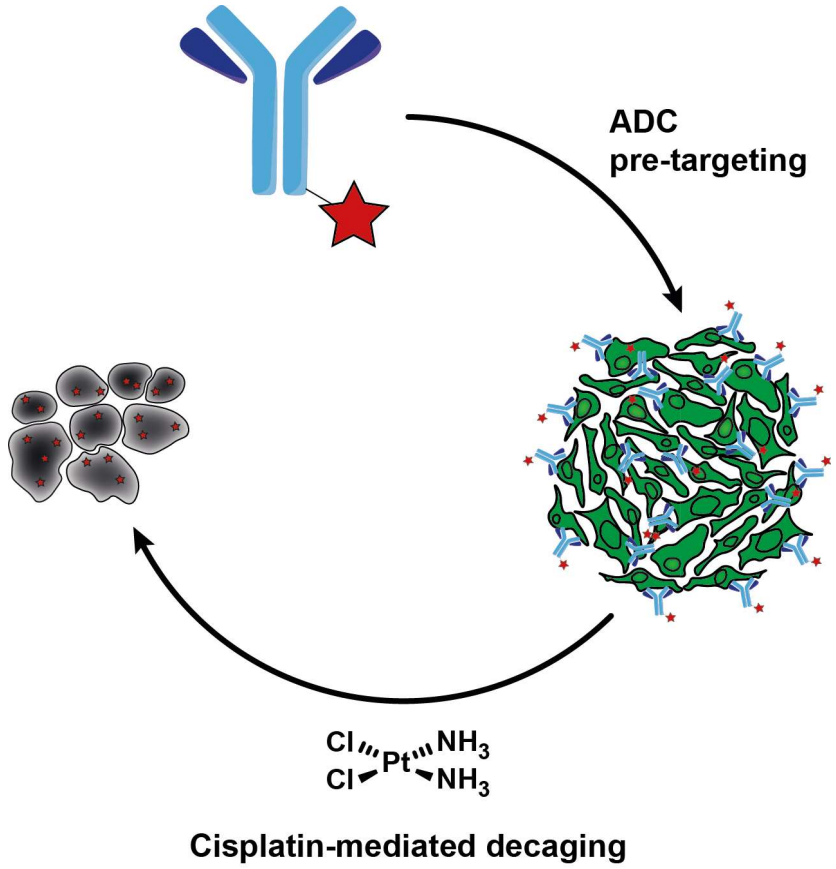

Figure 23: Cisplatin mediated release of drugs from ADCs.

The term "bioorthogonal" could perhaps never be a fitting description for reactions with cisplatin, a compound known to react with water,[218] DNA,[219] amino acids[218,220] and proteins.[221] However cisplatin is one of the most commonly used chemotherapy drugs, being used to treat up to 20% of cancer patients.[222] Its toxicity and effects on biological systems are therefore well known. Cisplatin was deemed a suitable reagent for the development of a drug decaging reaction as it is highly reactive (half-life in humans of ~30 mins[217]) yet can selectively accumulate in a tumour,[223] and even reach high concentrations (~1-2 µM in human tumours).[224]

4.2 Results and Discussion

When trying to design a decaging reaction that could be catalysed by platinum complexes, it is clear that platinum and gold share much of their chemistry.[225,226] Pt^{II} and Au^{III} are isoelectronic and highly electronegative so this is perhaps not surprising. Therefore reactions of both platinum and gold complexes were searched in the literature. A literature search was performed for reactions which

were: heterogeneous, aqueous and rapid at room temperature in air. Later such a reaction could be engineered to function with cisplatin or its metabolites. Fitting these criteria, the cyclisation of 4-pentynoic acid (**37**) (**Scheme 19a**) is well known in the literature to proceed within minutes[227–229] and has even been demonstrated with cisplatin.[230] The metal complexes catalyse a nucleophilic addition of an acid into an alkyne. Palladium mediated propargyl carbamate decaging relies on Pd^0 acting as a nucleophile adding to an alkyne[175,180] which causes allene formation and decarboxylation. An analogous mechanism using platinum or gold was devised using an acid as an internal nucleophile, which causes allene formation, decarboxylation and consequent drug release (**Scheme 19b**).

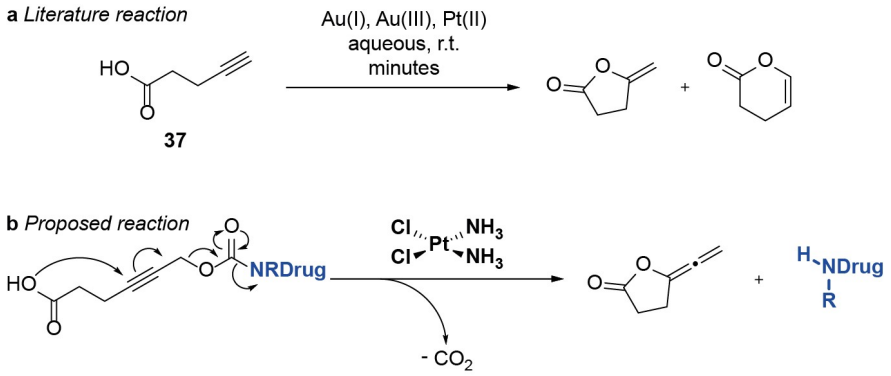

Scheme 19: a) Literature known cyclisation of 4-pentynoic acid (**37**).[227–230] **b)** Proposed decaging reaction.

A model compound pentynoic acid derivative **38** using dibenzylamine as a substitute for a drug was synthesised, and reacted with 0.1 equivalents of $NaAuCl_4$. This gold complex was chosen as a readily available, water soluble Au^{III} salt for model studies. The reaction was followed by ^1H NMR in 25% $MeOD/D_2O$ (**Figure 24**).

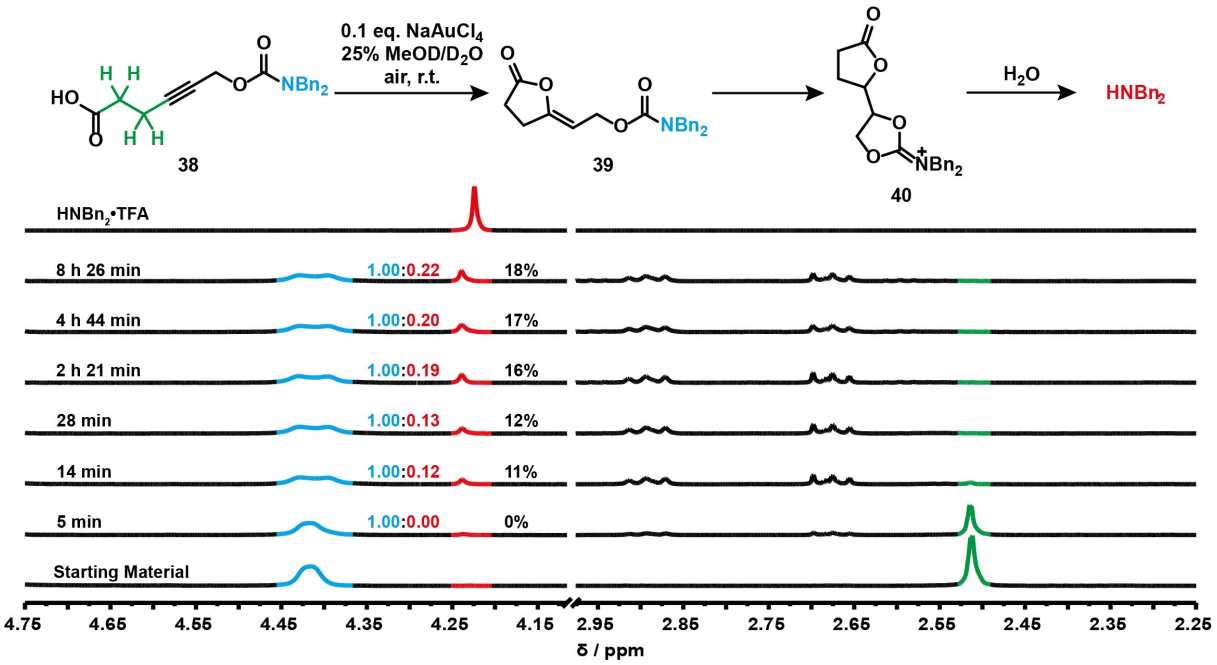

Figure 24: Decaging of pentynoic acid derivative **38** followed by ^{1}H NMR. General conditions: metal complex in D_2O (0.6 mL) was added in one portion to alkyne (~ 10 mg) in MeOD (0.2 mL). The reaction was mixed and transferred to an NMR tube at room temperature in air and sealed. Conversion was monitored by ^{1}H NMR and calculated based on the relative ratios of amine to amide/carbamate signals.

The cyclisation of an acid onto alkyne can be easily followed by the alkyl proton signals in **green** at ~2.50 ppm. These quickly disappear between the 14 and 28 minute timepoints. However this does not correspond to a similar growth in the signals of released dibenzylamine in **red** at ~4.25 ppm. After completion of the cyclisation of the acid onto the alkyne, the dibenzylamine signals slowly grow over the following 8 hours. This would suggest that the major mechanism of dibenzylamine release is not *via* the concerted allene-formation/elimination mechanism proposed in **Scheme 19b**. It is more likely that the cyclisation of the acid onto the alkyne occurs, but the intermediate is rapidly protonated before allene formation can occur. The stable cyclised intermediate **39** then contains a new, reactive alkene which can act as an electrophile for the carbamate carbonyl nucleophile. The carbonyl is a much weaker nucleophile than the acid which explains why it reacts much slower. The cyclisation of carbamate carbonyl onto alkene creates a cationic intermediate **40**, which is then slowly hydrolysed to release dibenzylamine (**Scheme 20**).

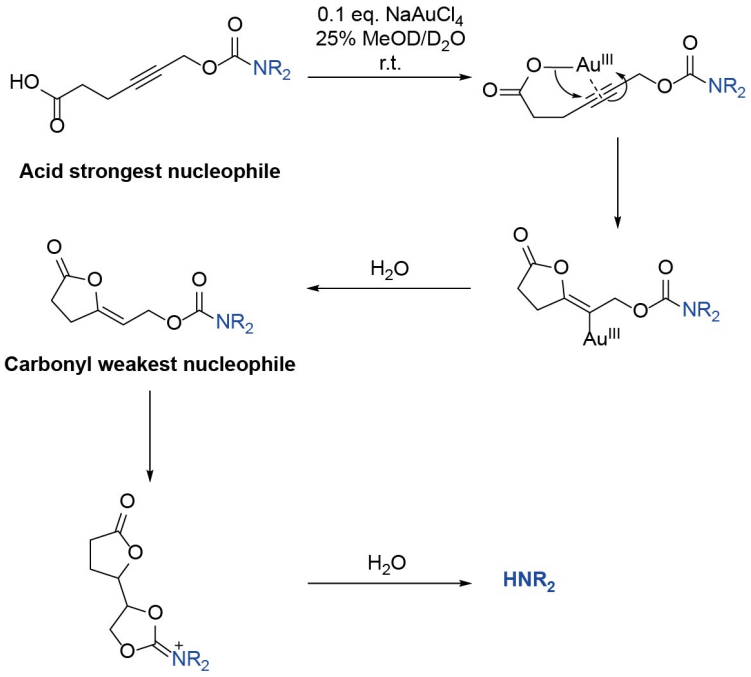

Scheme 20: Proposed mechanism for the decaging of acid bearing propargyl carbamate **38**.

If this proposed mechanism is correct then it should be possible to achieve a carbamate carbonyl cyclisation onto an alkyne directly without the need for the acid of compound **38**. A model terminal propargyl carbamate **41** was synthesised to study this transformation. In this case, dibenzylamine was replaced with morpholine to increase the water solubility of the propargyl carbamate. The decaging of this terminal propargyl carbamate **41** was followed by ^{1}H NMR under the same conditions as acid **38** (**Figure 25**).

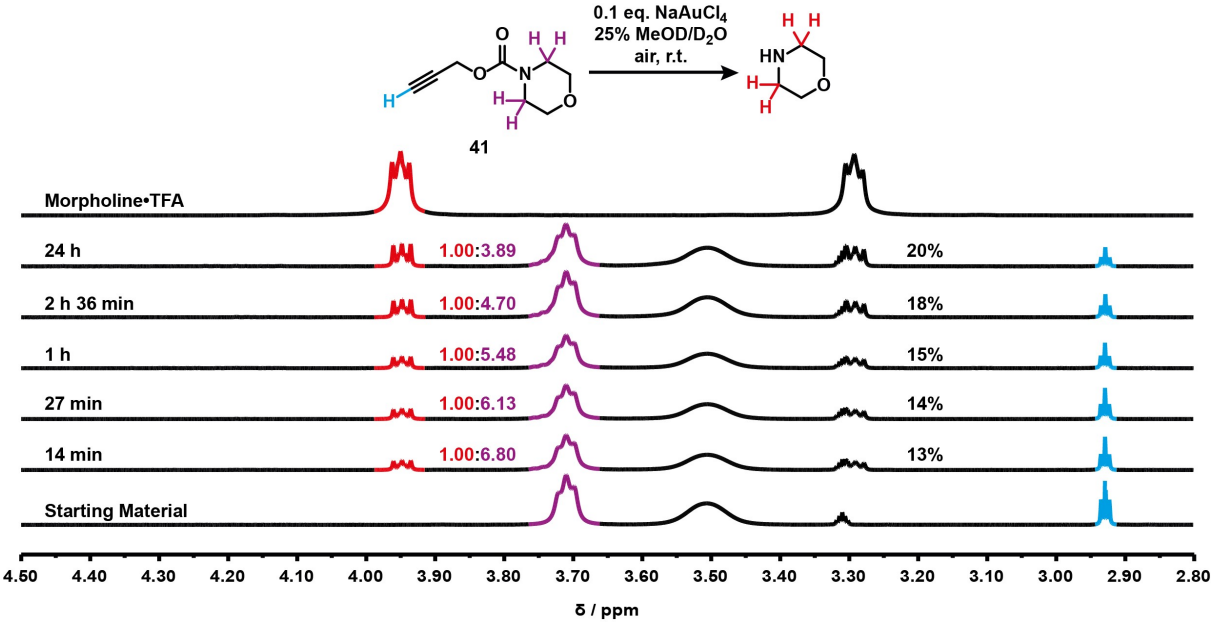

Figure 25: Decaging of terminal propargyl carbamate **41** monitored by ^{1}H NMR.

The morpholine signals in this reaction are used to calculate the conversion as they have the best resolution and are well separated in starting material and product. Another option would be to integrate the alkyne C*H* but complexation of gold to the alkyne could reduce the pKa of the C*H* sufficiently to cause deuteration (**Scheme 21**). Also, if the alkyne were to become hydrated or chlorinated, the morpholine signals in the products would presumably stay at a very similar chemical shift as the amide bond would be intact (**Scheme 21**).

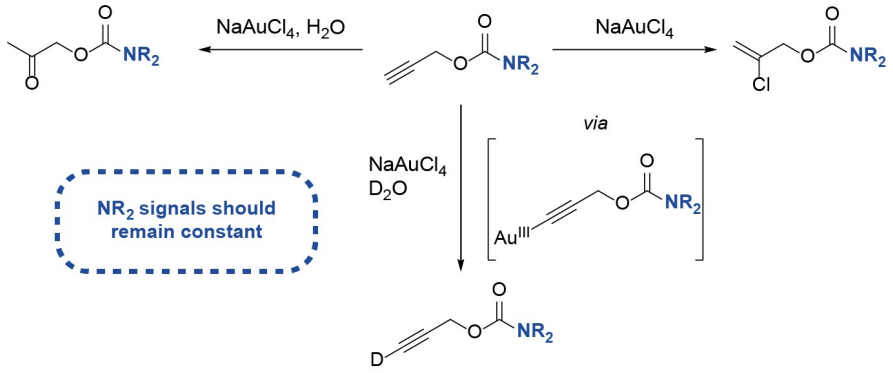

Scheme 21: Potential side reactions arising from the use of gold complexes.

Successful release of morpholine from carbamate **41** supports the hypothesis of carbamate carbonyl cyclisation onto the alkyne as the mechanism of decaging. This reaction even had slightly better conversion than acid **38**. It is however possible the decaging was simply Au^{III} acting as a Lewis acid and binding to the carbonyl oxygen, allowing direct hydrolysis. To verify that the mechanism did proceed *via* cyclisation, an aliphatic carbamate bearing no alkyne **42** was synthesised and subjected to the same conditions as previous decaging reactions (**Figure 26**).

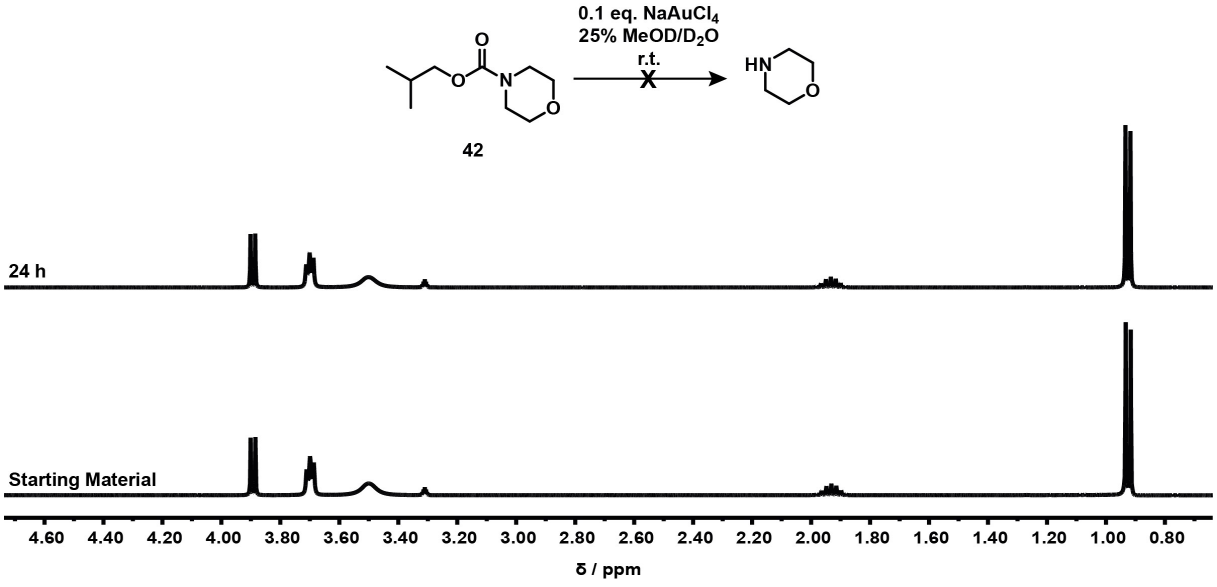

Figure 26: Stability study of aliphatic carbamate **42** monitored by ^{1}H NMR.

The aliphatic carbamate shows no sign of decomposition after 24 hours exposure to $NaAuCl_4$. This provides strong evidence that the mechanism of this decaging reaction passes *via* a cyclised carbocation which slowly hydrolyses. The data collected thus far however do not elucidate the rate-determining step of decaging. If the cyclisation step is faster than hydrolysis, then one would expect to see ^1H NMR signals arising from the cyclised intermediate of propargyl carbamate **41** (**Figure 25**). The ^1H NMR appears to show a mixture of only starting material and morpholine product, and therefore it could be assumed that cyclisation is the rate determining step. However, the cyclisation could also be rapid and reversible which could account for why there are no signals arising from a cyclised intermediate. Based on these mechanistic hypotheses, a similar decaging should be possible for amides. In fact, the intermediate cation would have mesomeric stabilisation from only one amide oxygen instead of two carbamate oxygens and would therefore be less stable and may hydrolyse faster. An amide analogue **43** of carbamate **41** was synthesised and subjected to the same decaging conditions (**Figure 27**).

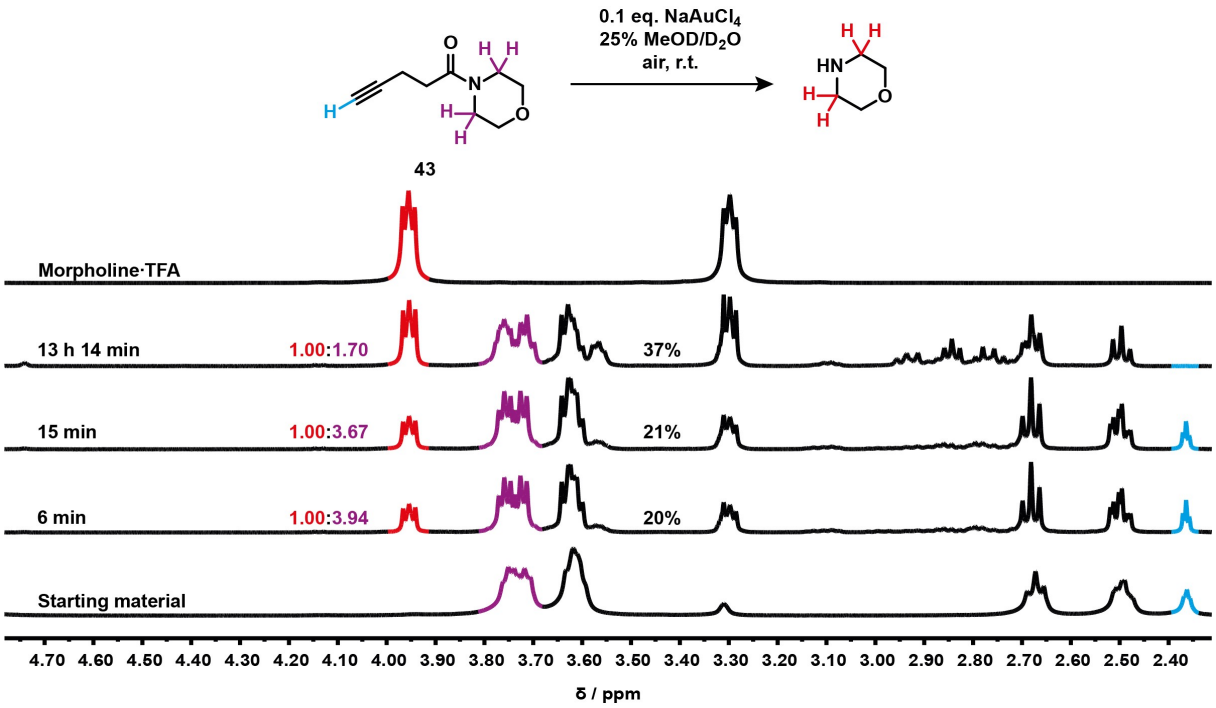

Figure 27: Decaging of tertiary amide **43** monitored by ^1H NMR.

Gratifyingly, the decaging of amide **43** had significantly better conversion than carbamate **41**. The decaging of amide **43** is also faster than carbamate **41** (20% at 15 min and 13% at 14 min respectively). This suggests that hydrolysis of the cyclised cationic intermediate is the rate determining step as amide **43** does not benefit from the same amount of mesomeric stabilisation as carbamate **41** after cyclisation (**Scheme 22**).

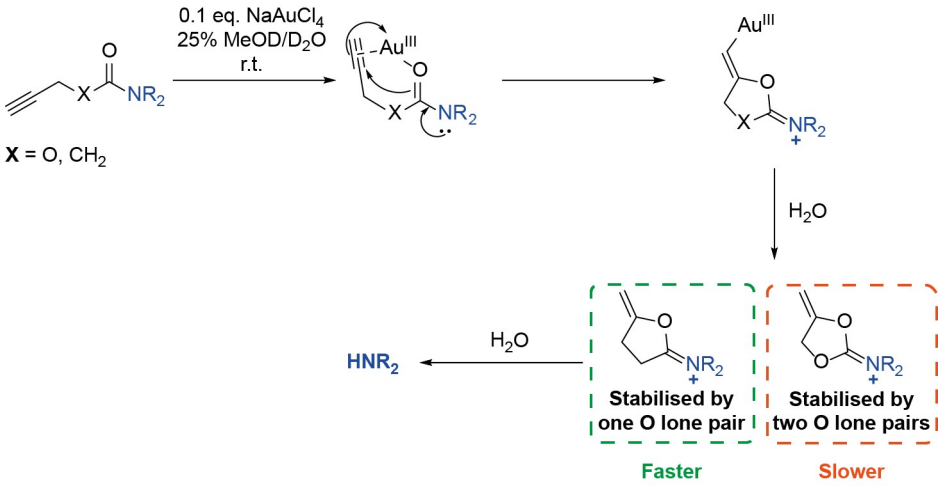

Scheme 22: Proposed decaging mechanism of carbamate **41** and amide **43**.

However it is very clear from these NMRs that even when the starting material alkyne C*H* signal is fully consumed, this does not lead to complete formation of the desired decaged product (**Figure 27**) – suggesting perhaps that the alkyne C*H* can be deuterated or the alkyne subject to side-reactions in the presence of the gold complex as proposed in **Scheme 21**. This is supported by the fact that after overnight reaction, no alkyne C*H* is remaining, and the propargylic methylene signals are a triplet and not doublet of triplets (**Figure 27**). Other potential side-reactions arising from the use of gold complexes could be alkyne hydration[231] and alkyne chlorination[232] (**Scheme 21**). Some signals in the 2.7-3.2 ppm region (**Figure 27**) suggest that these could be derived from the methylene groups in the starting material – perhaps after a side-reaction or cyclisation with the alkyne. However the integration of these peaks is insignificant when compared to the methylene signals in the starting material. It was also of interest to verify if this reaction would proceed with secondary amides. A secondary amide analogue **44** of tertiary amide **42** was synthesised and subjected to the same decaging conditions (**Figure 28**).

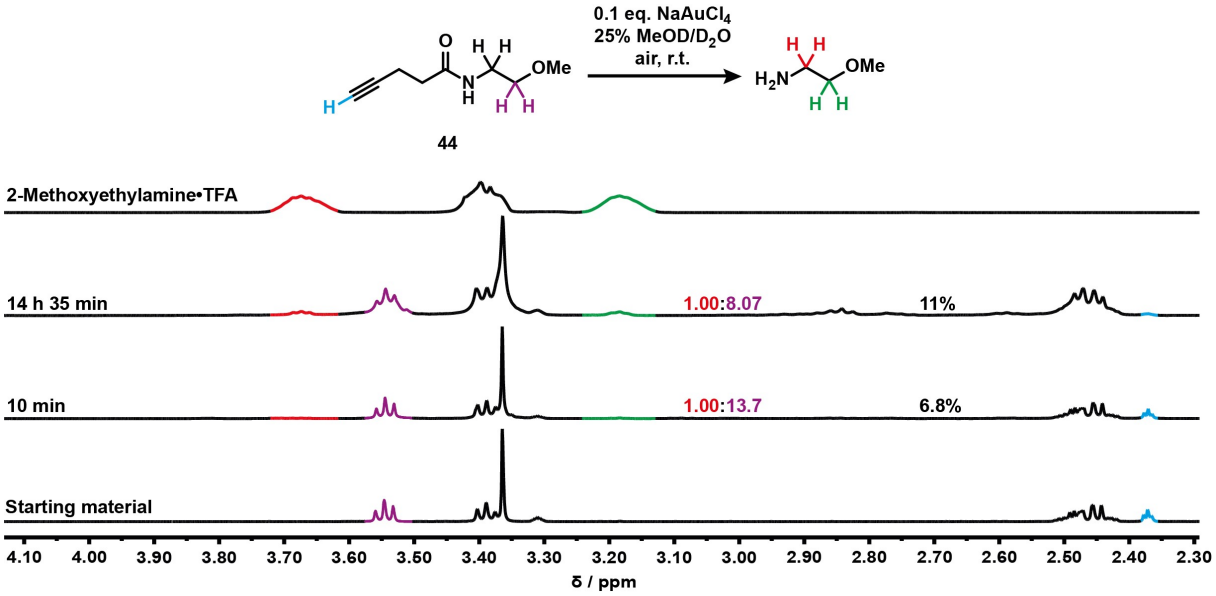

Figure 28: Decaging of secondary amide **44** monitored by ^{1}H NMR.

With tertiary amides such as **43**, the carbonyl oxygen acts as a nucleophile to attack the alkyne. In a secondary amide such as **44**, the amide nitrogen can also act as a nucleophile and attack the alkyne to give a stable cyclised product, thereby outcompeting the carbonyl oxygen and leading to a lower decaging conversion (**Scheme 23**).[233]

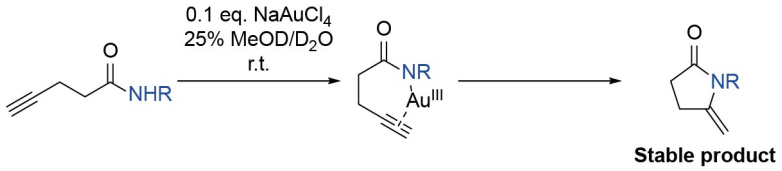

Scheme 23: Proposed mechanism of gold mediated cyclisation of secondary amide **44**.

These reactions developed first with the gold complex $NaAuCl_4$ were then tested for efficacy with platinum complexes including cisplatin (**Table 11**). As cisplatin has such a low half-life in circulation in humans, it was hoped that metabolites of cisplatin may also eventually be catalytically active in cellular or animal models. To act as a model for cisplatin metabolites, both K_2PtCl_4 and K_2PtCl_6 were trialled against these reactions. These offer "naked" sources of Pt^{II} and Pt^{IV} respectively which can be more catalytically active as they have labile chloride ligands.

Table 11: Summary of conversions for decaging reactions with gold and platinum complexes.

Catalyst	Compound	Structure	Conversion % (time)
0.1 eq. $NaAuCl_4 \cdot 2H_2O$	**41**	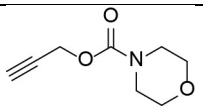	12% (4 min) 20% (24 h)
0.1 eq. $NaAuCl_4 \cdot 2H_2O$	**42**	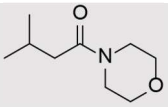	No change (24 h)
0.1 eq. $K_2Pt^{IV}Cl_6$	**41**	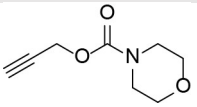	Trace product (overnight)
0.1 eq. $NaAuCl_4 \cdot 2H_2O$	**43**	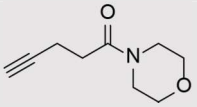	20% (6 min) 21% (15 min) 37% (13h 14 min)
0.1 eq. $K_2Pt^{IV}Cl_6$	**43**	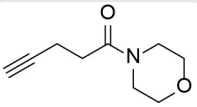	Traces (8 min) 40% (13 h 7 min)
0.1 eq. $K_2Pt^{II}Cl_4$	**43**	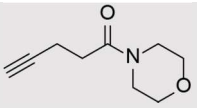	4% (10 min) 9% (4 h 21 min)
0.1 eq. cisplatin	**43**	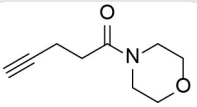	3% (overnight)
0.1 eq. $NaAuCl_4 \cdot 2H_2O$	**44**	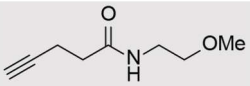	12% (14 h 35 min) 2% (10 min)
0.1 eq. $K_2Pt^{II}Cl_4$	**44**	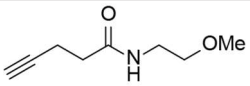	Small traces (overnight)
0.1 eq. $K_2Pt^{IV}Cl_6$	**44**	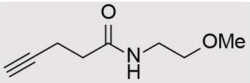	11% (14 h 45 min)

General procedure: Carbamates and amides (~10 mg) were dissolved in MeOD (0.2 mL) and gold or platinum complexes (0.1 eq.) were added in D_2O (0.6 mL) at room temperature in air. The reactions were transferred to an NMR tube then sealed.

Amides are generally much more metabolically stable than carbamates, and there are already several carbamate decaging reactions in the literature.[150,152,180] Therefore amide decaging was chosen as the most promising reaction for further development. In our initial results tertiary amides had shown much

better decaging conversions than secondary amides. Therefore drugs were sought which contained a secondary amine functionality which could be caged with 4-pentynoic acid (**37**) to give a tertiary amide.

Doxorubicin would be an ideal candidate as it is readily available in large quantities and its inherent fluorescence may later allow the tracking of platinum-cleavable antibody-doxorubicin conjugates. Unfortunately it bears only a primary amine, so methods were sought to synthesise a doxorubicin prodrug bearing a secondary amine. Fortunately, a doxorubicin analogue which had been reacted with acetone was known in the literature.[234] It was reported that the free base form of doxorubicin could be refluxed in anhydrous acetone to form cyclised product **pDox** (**45**). In the presence of water, doxorubicin analogue **pDox** (**45**) would decompose rapidly to release acetone and doxorubicin. However when acetylated the rate of decomposition of **pDoxAc** (**48**) was greatly reduced. It was hypothesised that if doxorubicin analogue **pDox** (**45**) could be converted to an amide with 4-pentynoic acid (**37**), then this could be decaged to release doxorubicin (**Scheme 24a**). Thus, doxorubicin prodrug **pDoxAm** (**46**) was synthesised to test its ability as a platinum cleavable doxorubicin prodrug. As negative controls, primary amide **DoxAm** (**47**) and acetylated **pDoxAc** (**48**) were synthesised as they should not react with platinum complexes efficiently to release doxorubicin (**Scheme 24b**).

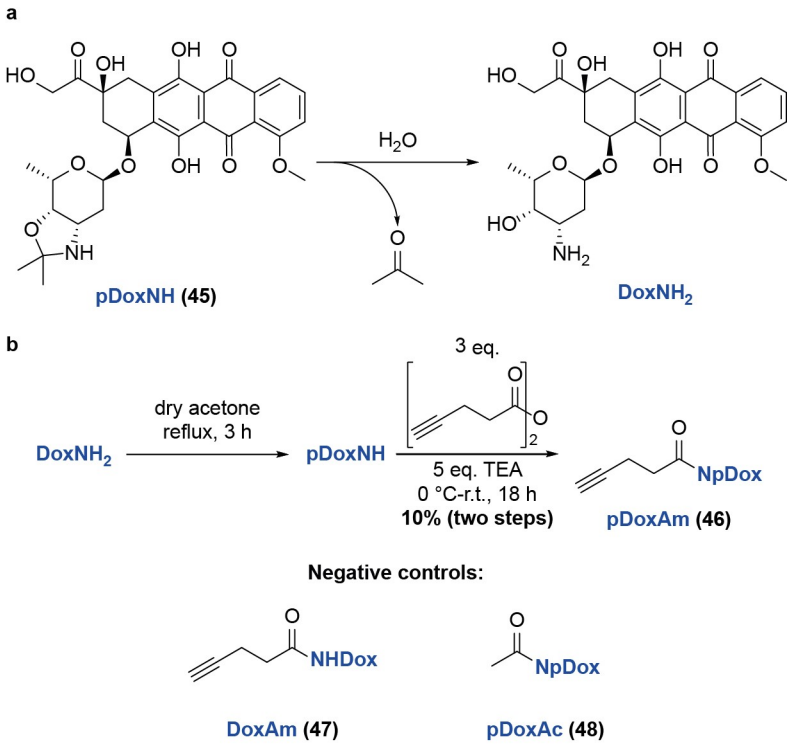

Scheme 24: a) Mechanism of doxorubicin release from **pDox** (**45**) **b)** Synthesis of **pDoxAm** (**46**) and structures of **DoxAm** (**47**) and **pDoxAc** (**48**).

The toxicity of doxorubicin prodrug **pDoxAm** (**46**) and negative controls **DoxAm** (**47**) and **pDoxAc** (**48**) were compared with that of free doxorubicin **Dox** (**Figure 29**).

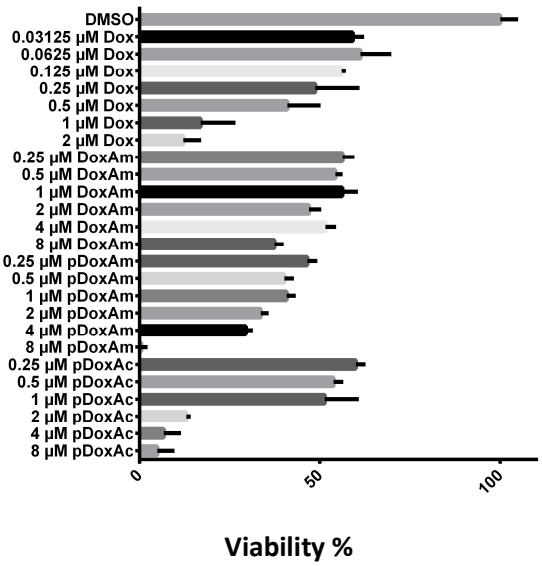

Figure 29: Toxicity of doxorubicin and derivatives in HeLa cells after 3 days as determined by Alamar Blue assay.

Unfortunately, the difference in toxicity between **pDoxAm** (**46**) and **Dox** was small (~2x). This would mean a very narrow margin in which to determine if the decaging reaction is working or not. Interestingly, while **pDoxAc** (**48**) and **pDoxAm** (**46**) were of similar toxicity, **DoxAm** (**47**) was much less toxic. This is likely due to ring strain in **pDox** (**45**) leading to weaker amides that are more easily hydrolysed. 5-Fluorouracil (**5-FU**) is a drug that is frequently used in decaging studies,[171,183,187] so this was caged with 4-pentynoic acid (**37**) to give **5-FU-am** (**49**) and the toxicity was tested (**Figure 30**).

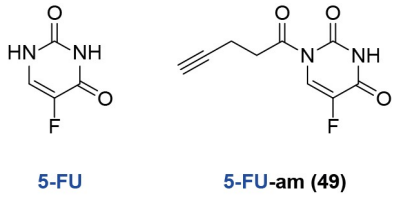

5-FU **5-FU-am (49)**

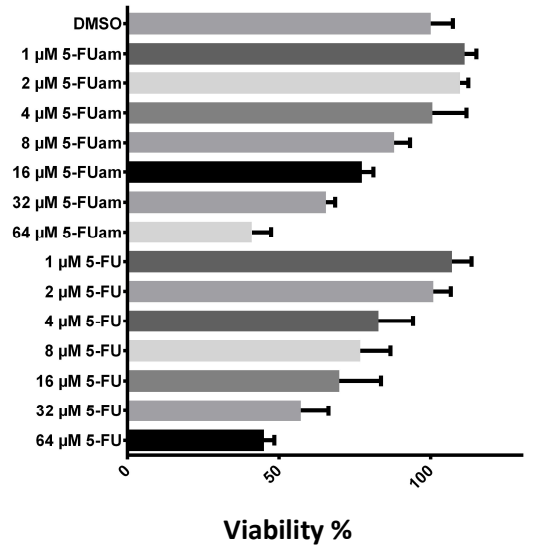

Figure 30: Toxicity screening of **5-FU** and **5-FU-am** (**49**).

In this case, the toxicity of **5-FU** and **5-FU-am** (**49**) are almost exactly the same. Presumably again this is due to the amide of **5-FU-am** (**49**) being unstable and hydrolysed to release **5-FU**. This led to a search for aliphatic secondary amine drugs which could be converted into stable amides. Monomethylauristatin E (**MMAE**) is a common ADC payload[16] which exerts its anti-cancer activity by inhibiting tubulin polymerisation. One of its most important interactions with tubulin comes from a salt bridge between its positively charged ammonium and a negatively charged aspartate side chain.[95] **MMAE** bears an aliphatic secondary amine which was caged with 4-pentynoic acid (**37**) to give **MMAE-am** (**50**) and tested for toxicity (**Figure 31**). **MMAE-am** (**50**) was expected to be less toxic than **MMAE** due to the loss of a positively charged amine.

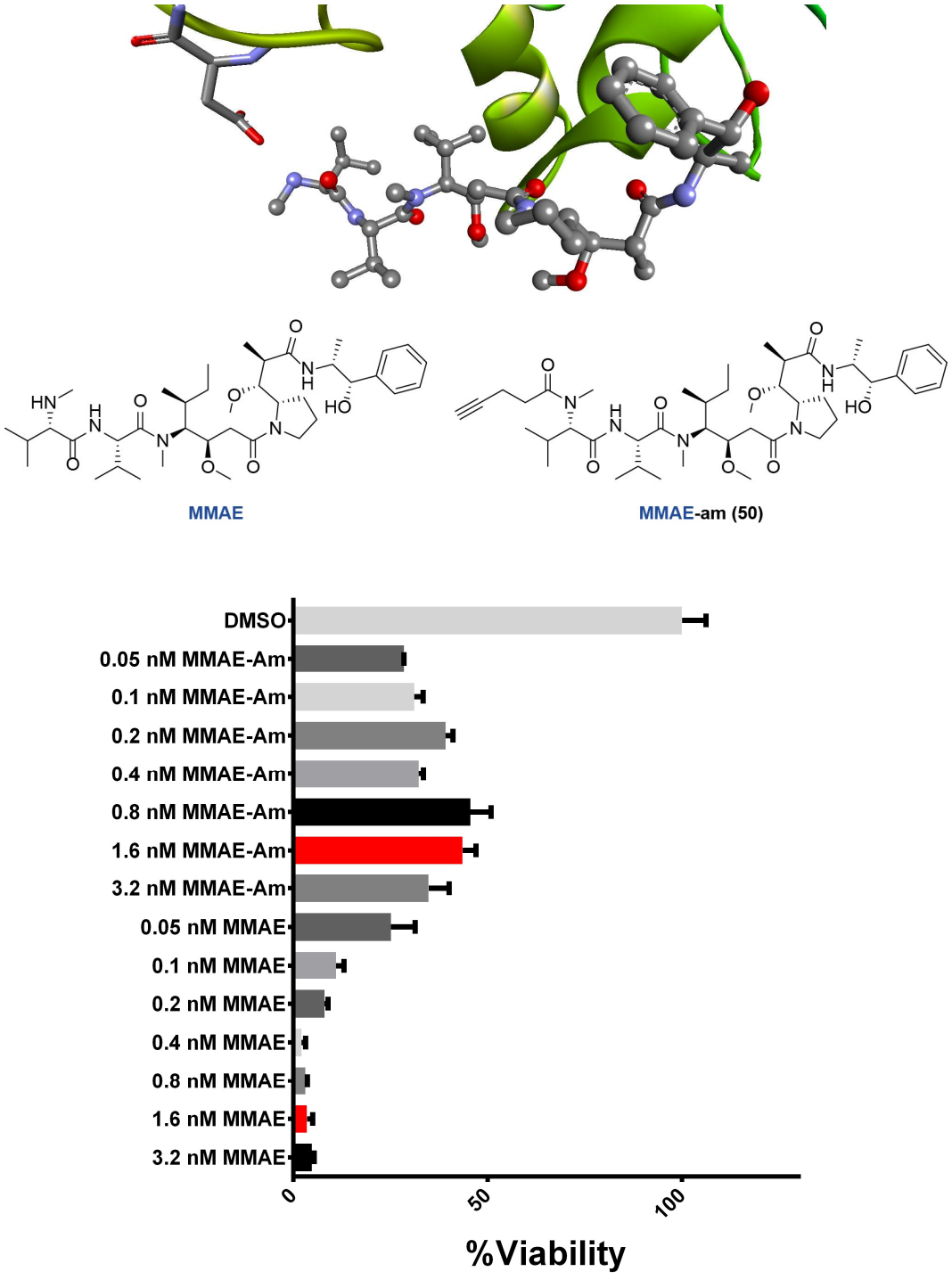

Figure 31: Binding mode of **MMAE** to its target tubulin including its important interaction with a positively charged ammonium and a negatively charged aspartate side chain. **MMAE-am** (**50**) was expected to disrupt this interaction and therefore lead to lower toxicity. Toxicity screening of **MMAE** and **MMAE-am** (**50**) in HeLa cells. Optimal concentrations are highlighted in **red**.

Encouragingly **MMAE-am** (**50**) was much less toxic than **MMAE**. Caging with 4-pentynoic acid (**37**) gives an approximately 10x difference in toxicity at the optimal concentration (1.6 nM). Hence, 1.6 nM **MMAE-am** was incubated for the same amount of time in cell culture with non-toxic concentrations

of platinum salts $K_2Pt^{II}Cl_4$ and $K_2Pt^{IV}Cl_6$ (**Figure 32**). Unfortunately, cisplatin and satraplatin were too toxic to achieve high concentrations in cell culture, and their non-toxic concentrations were deemed too low to achieve a reaction.

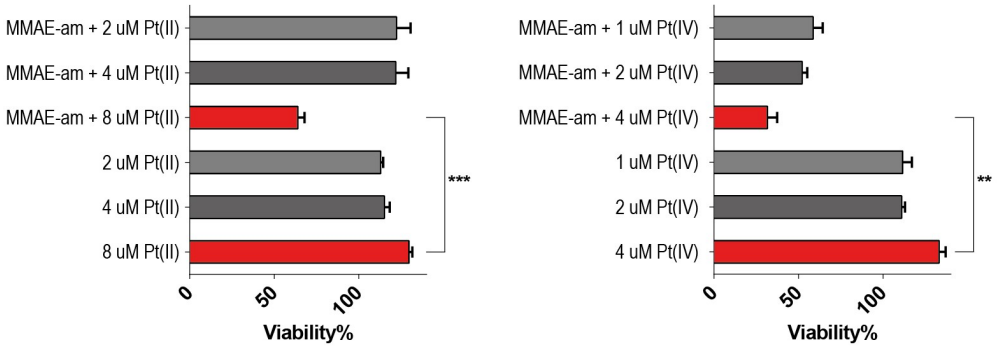

Figure 32: Decaging assay of $K_2Pt^{II}Cl_4$ (**Pt(II)**) and $K_2Pt^{IV}Cl_6$ (**Pt(IV)**) given twice daily at intervals of 8 h and 16 h as an aqueous solution for a total of 72 h. Optimal concentrations are highlighted in **red**. Concentration of **MMAE-am** (**50**) = 1.6 nM. Statistical significance was determined with a two-tailed unpaired t-test. ***p = 0.0001. **p = 0.0023.

Pleasingly, with increasing non-toxic concentrations of $K_2Pt^{II}Cl_4$ and $K_2Pt^{IV}Cl_6$ in the presence of **MMAE-am** (**50**) a large increase in toxicity is observed with 8 µM $K_2Pt^{II}Cl_4$ and 4 µM $K_2Pt^{IV}Cl_6$. Cisplatin and satraplatin were too toxic to achieve high concentrations. They would require sub-micromolar concentrations to not affect cell viability, meaning a very high reaction rate would be required in order to react efficiently with a nanomolar concentration of prodrug. It is also interesting to note that overconfluence of cells (> 100%) is observed for controls where cells are only treated with platinum complexes. It has been reported in the literature that platinum complexes can result in greater consumption of oxidative species by certain enzymes.[235] The study did not extend to live cell cultures and therefore this effect could not be observed for cancerous cells. However, low concentrations of $K_2Pt^{II}Cl_4$ and $K_2Pt^{IV}Cl_6$ leading to a reduction of oxidative stress on cancer cells could offer an explanation of this effect.

Around this time, a decaging reaction was reported of gold nanoparticles with a propargylated **5-FU** compound **pFU** (**51**). This was reported to be an efficient, bioorthogonal reaction which was even demonstrated in Zebrafish.[183] **pFU** (**51**) was tested for toxicity and decaging to verify whether it could potentially be reactive with platinum complexes despite not bearing the 4-pentynoic acid (**37**) caging group (**Figure 33**).

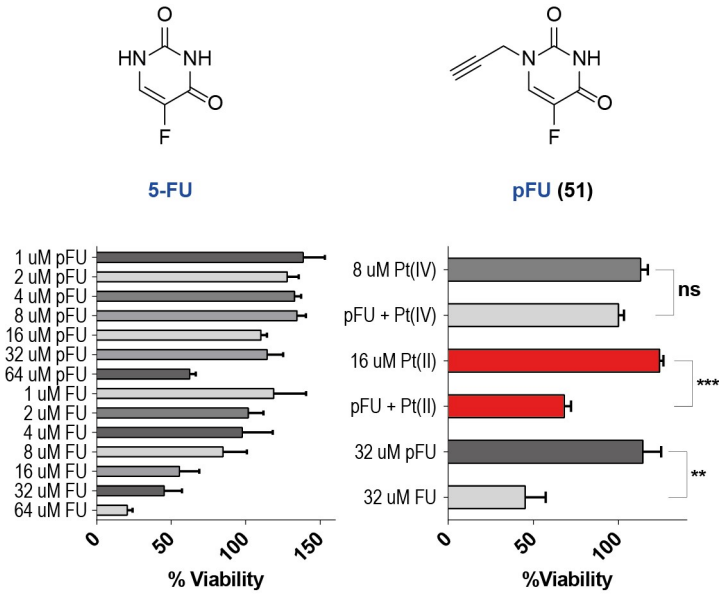

Figure 33: Structure, toxicity and decaging of **pFU** (**51**) in the presence of platinum complexes $K_2Pt^{II}Cl_4$ (**Pt(II)**) and $K_2Pt^{IV}Cl_6$ (**Pt(IV)**) as an aqueous solution for a total of 72 h. Optimal concentrations are highlighted in **red**. Statistical significance was determined with a two-tailed unpaired t-test. ***p = 0.0002. **p = 0.0018. ns = non-significant.

Pleasingly, **pFU** (**51**) and **5-FU** have a large difference in toxicity and showed efficient decaging with 16 µM $K_2Pt^{II}Cl_4$. Surprisingly no increase in toxicity could be seen with $K_2Pt^{IV}Cl_6$ despite it having been successful with **MMAE-am** (**50**) (**Figure 32**). With evidence that this platinum mediated decaging reaction can function in cell culture, an ADC linker was designed that should be able to release a drug payload in the presence of platinum complexes and perhaps cisplatin (**Figure 34**).

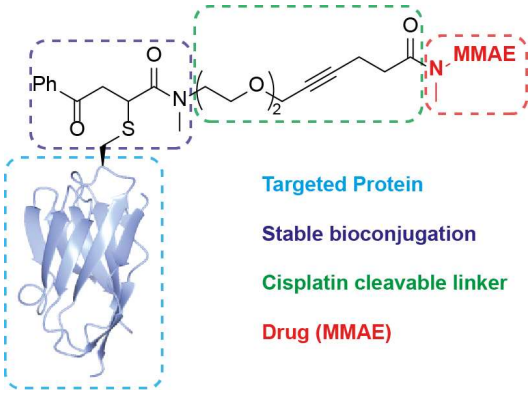

Figure 34: General structure of proposed targeted bioconjugates for the platinum mediated release of drug **MMAE**.

The linker bears the drug **MMAE** as a secondary amine toxic payload, and the alkyne is extended with two PEG units before a cysteine-selective acrylamide bioconjugation handle. An ether was deemed the safest choice of linker to extend the alkyne as ethers are not known to bind strongly with platinum complexes or undergo many platinum mediated reactions. The PEG also offers a spacer between the

protein surface and metal reagent as well as increased water solubility. The linker could be synthesised in 8 steps from commercially available 2-(2-aminoethoxy)ethanol (**52**) (**Scheme 25**).

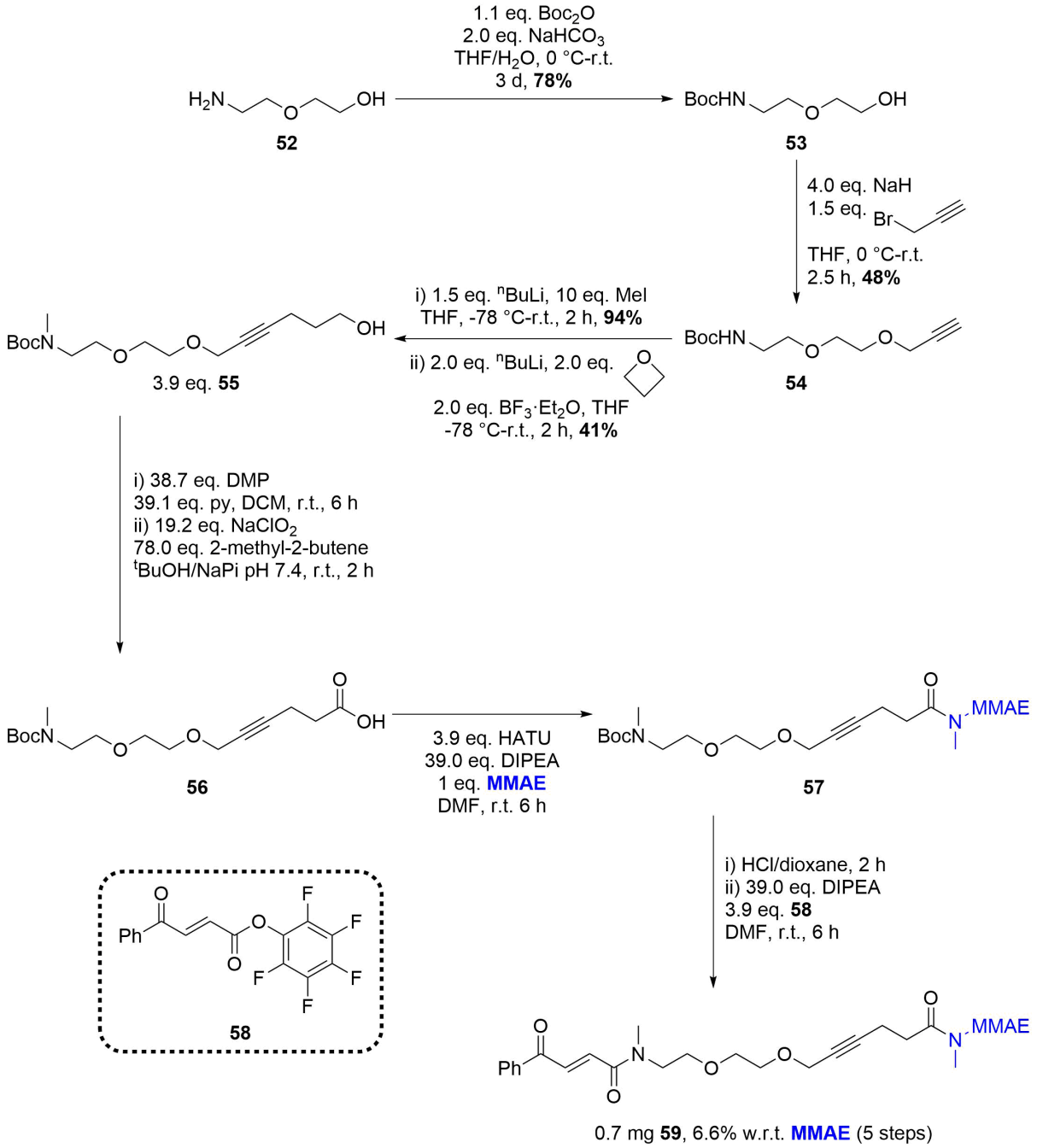

Scheme 25: Synthesis of platinum-cleavable bioconjugation linker **59**.

2-(2-Aminoethoxy)ethanol (**52**) was initially Boc protected to afford **53** in order to allow selective *O*-propargylation to give **54.** This was then *N*-methylated with ^{n}BuLi and MeI and subsequently the alkyne was lithiated with ^{n}BuLi and reacted with oxetane activated by Lewis acid $BF_3{\cdot}Et_2O$ to give alcohol **55**. Alcohol **55** was first oxidised to an aldehyde with Dess-Martin periodinane (**DMP**), and then the aldehyde to an acid *via* Pinnick oxidation to afford **56**. The crude acid **56** was coupled with **MMAE** using

HATU to give **57**, Boc deprotected in HCl/dioxane and finally reacted with activated ester **58** to give the desired product **59**. The acrylamide bioconjugation handle is unstable to Pinnick oxidation, and the presence of **MMAE** eliminates the possibility of intermediate purification by flash chromatography on silica as it renders the compounds too polar. Due to possible loss of product with repeated preparative HPLC purifications, it was decided that the product should only be purified after the final step. There were predictably many impurities in the chromatogram, and it required two successive purification procedures. With a pure sample of bioconjugation reagent **59** in hand, it was possible to selectively modify a model protein. A mutated Ubiquitin K63C (Ub) was selected as a small protein available in large quantities and at high concentration. This was reacted with an almost stoichiometric amount of acrylamide reagent **59** to give Ub-**59** with a small amount of Ub (**Figure 35**).

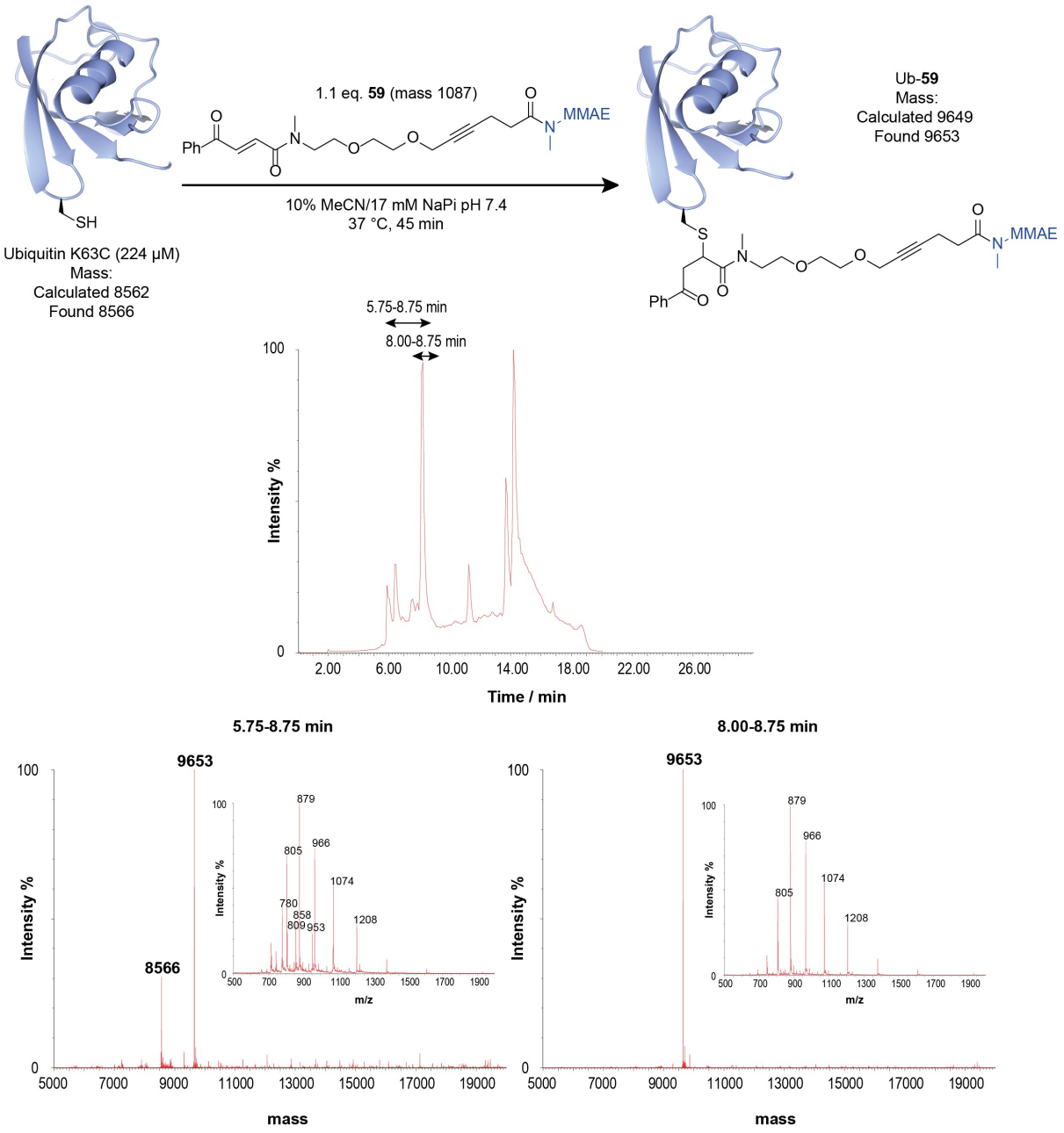

Figure 35: LC-MS analysis of the modification of Ubiquitin K63C (Ub) with acrylamide **59** to give Ub-**59**. The reaction was incomplete, however the retention times of starting material and product were sufficiently resolved that the product peak in the HPLC could be integrated to exclusively monitor the product. Ub was kindly provided by Dr Ester Jiménez-Moreno. Samples of the reaction mixture were injected without further preparation and LC-MS run under denaturing conditions.

While conversion was not complete, the starting material Ub and the product Ub-**59** were very well separated in the chromatogram. It was thought that this separation would be sufficient to allow monitoring of a decaging reaction with cisplatin. Reactions with palladium complexes on proteins typically require palladium scavenger 3-mercaptopropionic acid (**3-MPA**).[208,209,236,237] Therefore a screen of concentrations of **3-MPA** was performed to verify that the conjugate Ub-**59** was stable to thiols (**Figure 36**).

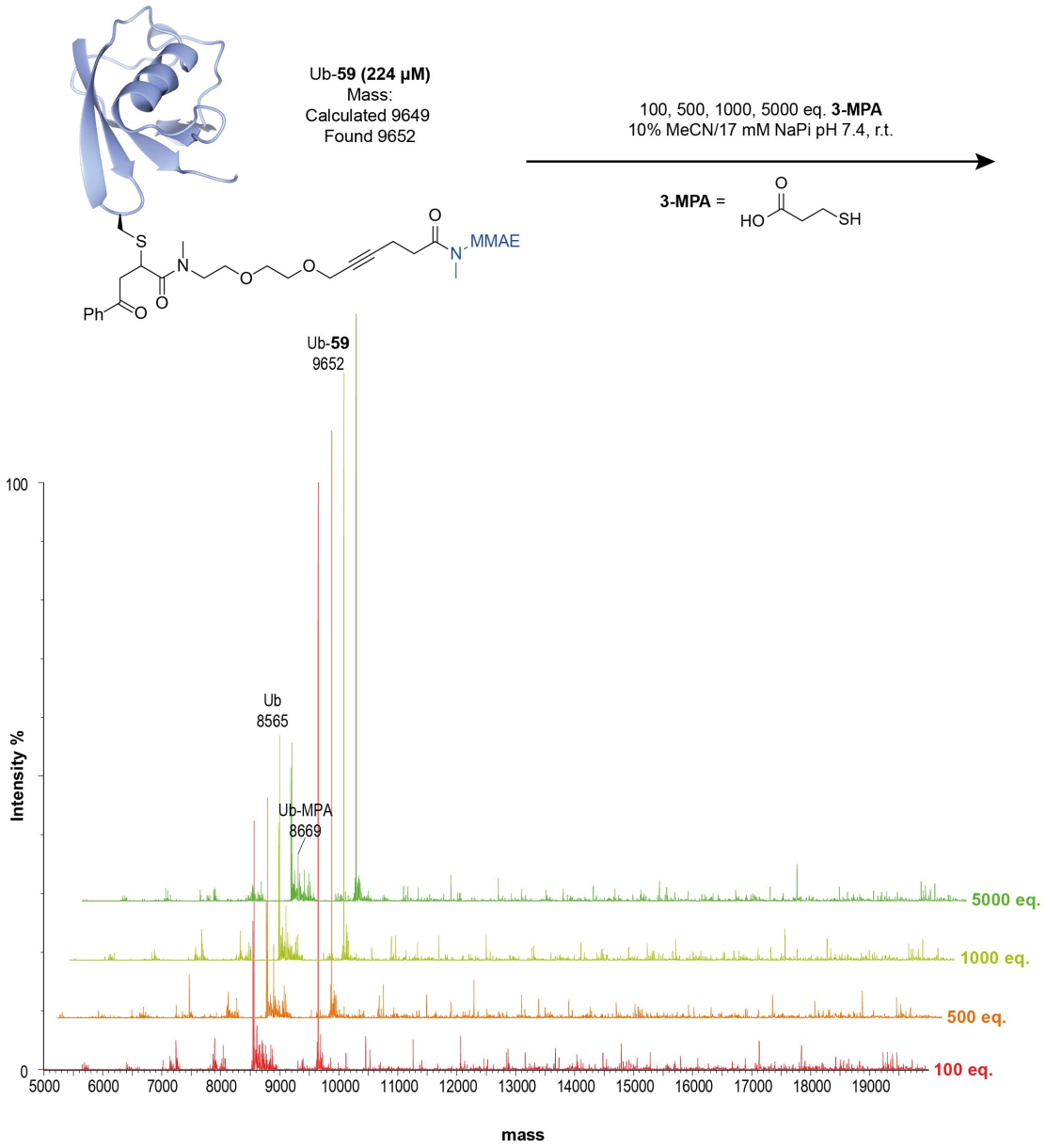

Figure 36: Stability study of conjugate Ub-**59** with varying concentrations of platinum scavenger **3-MPA**.

The conjugate Ub-**59** appeared stable to all concentrations of palladium scavenger **3-MPA** tested. Interestingly, free Ub can be seen to form disulfide bonds with **3-MPA** to form Ub-**MPA** (Mass calculated 8668, found 8669). 1000 equivalents of scavenger **3-MPA** was selected as a suitable concentration to study cisplatin mediated decaging of conjugate Ub-**59** as it should offer maximum scavenging of metals while not compromising protein stability. To study decaging, 10 equivalents of cisplatin in DMSO were added to conjugate Ub-**59** and after 1 hour the reaction was quenched with 1000 equivalents of scavenger **3-MPA** (**Figure 37**). DMSO was required as a co-solvent due to the limited water solubility of cisplatin.

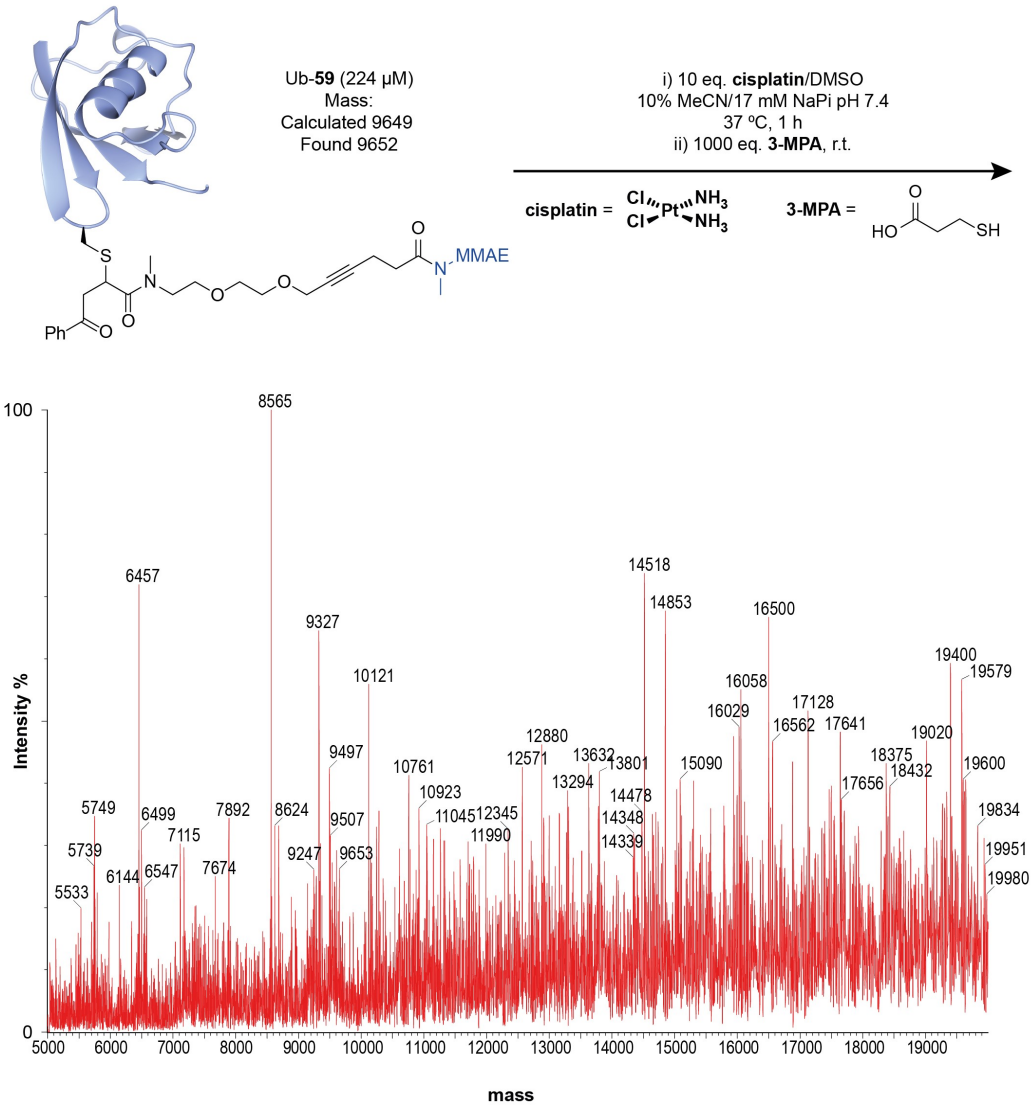

Figure 37: Unsuccessful decaging of conjugate Ub-**59** with cisplatin. The final DMSO concentration in the reaction was 1%.

The chaotic mass spectrum clearly indicated that the conditions of this experiment required further optimisation. While the mass of Ub can be seen (mass calculated 8562, found 8565) it is almost within the baseline of the spectrum. It was thought that the reaction would not be efficient enough to work with fewer than 10 equivalents of cisplatin, and therefore the equivalents of scavenger **3-MPA** were reduced to see if this had an effect on the mass spectrum (**Figure 38**).

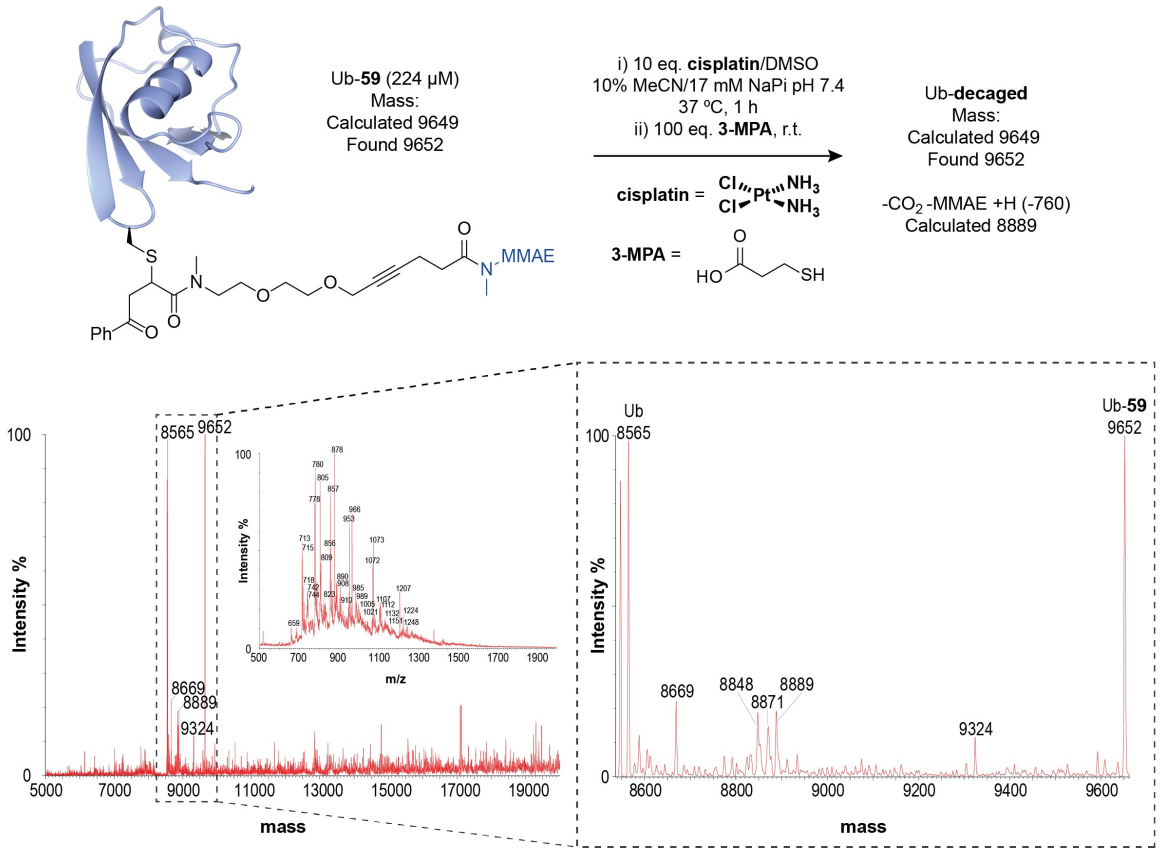

Figure 38: Successful decaging of conjugate Ub-**59** with cisplatin. The final DMSO concentration in the reaction was 1%.

Some evidence of decaging can be seen by MS, however masses of the products are unexpected. One should correspond to fragmentation of **MMAE** (mass 9324), whereas others should correspond to **MMAE** release followed by further reaction of the linker (mass 8848, 8871, 8889, **Figure 39**). Decarboxylation seems a particularly likely reaction to give the major products (mass calculated 8889, found 8889) as decarboxylation reactions are well known in the literature for gold complexes.[238–240] The peaks are not easily explained mechanistically but should correspond to further degradation of the linker (**Figure 39**).

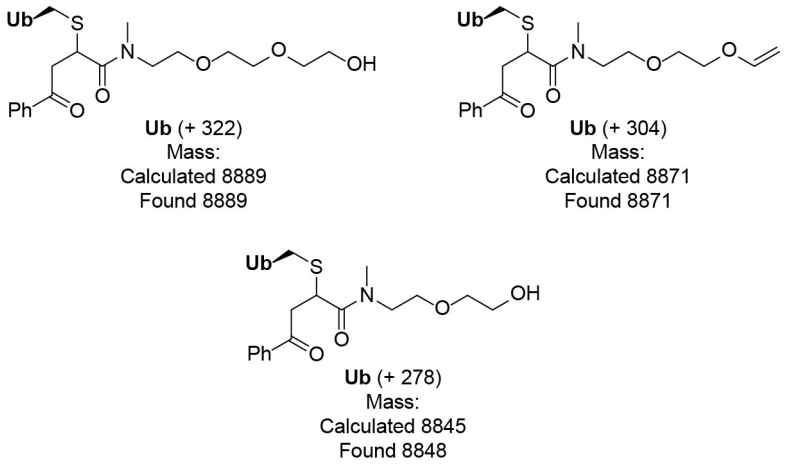

Figure 39: Potential explanations for product peaks observed after cisplatin decaging of conjugate Ub-**59**.

The mechanism as to how these compounds could form is unclear, and further decaging studies should be performed to investigate. Firstly, other platinum complexes such as $K_2Pt^{II}Cl_4$ and $K_2Pt^{IV}Cl_6$ should be reacted with conjugate Ub-**59** to see if the same products form. Small molecule analogues of Ub-**59** should also be synthesised to study the decaging by ^1H NMR, isolating all products for full characterisation. To see if conversion in the reaction between cisplatin and Ub-**59** could be increased, the reaction was allowed to progress for longer and also more equivalents of cisplatin were added (**Figure 40**).

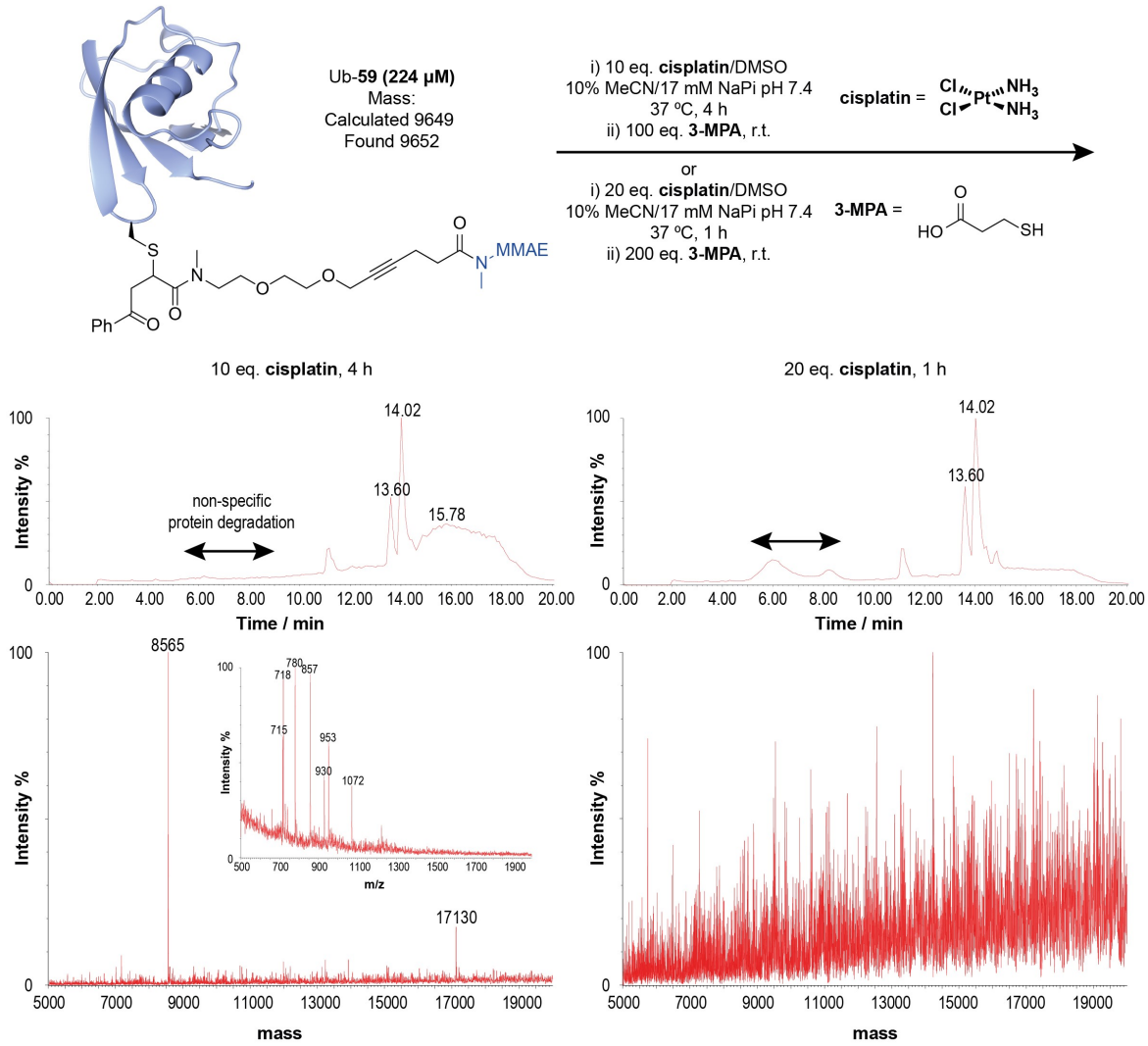

Figure 40: LC-MS analysis of attempted further optimisation of cisplatin mediated decaging of conjugate Ub-**59**.

Unfortunately, leaving the reaction with 10 equivalents for longer (4 h) appeared to result in protein degradation as evidenced by the decrease in protein peaks in the chromatogram. The mass spectrum appears to only show Ub and Ub dimer (Ub_2) which suggests that conjugate Ub-**59** degrades the fastest. After reaction of conjugate Ub-**59** with greater equivalents of cisplatin (20 eq.), protein peaks are still significant in the chromatogram. However integration of all protein peaks in the chromatogram leads to a mass spectrum in which no major protein peaks can be seen. This is likely due to non-specific binding of platinum to the proteins greatly reducing the intensity of any given species.

An IgG antibody was also selected for conjugation with acrylamide **59**. The F16* antibody[111,115,241] targets an alternatively spliced isoform of tenascin-C, a extracellular-matrix glycoprotein often overexpressed in tumours. As this is a non-internalising antibody, it was thought that this could later allow application to a solid-tumour model to test cisplatin mediated drug decaging. The F16* antibody

is a full IgG, but all interchain disulfide cysteines in the heavy chain have been mutated to serines. This leaves one reactive interchain disulfide cysteine per light chain (**Figure 41**).

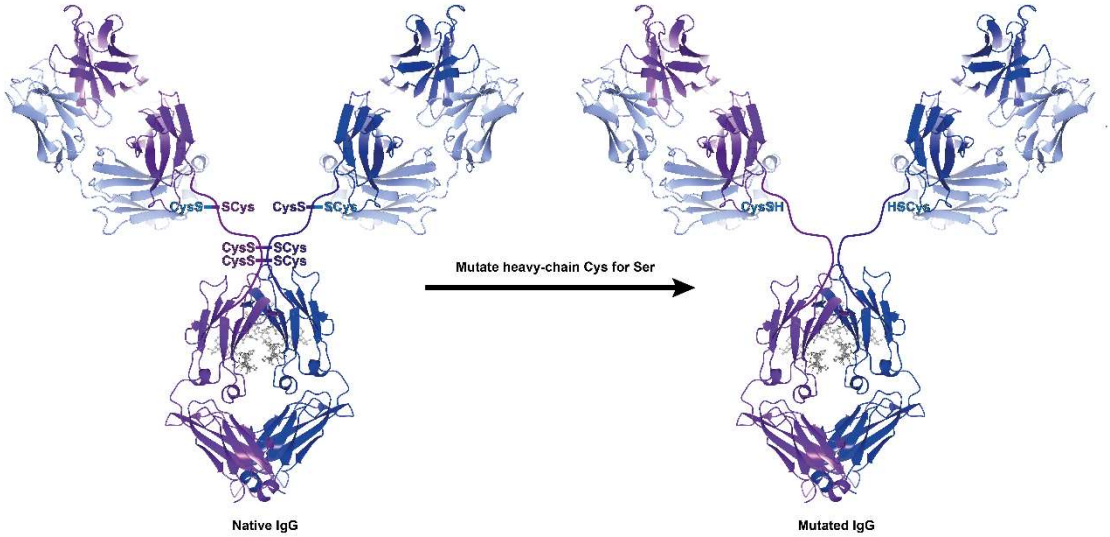

Figure 41: Native IgG antibody compared to mutated IgG antibody F16*, kindly provided by the group of Prof Dario Neri. Heavy chains are highlighted in **dark blue** and **purple**, light chains in light blue and glycosylation in **grey**.

The reduced F16* antibody can therefore easily be reacted with electrophiles to produce an ADC with a DAR of 2. In this case, the fully reduced F16* antibody was reacted with 40 equivalents of acrylamide **59** (**Figure 42**).

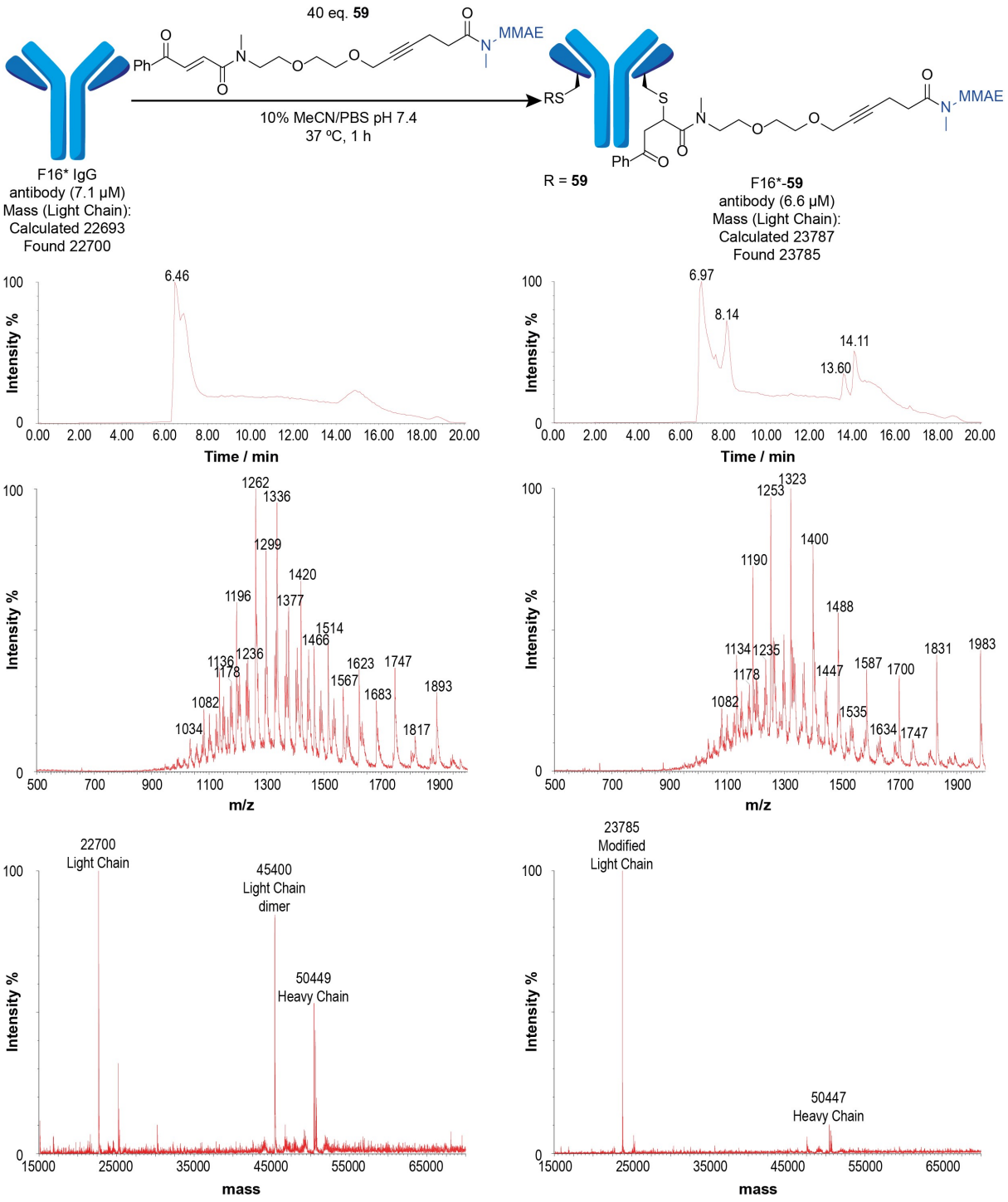

Figure 42: LC-MS analysis of the modification of IgG antibody F16* with acrylamide **59**. Samples of the reaction mixture were injected without further preparation and LC-MS run under denaturing conditions.

In the starting material (antibody F16*) the light chain (mass calculated 22693, found 22700) and the heavy chain are clearly visible. Interestingly, the dimer of the light chain is also visible from the formation of a light chain-light chain disulfide. After reaction with 40 equivalents of acrylamide **59** for 1 hour there is full conversion to the product F16***-59** (mass calculated 23787, found 23785) and negligible quantities of light chain dimer. Small molecule peaks in the chromatogram derived from

acrylamide **59** can be seen at 13.60 and 14.11 min of the reaction mixture. Dialysis of the reaction mixture was performed (**Figure 43**) using a dialysis device with a 3 kDa molecular weight cut-off. This allows small molecules of less than 3 kDa to diffuse across the membrane into a buffer solution while retaining the antibody.

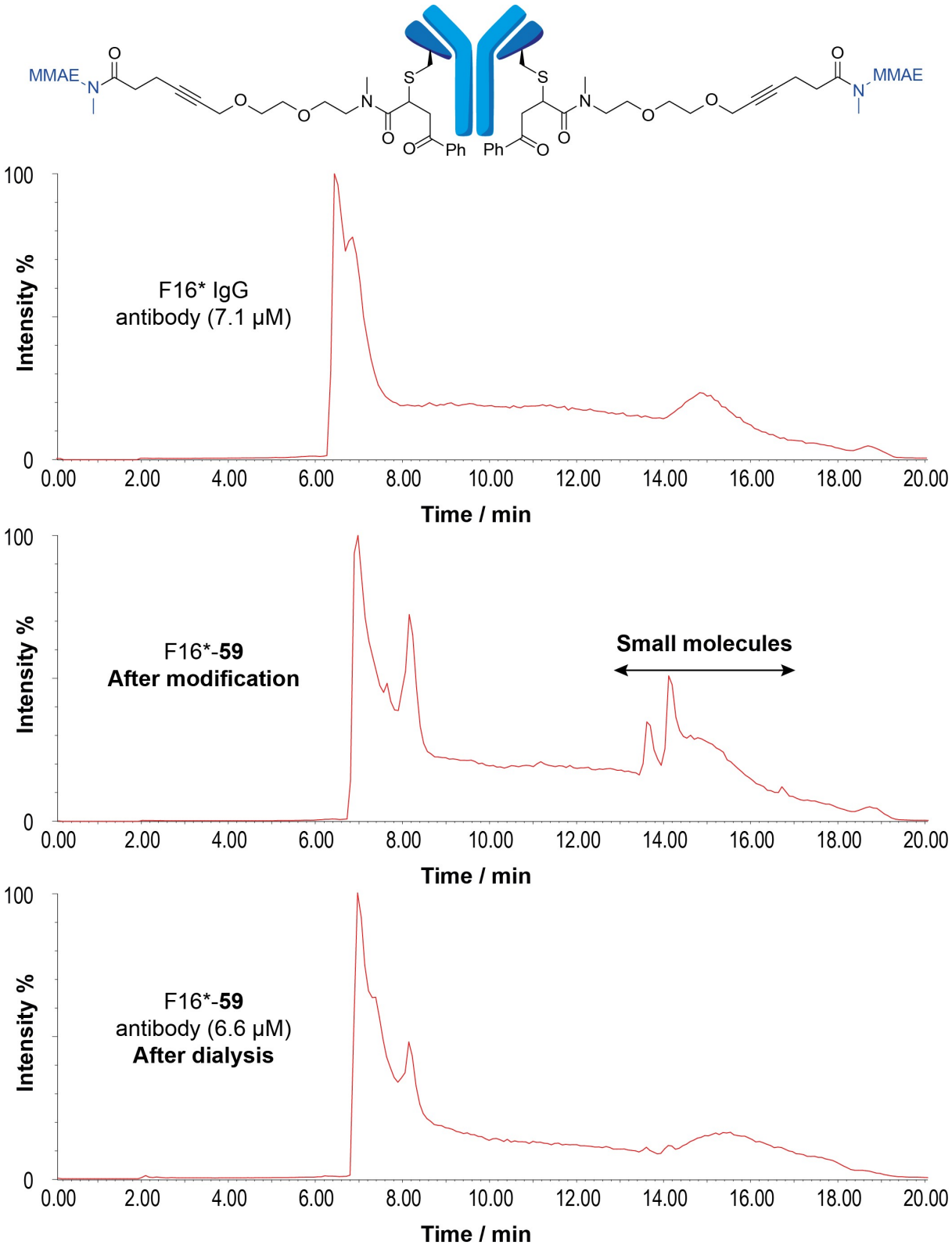

Figure 43: Chromatograms of F16* IgG antibody, crude reaction mixture of F16***-59** and purified F16***-59** after dialysis with a Slide-A-Lyzer™ MINI Dialysis Device into PBS (3 x).

The chromatograms show a decrease in the presence of small molecules to negligible levels after dialysis of the reaction mixture. This is important as any biological evaluation of the non-internalising,

cisplatin cleavable ADC would be effected by the presence of any **MMAE**-containing small molecules. With this purified ADC in hand, these biological studies will be performed first in cell culture with cancer cell lines, and then perhaps in mice.

4.3 Conclusions and Future Work

In this project, we have taken the concept of a cisplatin-mediated decaging reaction, developed mechanistic hypotheses as to how this may work, and successfully developed these hypotheses into decaging reactions that function with prodrugs in cell culture, as well as enabling the synthesis of a platinum-cleavable ADC. While our original mechanistic hypothesis of an acid-to-alkyne cyclisation was incorrect, careful study allowed this false-positive result to be turned into a functioning reaction that offers many advantages over other bioorthogonal decaging reactions. In order to fully understand the reaction, further study will be required as to the fate of the alkyne-bearing protecting groups after cleavage to ensure that they are non-toxic. The simplest method to achieve this would be to derivatise the terminal alkynes to make them non-volatile, and isolate any products after decaging. To further study platinum-cleavable linkers, Ub-**59** should be treated with platinum complexes such as $K_2Pt_2Cl_4$ and $K_2Pt_2Cl_6$ to see if their greater reactivity allows the detection of **MMAE** and protein degradation products by LC-MS. The ADC F16*-**59** should also be fully analysed by native MS as well as analytical size-exclusion chromatography to ensure that it is a single species and that bioconjugation does not result in excessive aggregation.

As cisplatin is known to accumulate in tumours it would also be interesting to see if this accumulated cisplatin could be used to cause drug decaging. For this, a 3D model of tumours would be necessary. In a collaboration with the Godinho Ferreira lab, patient derived samples of tumours will be implanted into Zebrafish embryos where they continue to grow for a short time.[242] First the Zebrafish will be incubated with cisplatin solutions to cause platinum accumulation in the tumour. The fish could then be washed, and incubated with **pFU** (**51**) to see if this then causes more tumour shrinkage than if the fish had just been incubated with cisplatin or **pFU** (**51**) alone (**Figure 44**). While this is very different from the final goal of non-internalising cisplatin-cleavable ADCs, it will tell us whether or not platinum mediated chemistry of cisplatin is feasible in a solid tumour with residual accumulated platinum.

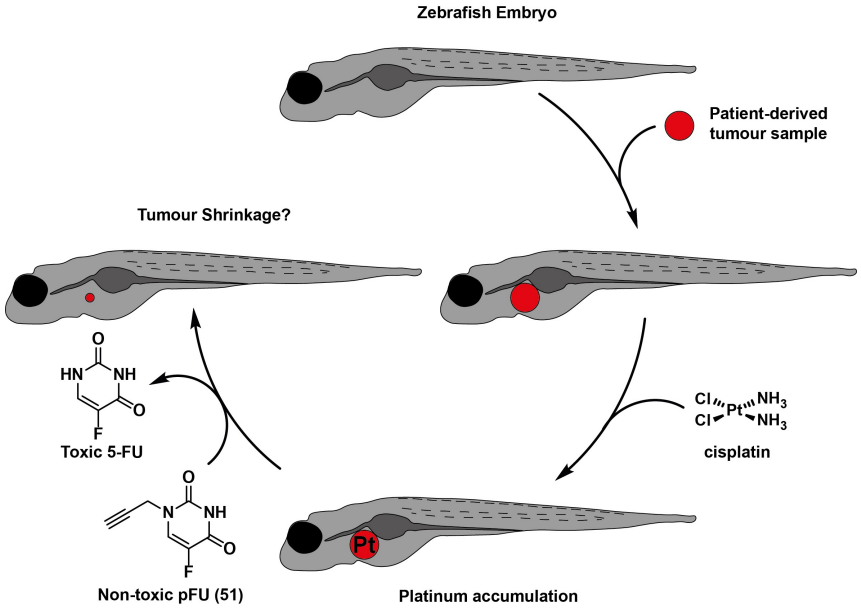

Figure 44: Proposed Zebrafish studies to be carried out in the lab of Dr Miguel Godinho Ferreira by Dr João Diogo Osório de Castro Conde.

Finally with the pure conjugate F16*-**59**, cancer cell cultures such as HeLa can be grown and first incubated with the ADC. Afterwards platinum complexes can be added to the culture to see if cell killing occurs. This would indicate that drug release is possible from an ADC in cell culture. Cellular studies with the F16* ADCs are not known in the literature and typically only mouse models are used. However it would still be useful to see whether or not drug release and cell killing can be induced from F16*-**59** in cell culture, as if F16*-**59** has low toxicity it would indicate that it is not being digested. It would also be interesting to see it would be possible to incubate cancerous cells with the ADC, wash out the excess ADC and then cause decaging with platinum complexes. This would indicate that drugs delivered to the close environment of cancerous cells can be much more efficacious than those in solution, and help elucidate whether a cisplatin cleavable ADC could be a therapeutic option in cancer. If these cellular decaging experiments seem promising, then tumour-xenograft models in mice will be performed. Firstly mice bearing tumours will be treated with the ADC F16*-**59**. Once the ADC F16*-**59** has accumulated to the maximum possible at its target site, cisplatin will be infused to see if this causes drug release and tumour shrinkage. In a second experiment, mice bearing tumours will be treated with cisplatin so that platinum complexes accumulate in the tumour. Afterwards the ADC F16*-**59** will be infused, and it will be interesting to see if the residual platinum complexes will be sufficient to cause significant decaging from an ADC and tumour shrinkage.

Chapter 5:

Experimental (Appendix)

5.1 General Experimental Details

Solvents, Reagents and Materials

All reactions were carried out under a positive pressure of argon dried over $CaCl_2$ unless otherwise stated. Oven dried glassware was heated to 140 °C and cooled under high vacuum. All reagents were purchased from commercial sources and were used as received. Distilled MeCN, DCM, MeOH, Et_2O and toluene were freshly distilled over CaH_2 under an atmosphere of argon. Distilled THF was pre-dried over CaH_2 and then distilled over $LiAlH_4$/Ph_3CH. Dry DMF was obtained from commercial sources and used directly. DIPEA and TEA were distilled over CaH_2 and stored under argon over 4 Å mol. sieves. Unless otherwise stated, water for HPLC or LC-MS was HPLC grade and water for synthesis was deionised. Flash column chromatography was performed on Material Harvest 60 Å silica and preparative TLC was performed on Merck PLC 60 F_{254} plates. Analytical TLC was visualized by UV at 254 nm, ninhydrin or $KMnO_4$ stain as appropriate.

Characterisation

IR spectrometry was carried out on a Perkin Elmer Spectrum One ATR FT-IR and melting points on a Stanford Research Systems OptiMelt. NMR spectra were recorded on Bruker 400-AVIII, DPX-400 or 500-AVIII HD Smart Probe as appropriate. The residual solvent peaks were used as an internal reference for chemical shift (^{1}H NMR $CHCl_3$ δ 7.27 ppm, DMSO δ 2.50 ppm, D_2O δ 4.79 ppm, MeOD δ 3.31 ppm; ^{13}C NMR $CDCl_3$ δ 77.0 ppm, DMSO δ 39.5 ppm). Data are presented as follows: chemical shift (ppm), multiplicity (br. = broad, s = singlet, d = doublet, t = triplet, q = quartet, hept = heptet, m = multiplet), coupling constant *J*, and integration. High resolution mass spectra were obtained with a Thermo Fischer Orbitrap or Waters Xevo LC-MS and ionized by electrospray (ESI). Absorbance and fluorescence spectra or endpoints were measured in a BMG Clariostar in Greiner 300 μL 96-well, U-bottom, clear polypropylene plates.

General method of fluorescence assay for decaging optimisation

200 μM solutions of 7-amino-4-methylcoumarin (**8**) (fluorophore) and caged-fluorophore derivatives were prepared in 10% deionised H_2O/DMF (v/v). Solutions of palladium catalysts were prepared to give twice their desired final concentration [Pd] in 10% deionised H_2O/DMF (v/v). 50 μL aliquots of caged fluorophore solutions were pipetted into a 96-well plate, and diluted with either 50 μL solvent or 50 μL palladium catalyst solution. Reaction progress was monitored at 23 °C by the fluorescence of 7-amino-4-methylcoumarin: λ_{abs} (max) 352 nm, λ_{em} (max) 415 nm, bandwidth 8 nm. The gain and focus

of the plate reader were automatically adjusted before each assay based on 100 µM 7-amino-4-methyl coumarin. All reactions were performed in triplicate.

General method of NMR screening for gold and platinum decaging optimisation

Amides or carbamates (~10 mg) were dissolved in MeOD (0.2 mL), and gold or platinum complexes dissolved in D_2O (0.6 mL). Sonication was required for complexes with limited aqueous solubility such as cisplatin. The solution of gold or platinum complex was then added to the solution of amide or carbamate and this marked as time t = 0 min. The reactions were monitored at various timepoints as well as after overnight reaction. After overnight reaction the conversion remains constant as the gold and platinum complexes have decomposed. All reactions were performed in air at room temperature.

Cell Studies

HEK (ATCC® CRL-1573™), MCF-7 (ATCC® HTB-22™) and HeLa (HeLa ATCC® CCL-2™) cells, kindly provided by the David Klenerman (Department of Chemistry, University of Cambridge, UK), Maria Mota (Instituto de Medicina Molecular, João Lobo Antunes, Portugal) and Shankar Balasubramanian (Department of Chemistry, University of Cambridge UK) groups respectively, were grown in a humidified incubator at 37 °C under 5% CO2 with 90% humidity, and split at approximately 80% confluence using Trypsin-EDTA solution 0.25%. HEK cells were grown in DMEM supplemented with heat-inactivated FBS, 100 units/mL penicillin, 100 µg/mL streptomycin and 0.25 µg/mL amphotericin B. MCF-7 and HeLa cells were grown in high glucose DMEM (+ pyruvate) supplemented with 10% heat-inactivated FBS, 100 units/mL penicillin and 100 µg/mL streptomycin, 1% non-essential amino acids, 2 mM GlutaMax™ and 10 mM HEPES. Cell viability experiments with MCF-7 and HeLa cells were performed without the presence of HEPES. All cell lines were grown to 80% confluency before seeding in 200 µL at 5000 (HEK), 3000 (MCF-7) and 5000 (HeLa) cells/well into a Corning Costar 96-well clear, flat bottom plate. AlamarBlue assays to determine toxicity were performed by adding 20 µL AlamarBlue solution to each well, and incubating (4 h for HEK cells, 6 h for MCF-7 and 6 h for HeLa). Determination of cell viability was as per supplier's guidelines. Briefly, for HEK and MCF-7 studies fluorescence was then measured at λ_{ex} 530-560 nm and λ_{em} 590 nm. The residual fluorescence of AlamarBlue in cell media was subtracted from each well as a background. Cell viability was calculated as 100 x F_{cells} / F_{DMSO}, where F is the fluorescence of a given well, cells refers to treated cells being studied and DMSO refers to a 1% DMSO control defined as 100% viable. For HeLa studies, absorbance was measured at 570 nm and 600 nm. The residual absorbance of cell media at 570 nm and 600 nm was subtracted from each well as a background. Cell viability was calculated as 100 x $(\varepsilon_{600\,nm} \cdot A_{570\,nm} - \varepsilon_{570\,nm} \cdot A_{600\,nm})_{cells}$ / $(\varepsilon_{600\,nm} \cdot A_{570\,nm} - \varepsilon_{570\,nm} \cdot A_{600\,nm})_{DMSO}$. All experiments were performed in triplicate.

ε refers to the molar extinction coefficient at the given wavelength, A refers to the absorbance of a well at the given wavelength, cells refers to treated cells and DMSO refers to a 1% DMSO control defined as 100% viable.

HPLC

HPLC was performed on a HPLC: Agilent Technologies 1100 Series G1313A system with a semi-preparative ColumnL YMC-Pack Pro C18, 250 x 10 mm L.D., S-5 µm, 12 nm, AS12S05-2510WT. Crude product was dissolved in 1:1 MeCN/H_2O and sterile filtered at 0.2 µm with EMD Millipore™ polyethersulfone syringe filters. 100 µL crude product aliquots were injected into the column and flow was maintained at 3.000 mL min^{-1} with solvent mixtures of MeCN/H_2O + 0.1% TFA. UV-vis absorbance was monitored at 254 nm to indicate when to begin manual collection of fractions. MeCN was evaporated from the fractions under a flow of compressed air, and the remaining H_2O/TFA solution flash frozen in liquid nitrogen then lyophilised.

LC-MS method for analysis of protein conjugation

For Chapter 3:

LC-MS was performed on a Xevo G2-S TOF mass spectrometer coupled to an Acquity UPLC system using an Acquity UPLC BEH300 C4 column (1.7 µm, 2.1% 50 mm). Solvents A (H_2O with 0.1% formic acid) and B (71% acetonitrile, 29% H_2O, and 0.1% formic acid) were used as the mobile phase at a flow rate of 0.2 mL min^{-1}. The gradient used was: 0-25 min 72% A/B-100% B, 25-27 min 100% B, 27-45 min 72% A/B. The electrospray source was operated with a capillary voltage of 2.0 kV and a cone voltage of 40 V. Nitrogen was used as the desolvation gas at a total flow of 850 L h^{-1}. Total mass spectra were reconstructed from the ion series using the MaxEnt algorithm preinstalled on MassLynx software (version 4.1 from Waters) according to the manufacturer's instructions. To obtain the ion series described, the major peak(s) of the chromatogram were selected for integration and further analysis.

For Chapter 4:

LC-MS was performed on a Waters Acquiry UPLC system equipped with a single quadrupole mass detector using an Acquity UPLC protein BEH C4 column, 300 Å, (1.7 mm, 2.1 × 50 mm). Solvents A (H_2O with 0.01% formic acid) and B (71% MeCN, 29% H_2O and 0.075% formic acid) were used as the mobile phase at a flow rate of 0.2 mL min^{-1}. The gradient used was: 0-12 min 28-71.2% A/B, 12-13 min 71.2-100% A/B, 13-16 min 100% A/B, 16-16.5 min 100%-28% A/B, 16.5-20 min 28% A/B. The electrospray source was operated with a capillary voltage of 3.0 kV and a cone voltage of 20 V. Nitrogen was used as the desolvation gas at a total flow of 800 L h^{-1} with cone volume at 1 L h^{-1}. Desolvation temperature

was set to 400 °C. Total mass spectra were reconstructed from the ion series using the MaxEnt algorithm preinstalled on MassLynx software (version 4.1 from Waters) according to the manufacturer's instructions. To obtain the ion series described, the major protein peak(s) of the chromatogram were selected for integration and further analysis.

Protein sequences

2Rb17c^{205} (Calculated mass: 14861.46)

EVQLQESGGG LVQPGGSLRL SCAASGFIFS NDAMTWVRQA PGKGLEWVSS INWSGTHTNY ADSVKGRFTI SRDNAKRTLY LQMNSLKDED TALYYCVTGY GVTKTPTGQG TQVTVSSHHH HHHSPSTPPT PSPSTPP**C**

Ubiquitin K63C (Calculated mass: 8566.77)

SAQIFVKTLT GKTITLEVEP SDTIENVKAK IQDKEGIPPD QQRLIFAGKQ LEDGRTLSDY NIQ**C**ESTLHL VLRLRGG

F16*^{115}

Light Chain (Calculated mass: 22693.2)

SSELTQDPAV SVALGQTVRI TCQGDSLRSY YASWYQQKPG QAPVLVIYGK NNRPSGIPDR FSGSSSGNTA SLTITGAQAE DEADYYCNSS VYTMPPVVFG GGTKLTVLGQ PKAAPSVTLF PPSSEELQAN KATLVCLISD FYPGAVTVAW KADSSPVKAG VETTTPSKQS NNKYAASSYL SLTPEQWKSH KSYSCQVTHE GSTVEKTVAP TE**C**S

Heavy Chain (Calculated mass: 48489.5)

EVQLLESGGG LVQPGGSLRL SCAASGFTFS RYGMSWVRQA PGKGLEWVSA ISGSGGSTYY ADSVKGRFTI SRDNSKNTLY LQMNSLRAED TAVYYCAKAH NAFDYWGQGT LVTVSSASTK GPSVFPLAPS SKSTSGGTAA LGCLVKDYFP EPVTVSWNSG ALTSGVHTFP AVLQSSGLYS LSSVVTVPSS SLGTQTYICN VNHKPSNTKV DKKVEPKSSD KTHTSPPSPA PELLGGPSVF LFPPKPKDTL MISRTPEVTC VVVDVSHEDP EVKFNWYVDG VEVHNAKTKP REEQYNSTYR VVSVLTVLHQ DWLNGKEYKC KVSNKALPAP IEKTISKAKG QPREPQVYTL PPSRDELTKN QVSLTCLVKG FYPSDIAVEW ESNGQPENNY KTTPPVLDSD GSFFLYSKLT VDKSRWQQGN VFSCSVMHEA LHNHYTQKSL SLSPGK

5.2 Synthetic Procedures for Chapter 3

Propargyl (7-amino-4-methylcoumarin)carbamate (7)

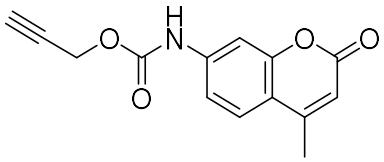

7-amino-4-methylcoumarin (**8**) (50 mg, 1 eq., 0.285 mmol) was dissolved in dry DMF (1.5 mL) in an oven dried flask. K_2CO_3 (118 mg, 1.5 eq., 0.428 mmol) was added and the solution chilled to 0 ˚C. Propargyl chloroformate (0.04 mL, 1.5 eq., 0.428 mmol) was then added dropwise and the reaction stirred for 30 min before pouring over icewater (25 mL). The precipitate was filtered and washed with icewater (4 x 3 mL) then EtOH (3 x 3 mL) to give the desired product a yellow solid (22 mg, 0.0855 mmol, 30%). The product was used without further purification. The data were in accordance with literature.[181]

^{1}H NMR (400 MHz, DMSO-d_6) δ 10.36 (br. s, 1H; N*H*), 7.71 (d, J = 8.56 Hz, 1H; $H_{aromatic(5)}$), 7.49 - 7.57 (m, 1H; $H_{aromatic(8)}$), 7.41 (d, J = 8.56 Hz, 1H; $H_{aromatic(6)}$), 6.25 (s, 1H; $H_{aromatic(3)}$), 4.82 (s, 2H; OCH_2), 3.57 - 3.64 (m, 1H; C≡C*H*), 2.39 (s, 3H; CH_3)

7-Isocyanato-4-methylcoumarin (8a)

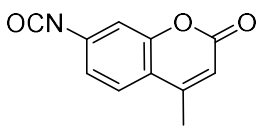

7-amino-4-methylcoumarin (**8**) (100 mg, 1 eq., 0.570 mmol) and triphosgene (85 mg, 0.5 eq., 0.285 mmol) were dissolved in freshly distilled toluene (20 mL) and refluxed for 0.5 h in oven dried glassware. The reaction mixture was then evaporated *in vacuo* to give the desired product which was used without further purification.

^{1}H NMR (400 MHz, DMSO-d_6) δ 7.41 (d, *J* = 8.56 Hz, 1H; H_5), 6.57 (dd, *J* = 1.47, 8.56 Hz, 1H; H_6), 6.41 (d, *J* = 1.47 Hz, 1H; H_8), 5.90 (s, 1H; H_3), 2.30 (s, 3H; CH_3)

MS(ESI): calcd. for $C_{11}H_8NO_3Na$ $[M+H]^+$ 202.0499, found 202.0492

Propargyl trityl thioether (9a)

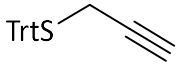

K_2CO_3 (750 mg, 3 eq., 5.43 mmol) was dried under high vacuum for 2 h before adding dry DMF (5 mL), followed by 80% propargyl bromide in toluene (0.6 mL, 3 eq., 5.43 mmol). Triphenylmethane thiol (500 mg, 1 eq., 1.81 mmol) was then added in one portion at room temperature and the reaction stirred at room temperature for 6 h. The reaction was then diluted in Et_2O (80 mL) and washed with icewater (2 x 30 mL), then icewater/brine (30 mL). The organics were dried over $MgSO_4$, and evaporated *in vacuo* to give the desired product as a light yellow solid (457 mg, 1.45 mmol, 80%).

R_f (petrol) 0.19

m.p. 127.5-130.5 ˚C

IR (ATR) / cm^{-1}: 3299, 3065, 1593, 1485, 1441

^{1}H NMR (400 MHz, $CDCl_3$) δ 7.44 (d, *J* = 7.58 Hz, 6H; $H_{aromatic}$), 7.30 - 7.35 (m, 6H; $H_{aromatic}$), 7.23 - 7.29 (m, 3H; $H_{aromatic}$), 2.83 (d, *J* = 2.5 Hz, 2H; CH_2), 2.19 (t, *J* = 2.5 Hz, 1H; C≡C*H*)

^{13}C NMR (101 MHz, $CDCl_3$) δ 144.0, 129.5, 128.1, 126.8, 79.1, 71.8, 67.2, 20.2

MS(ESI): calcd. for $C_{22}H_{18}SNa$ $[M+Na]^+$ 337.1021, found 337.1033

4-(Tritylthio)but-2-yn-1-ol (9b)

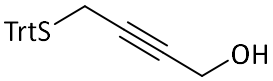

Propargyl trityl thioether (**9a**) (100 mg, 1 eq., 0.318 mmol) was added to an oven dried flask and dissolved in freshly distilled THF (5 mL). The solution was cooled to -78 ˚C before adding 2.5 M ^{n}BuLi in hexanes (0.14 mL, 1.1 eq., 0.350 mmol) dropwise. After 20 min stirring at -78 ˚C, $(CH_2O)_n$ (30 mg, 3 eq., 0.715 mmol) that had been previously dried under high vacuum overnight was added in one portion. After a further 20 min stirring, the reaction was warmed to room temperature and stirred for 4 h. The reaction mixture was poured over ice (30 mL) and extracted with EtOAc (2 x 50 mL). The organics were washed with icewater/brine (30 mL), dried over $MgSO_4$, filtered and evaporated. The crude material was purified by preparative TLC (2 mm, 25% EtOAc/petrol) to give the desired product as a yellow waxy solid (88 mg, 0.255 mmol, 80%).

R_f (25% EtOAc/petrol) 0.23

IR (ATR) / cm^{-1}: 3377, 3056, 2924, 1594, 1486, 1444

^{1}H NMR (400 MHz, $CDCl_3$) δ 7.46 (d, *J* = 7.7 Hz, 6H; $H_{aromatic}$), 7.34 (t, *J* = 7.7 Hz, 6H; $H_{aromatic}$), 7.23 - 7.29 (m, 3H; $H_{aromatic}$), 4.18 - 4.22 (m, 2H; SCH_2), 2.88 - 2.92 (m, 2H; CH_2O), 1.59 (br. s., 1H; O*H*)

^{13}C NMR (101 MHz, $CDCl_3$) δ 144.1, 129.6, 128.0, 126.9, 81.9, 81.2, 67.2, 51.2, 20.5

MS(ESI): calcd. for $C_{23}H_{20}O^{32}SNa$ $[M+Na]^+$ 367.1127, found 367.1129

4-(Tritylthio)but-2-ynl (7-amino-4-methylcoumarin)carbamate (9)

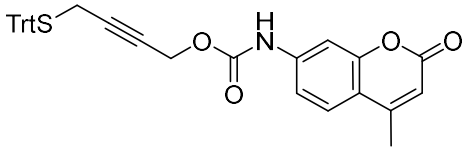

Isocyanate **8a** (57 mg, 1 eq., 0.283 mmol) and alcohol **9b** (98 mg, 1 eq., 0.283 mmol) were dissolved in freshly distilled THF (5 mL) at room temperature in an oven dried flask. Dibutyltin dilaurate (0.01 mL, 0.06 eq., 16.9 μmol) was added, and the reaction stirred for 1 h. The product was precipitated by dropwise addition of water (15 mL) and filtered. The precipitate was washed with MeOH (3 x 3 mL), Et_2O (3 x 3 mL) and petrol (3 x 3 mL), then dried *in vacuo* to give the desired product as an off-white powder (110 mg, 0.201 mmol, 71%).

m.p. 184.5-188.0 ˚C

IR (ATR) / cm^{-1}: 3278, 3084, 1739, 1697, 1625, 1591, 1531

^{1}H NMR (400 MHz, DMSO-d_6) δ 10.34 (s, 1H; N*H*), 7.71 (d, *J* = 8.60 Hz, 1H; H_5), 7.53 (d, *J* = 1.96 Hz, 1H; H_8), 7.41 (dd, *J* = 1.96, 8.60 Hz, 1H; H_6), 7.30 - 7.39 (m, 12H; $H_{aromatic}$), 7.23 - 7.29 (m, 3H; $H_{aromatic}$), 6.25 (s, 1H; H_3), 4.73 - 4.77 (m, 2H; OCH_2), 2.89 - 2.94 (m, 2H; SCH_2), 2.39 (s, 3H; CH_3)

^{13}C NMR (101 MHz, DMSO-d_6) δ 160.4, 154.3, 153.6, 152.9, 144.1, 142.9, 129.5, 128.6, 127.4, 126.6, 115.0, 114.7, 112.5, 105.0, 82.5, 78.7, 67.4, 53.1, 20.2, 18.5

MS(ESI): calcd. for $C_{34}H_{27}NO_4{}^{32}SNa$ $[M+Na]^+$ 568.1553, found 568.1549

tert-Butyl prop-2-yn-1-yl thioether (10a)

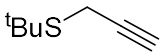

NaOH (106 mg, 1.2 eq., 2.66 mmol) was dissolved in MeOH (4.5 mL) before chilling to 0 ˚C and 80% propargyl bromide in toluene (0.37 mL, 1.5 eq., 3.33 mmol) was added. ^{t}BuSH (0.25 mL, 1 eq., 2.22 mmol) was then added in one portion and the reaction warmed to room temperature. After 3 h stirring, the reaction mixture was evaporated *in vacuo*, the residues diluted in water (30 mL) and extracted with DCM (3 x 20 mL). The organics were dried over $MgSO_4$ and evaporated *in vacuo* to give the desired product as a yellow oil (185 mg, 1.44 mmol, 65%). The data were in accordance with the literature.[243]

^{1}H NMR (400 MHz, $CDCl_3$) δ 3.26 (d, *J* = 2.74 Hz, 2H; C*H*$_2$), 2.17 (t, *J* = 2.65 Hz, 1H; C*H*), 1.37 (s, 9H (C*H*$_2$)$_3$)

4-(*tert*-Butylthio)but-2-yn-1-ol (10b)

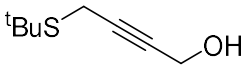

Alkyne **10a** (185 mg, 1 eq., 1.44 mmol) was dissolved in freshly distilled THF (10 mL) and chilled to -78 ˚C in an oven dried flask. 2.5 M ^{n}BuLi in hexanes (0.63 mL, 1.1 eq., 1.59 mmol) was then added dropwise. $(CH_2O)_n$ (65 mg, 1.5 eq., 2.16 mmol) was added after 10 min. The reaction was warmed to room temperature and stirred for 1 h before pouring over sat. aq. NH_4Cl (20 mL) and extracting with Et_2O (3 x 20 mL). The organics were dried over $MgSO_4$ and evaporated *in vacuo*. The crude material was purified by flash chromatography with 50% Et_2O/petrol on silica (26 g) to give the desired product as a light yellow oil (71 mg, 0.448 mmol, 31%). The data were in accordance with the literature.[244]

R_f (50% Et_2O/petrol) 0.31

^{1}H NMR (400 MHz, $CDCl_3$) δ 4.24 (t, *J* = 2.10 Hz, 2H; OC*H*$_2$), 3.30 (t, *J* = 2.10 Hz, 2H; SC*H*$_2$), 1.35 (s, 9H; (C*H*$_3$)$_3$)

4-(*tert*-Butylthio)but-2-yn-1-yl (7-amino-4-methylcoumarin)carbamate (10)

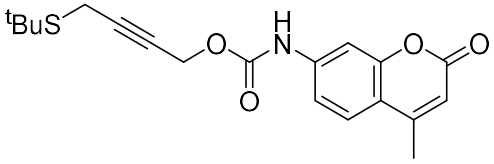

7-amino-4-methylcoumarin (**8**) (50 mg, 1 eq., 0.285 mmol) and triphosgene (42 mg, 0.5 eq., 0.143 mmol) were dissolved in freshly distilled toluene (10 mL) in and refluxed for 0.5 h in oven dried glassware before evaporating *in vacuo*. The crude isocyanate was then dissolved in freshly distilled THF (5 mL) at room temperature and alcohol **10b** (68 mg, 1.5 eq., 0.428 mmol) was added followed by dibutyltin dilaurate (0.01 mL, 0.06 eq., 20.4 µmol). After 1 h, the reaction was chilled to 0 ˚C and water (15 mL) was added dropwise to precipitate the product. The precipitate was filtered and washed with MeOH (3 mL), Et_2O (2 x 3 mL) and petrol (3 mL), then dried *in vacuo* to give the desired product as an off-white powder (34 mg, 0.0938 mmol, 33%).

m.p. 175.1-176.3 °C

IR (ATR) / cm^{-1}: 3263, 3058, 2963, 1721, 1686, 1620

^{1}H NMR (400 MHz, DMSO-d$_6$) δ 7.69 (d, *J* = 8.74 Hz, 1H; H_5), 7.52 (d, *J* = 2.06 Hz, 1H; H_8), 7.39 (dd, *J* = 2.06, 8.74 Hz, 1H; H_6), 6.24 (d, *J* = 1.28 Hz, 1H; H_3), 4.82 (t, *J* = 2.10 Hz, 2H; OCH_2), 3.44 (t, *J* = 2.10 Hz, 2H; SCH_2), 2.38 (d, *J* = 1.28 Hz, 3H; ArCH_3), 1.30 (s, 9H; (CH_3)$_3$)

^{13}C NMR (126 MHz, DMSO-d$_6$) δ 160.4, 154.3, 153.6, 153.0, 142.9, 126.5, 115.0, 114.7, 112.5, 105.0, 85.2, 77.0, 53.3, 43.5, 30.9, 18.5, 16.4

MS(ESI): calcd. for $C_{19}H_{21}NO_4SNa$ $[M+Na]^+$ 328.1084, found 328.1065

4-(Methylthio)but-2-yn-1-ol (24)

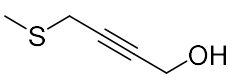

Sodium methanethiolate (500 mg, 1.5 eq., 7.13 mmol) was suspended in dry DMF (5 mL) in an oven dried flask, and chilled in a room temperature water bath. 80% propargyl bromide in toluene (0.53 mL, 1 eq., 4.76 mmol) was added dropwise, and the reaction stirred for 5 h. The reaction mixture was then poured over icewater basified to > pH 10 with sat. Na_2CO_3 solution (100 mL), and diluted with Et_2O (100 mL). The organics were washed with icewater basified to > pH 10 with sat. Na_2CO_3 solution (2 x

80 mL), then icewater/brine (50 mL), dried over $MgSO_4$ and then further dried over 4 Å mol. sieves. This solution was transferred *via* cannula to an oven dried flask, and then chilled to -78 ˚C. 2.5 M ^{n}BuLi in hexanes (2.85 mL, 1.5 eq., 7.13 mmol) was then added dropwise, and the reaction stirred for 10 min before $(CH_2O)_n$ (428 mg, 3.0 eq., 14.3 mmol) was added. The reaction was allowed to warm to room temperature and stirred for 1 h. The reaction mixture was washed with icewater (100 mL), and the aqueous layer was further extracted with Et_2O (100 mL). The organics were washed with brine (50 mL), dried over $MgSO_4$ and evaporated. The crude oil was purified by flash chromatography with 50% Et_2O/petrol on silica (49 g) to give the desired product as a malodorous, cloudy, viscous oil (146 mg, 1.25 mmol, 26%).

R_f (50% Et_2O/petrol) 0.26

^{1}H NMR (400 MHz, $CDCl_3$) δ 4.32 (s, 2H; OC*H*$_2$), 3.26 - 3.31 (m, 2H; SC*H*$_2$), 2.24 (s, 3H; C*H*$_3$)

^{13}C NMR (126 MHz, $CDCl_3$) δ 81.7, 81.0, 51.1, 21.7, 15.3

MS(ESI): calcd. for $C_5H_8O^{32}SNa$ $[M+Na]^+$ 139.0188, found 139.0188

4-(Methylthio)but-2-ynl (7-amino-4-methylcoumarin)carbamate (11)

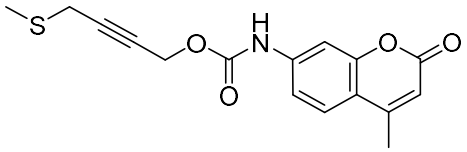

Isocyanate **8a** (40 mg, 1 eq., 0.199 mmol) and alcohol **24** (29 mg, 1.26 eq., 0.251 mmol) were dissolved in freshly distilled THF (5 mL) at room temperature. Dibutyltin dilaurate (0.01 mL, 0.08 eq., 17.4 μmol) was added, and the reaction stirred for 1 h. The reaction mixture was evaporated to ~¾ its volume, and the product precipitated by dropwise addition of water (4 mL). The precipitate was washed with water (4 x 3 mL), MeOH (3 x 3 mL), Et_2O (3 x 3 mL) and petrol (3 x 3 mL), then dried *in vacuo* to give the desired product as a white powder (38 mg, 0.121 mmol, 61%).

Decomp. 208 ˚C

IR (ATR) / cm^{-1}: 3276, 3172, 3100, 1738, 1687, 1627, 1593, 1534

^{1}H NMR (400 MHz, DMSO-d_6) δ 10.37 (br. s, 1H; N*H*), 7.71 (d, *J* = 8.51 Hz, 1H; *H*$_5$), 7.53 (d, *J* = 1.36 Hz, 1H; *H*$_8$), 7.41 (dd, *J* = 1.36, 8.51 Hz, 1H; *H*$_6$), 6.25 (s, 1H; *H*$_3$), 4.85 - 4.88 (m, 2H; OC*H*$_2$), 3.41 - 3.44 (m, 2H; SC*H*$_2$), 2.39 (s, 3H; C*H*$_3$), 2.16 (s, 3H; SC*H*$_3$)

^{13}C NMR (101 MHz, DMSO-d_6) δ 160.5, 154.3, 153.6, 152.9, 142.8, 126.5, 115.0, 114.7, 112.5, 105.0, 83.8, 77.6, 53.3, 20.9, 18.5, 15.0

MS(ESI): calcd. for $C_{16}H_{15}NO_4{}^{32}SNa$ $[M+Na]^+$ 340.0614, found 340.0598

4-(Dimethylamino)but-2-yn-1-ol (12a)

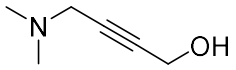

A solution of 2.5 M ^{n}BuLi in hexanes (1.17 mL, 1.2 eq., 2.92 mmol) in freshly distilled THF (12 mL) was chilled to -78 ˚C in an oven dried flask, and 3-dimethylamino-1-propyne (0.26 mL, 1 eq., 2.44 mmol) added dropwise. After 1 h, $(CH_2O)_n$ (146 mg, 2 eq., 4.88 mmol) was added in one portion and the reaction allowed to warm to room temperature. After 1 h, the reaction was quenched with brine (20 mL) and extracted with EtOAc (3 x 20 mL). The organics were dried over $MgSO_4$ and evaporated *in vacuo* to give the desired product as a yellow oil (219 mg, 1.93 mmol, 80%). The data were in accordance with the literature.[245]

^{1}H NMR (400 MHz, $CDCl_3$) δ 4.27 (t, *J* = 2.15 Hz, 2H; OC*H*$_2$), 3.25 (t, *J* = 2.15 Hz, 2H; NC*H*$_2$), 2.29 (s, 6H; C*H*$_3$)

4-(Dimethylamino)but-2-ynl (7-amino-4-methylcoumarin)carbamate (12)

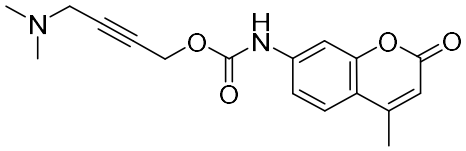

7-amino-4-methylcoumarin (**8**) (60 mg, 1 eq., 0.339 mmol) and triphosgene (50 mg, 0.5 eq., 0.169 mmol) were dissolved in freshly distilled toluene (10 mL) and refluxed for 0.5 h in oven dried glassware before evaporating *in vacuo*. The crude isocyanate was then suspended in freshly distilled THF (5 mL) at room temperature and alcohol **12a** (57 mg, 1.5 eq., 0.508 mmol) was added followed by dibutyltin dilaurate (0.01 mL, 0.06 eq., 20.4 μmol). After 1 h, the product was precipitated by the dropwise addition of water (10 mL), chilling to 0 ˚C, and dropwise addition of Na_2CO_3 until pH 10. Futher water (5 mL) was added dropwise and the suspension stirred for 10 min. The precipitate was filtered and washed with MeOH (3 mL), Et_2O (2 x 3 mL) and petrol (3 mL), then dried *in vacuo* to give the desired product as an off-white powder (37 mg, 0.117 mmol, 35%).

Decomp. 178 ˚C

IR (ATR) / cm^{-1}: 3277, 2954, 2931, 2856, 1736,, 1687, 1624, 1591, 1530

^{1}H NMR (500 MHz, DMSO-d_6) δ 7.71 (d, *J* = 8.78 Hz, 1H; H_5), 7.54 (d, *J* = 1.91 Hz, 1H; H_8), 7.41 (dd, *J* = 1.91, 8.78 Hz, 1H; H_6), 6.25 (s, 1H; H_3), 4.85 - 4.88 (m, 2H; OCH_2), 3.25 - 3.30 (m, 2H; NCH_2), 2.39 (s, 3H; CH_3), 2.17 (s, 6H; N(CH_3)$_2$)

^{13}C NMR (126 MHz, DMSO-d_6) δ 160.5, 154.3, 153.6, 153.0, 143.0, 126.6, 115.0, 114.8, 112.5, 105.0, 82.9, 80.1, 53.2, 47.6, 44.1, 18.5

MS(ESI): calcd. for $C_{15}H_{20}N_2O_4Na$ $[M+Na]^+$ 315.1215, found 315.1322

Propargyl trityl ether (13a)

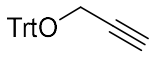

Propargyl alcohol (1.75 mL, 1 eq., 30.0 mmol) was dissolved in distilled DCM (15 mL) with 4 Å mol. sieves. DMAP (73 mg, 0.02 eq., 0.600 mmol) and pyridine (2.45 mL, 1.01 eq., 30.0 mmol) were added, followed by triphenylmethyl chloride (9.2 g, 1.1 eq., 33.0 mmol) in one portion and the reaction stirred at room temperature for 18 h. The reaction was then poured onto ice (200 mL) and then acidified to < pH 2 with 3 M HCl. The aqueous mixture was then extracted with EtOAc (3 x 150 mL). The organics were washed with icewater/brine (200 mL), dried over $MgSO_4$ and evaporated *in vacuo*. The crude material was dry-loaded onto silica (30 g) with EtOAc, and purified by flash chromatography with a gradient of 1-5% Et_2O/petrol, on silica (188 g) to give the product as a white powder (4.04 g, 13.5 mmol, 45%). The data were in accordance with literature.[246]

4-(Trityloxy)but-2-yn-1-ol (13b)

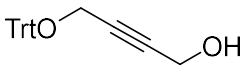

Propargyl trityl ether (**13a**) (2.0 g, 1 eq., 6.70 mmol) and $(CH_2O)_n$ (604 mg, 3 eq., 20.1 mmol) were dried separately under high vacuum overnight, before dissolving **13a** in distilled THF (40 mL) and chilling the solution to -78 ˚C in an oven dried flask. 2.5 M ^{n}BuLi in hexanes (2.95 mL, 1.1 eq., 7.37 mmol) was then added dropwise, and the reaction stirred at -78 ˚C for 10 mins. $(CH_2O)_n$ was then added in one portion, and the reaction stirred for 2 h before warming to room temperature and stirring for a further 1 h. The

reaction was poured over ice (100 mL) and extracted with EtOAc (3 x 100 mL). The organics were washed with icewater/brine (50 mL), dried over $MgSO_4$ and evaporated *in vacuo*. The crude material was dry-loaded onto silica (10 g) and purified by flash chromatography with 30% EtOAc/petrol on silica (193 g) to give product as a white powder (1.71 g, 5.23 mmol, 78%). The data were in accordance with literature.[247]

^{1}H NMR (400 MHz, $CDCl_3$) δ 7.51 (d, *J* = 7.5 Hz, 6H; $H_{aromatic}$), 7.35 (t, *J* = 7.5 Hz, 6H; $H_{aromatic}$), 7.28 (t, *J* = 7.09 Hz, 3H; $H_{aromatic}$), 4.29 (s, 2H; CH_2), 3.87 (s, 2H; CH_2)

4-(Trityloxy)but-2-ynl (7-amino-4-methylcoumarin)carbamate (13)

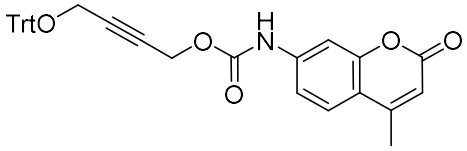

Isocyanate **8a** (40 mg, 1 eq., 0.199 mmol) and alcohol **13b** (72 mg, 1.1 eq., 0.219 mmol) were dissolved in freshly distilled THF (5 mL) at room temperature in an oven dried flask. Dibutyltin dilaurate (0.01 mL, 0.08 eq., 16.9 μmol) was added, and the reaction stirred for 1 h. The product was precipitated by dropwise addition of water (15 mL) and filtered. The precipitate was washed with MeOH (3 x 3 mL), Et_2O (3 x 3 mL) and petrol (3 x 3 mL), then dried *in vacuo* to give the desired product as a white powder (77 mg, 0.145 mmol, 73%).

m.p. 192.1-194.9 ˚C

IR (ATR) / cm^{-1}: 3281, 1734, 1697, 1619, 1582, 1534

^{1}H NMR (400 MHz, DMSO-d_6) δ 10.38 (s, 1H; N*H*), 7.71 (d, *J* = 8.86 Hz, 1H; H_5), 7.55 (d, *J* = 1.70 Hz, 1H; H_8), 7.42 (dd, *J* = 1.70, 8.86 Hz, 1H; H_6), 7.33 - 7.40 (m, 12H; $H_{aromatic}$), 7.24 - 7.32 (m, 3H; $H_{aromatic}$), 6.25 (s, 2H; H_3), 4.84 - 4.87 (m, 2H; OCH_2), 3.77 - 3.80 (m, 2H; OCH_2), 2.39 (s, 3H; CH_3)

^{13}C NMR (101 MHz, DMSO-d_6) δ 160.4, 154.3, 153.6, 152.9, 143.5, 142.9, 128.5, 127.7, 126.6, 115.0, 114.7, 112.5, 105.0, 87.4, 83.6, 80.8, 67.5, 53.0, 25.6, 18.5

MS(ESI): calcd. for $C_{34}H_{27}NO_5Na$ $[M+Na]^+$ 552.1781, found 552.1763

4-Methoxybut-2-yn-1-ol (25)

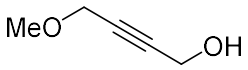

Methyl propargyl ether (0.85 mL, 1 eq., 10.0 mmol) was dissolved in freshly distilled THF (30 mL) in an oven dried flask. The solution was cooled to 0 ˚C, and 2.5 M ^{n}BuLi in hexanes (4.4 mL, 1.1 eq., 11.0 mmol) was added dropwise. The reaction was stirred for 30 min at 0 ˚C before $(CH_2O)_n$ (0.45 g, 1.5 eq., 15.0 mmol) was added in one portion. After 1 h at 0 ˚C, the reaction was diluted with sat. NH_4Cl solution (50 mL) and extracted with EtOAc (3 x 80 mL). The organics were washed with icewater/brine (50 mL), dried over $MgSO_4$ and evaporated *in vacuo* to yield the product as a light yellow liquid (738 mg, 7.37 mmol, 74%). The data were in accordance with the literature.[248]

^{1}H NMR (400 MHz, $CDCl_3$) δ 4.27 - 4.33 (m, 2H; OC*H*$_2$), 4.10 - 4.16 (m, 2H; OC*H*$_2$), 3.38 (s, 3H; OC*H*$_3$), 2.74 (br. s, 1H; O*H*)

4-Methoxybut-2-ynl (7-amino-4-methylcoumarin)carbamate (14)

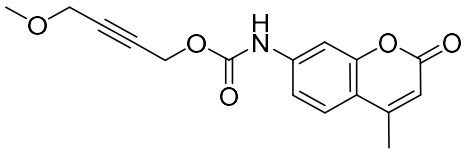

Isocyanate **8a** (40 mg, 1 eq., 0.199 mmol) and alcohol **25** (25 mg, 1.26 eq., 0.249 mmol) were dissolved in freshly distilled THF (5 mL) at room temperature in an oven dried flask. Dibutyltin dilaurate (0.01 mL, 0.08 eq., 16.9 μmol) was added, and the reaction stirred for 1 h. The precipitate was filtered washed with water (4 x 3 mL), MeOH (4 x 3 mL), Et_2O (3 x 3 mL) and petrol (3 x 3 mL), then dried *in vacuo* to give the desired product as an off-white powder (27 mg, 0.0896 mmol, 45%).

Decomp. 186 ˚C

IR (ATR) / cm^{-1}: 2928, 2323, 1726, 1689, 1618

^{1}H NMR (500 MHz, DMSO-d_6) δ 10.37 (br. s, 1H; N*H*), 7.70 (d, *J* = 8.78 Hz, 1H; *H*$_5$), 7.53 (d, *J* = 1.91 Hz, 1H; *H*$_8$), 7.40 (dd, *J* = 1.91, 8.78 Hz, 1H; *H*$_6$), 6.24 (d, *J* = 0.92 Hz, 1H; *H*$_3$), 4.89 (br. t, *J* = 1.80 Hz, 1H; OC*H*$_2$), 4.16 (br. t, *J* = 1.80 Hz, 1H; OC*H*$_2$), 3.27 (s, 3H; OC*H*$_3$), 2.39 (d, *J* = 0.92 Hz, 3H; C*H*$_3$)

^{13}C NMR (126 MHz, DMSO-d_6) δ 160.5, 154.2, 153.6, 152.9, 142.8, 126.6, 115.0, 114.8, 112.5, 105.0, 83.6, 81.6, 59.4, 57.4, 53.1, 18.5

MS(ESI): calcd. for $C_{16}H_{15}NO_5Na$ $[M+Na]^+$ 324.0842, found 324.0827

Hex-2-yn-1-yl (7-amino-4-methylcoumarin)carbamate (15)

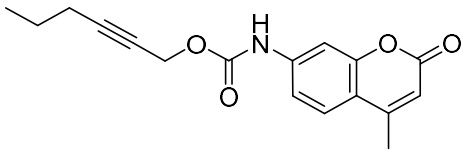

Triphosgene (85 mg, 1 eq., 0.285 mmol) was dissolved in DCM (10 mL) previously dried over 4 Å mol. sieves and then chilled to 0 ˚C. 2-hexyn-1-ol (0.09 mL, 3 eq., 0.856 mmol) was added dropwise followed by pyridine (0.07 mL, 3 eq., 0.856 mmol). The reaction was allowed to warm to room temperature and stirred for 3 h before evaporating *in vacuo*. The crude solids were triturated with freshly distilled Et_2O (3 x 4 mL) and the filtrate evaporated *in vacuo* to give the crude chloroformate. This was added dropwise to a suspension of 7-amino-4-methylcoumarin (**8**) (50 mg, 1 eq., 0.285 mmol) and K_2CO_3 (59 mg, 1.5 eq., 0.428 mmol) in dry DMF (1 mL). To ensure complete addition, the chloroformate flask was rinsed with further dry DMF (0.5 mL). The reaction was stirred at 0 ˚C for 30 min then icewater (5 mL) was added slowly dropwise before pouring the mixture over icewater (20 mL). The precipitate was filtered and washed with icewater (4 x 3 mL) then EtOH (3 x 3 mL) to give the desired product as an off-white powder (27 mg, 0.0902 mmol, 32%).

Decomp. 208 ˚C

IR (ATR) / cm^{-1}: 3276, 2958, 1734, 1688, 1622, 1590, 1528

^{1}H NMR (400 MHz, DMSO-d_6) δ 10.32 (br. s, 1H; N*H*), 7.70 (d, J = 8.56 Hz, 1H; $H_{aromatic(5)}$), 7.53 (s, 1H; $H_{aromatic(8)}$), 7.41 (d, J = 8.56 Hz, 1H; $H_{aromatic(6)}$), 6.24 (s, 1H; $H_{aromatic(3)}$), 4.80 (s, 2H; OCH_2), 2.39 (s, 3H; CH_3), 2.23 (t, J = 6.9 Hz, 2H; C$H_2$$CH_2$), 1.48 (sxt, J = 6.9 Hz, 2H; C$H_2$$CH_3$), 0.94 (t, J = 6.9 Hz, 3H; CH_2CH_3)

^{13}C NMR (126 MHz, DMSO-d_6) δ 165.2, 159.0, 158.4, 157.8, 147.7, 131.2, 119.7, 119.5, 117.2, 109.7, 92.5, 80.2, 58.2, 26.6, 25.1, 23.2, 18.4

MS(ESI): calcd. for $C_{17}H_{17}O_4NNa$ $[M+Na]^+$ 322.1050, found 322.1043

4-Chlorobut-2-yn-1-ol (32)

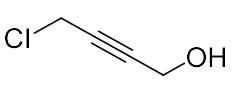

Propargyl chloride (0.2 mL, 1 eq., 2.68 mmol) was dissolved in freshly distilled Et_2O (10 mL) and chilled to -78 ˚C in an oven dried flask. 2.5 M ^{n}BuLi in hexanes (0.96 mL, 0.91 eq., 2.44 mmol) was then added quickly dropwise. After 10 min, $(CH_2O)_n$ (96 mg, 1.2 eq., 3.22 mmol) was added in one portion. The reaction was warmed to room temperature and stirred for 1 h before pouring over sat. aq. NH_4Cl (20 mL) and extracting with Et_2O (3 x 20 mL). The organics were dried over $MgSO_4$ and evaporated *in vacuo* to give the desired product as an orange oil (209 mg, 2.00 mmol, 72%). The data were in accordance with the literature.[249]

R_f (1% MeOH/DCM) 0.27

^{1}H NMR (400 MHz, $CDCl_3$) δ 4.23 - 4.26 (m, 2H), 4.13 (t, J = 1.92 Hz, 2H)

Methyl *N*-(*tert*-butoxycarbonyl)-*S*-(4-hydroxybut-2-yn-1-yl)-*L*-cysteinate (16a)

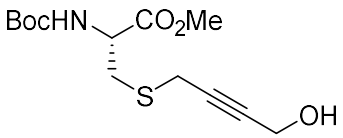

KOAc (1.514 g, 3.5 eq., 15.0 mmol) was suspended in acetone (100 mL) and propargyl chloride **32** (0.67 g, 1.5 eq., 6.44 mmol) added. BocCysOMe (1.01 g, 1 eq., 4.29 mmol) was then added and the reaction stirred at room temperature for 20 h. The reaction was then evaporated *in vacuo*, and purified by flash chromatography with 40% EtOAc/petrol on silica (60 g) to give the desired product as a light orange oil (1.01 g, 3.33 mmol, 78%).

R_f (50% EtOAc/petrol) 0.16

IR (ATR) / cm^{-1}: 3382, 2978, 1742, 1698, 1511

^{1}H NMR (400 MHz, $CDCl_3$) δ 5.41 - 5.53 (m, 1H; N*H*), 4.53 - 4.70 (m, 1H; αC*H*), 4.23 (br. s, 1H; O*H*), 3.74 (s, 3H; CH_3), 3.21 - 3.39 (m, 2H; SCH_2), 2.95 - 3.18 (m, 2H; βCH_2), 1.41 (s, 9H; (CH_3)$_3$)

^{13}C NMR (101 MHz, $CDCl_3$) δ 171.6, 155.3, 82.8, 80.6, 80.4, 53.3, 52.6, 50.8, 33.8, 28.3, 20.2

MS(ESI): calcd. for $C_{13}H_{22}NO_5S$ $[M+H]^+$ 304.1219, found 304.1213

Methyl *N*-(*tert*-butoxycarbonyl)-*S*-(4-(((7-amino-4-methylcoumarin)carbamoyl)oxy)but-2-yn-1-yl)-*L*-cysteinate (16)

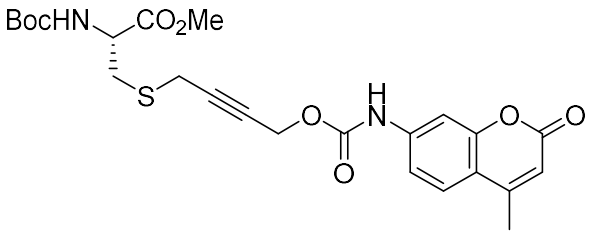

7-amino-4-methylcoumarin (**8**) (35 mg, 1 eq., 0.200 mmol) and triphosgene (30 mg, 0.5 eq., 0.100 mmol) were dissolved in freshly distilled toluene (10 mL) and refluxed for 0.5 h in oven dried glassware before evaporating *in vacuo*. The crude isocyanate was then dissolved in freshly distilled THF (3 mL) at room temperature and alcohol **16a** (85 mg, 1.4 eq., 0.280 mmol) in further THF (2 mL) was added followed by dibutyltin dilaurate (0.01 mL, 0.08 eq., 16.9 µmol). After 1 h, the reaction was evaporated *in vacuo* and re-dissolved in DCM (10 mL). 10% aqueous KF (10 mL) was added and stirred for 10 min before the layers were separated. The aqueous layer was extracted with DCM (2 x 10 mL) and the organics were dried over $MgSO_4$, filtered and evaporated *in vacuo*. The crude solids were triturated with MeOH (3 x 3 mL), Et_2O (3 x 3 mL) and petrol (3 x 3 mL) to give the desired product as an off-white powder (41 mg, 0.0821 mmol, 41%).

m.p. 137-139 °C

IR (ATR) / cm^{-1}: 3284, 3082, 2986, 1741, 1683, 1624

^{1}H NMR (500 MHz, DMSO-d_6) δ 10.39 (s, 1H; N*H*), 7.72 (d, *J* = 8.85 Hz, 1H; H_5), 7.54 (d, *J* = 1.83 Hz, 1H; H_8), 7.41 (dd, *J* = 1.83, 8.85 Hz, 1H; H_6), 6.25 (d, *J* = 0.92 Hz, 1H; H_3), 4.92 (t, *J* = 1.83 Hz, 1H; OCH_2), 4.55 (t, *J* = 1.83 Hz, 1H; OCH_2), 4.12 - 4.17 (m, 1H; αC*H*), 3.64 - 3.66 (m, 3H; CO_2CH_3), 2.78 - 2.95 (m, 2H; SCH_2), 2.67 - 2.74 (m, 1H; SCH_2), 2.55 - 2.62 (m, 1H; SCH_2), 2.40 (s, 3H; ArCH_3), 1.40 (s, 9H; (CH_3)$_3$)

^{13}C NMR (126 MHz, DMSO-d_6) δ 171.2, 160.0, 155.3, 153.8, 153.2, 152.4, 142.3, 126.1, 114.8, 114.2, 112.0, 104.3, 82.1, 81.2, 78.4, 56.1, 52.4, 51.9, 30.6, 28.1, 25.3, 18.0

MS(ESI): calcd. for $C_{24}H_{28}N_2O_8SNa$ $[M+Na]^+$ 527.1459, found 527.1443

$Pd(COD)Cl_2$

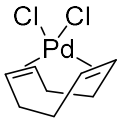

$PdCl_2$ (200 mg, 1 eq., 1.13 mmol) was suspended in concentrated HCl (~37%, 0.5 mL) and gently warmed until fully dissolved. The solution was cooled to room temperature and then diluted with absolute ethanol (15 mL). The solution was filtered, and the residues washed with further ethanol (2 mL). To the filtrate 1,5-cyclooctadiene (0.3 mL, 2.16 eq., 2.44 mmol) was added and the reaction was stirred for 5 min before being left to stand for 10 min. The yellow precipitate was filtered and washed with Et_2O (3 x 3 mL) to give the desired product as a bright yellow powder (216 mg, 0.756 mmol, 67%). The data were in accordance with the literature.[250,251]

^{1}H NMR (400 MHz, $CDCl_3$) δ 6.35 – 6.27 (m, 4H; C$H_{alkenyl}$), 2.98 – 2.85 (m, 4H; CH_{alkyl}), 2.63 – 2.51 (m, 4H; CH_{alkyl})

Methyl *S*-(4-hydroxybut-2-yn-1-yl)-*L*-cysteinate (20a)

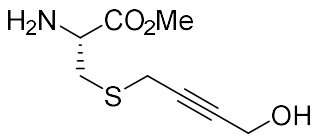

Alcohol **16a** (1.01 g, 1 eq., 3.33 mmol) was dissolved in DCM (10 mL) and TFA (1 mL) added. After 3 h, the reaction was evaporated *in vacuo* and purified by flash chromatography with 5% TEA/8% MeOH/DCM on silica (10 g), then 5% MeOH/EtOAc on silica (30 g) then 8% MeOH/EtOAc on silica (60 g) to give the desired product (542 mg, 2.66 mmol, 80%). The product could not be fully separated from triethylamine salts and was used crude.

R_f (8% MeOH/EtOAc) 0.19

^{1}H NMR (400 MHz, $CDCl_3$) δ 4.26 (t, J = 2.20 Hz, 2H; OCH_2), 3.80 (dd, J = 4.85, 7.23 Hz, 1H; α*H*), 3.76 (s, 3H; CH_3), 3.32 (td, J = 2.13, 4.35 Hz, 2H; SCH_2), 3.11 (dd, J = 4.76, 13.90 Hz, 1H; β*H*), 2.98 (dd, J = 7.14, 13.72 Hz, 1H; β*H*), 2.56 (br. s., 3H; O*H*/NH_2)

Methyl *N*-acetyl-*S*-(4-hydroxybut-2-yn-1-yl)-*L*-cysteinate (20b)

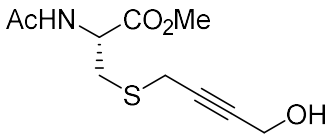

Alcohol **20a** (191 mg, 1 eq., 0.940 mmol) was dissolved in DCM (10 mL) and TEA (0.2 mL, 1.5 eq., 1.41 mmol) was added, followed by AcCl (0.08 mL, 1.2 eq., 1.13 mmol) at room temperature. After 4 h the reaction was evaporated *in vacuo* and purified by flash chromatography with 1% HCOOH/EtOAc to give the desired product as a light yellow oil (53 mg, 0.216 mmol, 23%).

R_f (1% HCOOH/EtOAc) 0.33

^{1}H NMR (500 MHz, $CDCl_3$) δ 6.57 (br. d, J = 6.70 Hz, 1H; N*H*), 4.92 - 4.97 (m, 1H; α*H*), 4.28 - 4.31 (m, 2H; OCH_2), 3.81 (s, 3H; OCH_3), 3.40 (td, J = 1.98, 16.78 Hz, 1H; β*H*), 3.31 - 3.34 (m, 1H; β*H*), 3.28 - 3.30 (m, 1H; SC*H*), 3.09 (dd, J = 5.65, 14.19 Hz, 1H; SC*H*), 2.10 (s, 3H; COCH_3)

^{13}C NMR (126 MHz, $CDCl_3$) δ 171.3, 170.9, 83.3, 80.4, 52.9, 52.5, 50.9, 33.1, 23.2, 20.4

IR (ATR) / cm^{-1}: 3275, 2954, 1740, 1655, 1537

MS(ESI): calcd. For $C_{10}H_{16}O_4N^{32}S$ $[M+H]^+$ 246.0795, found 246.0791

Methyl *N*-acetyl-*S*-(4-(((7-amino-4-methylcoumarin)carbamoyl)oxy)but-2-yn-1-yl)-*L*-cysteinate (20)

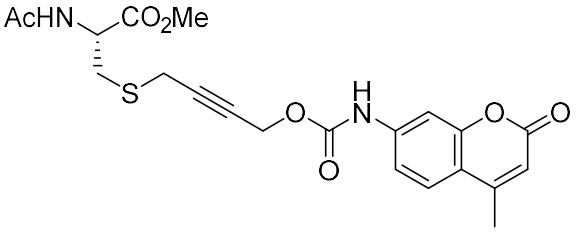

7-amino-4-methylcoumarin (**8**) (50 mg, 1 eq., 0.285 mmol) and triphosgene (42 mg, 0.5 eq., 0.143 mmol) were dissolved in freshly distilled toluene (10 mL) and refluxed for 0.5 h in oven dried glassware before evaporating *in vacuo*. The crude isocyanate was then dissolved in freshly distilled THF (3 mL) at room temperature and alcohol **20b** (77 mg, 1.1 eq., 0.314 mmol) added in further THF (2 mL) followed by dibutyltin dilaurate (0.01 mL, 0.06 eq., 16.9 µmol). After 1 h, the reaction was evaporated *in vacuo* and re-dissolved in DCM (10 mL). 10% aqueous KF (10 mL) was added and stirred for 10 min before the layers were separated. The aqueous layer was extracted with DCM (2 x 10 mL) and the organics were dried over $MgSO_4$, filtered and evaporated *in vacuo*. The crude solids were triturated with MeOH (3 x

3 mL), Et_2O (3 x 3 mL) and petrol (3 x 3 mL) to give the desired product as a yellow powder (46 mg, 0.103 mmol, 36%).

Decomp. 184 °C

^{1}H NMR (500 MHz, DMSO-d_6) δ 10.35 (br. s, 1H; N*H*CO_2), 8.41 (d, *J* = 7.90 Hz, 1H; N*H*CO), 7.71 (d, *J* = 8.54 Hz, 1H; H_5), 7.53 (d, *J* = 1.83 Hz, 1H; H_8), 7.40 (dd, *J* = 2.14, 8.54 Hz, 1H; H_6), 6.25 (d, *J* = 0.92 Hz, 1H; H_3), 4.85 - 4.87 (m, 2H; OCH_2), 4.47 - 4.56 (m, 1H; α*H*), 3.64 (s, 3H; OCH_3), 3.48 - 3.52 (m, 2H; SCH_2), 3.05 (dd, *J* = 5.34, 13.89 Hz, 1H; β*H*), 2.86 (dd, *J* = 8.70, 13.89 Hz, 1H; β*H*), 2.39 (d, *J* = 0.61 Hz, 3H; ArCH_3), 1.87 (s, 3H; COCH_3)

^{13}C NMR (126 MHz, DMSO-d_6) δ 171.7, 169.9, 160.5, 154.3, 153.6, 153.0, 142.9, 126.5, 115.0, 114.7, 112.5, 105.0, 83.4, 78.1, 53.2, 52.6, 52.0, 32.9, 22.7, 19.4, 18.5

IR (ATR) / cm^{-1}: 3279, 1739, 1687, 1625

MS(ESI): calcd. For $C_{21}H_{23}O_7N_2S$ $[M+H]^+$ 447.1220, found 447.1205

Methyl *S*-(4-hydroxybut-2-yn-1-yl)-*L*-cysteinate hydrochloride (21a)

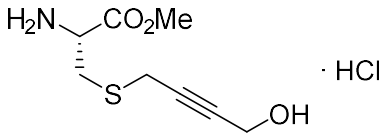

In an oven dried flask, freshly distilled MeOH (10 mL) was chilled to 0 °C and AcCl (0.06 mL) added. The reaction was warmed to room temperature, and then re-chilled to 0 °C before amine **19a** (80 mg, 1 eq., 0.394 mmol) was added. After 5 min the reaction was evaporated *in vacuo* to give the desired product as a clear oil (88 mg, 0.367 mmol, 93%) which was used without further purification.

Methyl *S*-(4-(((7-amino-4-methylcoumarin)carbamoyl)oxy)but-2-yn-1-yl)-*L*-cysteinate (21)

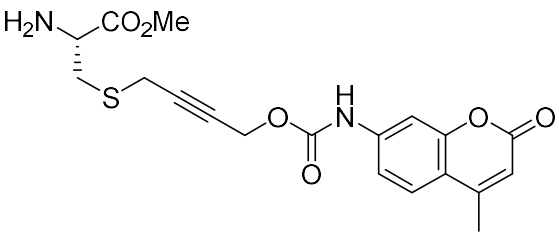

7-amino-4-methylcoumarin (**8**) (50 mg, 1 eq., 0.285 mmol) and triphosgene (42 mg, 0.5 eq., 0.143 mmol) were dissolved in freshly distilled toluene (10 mL) and refluxed for 0.5 h in oven dried glassware before evaporating *in vacuo*. The crude isocyanate was then dissolved in freshly distilled THF (3 mL) at room temperature and alcohol **21a** (88 mg, 1.29 eq., 0.367 mmol) in further THF (2 mL) was added followed by dibutyltin dilaurate (0.01 mL, 0.06 eq., 16.94 µmol). After 1 h, the reaction was evaporated *in vacuo* and re-dissolved in DCM (10 mL). 10% aqueous KF (10 mL) was added and stirred for 10 min before the aqueous layer was basified to pH > 10 with sat. aq. Na_2CO_3 and the layers were separated. The aqueous layer was extracted with DCM (2 x 10 mL) and the organics were dried over $MgSO_4$, filtered and evaporated *in vacuo*. The crude solids were triturated with MeOH (3 x 3 mL), Et_2O (3 x 3 mL) and petrol (3 x 3 mL) to give the desired product as a dark yellow powder (52 mg, 0.129 mmol, 45%).

m.p. 109-111 °C

^{1}H NMR (500 MHz, DMSO-d_6) δ 9.33 (s, 1H; N*H*CO_2), 7.64 (d, *J* = 8.54 Hz, 1H; H_5), 7.57 (d, *J* = 2.14 Hz, 1H; H_5), 7.26 (dd, *J* = 1.98, 8.70 Hz, 1H; H_8), 6.89 (d, *J* = 7.93 Hz, 1H; H_6), 6.20 (d, *J* = 0.92 Hz, 1H; H_3), 5.16 (t, *J* = 5.95 Hz, 1H; N*H*), 4.56 - 4.64 (m, 1H; N*H*), 4.07 - 4.10 (m, 2H; OCH_2), 3.70 (s, 3H; OCH_3), 3.45 - 3.49 (m, 2H; SCH_2), 3.13 (dd, *J* = 4.88, 13.73 Hz, 1H; β*H*), 3.04 (dd, *J* = 7.32, 13.73 Hz, 1H; β*H*), 2.38 (d, *J* = 0.61 Hz, 3H; CH_3CO)

^{13}C NMR (126 MHz, DMSO-d_6) δ 172.0, 160.6, 154.6, 154.5, 153.7, 144.1, 126.4, 114.4, 114.0, 111.8, 104.3, 83.7, 80.1, 52.8, 52.5, 49.5, 33.4, 19.8, 18.4

IR (ATR) / cm^{-1}: 3381, 2922, 1717, 1677, 1618

MS(ESI): calcd. For $C_{19}H_{21}O_6N_2S$ $[M+H]^+$ 405.1120, found 405.1114

Pd(NBD)Cl$_2$

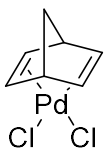

$PdCl_2$ (100 mg, 1 eq., 0.564 mmol) was suspended in concentrated HCl (~37%, 0.25 mL) and gently warmed until fully dissolved. The solution was cooled to room temperature and then diluted with absolute ethanol (7.5 mL). The solution was filtered, and the residues washed with further ethanol (1 mL). To the filtrate was added norbornadiene (0.12 mL, 2.16 eq., 1.22 mmol) and the reaction was

stirred for 5 min before being left to stand for 10 min. The yellow precipitate was filtered and washed with Et_2O (3 x 3 mL) to give the desired product as a bright yellow powder (94 mg, 0.349 mmol, 62%).[251,252]

^{1}H NMR (400 MHz, DMSO-d_6) δ 6.74 (t, *J* = 1.92 Hz, 4H; C$H_{alkenyl}$), 3.56 – 3.52 (m, 2H; C$H_{bridgehead}$), 1.87 (t, *J* = 1.56 Hz, 2H; C$H_{bridging}$)

But-3-yn-1-yl trityl thioether (22a)

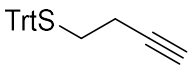

K_2CO_3 (1.5 g, 3 eq., 10.9 mmol) was suspended in DMF (10 mL) in an oven dried flask. 4-bromo-1-butyne (577 mg, 1.2 eq., 4.34 mmol) was added followed by triphenylmethane thiol (1 g, 1 eq., 3.62 mmol) in one portion. After 6 h stirring at room temperature, the reaction was diluted in Et_2O (100 mL) and washed with water basified to pH > 10 with sat. aq. Na_2CO_3 (2 x 50 mL), then brine (50 mL). The organics were dried over $MgSO_4$, filtered and dry-loaded directly onto silica (5 g). The crude material was purified by flash chromatography on silica (50 g) with 5% Et_2O/petrol to give the desired product as a white powder (886 mg, 2.73 mmol, 75%).

R_f (5% Et_2O/petrol) 0.41

m.p. 73.5-76.5 °C

IR (ATR) / cm^{-1}: 3292, 3057, 3030, 2932, 1594, 1488, 1443

^{1}H NMR (400 MHz, $CDCl_3$) δ 7.46 (d, *J* = 7.32 Hz, 6H), 7.32 (t, *J* = 7.32 Hz, 6H), 7.22 - 7.29 (m, 3H), 2.41 (t, *J* = 7.45 Hz, 2H), 2.15 (dt, *J* = 2.55, 7.45 Hz, 2H), 2.00 (t, *J* = 2.55 Hz, 1H)

^{13}C NMR (101 MHz, $CDCl_3$) δ 144.7, 129.6, 127.9, 126.7, 82.6, 69.2, 66.8, 30.8, 18.5

MS(ESI): calcd. for $C_{23}H_{19}{}^{32}S$ $[M-H]^-$ 327.1207, found 327.1205

5-(Tritylthio)pent-2-yn-1-ol (22b)

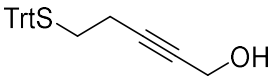

Propargyl thioether **22a** (645 mg, 1 eq., 1.96 mmol) was dissolved in freshly distilled THF (20 mL) in an oven dried flask and chilled to -78 °C. 1.6 M ^{n}BuLi in hexanes (1.5 mL, 1.2 eq., 2.36 mmol) was then added dropwise. After 10 mins, $(CH_2O)_n$ (88 mg, 1.5 eq., 2.95 mmol) was then added in one portion and the reaction warmed to room temperature. After 1 h the reaction was quenched with sat. aq. NH_4Cl (30 mL) and the phases separated. The aqueous layer was further extracted with EtOAc (2 x 30 mL). The organics were dried over $MgSO_4$, filtered and evaporated directly onto silica (5 g) and purified by flash chromatography on silica (50 g) with a gradient of 25-50% EtOAc/petrol to give the desired product as a yellow amorphous solid (677 mg, 1.89 mmol, 99%).

R_f (40% EtOAc/petrol) 0.33

m.p. 99.2-101.5 °C

IR (ATR) / cm^{-1}: 3365, 3057, 3018, 2929, 2870, 1594, 1488, 1443

^{1}H NMR (400 MHz, $CDCl_3$) δ 7.43 (d, *J* = 7.40 Hz, 6H; $H_{aromatic}$), 7.30 (t, *J* = 7.40 Hz, 6H; $H_{aromatic}$), 7.23 (t, *J* = 7.40 Hz, 3H; $H_{aromatic}$), 4.19 - 4.23 (m, 2H; OCH_2), 2.37 (t, *J* = 7.50 Hz, 2H; SCH_2), 2.18 (tt, *J* = 1.70, 7.20 Hz, 2H; CH_2CC), 1.58 - 1.64 (m, 1H; O*H*)

^{13}C NMR (101 MHz, $CDCl_3$) δ 144.7, 129.6, 127.9, 126.7, 84.5, 79.3, 66.8, 51.3, 30.9, 18.8

MS(ESI): calcd. for $C_{24}H_{22}O^{32}SNa$ $[M+Na]^+$ 381.1284, found 381.1293

5-(Tritylthio)pent-2-yn-1-yl (7-amino-4-methylcoumarin)carbamate (22)

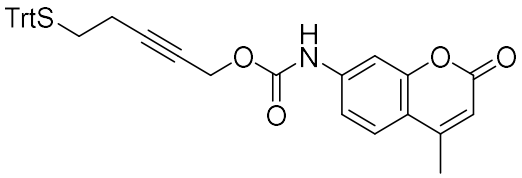

7-amino-4-methylcoumarin (**8**) (50 mg, 1 eq., 0.285 mmol) and triphosgene (42 mg, 0.5 eq., 0.143 mmol) were dissolved in freshly distilled toluene (10 mL) and refluxed for 0.5 h in oven dried glassware before evaporating *in vacuo*. The crude isocyanate was then dissolved in freshly distilled THF (5 mL) at room temperature and alcohol **22b** (123 mg, 1.2 eq., 0.342 mmol) added followed by dibutyltin dilaurate (0.01 mL, 0.08 eq., 16.9 µmol). After 1 h, the reaction was evaporated *in vacuo* to ~½ volume and chilled to 0 °C. Water (10 mL) was added dropwise and the precipitate filtered. The crude solids were triturated with MeOH (2 x 3 mL), Et_2O (2 x 3 mL) and petrol (2 x 3 mL) to give the desired product as an off-white powder (63 mg, 0.191 mmol, 67%).

m.p. 188.8-190.0 °C

IR (ATR) / cm^{-1}: 3277, 3176, 3085, 3057, 2926, 2956, 2854, 1738, 1697, 1624

^{1}H NMR (400 MHz, DMSO-d_6) δ 10.33 (s, 1H; N*H*), 7.69 (d, *J* = 8.86 Hz, 1H; H_5), 7.53 (d, *J* = 2.04 Hz, 1H; H_8), 7.40 (dd, *J* = 1.87, 8.69 Hz, 1H; H_6), 7.30 - 7.36 (m, 12H; H_{trityl}), 7.22 - 7.27 (m, 3H; H_{trityl}), 6.25 (s, 1H; H_2), 4.78 (s, 2H; OCH_2), 2.39 (s, 3H; CCH_3), 2.18 - 2.28 (m, 4H; SCH_2/CCCH_2)

^{13}C NMR (101 MHz, DMSO-d_6) δ 160.5, 154.2, 153.6, 153.0, 144.7, 142.9, 129.5, 128.5, 127.2, 126.5, 115.0, 114.7, 112.5, 105.0, 85.9, 76.2, 66.7, 53.3, 30.8, 18.5, 18.4

MS(ESI): calcd. for $C_{35}H_{29}NO_4{}^{32}S$ $[M+Na]^+$ 582.1715, found 582.1709

5-(Methylthio)pent-2-yn-1-ol (23a)

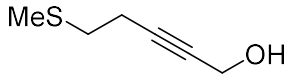

K_2CO_3 (1.77 g, 2.5 eq., 12.8 mmol) was dissolved in water (20 mL) and 4-bromo-1-butyne (750 mg, 1.1 eq., 5.64 mmol) was added. Sodium methanethiolate (359 mg, 1 eq., 5.13 mmol) was then added at room temperature and the reaction stirred for 5 h. The reaction was extracted with Et_2O (3 x 20 mL) and the organics dried over $MgSO_4$, then filtered directly onto 4 Å mol. sieves in an oven dried flask. The solution was then filtered *via* cannula into an oven dried flask and chilled to -78 °C. 1.6 M ^{n}BuLi in hexanes (4.81 mL, 1.5 eq., 7.69 mmol) was added dropwise followed by $(CH_2O)_n$ (308 mg, 2 eq., 10.3 mmol) after 10 min. The reaction was warmed to room temperature and stirred for 1 h before quenching with sat. aq. NH_4Cl (30 mL) and separating. The organics were dried over $MgSO_4$, filtered and evaporated. The crude material was purified by flash chromatography on silica (30 g) with 50% Et_2O/petrol to give the desired product as a clear oil (262 mg, 2.01 mmol, 39%) which contains traces of Et_2O and petrol.

R_f (50% Et_2O/Petrol) 0.24

IR (ATR) / cm^{-1}: 3345, 2917, 2865, 1431

^{1}H NMR (500 MHz, $CDCl_3$) δ 4.27 (br. s., 2H; OCH_2), 2.68 (t, *J* = 7.02 Hz, 2H; SCH_2), 2.54 (t, *J* = 6.71 Hz, 2H; CH_2CC), 2.16 (s, 3H; SCH_3), 1.88 (br. s, 1H; O*H*)

^{13}C NMR (126 MHz, $CDCl_3$) δ 84.4, 79.4, 51.2, 33.1, 19.7, 15.6

MS(ESI): calcd. for $C_6H_{11}O^{32}S$ $[M+H]^+$ 131.0525, found 131.0530

5-(Methylthio)pent-2-yn-1-yl (7-amino-4-methylcoumarin)carbamate (23)

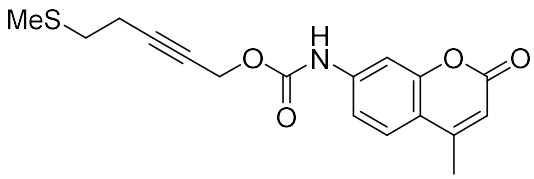

7-amino-4-methylcoumarin (**8**) (50 mg, 1 eq., 0.285 mmol) and triphosgene (42 mg, 0.5 eq., 0.143 mmol) were dissolved in freshly distilled toluene (10 mL) and refluxed for 0.5 h in oven dried glassware before evaporating *in vacuo*. The crude isocyanate was then dissolved in freshly distilled THF (5 mL) at room temperature and alcohol **23a** (56 mg, 1.5 eq., 0.428 mmol) was added followed by dibutyltin dilaurate (0.01 mL, 0.08 eq., 16.9 µmol). After 1 h, the reaction was evaporated *in vacuo* to ~½ volume and chilled to 0 °C. Water (10 mL) was added dropwise and the precipitate filtered. The crude solids were triturated with MeOH (2 x 3 mL), Et_2O (2 x 3 mL) and petrol (2 x 3 mL) to give the desired product as a white powder (63 mg, 0.190 mmol, 66%).

m.p. 175.6-177.8 °C

IR (ATR) / cm^{-1}: 3277, 3174, 3100, 2956, 2920, 1735, 1687, 1625

^{1}H NMR (400 MHz, DMSO-d_6) δ 10.33 - 10.37 (m, 1H; N*H*), 7.70 (d, *J* = 8.86 Hz, 1H; H_5), 7.53 (d, *J* = 1.70 Hz, 1H; H_8), 7.40 (dd, *J* = 1.70, 8.52 Hz, 1H; H_6), 6.24 (s, 1H; H_2), 4.80 - 4.82 (m, 2H; OCH_2), 2.59 - 2.65 (m, 2H; SCH_2/CCCH_2), 2.52 - 2.58 (m, 2H; SCH_2/CCCH_2), 2.39 (s, 3H; CCH_3), 2.09 (s, 3H; SCH_3)

^{13}C NMR (101 MHz, DMSO-d_6) δ 160.4, 154.2, 153.6, 153.0, 142.9, 126.5, 115.0, 114.7, 112.5, 104.9, 86.6, 76.0, 53.4, 32.4, 19.4, 18.5, 15.1

MS(ESI): calcd. for $C_{17}H_{18}O_4N^{32}S$ $[M+H]^+$ 332.0951, found 332.0960

2-(2-(2-Ethoxyethoxy)ethoxy)ethyl tosylate (30)

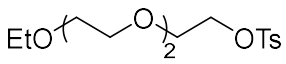

Triethylene glycol monoethylether **29** (25 mL, 1 eq., 143 mmol) was dissolved in TEA (100 mL, 5 eq., 720 mmol) and chilled to 0 °C. TsCl (30 g, 1.1 eq., 157 mmol) was added over 5 min and the reaction allowed to warm to room temperature after 15 min and stirred for 5 h. The reaction mixture was

poured slowly over a mixture of ice (200 mL) and conc. HCl (150 mL) and then extracted with Et_2O (3 x 100 mL). The combined organics were washed with brine (100 mL) and sat. aq. $NaHCO_3$ (100 mL), dried over $MgSO_4$, filtered and evaporated to give the desired product as a light yellow oil (42.759 g, 129 mmol, 90%). The data were in accordance with the literature.[253]

^{1}H NMR (400 MHz, $CDCl_3$) δ 7.79 (d, J = 8.05 Hz, 2H; H_{aryl}), 7.34 (d, J = 8.05 Hz, 2H; H_{aryl}), 4.14 - 4.17 (m, 2H; SO_2CH_2), 3.66 - 3.70 (m, 2H; $SO_2CH_2CH_2$), 3.54 - 3.63 (m, 8H; OCH_2CH_2O), 3.51 (q, J = 7.06 Hz, 2H; OCH_2CH_3), 2.44 (s, 3H; $ArCH_3$), 1.20 (t, J = 7.06 Hz, 3H; OCH_2CH_3)

_S_-(2-(2-(2-Ethoxyethoxy)ethoxy)ethyl)thioacetate (31)

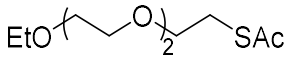

Tosylate **30** (2.0 g, 1.0 eq., 6.02 mmol) was dissolved in acetone (50 mL) and degassed by five evacuation/refill cycles. KSAc (1.37 g, 2.0 eq., 12.0 mmol) was then added in one portion and the reaction stirred for 20 h. The reaction was evaporated then diluted in sat. aq. $NaHCO_3$ (60 mL) and extracted with DCM (4 x 30 mL) and evaporated *in vacuo*. This gave the desired product as an orange oil (1.22 g, 5.17 mmol, 86%) which was used crude without further purification.

^{1}H NMR (400 MHz, $CDCl_3$) δ 3.55 - 3.65 (m, 10H; OCH_2), 3.51 (q, J = 7.06 Hz, 2H; OCH_2CH_3), 3.08 (t, J = 6.50 Hz, 2H; CH_2SAc), 2.32 (s, 3H; SAc), 1.19 (t, J = 7.06 Hz, 3H; OCH_2CH_3)

3,6,9-Trioxa-12-thiahexadec-14-yn-16-ol (33)

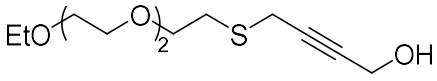

A 1 M solution of NaOMe was prepared by dissolving Na (553 mg, 24.1 mmol) in freshly distilled MeOH (24 mL). An portion of this solution (6.3 mL, 2.06 eq., 6.28 mmol) was added to thioester **32** (721 mg, 1 eq., 3.05 mmol) in an oven dried flask and the reaction stirred at room temperature for 1.5 h. Propargyl alcohol **32** (478 mg, 1.5 eq., 4.58 mmol) was then added in one portion and the reaction stirred for a further 20 h. The reaction was then evaporated and purified by flash chromatography with a gradient of 50-70% EtOAc/petrol on silica (80 g) to give the desired product as an orange oil (581 mg, 2.21 mmol, 73%).

R_f (50% EtOAc/petrol) 0.10

IR (ATR) / cm^{-1}: 3407, 2866

^{1}H NMR (500 MHz, $CDCl_3$) δ 4.29 - 4.31 (m, 2H; OC*H*$_2$C≡C), 3.74 (t, J = 6.71 Hz, 2H; SCH$_2$C*H*$_2$O), 3.66 - 3.69 (m, 6H; OC*H*$_2$), 3.60 - 3.63 (m, 2H; C*H*$_2$OCH$_2$CH$_3$), 3.55 (q, J = 7.02 Hz, 2H; OC*H*$_2$CH$_3$), 3.39 (t, J = 1.98 Hz, 2H; SC*H*$_2$C≡C), 2.91 (t, J = 6.71 Hz, 2H; SC*H*$_2$CH$_2$O), 1.89 - 1.95 (m, 1H; O*H*), 1.24 (t, J = 7.02 Hz, 3H; OCH$_2$C*H*$_3$)

^{13}C NMR (126 MHz, $CDCl_3$) δ 81.7, 81.6, 70.8, 70.6, 70.6, 70.4, 69.8, 66.7, 51.1, 30.7, 20.1, 15.1

MS(ESI): calcd. for $C_{12}H_{22}O_4{}^{32}S$ $[M+H]^+$ 263.1259, 263.1256

3,6,9-Trioxa-12-thiahexadec-14-yn-16-yl (7-amino-4-methylcoumarin)carbamate (28)

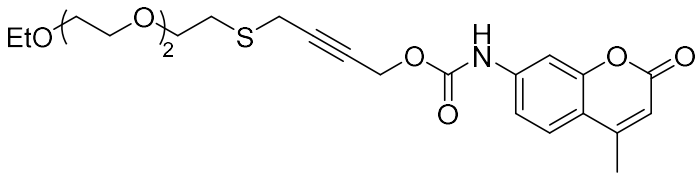

7-amino-4-methylcoumarin (**8**) (50 mg, 1 eq., 0.285 mmol) and triphosgene (42 mg, 0.5 eq., 0.143 mmol) were dissolved in freshly distilled toluene (10 mL) and refluxed for 0.5 h in oven dried glassware before evaporating *in vacuo*. The crude isocyanate was then dissolved in freshly distilled THF (5 mL) at room temperature and alcohol **33** (97 mg, 1.3 eq., 0.371 mmol) was added followed by dibutyltin dilaurate (0.01 mL, 0.06 eq., 17.1 µmol). After 1 h, the reaction was evaporated *in vacuo*. The crude viscous oil was treated with petrol (15 mL) and then evaporated again. The crude waxy solid was triturated with petrol (5 x 3 mL) and Et_2O (5 x 3 mL) then dried *in vacuo* to give the desired product as a light brown waxy solid (100 mg, 0.216 mmol, 87%).

IR (ATR) / cm^{-1}: 3278, 3173, 3094, 2868, 17.36, 1687

^{1}H NMR (400 MHz, DMSO-d_6) δ 10.37 (s, 1H; N*H*), 7.71 (d, J = 8.69 Hz, 1H; *H*$_5$), 7.54 (d, J = 1.36 Hz, 1H; *H*$_8$), 7.41 (dd, J = 1.36, 8.69 Hz, 1H; *H*$_6$), 6.25 (s, 1H; *H*$_3$), 4.86 (s, 2H; OC*H*$_2$C≡C), 3.61 (t, J = 6.47 Hz, 2H; SCH$_2$C*H*$_2$O), 3.37 - 3.54 (m, 12H; O(C*H*$_2$)$_2$O+SC*H*$_2$C≡C+OC*H*$_2$CH$_3$), 2.78 (t, J = 6.47 Hz, 2H; SC*H*$_2$CH$_2$O), 2.39 (s, 3H; ArC*H*$_3$), 1.09 (t, J = 6.98 Hz, 3H; OCH$_2$C*H*$_3$)

^{13}C NMR (101 MHz, DMSO-d_6) δ 160.4, 154.3, 153.6, 153.0, 142.9, 126.5, 115.0, 114.7, 112.5, 105.0, 84.2, 77.6, 70.3, 70.3, 70.2, 70.0, 69.6, 66.0, 53.3, 30.9, 19.4, 18.5, 15.6

MS(ESI): calcd. for $C_{23}H_{30}NO_7{}^{32}S$ $[M+H]^+$ 464.1743, found 464.1752

3,6,9-Trioxa-12-thiahexadec-14-yn-16-yl (4-nitrophenyl) carbonate (34)

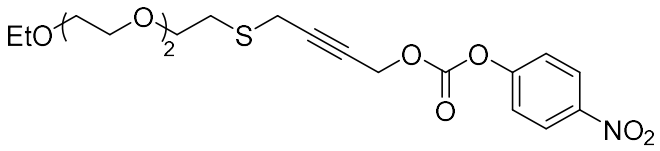

Alcohol **33** (200 mg, 1 eq., 0.762 mmol) was dissolved in freshly distilled DCM (12 mL) in an oven dried flask and *p*-nitrophenylchloroformate (231 mg, 1.5 eq., 1.14 mmol) was added. DIPEA (0.27 mL, 2.0 eq., 1.52 mmol) was added dropwise and the reaction stirred for 20 h. The reaction was evaporated and purified by flash chromatography with 50% EtOAc/petrol on silica (60 g). Crude fractions were evaporated, the material dissolved in DCM (50 mL) and washed with dilute aq. $NaHCO_3$ (30 mL). The aqueous layer was extracted with DCM (25 mL) and the combined organics dried over $MgSO_4$, filtered and evaporated *in vacuo* to give the desired product as a light yellow oil (192 mg, 0.449 mmol, 59%).

R_f (50% EtOAc/Petrol) 0.30

IR (ATR) / cm^{-1}: 2869, 1768

^{1}H NMR (400 MHz, $CDCl_3$) δ 8.30 (d, J = 9.20 Hz, 2H; $H_{aromatic}$), 7.42 (d, J = 9.20 Hz, 2H; $H_{aromatic}$), 4.92 (t, J = 1.70 Hz, 2H; OCH_2C≡C), 3.73 (t, J = 6.56 Hz, 2H; SCH_2CH_2O), 3.63 - 3.69 (m, 6H; OCH_2), 3.58 - 3.63 (m, 2H; C$H_2OCH_2CH_3$), 3.53 (q, J = 7.07 Hz, 2H; OCH_2CH_3), 3.41 (t, J = 1.87 Hz, 2H), 2.88 (t, J = 6.56 Hz, 2H; SCH_2CH_2O), 1.22 (t, J = 7.07 Hz, 3H; OCH_2CH_3)

^{13}C NMR (101 MHz, $CDCl_3$) δ 155.3, 152.0, 145.5, 125.3, 121.8, 85.2, 75.2, 70.8, 70.7, 70.6, 70.4, 69.8, 66.6, 57.1, 31.1, 20.0, 15.2

MS(ESI): calcd. for $C_{19}H_{26}NO_8{}^{32}S$ $[M+H]^+$ 428.1374, found 428.1360

cDox (35)

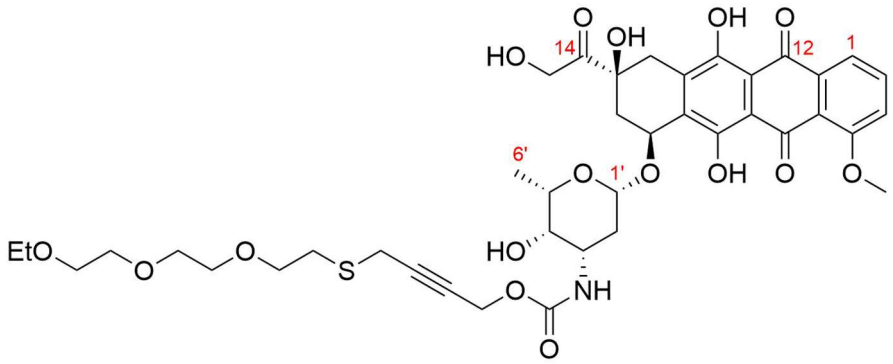

Carbonate **34** (48 mg, 1.3 eq., 112 µmol) was dissolved in DMF and doxorubicin hydrochloride (50 mg, 1.0 eq., 86.2 µmol) was added. DIPEA (37 µL, 2.5 eq., 216 µmol) was then added in one portion and the reaction stirred for 3 h then diluted with EtOAc (75 mL), washed with water (2 x 30 mL) and brine (30 mL). The organics were dried over $MgSO_4$, filtered and evaporated *in vacuo*. The crude material was purified by flash chromatography with 5% MeOH/DCM on silica (30 g) to give the desired product as a red waxy solid (55 mg, 65.6 µmol, 76%).

R_f (5% MeOH/DCM) 0.38

IR (ATR) / cm^{-1}: 3441, 2931, 1721

^{1}H NMR (500 MHz, $CDCl_3$) δ 13.98 (s, 1H; $H_{6/11}$), 13.25 (s, 1H; $H_{6/11}$), 8.05 (d, *J* = 7.63 Hz, 1H; H_1), 7.80 (dd, *J* = 7.63, 8.24 Hz, 1H; H_2), 7.41 (d, *J* = 8.24 Hz, 1H; H_3), 5.52 – 5.48 (m, 1H; $H_{1'}$), 5.43 (d, *J* = 8.54 Hz, 1H; N*H*), 5.31 – 5.27 (m, 1H; H_7), 4.78 (d, *J* = 3.05 Hz, 2H; H_{14}), 4.68 (d, *J* = 15.4 Hz, 1H; H_9), 4.59 (d, *J* = 13.9 Hz, 2H; $OCH_2C{\equiv}C$), 4.12 (q, *J* = 6.7 Hz, 1H; $H_{5'}$), 4.10 (s, 3H; OCH_3), 3.84 - 3.92 (m, 1H; $H_{3'}$),3.63 - 3.73 (m, 10H; SCH_2CH_2O + CH_2O + $H_{4'}$ + $H_{3'}$), 3.59 - 3.63 (m, 2H; $CH_2OCH_2CH_3$), 3.54 (q, *J* = 7.02 Hz, 2H; OCH_2CH_3), 3.34 (br. s., 2H; $C{\equiv}CCH_2S$), 3.31 (d, *J* = 2.2 Hz, 2H; $C_{4'/9}OH$), 3.27 (dd, *J* = 18.9, 2.0 Hz, 1H; H_{10}), 3.02 (s, 2H; $C_{14}OH$), 2.97 (d, *J* = 14.6 Hz, 1H; H_{10}), 2.85 (dt, J = 2.14, 6.70 Hz, 2H; SCH_2CH_2O), 2.50 - 2.55 (m, 1H; $C_{4'/9}OH$), 2.36 (d, J = 14.65 Hz, 1H; H_8), 2.19 (dd, *J* = 3.66, 14.65 Hz, 1H; H_8), 1.82 - 1.87 (m, 2H; $H_{2'}$), 1.31 (d, *J* = 6.41 Hz, 3H; $C_{6'}$-CH_3), 1.22 (t, *J* = 7.02 Hz, 3H; OCH_2CH_3)

^{13}C NMR (126 MHz, $CDCl_3$) δ 213.9, 187.1, 186.7, 161.1, 156.2, 155.7, 154.8, 135.8, 135.5, 133.6, 133.6, 120.9, 119.9, 118.5, 111.6, 111.4, 100.7, 82.7, 77.6, 76.6, 70.7, 70.7, 70.5, 70.3, 69.7, 69.6, 69.3, 67.4, 66.7, 65.6, 56.7, 53.0, 47.2, 35.6, 34.0, 31.5, 30.0, 20.0, 16.9, 15.1

MS(ESI): calcd. for $C_{40}H_{49}NO_{16}{}^{32}SNa$ $[M+Na]^+$ 854.2664, found 854.2648

*Synthesis of Compounds **36a-e** and **36** performed by Laura Sinatra*

tert-Butyl (2-(2-(2-(2-hydroxyethoxy)ethoxy)ethoxy)ethyl)carbamate (36a)

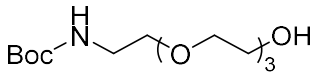

A solution of Boc_2O (207 mg, 1.5 eq., 1.13 mmol) in EtOH (0.5 mL) was added to 2-(2-2-2-aminoetriethoxy)ethanol (150 mg, 1.0 eq., 0.753 mmol) in EtOH (1.0 mL). The reaction mixture was stirred at room temperature for 18 h and the solvent was evaporated *in vacuo*. The residue was dissolved in DCM (20 mL) then washed with 1 M HCl (20 mL), sat. aq. $NaHCO_3$ (20 mL) and brine (20 mL). The organic layer was dried over $MgSO_4$, filtered and evaporated *in vacuo*. The crude material was purified by flash chromatography on silica with 0-10% MeOH/DCM to give the desired product as a pale yellow oil (186 mg, 0.473 mmol, 63%). The data were in accordance with the literature.[253]

R_f (5% MeOH/DCM) 0.41

^{1}H NMR (400 MHz, $CDCl_3$) δ 3.75 – 3.68 (m, 4H; OCH_2CH_2O), 3.68 – 3.60 (m, 8H; OCH_2CH_2O), 3.53 (dd, *J* = 5.5, 4.5 Hz, 2H; OCH_2CH$_2$N), 3.31 (dd, *J* = 5.5, 4.5 Hz, 2H; CH_2NH), 1.44 (s, 9H; C(CH_3)$_3$)

2,2-Dimethyl-4-oxo-3,8,11,14-tetraoxa-5-azahexadecan-16-yl 4-methylbenzenesulfonate (36b)

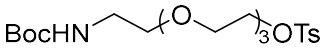

Carbamate **36a** (180 mg, 1.0 eq., 0.617 mmol) was dissolved in freshly distilled DCM (1.0 mL) in an oven dried flask. TEA (422 µL, 5.0 eq., 3.05 mmol) and DMAP (3.66 mg, 0.05 eq., 0.0305 mmol) were added and the reaction was cooled to 0 °C. TsCl (173 mg, 1.5 eq., 0.926 mmol) was added slowly, the reaction allowed to warm to room temperature and stirred for 20 h. Then the reaction was diluted with DCM (20 mL) and washed with 1 M HCl (20 mL). The aqueous layer was extracted with DCM (3 x 20 mL). The organic layers were combined, washed with brine (50 mL), dried over $MgSO_4$, filtered and evaporated *in vacuo*. The crude product was purified by flash chromatography on silica with 0-5% MeOH/DCM to give the desired product as light yellow oil (257 mg, 0.574 mmol, 93 %). The data were in accordance with the literature.[253]

R_f (5% MeOH/DCM) 0.46

^{1}H NMR (400 MHz, $CDCl_3$) δ 7.80 (d, *J* = 8.3 Hz, 2H; H_{aryl}), 7.34 (d, *J* = 8.1 Hz, 2H; H_{aryl}), 4.16 (dd, *J* = 9.7, 1.1 Hz, 2H; SO_2CH_2), 3.70 (dd, *J* = 5.6, 4.1 Hz, 2H; $SO_2CH_2CH_2$), 3.60 (m, *J* = 1.7 Hz, 8H; OCH_2CH_2O), 3.53 (t, *J* = 5.2 Hz, 2H; OCH_2CH$_2$N), 3.30 (q, *J* = 5.5 Hz, 2H; CH_2NH), 2.45 (s, 3H; ArCH_3), 1.44 (s, 9H; C(CH_3)$_3$)

***S*-(2,2-Dimethyl-4-oxo-3,8,11,14-tetraoxa-5-azahexadecan-16-yl) ethanethioate (36c)**

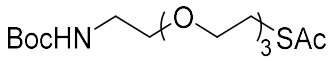

Tosylate **36b** (182 mg, 1.0 eq., 0.407 mmol) was dissolved in acetone (6 mL) and degassed by five evacuation/refill cycles. KSAc (278 mg, 6.0 eq., 2.44 mmol) was added in one portion and the reaction stirred for 20 h at room temperature. The reaction was then evaporated *in vacuo*, the crude material diluted in sat. aq. $NaHCO_3$ (30 mL) and extracted with DCM (3 x 30 mL). The organic layers were combined, washed with 5% NaOH (2x 50 mL) and evaporated *in vacuo*. The crude product was purified by flash chromatography on silica with 5% MeOH/DCM to give the desired product as a yellow oil (139 mg, 0.394 mmol, 97%).

R_f (5% MeOH/DCM) 0.46

^{1}H NMR (400 MHz, $CDCl_3$) δ 3.66 – 3.57 (m, 10H, OCH_2CH_2O), 3.54 (t, *J* = 5.1 Hz, 2H, OCH_2CH_2N), 3.31 (q, *J* = 5.4 Hz, 2H, CH_2NH), 3.09 (t, *J* = 6.5 Hz, 2H, CH_2SCH_3), 2.33 (s, 3H, CH_2SCH_3), 1.43 (s, 9H, C(CH_3)$_3$)

^{13}C NMR (75 MHz, DMSO-d_6) δ 195.6, 156.1, 70.7, 70.7, 70.5, 70.4, 69.9, 40,5, 30.7, 29.0, 28.6

IR (ATR) / cm^{-1}: 3354, 2977, 2869, 1690, 1513

MS(ESI): calcd. for $C_{15}H_{29}NO_6{}^{32}SNa$ $[M+Na]^+$ 374.1613, found 374.1599

***tert*-Butyl (16-hydroxy-3,6,9-trioxa-12-thiahexadec-14-yn-1-yl)carbamate (36d)**

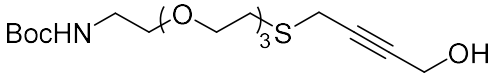

Thioester **36c** (120 mg, 1.0 eq., 0.341 mmol) was dissolved in freshly distilled MeOH (2 mL). A 1 M solution of NaOMe was prepared by dissolving Na (553 mg, 24.05 mmol) in freshly distilled MeOH (24 mL). A portion of this solution (0.59 mL, 2.0 eq., 0.683 mmol) was added to thioester **36c** in an oven dried flask and the reaction stirred for 1.5 h. Propargyl chloride **32** (48 mg, 1.35 eq., 0.460 mmol) was then added in one portion and the reaction stirred for further 20 h. The reaction was then evaporated *in vacuo* and purified by flash chromatography on silica with 0-33% MeOH/DCM to give the desired product as a yellow oil (109 mg, 0.290 mmol, 85%).

R_f (5% MeOH/DCM) 0.40

^{1}H NMR (400 MHz, $CDCl_3$) δ 5.18 (s, 1H, O*H*), 4.29 – 4.27 (m, 2H, OC*H*$_2$C≡C), 3.74 (t, *J* = 6.5 Hz, 2H, SCH$_2$C*H*$_2$O), 3.68 – 3.60 (m, 8H, OC*H*$_2$C*H*$_2$O), 3.55 (q, *J* = 5.1 Hz, 2H, OC*H*$_2$CH$_2$N), 3.38 (t, *J* = 2.2 Hz, 2H, SC*H*$_2$C≡C), 3.36 – 3.28 (m, 2H, C*H*$_2$NH), 2.88 (t, *J* = 6.5 Hz, 2H, CH$_2$SCH$_2$), 1.45 (s, 9H, C(C*H*$_3$)$_3$)

^{13}C NMR (75 MHz, DMSO-d_6) δ 156.3, 81.8, 81.7, 79.4, 71.0, 70.8, 70.7, 70.4, 66.0, 51.2, 40.5, 31.0, 28.6, 20.3, 15.4

IR (ATR) / cm^{-1}: 3368, 2868, 1691, 1515

MS(ESI): calcd. for $C_{17}H_{31}NO_6{}^{32}S$ $[M+H]^+$ 378.1945, found 378.1941

(*E*)-*N*-(16-Hydroxy-3,6,9-trioxa-12-thiahexadec-14-yn-1-yl)-4-oxo-4-phenylbut-2-enamide (36e)

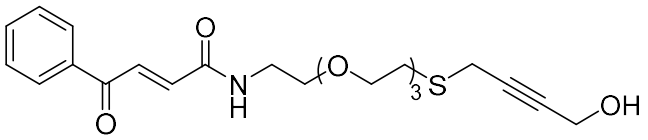

Alcohol **36d** (60 mg, 1.0 eq., 0.159 mmol) was dissolved in 20% TFA in DCM (1 mL) and stirred for 3 h. Afterwards the solvent was evaporated *in vacuo* and the crude product was dissolved in dry DMF (0.75 mL) in an oven dried flask. DIPEA (31 µL, 2.0 eq, 0.32 mmol) was added to the solution. 3-benzoylacrylic acid (28 mg, 1.0 eq., 0.16 mmol) and HBTU (72 mg, 1.2 eq., 0.19 mmol) were dissolved in dry DMF (0.75 mL) and DIPEA (31 µL, 2.0 eq., 0.318 mmol) was added. This solution was stirred for 15 min and added dropwise to the crude amine in DMF at 0 °C. The reaction was allowed to warm to room temperature and stirred for 18 h. The solvent was evaporated *in vacuo* and coevaporated 3 times with toluene. The crude product was dissolved in DCM (20 mL) and washed with 1 M HCl (3x 20 mL), $NaHCO_3$ sat. (3x 20 mL) and brine (3x 20 mL). The organic layer was dried over $MgSO_4$, filtered and evaporated *in vacuo*. The crude material was purified by flash chromatography on silica with 0-5% MeOH/DCM to give the desired product as brown waxy oil (15.1 mg, 35.2 µmol, 22% over two steps).

R$_f$ (5% MeOH/DCM) 0.26

^{1}H NMR (400 MHz, $CDCl_3$) δ 8.06 – 8.03 (m, 2H; *H*$_{aryl}$), 7.98 (d, *J* = 15.1 Hz, 1H; *H*C=CH), 7.65 – 7.59 (m, 1H; *H*$_{aryl}$), 7.51 (dd, *J* = 8.4, 7.0 Hz, 2H; *H*$_{aryl}$), 7.31 (s, 1H; N*H*), 7.04 (d, *J* = 15.1 Hz, 1H; HC=C*H*), 4.28 (t, *J* = 2.1 Hz, 2H; OC*H*$_2$C≡C), 3.74 (t, *J* = 6.6 Hz, 2H; SCH$_2$C*H*$_2$O), 3.71 – 3.64 (m, 10H; OC*H*$_2$C*H*$_2$O), 3.62 (dd, *J* = 7.4, 3.3 Hz, 2H; SC*H*$_2$C≡C), 3.32 (t, *J* = 2.1 Hz, 2H; C*H*$_2$NH), 2.86 (t, *J* = 6.6 Hz, 2H; CH$_2$SCH$_2$), 2.39 (s, 1 H; O*H*)

^{13}C NMR (75 MHz, DMSO-d_6) δ 189.9, 164.4, 136.9, 135.6, 133.7, 133.0, 128.9, 128.8, 81.8, 81.4, 70.8, 70.6, 70.5, 70.2, 70.1, 69.6, 51.0, 39.9, 30.8, 20.1

IR (ATR) / cm^{-1}: 3279, 3070, 2917, 2867, 1646, 1596, 1579, 1535

MS(ESI): calcd. for $C_{22}H_{29}NO_6{}^{32}SNa$ $[M+Na]^+$ 458.1608, found 458.1597

(*E*)-*N*-(16-Hydroxy-3,6,9-trioxa-12-thiahexadec-14-yn-1-yl)-4-oxo-4-phenylbut-2-enamide doxorubicin carbamate (36)

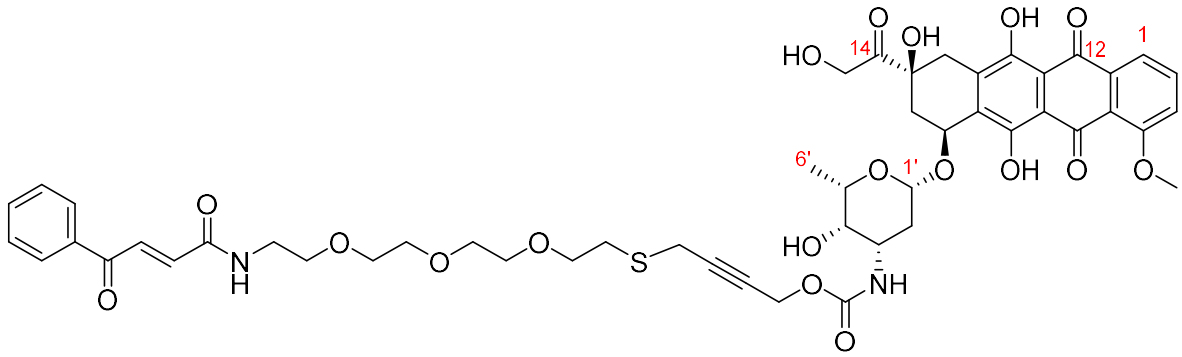

Alcohol **36e** (15 mg, 1.0 eq., 34.4 µmol) was dissolved in DCM (1 mL) and *p*-nitrophenylchloroformate (11 mg, 1.57 eq., 54.1 µmol) was added in an oven dried flask. DIPEA (18 µL, 3.0 eq., 0.103 mmol) was added dropwise and the reaction stirred for 20 h. Then it was diluted with DCM (20 mL) and washed with dilute aq. $NaHCO_3$ (20 mL). The aqueous layer was extracted with DCM (2 x 20 mL) and the combined organic layer was dried over $MgSO_4$, filtered and evaporated under reduced pressure. The residue was dissolved in dry DMF (1 mL) and doxorubicin hydrochloride (20 mg, 1.0 eq., 0.035 mmol) and DIPEA (18 µL, 3.0 eq., 0.11 mmol) were then added in one portion and the reaction stirred for 18 h. Afterwards DMF was coevaporated with toluene (3 x 5 mL). The crude product was purified by flash chromatography on silica with 0-5% MeOH/DCM and then purified by preparative TLC (1 mm, 5% MeOH/DCM) to give the desired product as a red waxy solid (15 mg, 15.1 µmol, 43% over two steps).

R_f (5% MeOH/DCM) 0.21

^{1}H NMR (400 MHz, $CDCl_3$) δ 13.97 (s, 1H, $H_{6/11}$), 13.27 (s, 1H, $H_{6/11}$), 8.08 – 8.00 (m, 3H, H_1, H_{aryl}), 7.96 (d, *J* = 15.0 Hz, 1H, *H*C=CH), 7.79 (dd, *J* = 8.5, 7.7 Hz, 1H, H_{aryl}), 7.60 (t, *J* = 7.4 Hz, 1H, H_{Aryl}), 7.50 (t, *J* = 7.6 Hz, 2H, H_{aryl}), 7.39 (dd, *J* = 8.6, 1.1 Hz, 1H, H_{aryl}), 7.22 (s, 1 H, N*H*), 7.05 (d, *J* = 15.1 Hz, 1H, HC=C*H*), 5.64 (d, *J* = 8.6 Hz, 1H, N*H*), 5.57 – 5.49 (m, 1H, H_1), 5.31 (s, 1H, H_7), 4.77 (s, 2H, H_{14}), 4.70 (s, 1H, H_9), 4.65 (d, *J* = 19.5 Hz, 2H, OCH_2C≡C), 4.50 (d, *J* = 15.4 Hz, 2H), 4.22 (s, 1H, $H_{5'}$), 4.08 (s, 3H, OCH_3), 3.87 (s, 1H, $H_{3'}$), 3.78 – 3.54 (m, 16H, SCH_2CH_2O + CH_2O + $H_{4'}$ + $H_{3'}$), 3.31 (d, *J* = 2.5 Hz, 2H, C≡CCH_2S), 3.27 (d, *J*

= 2.0 Hz, 1H, H_{10}), 3.15 (d, *J* = 6.3 Hz, 1H, H_{10}), 2.86 – 2.80 (m, 2H, SCH_2CH_2O), 2.36 (d, *J* = 14.6 Hz, 1H, H_8), 2.22 – 2.12 (m, 1H, H_8), 1.90 – 1.80 (m, 2H, $H_{2'}$), 1.31 (d, *J* = 6.5 Hz, 3H, $C_{6'}$-CH_3)

^{13}C NMR (75 MHz, DMSO-d_6) δ 213.90, 189.70, 187.16, 186.77, 164.48, 161.07, 156.24, 155.72, 154.84, 154.75, 136.92, 135.75, 135.56, 135.37, 133.70, 133.62, 133.09, 128.84, 120.96, 119.86, 118.43, 111.62, 111.44, 100.80, 82.76, 70.86, 70.55, 70.42, 70.26, 70.20, 69.56, 69.30, 67.98, 67.48, 65.57, 56.70, 52.94, 47.33, 39.92, 35.67, 34.03, 30.75, 30.06, 29.71, 25.62, 20.03, 17.00

IR (ATR) / cm^{-1}: 3694, 3327, 2925, 2335, 2191, 2064, 1974,1721, 1646, 1579

MS(ESI): calcd. for $C_{50}H_{56}N_2O_{18}{}^{32}S$ $[M+H]^+$ 1027.3141, found 1027.3108

5.3 Synthetic Procedures for Chapter 4

tert-Butyldimethyl(pent-4-yn-1-yloxy)silane (38a)

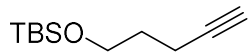

4-pentyn-1-ol (1.00 g, 1.00 eq., 11.9 mmol) was dissolved in DCM (20 mL) and TBSCl (1.88 g, 1.05 eq., 12.5 mmol) was added followed by imidazole (1.62 g, 2.00 eq., 23.8 mmol). The reaction was stirred for 2 h at room temperature, then poured over water (50 mL) and acidified to pH < 2 with 3 M HCl. The layers were separated and the aqueous layer further extracted with DCM (2 x 30 mL). The organics were dried over $MgSO_4$ and evaporated *in vacuo* to give the desired product as a clear oil (2.15 g, 10.9 mmol, 91%). The data were in accordance with the literature.[254]

^{1}H NMR (400 MHz, $CDCl_3$) δ 3.70 (t, *J* = 6.0 Hz, 2H; OC*H*$_2$), 2.27 (td, *J* = 7.1, 2.7 Hz, 2H; C*H*$_2$C≡CH), 1.93 (t, *J* = 2.7 Hz, 1H; C≡C*H*), 1.76 – 1.68 (m, 2H; OCH$_2$C*H*$_2$), 0.90 (s, 9H; C(C*H*$_3$)$_3$), 0.06 (s, 6H; Si(C*H*$_3$)$_2$)

6-((_tert_-Butyldimethylsilyl)oxy)hex-2-yn-1-ol (38b)

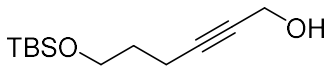

Alkyne **38a** (7.79 g, 1.0 eq., 39.3 mmol) was dissolved in freshly distilled THF (50 mL) in an oven dried flask and chilled to -78 °C. 1.6 M ^{n}BuLi in hexanes (29.5 mL, 1.2 eq., 47.2 mmol) was added dropwise and the reaction stirred for 10 min. $(CH_2O)_n$ (1.53 g, 1.3 eq., 51.1 mmol) was added and the reaction allowed to warm to room temperature, then stirred for 1 h. The reaction was then poured over sat. aq. NH_4Cl (150 mL) and separated. The aqueous layer was extracted wtih EtOAc (2 x 100 mL). The combined organics were dried over $MgSO_4$ and evaporated *in vacuo*. The crude material was purified by flash chromatography with 1% TEA, 20% EtOAc/petrol on silica (150 g) to give the product (8.65 g, 37.4 mmol, 96%) as a light yellow oil. The data were in accordance with the literature.[254]

R$_f$ (20% EtOAc/petrol) 0.18

^{1}H NMR (400 MHz, $CDCl_3$) δ 4.28 – 4.21 (m, 2H; HOC*H*$_2$), 3.68 (t, *J* = 6.0 Hz, 2H; TBSOC*H*$_2$), 2.30 (tt, *J* = 7.1, 2.2 Hz, 2H; C*H*$_2$C≡CH$_2$), 1.77 – 1.65 (m, 2H; OCH$_2$C*H*$_2$), 1.49 – 1.44 (m, 1H; O*H*), 0.89 (s, 9H; C(C*H*$_3$)$_3$), 0.05 (s, 6H; Si(C*H*$_3$)$_2$)

6-((*tert*-Butyldimethylsilyl)oxy)hex-2-yn-1-yl dibenzylcarbamate (38c)

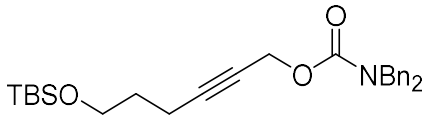

Alcohol **38b** (200 mg, 1.0 eq., 0.875 mmol) was dissolved in freshly distilled MeCN (12 mL) in an oven dried flask and DSC (336 mg, 1.5 eq., 1.31 mmol) added in one portion at room temperature. DIPEA (0.46 mL, 3.0 eq., 2.63 mmol) was added dropwise and the reaction stirred for 5 h. Bn_2NH (0.42 mL, 2.5 eq., 2.19 mmol) was added dropwise and the reaction stirred a further 2 h then evaporated *in vacuo*. The crude oil was diluted in 3 M HCl (50 mL) and extracted with EtOAc (2 x 50 mL). The organics were washed with brine (30 mL), dried over $MgSO_4$ and evaporated *in vacuo*. The crude material was purified by flash chromatography with 1% TEA, 10% EtOAc/petrol on silica (50 g) to give the product (304 mg, 0.673 mmol, 77%) as a clear oil.

R_f (10% EtOAc/petrol) 0.32

IR (ATR) /cm^{-1}: 2952, 2929, 1702, 1605

^{1}H NMR (400 MHz, $CDCl_3$) δ 7.37 – 7.20 (m, 10H; $H_{aromatic}$), 4.81 (t, *J* = 2.2 Hz, 2H; CO_2CH_2), 4.43 (d, *J* = 12.7 Hz, 4H; $N(CH_2)_2$), 3.69 (t, *J* = 6.1 Hz, 2H; $TBSOCH_2$), 2.33 (tt, *J* = 7.1, 2.2 Hz, 2H; $CH_2C{\equiv}CH_2$), 1.79 – 1.67 (m, 2H; OCH_2CH_2), 0.89 (s, 9H; $C(CH_3)_3$), 0.05 (s, 6H; $Si(CH_3)_2$)

^{13}C NMR (101 MHz, $CDCl_3$) δ 156.17, 137.16, 128.59, 128.17, 127.74, 127.46, 86.93, 74.82, 61.54, 54.11, 49.31, 48.88, 31.50, 25.93, 18.33, 15.26, -5.33

MS(ESI): calcd. for $C_{27}H_{37}NO_3Si$ $[M+H]^+$ 452.2616, found 452.1862

6-Hydroxyhex-2-yn-1-yl dibenzylcarbamate (38d)

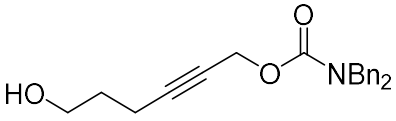

Silane **38c** (207 mg, 1.0 eq., 0.458 mmol) was dissolved in freshly distilled MeOH (15 mL) and chilled to 0 °C. AcCl (8 drops) was added, and the reaction stirred for 0.5 h. The reaction was evaporated *in vacuo* and purified by flash chromatography with 40% EtOAc/petrol on silica (50 g) to give the desired product (150 mg, 0.445 mmol, 97%) as a clear oil.

R_f (40% EtOAc/petrol) 0.18

IR (ATR) /cm^{-1}: 3438, 3032, 2943, 1690

^{1}H NMR (400 MHz, $CDCl_3$) δ 7.36 – 7.19 (m, 10H; $H_{aromatic}$), 4.79 (t, *J* = 2.2 Hz, 2H; CO_2CH_2), 4.42 (d, *J* = 13.8 Hz, 4H; NCH_2), 3.75 (t, *J* = 6.5 Hz, 2H; $HOCH_2$), 2.37 (tt, *J* = 6.5, 2.2 Hz, 2H; $C{\equiv}CCH_2$), 1.82 – 1.73 (m, 2H; OCH_2CH_2)

^{13}C NMR (101 MHz, $CDCl_3$) δ 156.17, 137.12, 128.60, 128.16, 127.69, 127.48, 86.43, 75.41, 61.57, 54.02, 49.39, 48.92, 31.02, 15.38

MS(ESI): calcd. For $C_{21}H_{25}NO_3$ $[M+H]^+$ 338.1756 , found 338.1757

6-((Dibenzylcarbamoyl)oxy)hex-4-ynoic acid (38)

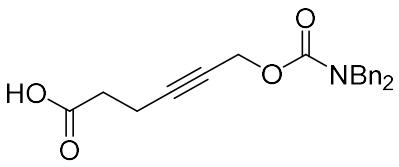

Alcohol **38d** (95 mg, 1.0 eq., 0.282 mmol) was dissolved in DCM (10 mL) and pyridine (68.3 µL, 3.0 eq., 0.845 mmol) was added followed by DMP (179 mg, 1.5 eq., 0.422 mmol). The reaction was stirred for 2 h at room temperature before diluting with 1:1 10% aq. $Na_2S_2O_3$/sat. aq. Na_2CO_3 (10 mL) and stirring for 30 min. The layers were separated and the aqueous layer extracted with DCM (2 x 10 mL). The organics were washed with water (10 mL), dried over $MgSO_4$ and evaporated *in vacuo*. The crude material was dissolved in ^{t}BuOH (4 mL) and diluted with 50 mM pH 7.4 NaPi (4 mL). 2-methyl-2-butene (0.3 mL, 10 eq., 2.82 mmol) was added followed by $NaClO_2$ (60 mg, 2.0 eq., 0.563 mmol) and the reaction stirred for at room temperature. After 2 h, the reaction was evaporated then diluted with 3 M HCl (20 mL) and extracted with DCM (3 x 15 mL). The organics were dried over $MgSO_4$ and evaporated *in vacuo*. The crude material was purified by flash chromatography with 60% EtOAc/petrol on silica (30 g) to give the product (76 mg, 0.217 mmol, 77%) as a white powder.

R_f (80% EtOAc/petrol) 0.10

IR (ATR) /cm^{-1}: 3030, 2350, 1705

^{1}H NMR (400 MHz, $CDCl_3$) δ 7.38 – 7.17 (m, 10H; $H_{aromatic}$), 4.79 (t, *J* = 2.0 Hz, 2H; OCH_2), 4.42 (d, *J* = 14.8 Hz, 4H; NCH_2), 2.64 – 2.51 (m, 4H; $(CH_2)_2CO_2H$)

^{13}C NMR (101 MHz, $CDCl_3$) δ 176.95, 156.13, 137.06, 128.61, 128.16, 127.71, 127.50, 84.78, 75.71, 53.90, 49.40, 48.92, 32.97, 14.46

MS(ESI): calcd. For $C_{21}H_{22}NO_4$ $[M+H]^+$ 352.1549, found 352.1550

Propargyl morpholine-4-carboxylate (41)

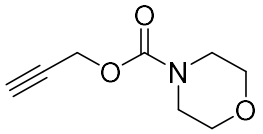

DIPEA (0.27 mL, 1.5 eq., 1.55 mmol) was dissolved in freshly distilled DCM (5 mL) in an oven dried flask and propargyl chloroformate (0.15 mL, 1.5 eq., 1.55 mmol) was added, followed by dropwise morpholine (90.4 µL, 1.0 eq., 1.03 mmol) at room temperature. After 1 h, the reaction was diluted with 3 M HCl (20 mL) and extracted with DCM (3 x 10 mL). The organics were dried over $MgSO_4$ and evaporated *in vacuo*. The crude material was purified by flash chromatography with 30% EtOAc/petrol on silica (50 g) to give the product (138 mg, 0.816 mmol, 79%) as a white powder.

R_f (30% EtOAc/petrol) 0.19

m.p. 42.5-44.4 °C

IR (ATR) /cm^{-1}: 3676, 3244, 2988, 2975, 2902, 1716, 1690

^{1}H NMR (400 MHz, $CDCl_3$) δ 4.70 (d, *J* = 2.4 Hz, 2H; OCH_2), 3.65 (s, 4H; O(CH_2)$_2$), 3.52 – 3.44 (m, 4H; N(CH_2)$_2$), 2.47 (t, *J* = 2.4 Hz, 1H; C≡C*H*)

^{13}C NMR (101 MHz, $CDCl_3$) δ 154.39, 78.29, 74.64, 66.48, 53.07, 44.32, 43.99

MS(ESI): calcd. for $C_8H_{12}NO_3$ $[M+H]^+$ 170.0817, found 170.0818

***iso*-Butyl morpholine-4-carboxylate (42)**

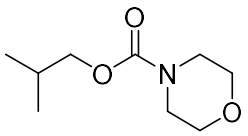

iso-Butyl chloroformate (0.23 mL, 1.5 eq., 1.72 mmol) was dissolved in freshly distilled DCM (6 mL) in an oven dried flask and DIPEA (0.3 mL, 1.5 eq., 1.72 mmol) was added. Morpholine (0.1 mL, 1 eq., 1.25 mmol) was then added dropwise and the reaction stirred for 1 h at room temperature. The reaction was diluted with 3 M HCl (20 mL) and extracted with DCM (3 x 10 mL). The organics were dried over $MgSO_4$ and evaporated *in vacuo*. The crude material was purified by flash chromatography with 20% EtOAc/petrol on silica (50 g) to give the product (194 mg, 1.04 mmol, 90%) as a clear oil.

R_f (20% EtOAc/petrol) 0.15

IR (ATR) /cm^{-1}: 3677, 2963, 2901, 1698

^{1}H NMR (400 MHz, $CDCl_3$) δ 3.87 (dd, *J* = 6.7, 0.9 Hz, 2H; OCH_2), 3.65 (t, *J* = 4.8 Hz, 4H; O(CH_2)$_2$), 3.50 – 3.42 (m, 4H; N(CH_2)$_2$), 1.92 (hept, *J* = 6.7 Hz, 1H; CH(CH_3)$_2$), 0.92 (dd, *J* = 6.7, 0.9 Hz, 6H; (CH_3)$_2$)

^{13}C NMR (101 MHz, $CDCl_3$) δ 155.59, 71.65, 66.61, 44.00, 27.97, 19.08

MS(ESI): calcd. for $C_9H_{18}NO_3$ $[M+H]^+$ 188.1287, found 188.1280

1-Morpholinopent-4-yn-1-one (43)

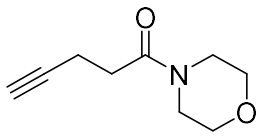

4-pentynoic acid (**37**) (150 mg, 1.0 eq., 1.53 mmol) was dissolved in DCM (20 mL) and morpholine (134 µL, 1.0 eq., 1.53 mmol) was added followed by DCC (284 mg, 0.9 eq., 1.38 mmol) and the reaction stirred for 6 h at room temperature. The reaction was filtered, and the filtrate evaporated then purified by flash chromatography with 50% EtOAc/petrol on silica (50 g) to give the desired product (132 mg, 0.789 mmol, 57%) as a white powder.

R_f (50% EtOAc/petrol) 0.10

m.p. 83.0-84.6 °C

IR (ATR) /cm^{-1}: 3676, 3223, 2967, 2919, 1636

^{1}H NMR (400 MHz, $CDCl_3$) δ 3.68 – 3.64 (m, 4H; O(CH_2)$_2$), 3.63 – 3.60 (m, 2H; NCH_2), 3.50 – 3.43 (m, 2H; NCH_2), 2.57 – 2.52 (m, 4H; (CH_2)$_2$C≡C), 1.98 – 1.95 (m, 1H; C≡CH)

^{13}C NMR (101 MHz, $CDCl_3$) δ 169.52, 83.35, 68.83, 66.88, 66.57, 45.79, 42.02, 31.97, 14.45

MS(ESI): calcd. for $C_9H_{14}NO_2$ $[M+H]^+$ 168.1025, found 168.1026

N-(2-Methoxyethyl)pent-4-ynamide (44)

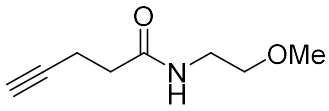

4-pentynoic acid (**37**) (100 mg, 1.0 eq., 1.02 mmol) was dissolved in DCM (10 mL) and TEA (0.43 mL, 3.0 eq., 3.06 mmol) was added, followed by EDC·HCl (195 mg, 1.0 eq., 1.02 mmol) at room temperature. The reaction was stirred for 1 h before 2-methoxyethylamine (88.6 µL, 1.0 eq., 1.02 mmol) was added dropwise. The reaction was stirred for a further 6 h before diluting with 3 M HCl (20 mL) and extracting with DCM (3 x 10 mL). The organics were dried over $MgSO_4$, filtered and evaporated *in vacuo*. The crude material was purified by flash column chromatography with 75% EtOAc/petrol on silica (50 g) to give the desired product (32 mg, 0.206 mmol, 20%) as a clear oil.

R_f (75% EtOAc/petrol) 0.14

IR (ATR) /cm^{-1}: 3288, 2926, 1650, 1545

^{1}H NMR (400 MHz, $CDCl_3$) δ 6.07 (br. s, 1H; N*H*), 3.43 (d, *J* = 2.7 Hz, 4H; OCH_2 + NCH_2), 3.32 (s, 3H; OCH_3), 2.50 (td, *J* = 7.3, 2.2 Hz, 2H; C≡C*H*), 2.38 (t, *J* = 7.3 Hz, 2H), 1.96 (t, *J* = 2.7 Hz, 1H; C≡C*H*)

^{13}C NMR (101 MHz, $CDCl_3$) δ 170.95, 82.94, 71.14, 69.19, 58.72, 39.21, 35.27, 14.85

MS(ESI): calcd. for $C_8H_{14}NO_2$ $[M+H]^+$ 156.1019, found 156.1017

pDoxAm (46)

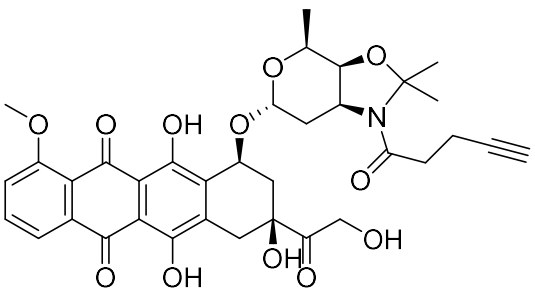

Doxorubicin hydrochloride (100 mg, 1 eq., 172.42 µmol) was suspended in chloroform (20 mL) and TEA (10 drops) added until fully dissolved. Water (10 mL) was then added and the layers separated. The

aqueous layer was extracted with chloroform (10 mL) and the combined organics evaporated *in vacuo*. Acetone (30 mL) and 4 Å mol. sieves were added and the reaction refluxed for 3 h. The reaction was cooled to room temperature then chilled to 0 ˚C before adding TEA (72 µL, 3 eq., 517.26 µmol). 4-pentynoic acid (**37**) (51 mg, 3 eq., 517.26 µmol) was dissolved in $CDCl_3$ and TEA (72 µL, 3 eq., 517.26 µmol) was added followed by $SOCl_2$ (19 µL, 1.5 eq., 258.63 µmol). The reaction was monitored by ^1H NMR until complete formation of anhydride after 2 h. The crude anhydride in $CDCl_3$ was added to pDox (**45**) in acetone at 0 ˚C. The reaction was allowed to come to room temperature and stirred for 18 h, then formic acid (5 drops) was added and the reaction dry-loaded directly onto silica (2 g). The crude product was purified by flash chromatography on silica (50 g) with 10% MeOH/DCM, then on silica (30 g) with 0-10% MeOH/DCM, then again on silica (50 g) w(ith 4-10% MeOH/DCM to give the desired product (11 mg, 16.57 µmol, 10%) as a red powder.

^{1}H NMR (500 MHz, $CDCl_3$) δ 14.02 (s, 1H; OH_{phenol}), 13.26 (s, 1H; OH_{phenol}), 8.04 (dd, *J* = 7.7, 1.1 Hz, 1H; $H_{1/3}$), 7.80 (dd, *J* = 8.6, 7.7 Hz, 1H; H_2), 7.41 (dd, *J* = 8.6, 1.1 Hz, 1H; $H_{1/3}$), 5.53 (t, *J* = 8.1 Hz, 1H; $H_{1'}$), 5.32 (dd, *J* = 4.1, 2.1 Hz, 1H; H_7), 4.75 (s, 2H; CH_2OH), 4.56 (s, 1H; 9-O*H*), 4.30 (qd, *J* = 6.7, 2.2 Hz, 1H; $H_{5'}$), 4.09 (s, 3H; OMe), 3.99 – 3.89 (m, 2H; $H_{3'/4'}$), 3.31 (dd, *J* = 18.8, 2.1 Hz, 1H; H_{10}), 3.05 (d, *J* = 18.8 Hz, 1H; H_{10}), 2.51 – 2.45 (m, 3H; NHCOCH_2 + H_8), 2.41 – 2.30 (m, 2H; CH_2C≡C), 2.23 – 2.16 (m, 1H; H_8), 2.10 – 2.03 (m, 1H; $H_{2'}$), 1.87 (t, *J* = 2.4 Hz, 1H; C≡C*H*), 1.80 (ddd, *J* = 14.2, 10.5, 4.0 Hz, 1H; $H_{2'}$), 1.70 (s, 3H; CMe_2), 1.57 (s, 3H; CMe_2), 1.41 (d, *J* = 6.7 Hz, 3H; 5'-Me)

^{13}C NMR (126 MHz, $CDCl_3$) δ 213.41, 187.18, 186.83, 167.01, 161.10, 156.18, 155.61, 135.87, 135.48, 133.48, 133.34, 120.87, 119.87, 118.49, 111.76, 111.62, 100.45, 95.26, 83.29, 72.33, 70.14, 68.74, 65.45, 63.95, 56.71, 50.95, 35.40, 34.07, 33.82, 31.65, 29.71, 26.89, 23.90, 16.79, 14.18

MS(ESI): calcd. for $C_{35}H_{38}NO_{12}$ $[M+H]^+$ 664.2389, found 664.2375

DoxAm (47)

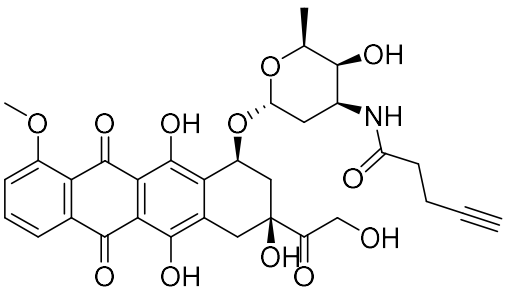

Doxorubicin hydrochloride (50 mg, 1 eq., 86.21 µmol) and 4-pentynoic acid (**37**) (17 mg, 2 eq., 172.42 µmol) were dissolved in DCM (12 mL) and TEA (60.1 µL, 5 eq., 431.05 µmol) was added followed by TBTU (55 mg, 2 eq., 172.42 µmol). The reaction was stirred at room temperature for 6 h. The reaction was diluted with DCM (20 mL) and washed with water (20 mL). The aqueous layer was washed with DCM (10 mL), and the combined organics dried over $MgSO_4$, filtered and evaporated *in vacuo* directly onto silica (2 g). The crude product was purified by flash chromatography on silica (50 g) with 7-10% MeOH, 1% HCOOH/DCM. The product containing fractions were dry-loaded onto silica (1 g) and purified by flash chromatography on silica (50 g) with 5-10% MeOH/DCM to give the desired product (42 mg, 67.35 µmol, 78%) as a bright red amorphous solid.

IR (ATR) /cm^{-1}: 3297, 2925, 2854, 1724, 1618, 1579

^{1}H NMR (400 MHz, $CDCl_3$) δ 13.95 (s, 1H; OH_{phenol}), 13.20 (s, 1H; OH_{phenol}), 8.02 (dd, *J* = 8.1, 1.1 Hz, 1H; $H_{1/3}$), 7.77 (t, *J* = 8.1 Hz, 1H; H_2), 7.38 (dd, *J* = 8.1, 1.1 Hz, 1H; $H_{1/3}$), 6.00 (d, *J* = 8.4 Hz, 1H; N*H*), 5.49 (d, *J* = 4.1 Hz, 1H; $H_{1'}$), 5.28 – 5.22 (m, 1H; H_7), 4.75 (s, 2H; CH_2OH), 4.51 (s, 1H; 9-O*H*), 4.20 – 4.11 (m, 2H; $H_{5'}$), 4.06 (s, 3H; OMe), 3.65 (s, 1H; $H_{3'}$), 3.25 (dd, *J* = 18.9, 1.9 Hz, 1H; H_{10}), 2.97 (d, *J* = 18.9 Hz, 1H; H_{10}), 2.50 – 2.42 (m, 2H; NHCOCH_2), 2.37 – 2.28 (m, 3H; CH_2C≡C + H_8), 2.16 (dd, *J* = 14.8, 4.1 Hz, 1H; H_8), 1.98 (t, *J* = 2.6 Hz, 1H; C≡C*H*), 1.86 (dd, *J* = 13.3, 5.2 Hz, 1H; $H_{2'}$), 1.77 (td, *J* = 13.3, 4.1 Hz, 1H; $H_{2'}$), 1.29 (d, *J* = 6.6 Hz, 3H; 5'-Me)

^{13}C NMR (101 MHz, $CDCl_3$) δ 213.88, 187.05, 186.59, 170.28, 160.99, 156.18, 155.60, 135.78, 135.45, 133.58, 133.52, 120.78, 119.85, 118.42, 111.55, 111.36, 100.70, 82.84, 69.72, 69.45, 69.43, 67.16, 65.56, 56.65, 45.28, 35.67, 35.28, 33.95, 29.90, 29.70, 16.85, 14.92

MS(ESI): calcd. for $C_{32}H_{34}NO_{12}$ $[M+H]^+$ 624.2076, found 624.2062

pDoxAc (48)

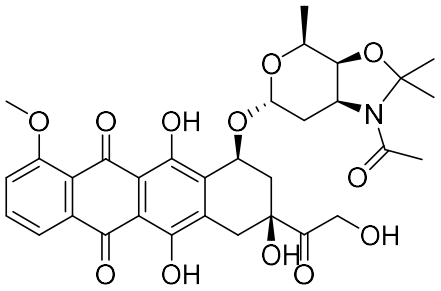

Doxorubicin hydrochloride (100 mg, 1 eq., 172.42 µmol) was suspended in chloroform (20 mL) and TEA (10 drops) was added until fully dissolved. Water (10 mL) was then added and the layers separated.

The aqueous layer was extracted with chloroform (10 mL) and the combined organics evaporated *in vacuo*. Acetone (30 mL) and 4 Å mol. sieves were added and the reaction refluxed for 3 h. The reaction was cooled to room temperature. then chilled in ice before adding TEA (48 µL, 2 eq., 344.84 µmol) followed by acetic anhydride (26 mg, 1.5 eq., 258.63 µmol). The reaction was allowed to come to room temperature and stirred for 18 h, then formic acid (5 drops) was added and the reaction dry-loaded directly onto silica (2 g). The crude product was purified by flash chromatography on silica (50 g) with 10% MeOH/DCM, then on silica (30 g) with 0-10% MeOH/DCM, then again on silica (50 g) with 4-10% MeOH/DCM to give the product (13 mg, 20.78 µmol, 12%) as a red powder.

IR (ATR) /cm^{-1}: 3476, 2925, 2855, 1724, 1618, 1579

^{1}H NMR (400 MHz, $CDCl_3$) δ 13.98 (s, 1H; OH_{phenol}), 13.21 (s, 1H; OH_{phenol}), 8.01 (dd, *J* = 7.8, 1.1 Hz, 1H; $H_{1/3}$), 7.78 (t, *J* = 8.1 Hz, 1H; H_2), 7.39 (dd, *J* = 8.6, 1.1 Hz, 1H; $H_{1/3}$), 5.53 – 5.49 (m, 1H; $H_{1'}$), 5.31 – 5.26 (m, 1H; H_7), 4.74 (s, 2H; CH_2OH), 4.55 (s, 1H; 9-O*H*), 4.32 – 4.23 (m, 1H; $H_{5'}$), 4.08 (s, 3H; OMe), 3.93 – 3.89 (m, 1H; $H_{3'/4'}$), 3.89 – 3.83 (m, 2H; $H_{3'/4'}$), 3.26 (dd, *J* = 18.9, 1.9 Hz, 1H; H_{10}), 3.05 – 2.95 (m, 2H; H_{10}), 2.38 (d, *J* = 14.8 Hz, 1H; H_8), 2.22 – 2.13 (m, 1H; H_8), 2.11 – 2.02 (m, 1H; $H_{2'}$), 1.97 (s, 3H; Ac), 1.79 (ddd, *J* = 13.9, 10.3, 3.9 Hz, 1H; $H_{2'}$), 1.69 (s, 3H; CMe_2), 1.56 (s, 3H; CMe_2), 1.39 (d, *J* = 6.7 Hz, 3H; 5'-Me)

^{13}C NMR (101 MHz, $CDCl_3$) δ 213.43, 187.13, 186.74, 166.61, 161.08, 156.16, 155.53, 135.90, 135.40, 133.51, 133.32, 120.77, 119.86, 118.51, 111.63, 111.53, 100.42, 95.03, 72.19, 70.06, 65.45, 64.00, 56.71, 51.78, 35.33, 34.02, 31.55, 29.70, 26.86, 23.88, 23.56, 16.79

MS(ESI): calcd. for $C_{32}H_{36}NO_{12}$ $[M+H]^+$ 626.2232, found 626.2218

FU-am (49)

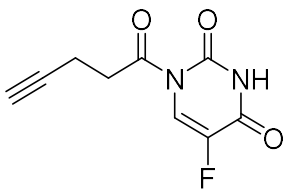

5-Fluorouracil (50 mg, 1.0 eq., 384.38 µmol), EDC·HCl (81 mg, 1.1 eq., 422.82 µmol) and 4-pentynoic acid (**37**) (45 mg, 1.2 eq., 461.26 µmol) were dissolved in DMF (1 mL). TEA (0.21 mL, 4.0 eq., 1.54 mmol) was added and the reaction stirred at room temperature for 20 h. The reaction was evaporated, then diluted in EtOAc and washed with dilute $NaHCO_3$ (10 mL), 3 M HCl (10 mL) and brine (10 mL). The

organics were dried over $MgSO_4$, filtered and evaporated *in vacuo*. The crude material was purified by filtration over silica (5 g) in EtOAc to give the product (22 mg, 104.69 µmol, 27%) as a white powder.

IR (ATR) /cm^{-1}: 3251, 3083, 2921, 1743, 1693, 1681

^{1}H NMR (500 MHz, $CDCl_3$) δ 8.90 (s, 1H; N*H*), 8.30 (d, *J* = 6.6 Hz, 1H; H_6), 3.39 (t, *J* = 6.9 Hz, 2H; CH_2CO), 2.63 (td, *J* = 6.9, 2.7 Hz, 2H; CH_2CC), 2.00 (t, *J* = 2.7 Hz, 1H; H_{alkyne})

^{13}C NMR (126 MHz, $CDCl_3$) δ 170.16 , 156.31 (d, *J* = 28.6 Hz), 147.66 , 141.44 (d, *J* = 245.0 Hz), 121.43 (d, *J* = 36.8 Hz), 81.83 , 69.48 , 38.33 , 29.68 , 14.01

MS(ESI): calcd. for $C_9H_6FN_2O_3$ $[M-H]^-$ 209.0362 , found 209.0363

MMAE-am (50)

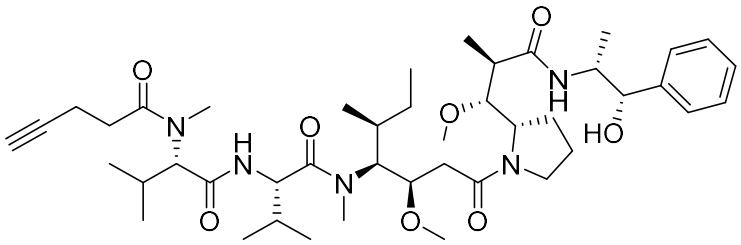

4-pentynoic acid (**37**) (1.4 mg, 2.0 eq., 13.9 µmol) was dissolved in DMF (0.5 mL) and HBTU (5.3 mg, 2.0 eq., 13.9 µmol) was added followed by DIPEA (6 µL, 5.0 eq., 34.8 µmol) at room temperature. After 10 min, **MMAE** (5 mg, 1.0 eq., 6.96 µmol) was added in one portion. The reaction was stirred for 6 h then evaporated *in vacuo*. The crude product was dissolved in DCM (10 mL) and washed with 3 M HCl (5 mL), water basified to ~pH 8 with sat. aq. $NaHCO_3$ solution (5 mL) and water (5 mL). The organics were dried over $MgSO_4$, filtered and evaporated *in vacuo*. The crude material was purified by preparative HPLC with a gradient of 50-95% H_2O/MeCN + 0.1% TFA for 0-15 min, then 95% for 15-20 min, then 95-50% for 20-22 min to give the desired product (4 mg, 5.01 µmol, 72%).

MMAE R_t = 4.3 min – peak confirmed by high-res mass spec

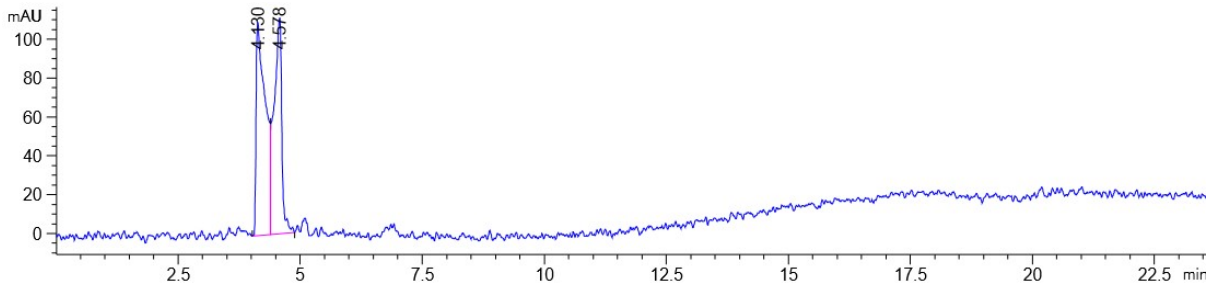

Reaction mixture, **MMAE-am** (**50**), R_t = 12.4 min – peak confirmed by high-res mass spec

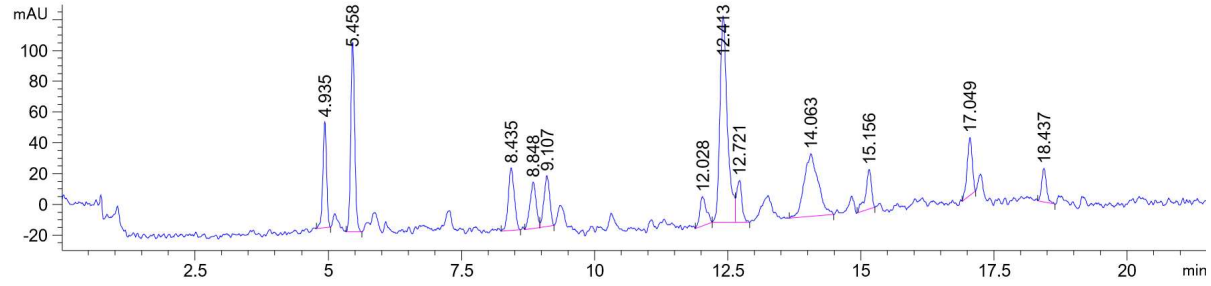

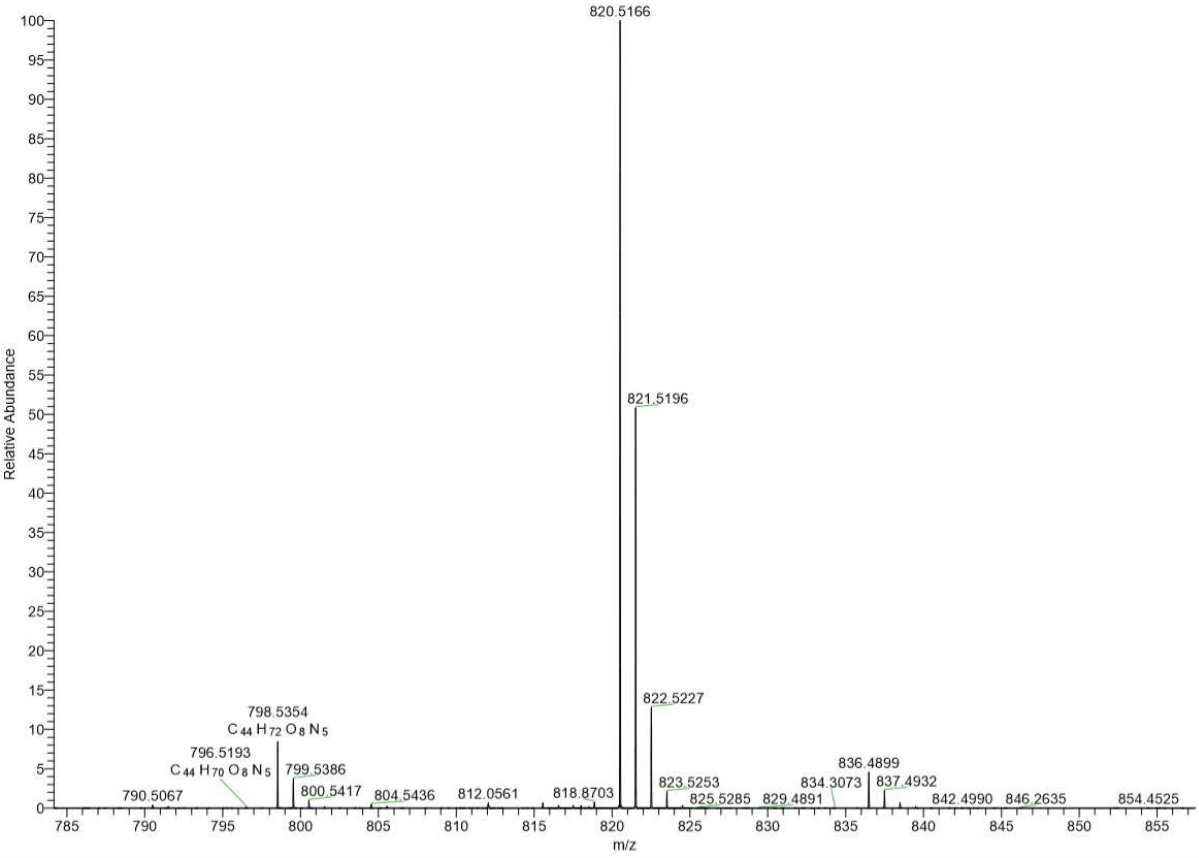

MS(ESI): calcd. for $C_{44}H_{72}O_8N_5$ $[M+H]^+$ 798.5375, found 798.5354

MS(ESI): calcd. for $C_{44}H_{71}O_8N_5Na$ $[M+Na]^+$ 820.5194, found 820.5166

MMAEam decaging (5 h) R_t = 3.5 min – peak confirmed by high-res mass spec

MMAE-am (2.1 mg, 1.0 eq., 2.63 µmol) was reacted with $NaAuCl_4$ (10.5 mg, 10 eq., 26.3 µmol) in 1:1 MeCN:H_2O for 5 h. A 0.5 mL aliquot was taken and the reaction quenched by addition of vitamin A (2.6 mg, 22 eq., 14.8 µmol). This reduces the gold complexes to a brown precipitate, which can then be filtered before HPLC.

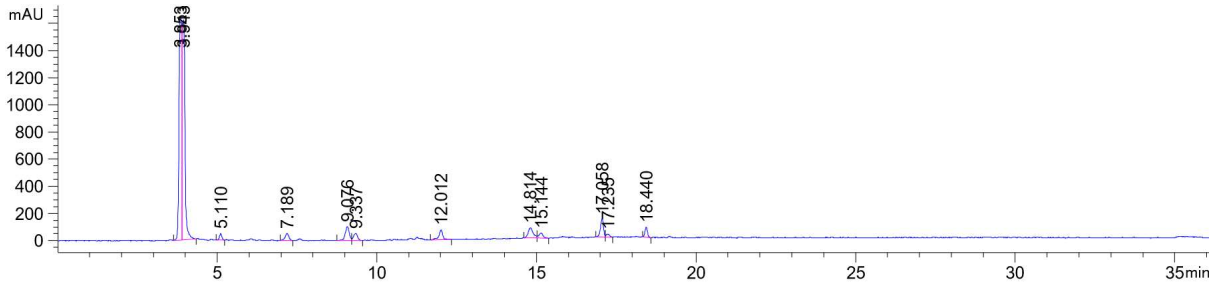

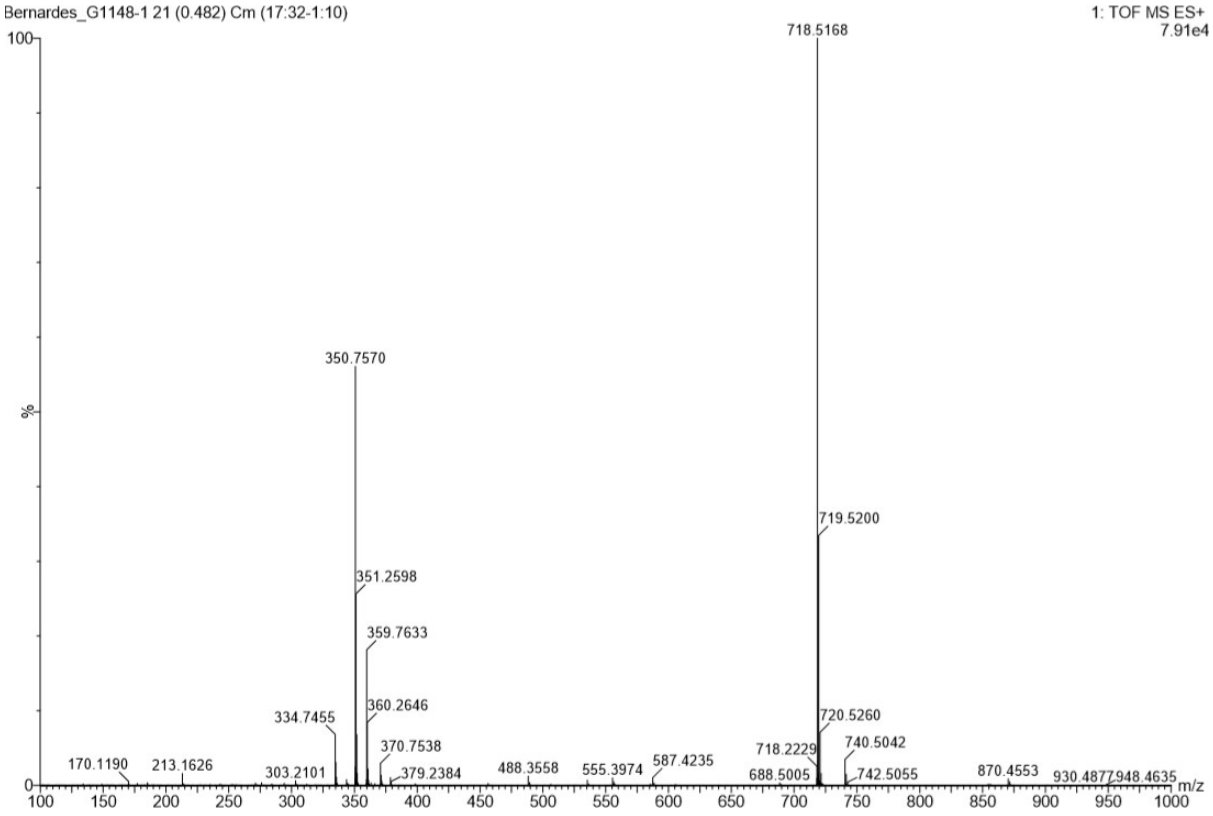

MS(ESI): calcd. for $C_{39}H_{68}O_7N_5$ $[M+H]^+$ 718.5113, found 718.5168

pFU (51)

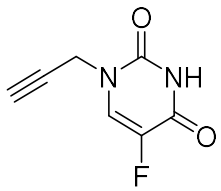

5-Fluorouracil (400 mg, 1.0 eq., 3.08 mmol) was dissolved in dry DMF and DBU (460 µL, 1.0 eq., 3.08 mmol) was added at room temperature followed by 80% propargyl bromide in toluene (343 µL, 1.0 eq., 3.08 mmol). The reaction was stirred at room temperature for 20 h then evaporated *in vacuo* at 50 °C. The crude product was purified by flash column chromatography on silica (100 g) with a gradient

of 50-75% EtOAc/petrol to give the desired product (136 mg, 0.808 mmol, 26%) as a white powder. The data were in accordance with the literature.[187]

^{1}H NMR (400 MHz, $CDCl_3$) δ 7.56 (d, *J* = 5.4 Hz, 1H; $H_{aromatic}$), 4.56 (d, *J* = 2.6 Hz, 2H; CH_2), 2.55 (d, *J* = 2.6 Hz, 1H; C≡C*H*)

tert-Butyl (2-(2-hydroxyethoxy)ethyl)carbamate (53)

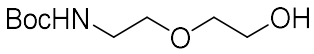

2-(2-aminoethoxy)ethan-1-ol **52** (5 mL, 1.0 eq., 49.8 mmol) was dissolved in THF (100 mL) and Boc_2O (12.0 g, 1.1 eq., 54.8 mmol) was added in one portion at 0 °C. $NaHCO_3$ (8.37 g, 2.0 eq., 99.7 mmol) dissolved in water (60 mL) was then added dropwise to the reaction over 10 min. The reaction was warmed to room temperature and stirred for 3 days then evaporated to ~½ volume *in vacuo*. EtOAc (100 mL) was added and washed with 3 M HCl (50 mL). The aqueous layer was extracted with EtOAc (50 mL) and the combined organics were washed with brine (50 mL), dried over $MgSO_4$, filtered and evaporated *in vacuo* to give the desired product (7.93 g, 49.8 mmol, 78%) as a clear oil. The data were in accordance with the literature.[255]

^{1}H NMR (400 MHz, $CDCl_3$) δ 4.90 (br. s, 1H; N*H*), 3.76 – 3.71 (m, 2H; CH_2OH), 3.59 – 3.52 (m, 4H; OCH_2), 3.36 – 3.28 (m, 2H; NCH_2), 1.45 (s, 9H; (CH_3)$_3$)

tert-Butyl (2-(2-(prop-2-yn-1-yloxy)ethoxy)ethyl)carbamate (54)

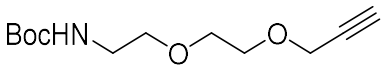

Alcohol **53** (1.0 g, 1.0 eq., 4.87 mmol) was dissolved in freshly distilled THF (25 mL) in an oven dried flask and chilled to 0 °C. 60% NaH in mineral oil (779 mg, 4.0 eq., 19.49 mmol) was added, followed by 80% propargyl bromide in toluene (0.65 mL, 1.5 eq., 7.31 mmol) and the reaction allowed to warm to room temperature. After 2.5 h, the reaction was quenched with sat. aq. NH_4Cl (50 mL) and separated. The aqueous layer was extracted with EtOAc (2 x 30 mL) and the combined organics dried over $MgSO_4$, filtered and evaporated *in vacuo*. The crude product was purified by flash chromatography on silica (200 g) with 35% EtOAc/petrol to give the desired product (563 mg, 2.31 mmol, 48%) as a clear oil. The data were in accordance with the literature.[256]

R_f (30% EtOAc/petrol) 0.20

^{1}H NMR (400 MHz, $CDCl_3$) δ 4.96 (s, 1H; N*H*), 4.21 – 4.17 (m, 2H; CH_2C≡C), 3.70 – 3.66 (m, 2H; OCH_2), 3.65 – 3.60 (m, 2H; OCH_2), 3.53 (t, *J* = 5.4 Hz, 2H; NCH$_2$CH_2), 3.31 (q, *J* = 5.4 Hz, 2H; NCH_2), 2.43 (td, *J* = 2.4, 0.8 Hz, 1H; C≡C*H*), 1.43 (s, 9H; (CH_3)$_3$)

tert-Butyl (2-(2-((6-hydroxyhex-2-yn-1-yl)oxy)ethoxy)ethyl)methylcarbamate (55)

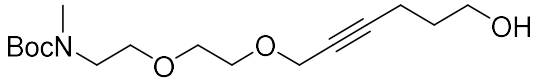

Alkyne **54** (239 mg, 1.0 eq., 0.982 mmol) was dissolved in freshly distilled THF (15 mL) in an oven dried flask then chilled to -78 °C. 1.6 M ^{n}BuLi in hexanes (0.92 mL, 1.5 eq., 1.47 mmol) was added dropwise and stirred for 10 min. MeI (0.61 mL, 10 eq., 9.82 mmol) was added dropwise and the reaction warmed to room temperature. After 2 h the reaction was quenched with sat. aq. NH_4Cl (30 mL) and extracted with EtOAc (3 x 10 mL). The combined organics were dried over $MgSO_4$, filtered and evaporated *in vacuo* to give crude methylated product (237 mg, 0.921 mmol, 94%). The crude material was dissolved in freshly distilled THF (15 mL) and chilled to -78 °C. 1.6 M ^{n}BuLi in hexanes (1.15 mL, 2.0 eq., 1.84 mmol) was added dropwise and stirred for 10 min. Trimethylene oxide (120 µL,2.0 eq., 1.84 mmol) was added followed by $BF_3{\cdot}Et_2O$ (0.23 mL, 2.0 eq., 1.84 mmol), then the reaction was warmed to room temperature and stirred for 2 h. The reaction was quenched with sat. aq. NH_4Cl (30 mL) and extracted with EtOAc (3 x 10 mL). The combined organics were dried over $MgSO_4$, filtered and evaporated *in vacuo*. The crude material was purified by flash chromatography on silica (50 g) with 80% EtOAc/petrol to give the desired product (119 mg, 0.377 mmol, 41%) as a clear oil.

R_f (80% EtOAc/petrol) 0.29

^{1}H NMR (400 MHz, $CDCl_3$) δ 4.16 (t, *J* = 2.2 Hz, 2H; OCH_2C≡C), 3.73 (t, *J* = 6.7 Hz, 2H; CH_2OH), 3.66 – 3.49 (m, 7H; N*H* + OCH_2), 3.38 (br. s, 2H; NCH_2), 2.90 (s, 3H; NCH_3), 2.33 (tt, *J* = 6.7, 2.2 Hz, 2H; C≡CCH_2CH$_2$), 1.75 (tt, *J* = 6.7 Hz, 2H; CH$_2$CH_2CH$_2$), 1.43 (s, 9H; (CH_3)$_3$)

^{13}C NMR (101 MHz, $CDCl_3$) δ 155.77, 86.28, 79.42, 76.39, 70.30, 69.58, 68.91, 61.56, 58.95, 48.37, 35.32, 31.18, 28.45, 15.31

MS(ESI): calcd. for $C_{16}H_{29}NO_5Na$ $[M+Na]^+$ 338.1938, found 338.1935

Perfluorophenyl (*E*)-4-oxo-4-phenylbut-2-enoate (58)

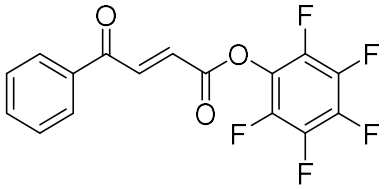

3-benzoylacrylic acid (250 mg, 1.0 eq., 1.42 mmol) was dissolved in freshly distilled DCM (8 mL) and DIPEA (495 µL, 2.0 eq., 2.84 mmol) was added .The solution was chilled to 0 °C and then pentafluorophenyl trifluoroacetate (265 µL, 1.1 eq., 1.56 mmol) was added and then the reaction warmed to room temperature. After 3 h, the reaction was filtered through silica (30 g) in DCM and then evaporated *in vacuo* to give the desired product (466 mg, 1.36 mmol, 96%) as a yellow solid which was used without further purification.

Acrylamide-(platinum cleavable linker)-MMAE (59)

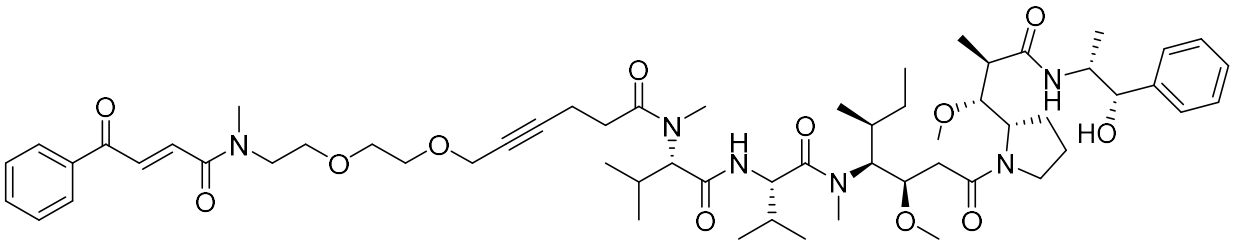

Alcohol **55** (12 mg 3.9 eq., 38.1 µmol) was dissolved in freshly distilled DCM (5 mL) and pyridine (30.8 µL, 39.1 eq., 381 µmol) was added followed by DMP (48 mg, 11.6 eq., 113 µmol) at room temperature. After 2 h, further DMP (48 mg, 11.6 eq., 113 µmol) was added, and again after 2 h DMP (64 mg, 15.5 eq., 151 µmol) was added. After 2 h, 10% aq. $Na_2S_2O_3$ and basified to pH < 10 with sat. aq. Na_2CO_3 and stirred for 1 h at room temperature. The layers were separated and the aqueous layer extracted with DCM (3 x 10 mL). The organics were dried over $MgSO_4$, filtered and evaporated *in vacuo*. To the crude aldehyde, ^{t}BuOH (1 mL), 50 mM pH 7.4 NaPi (1 mL), 2-methyl-2-butene (80.6 µL, 78.0 eq., 761 µmol) and $NaClO_2$ (17 mg, 19.2 eq., 188 µmol) were added at room temperature and the reaction stirred for 2 h. The reaction was evaporated *in vacuo* to ~½ volume, diluted to 3 M HCl (20 mL) and extracted with DCM (3 x 10 mL). The organics were dried over $MgSO_4$, filtered and evaporated *in vacuo*. The crude acid was dissolved in dry DMF (2 mL) and DIPEA (66.2 µL, 39.0 eq., 380 µmol) was added followed by HATU (14 mg, 3.9 eq., 38.0 µmol). After 1 h, MMAE (7 mg, 1.0 eq., 9.75 µmol) was added and the reaction stirred for 6 h before evaporating *in vacuo* at 40 °C. The crude product was dissolved in $CHCl_3$ (5 mL) and washed with water (5 mL). The crude material was dissolved in 4 M HCl/dioxane (2 mL) at room temperature and stirred for 2 h. The reaction was evaporated *in vacuo*, and the crude ammonium chloride dissolved in dry DMF (1 mL) and DIPEA (66.2 µL, 39.0 eq., 380 µmol) was added followed by

activated ester **58** (13 mg, 3.9 eq., 38.0 µmol). The reaction was stirred for 6 h, evaporated *in vacuo*, then redissolved in 1:1 MeCN:H_2O, filtered and purified by preparative HPLC to give the desired product (0.7 mg, 0.644 µmol, 6.6%).

1st purification:

50% MeCN/H_2O + 0.1% TFA: $\mathbf{R_t}$ = 12.5-14.0 min – peak confirmed by high-res mass spec.

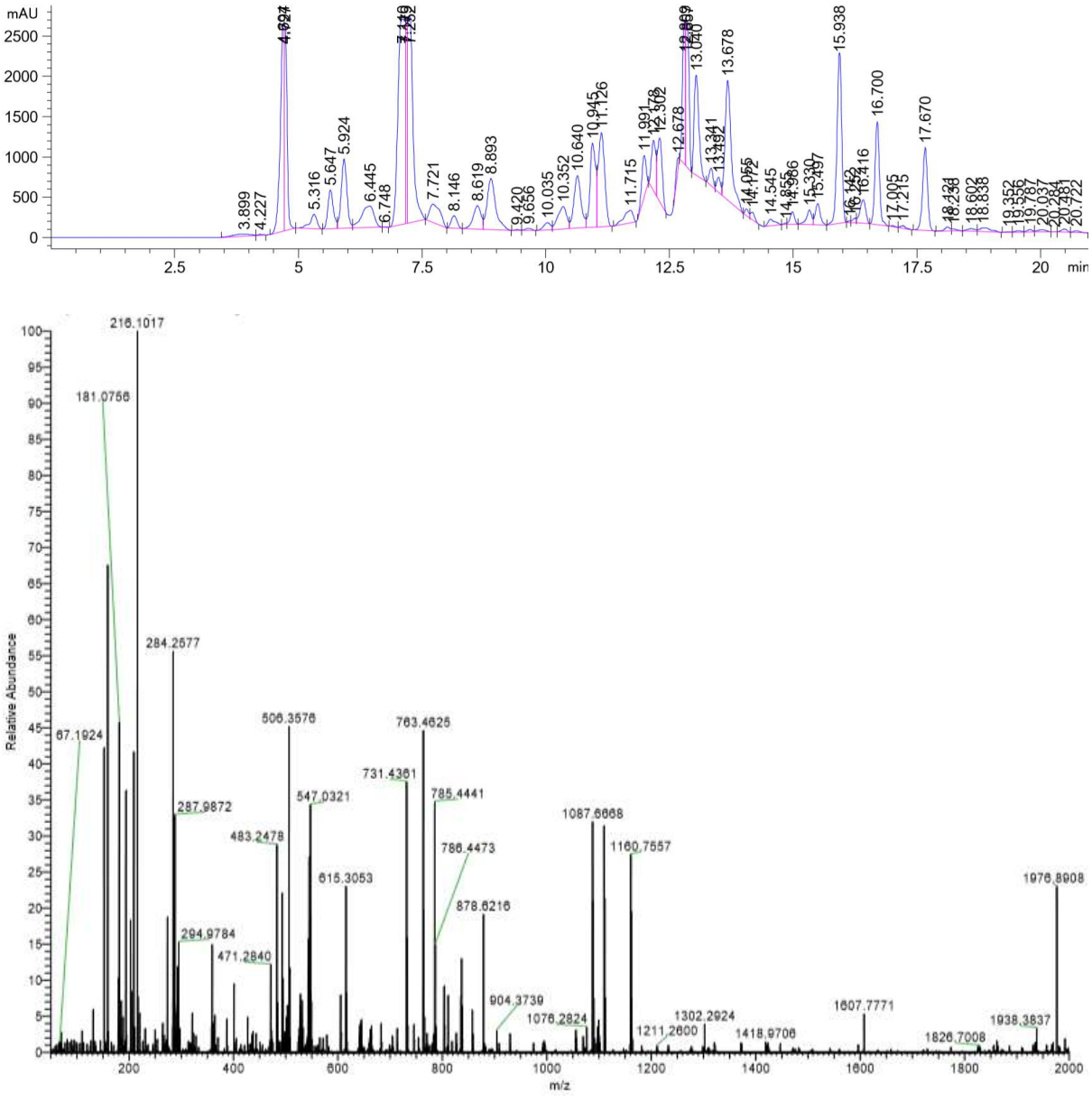

MS(ESI): calcd. for $C_{60}H_{91}N_6O_{12}$ $[M+H]^+$ 1087.6689, found 1087.6669

2nd purification:

0-20 min 40% MeCN/H_2O + 0.1% TFA, 20-30 min 40-70% MeCN/H_2O + 0.1% TFA: $\mathbf{R_t}$ = 29.3 min – peak confirmed by high-res mass spec.

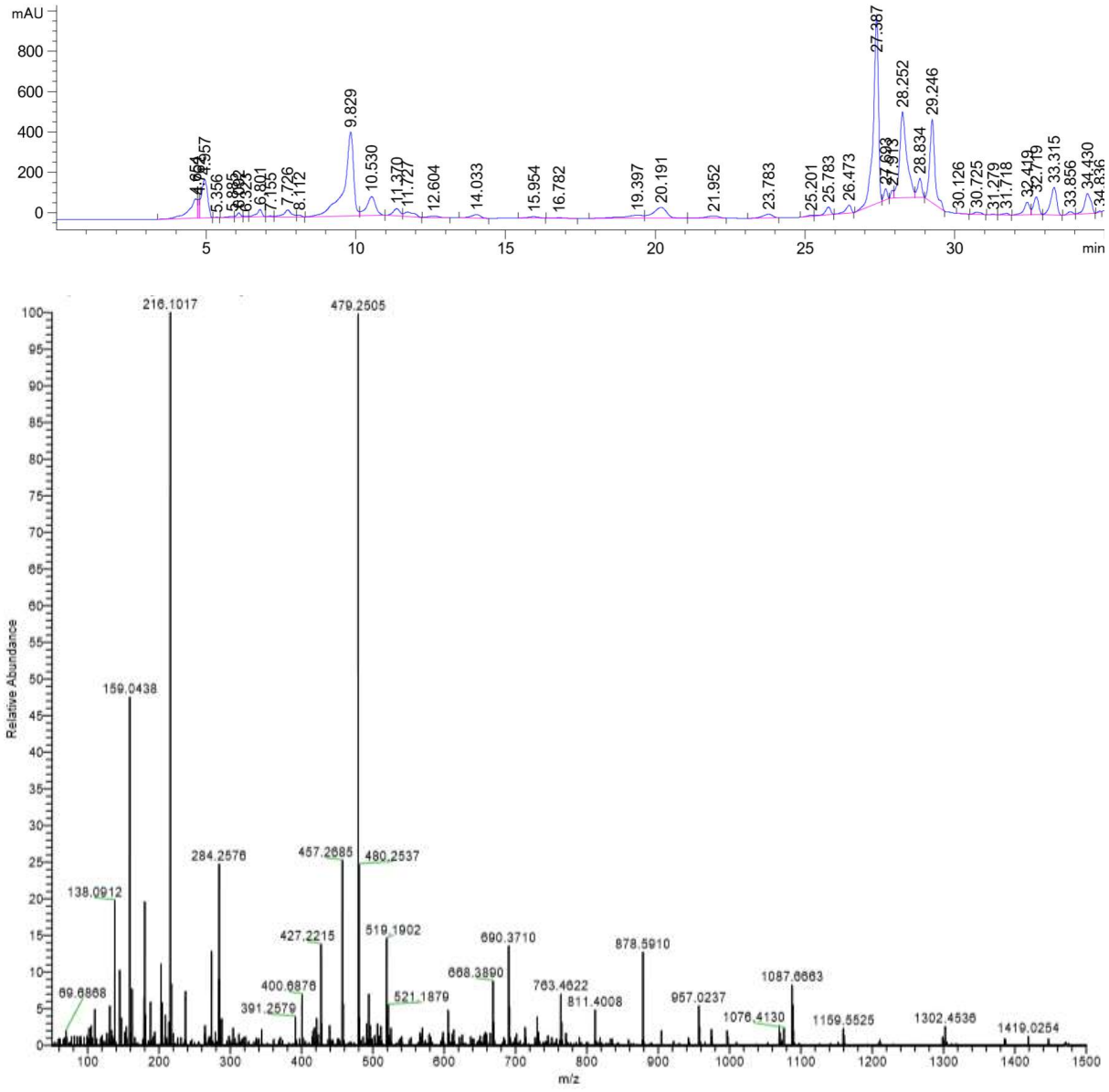

MS(ESI): calcd. for $C_{60}H_{91}N_6O_{12}$ $[M+H]^+$ 1087.6689, found 1087.6663

5.4 NMR spectra for Chapter 3

Propargyl trityl thioether (9a)

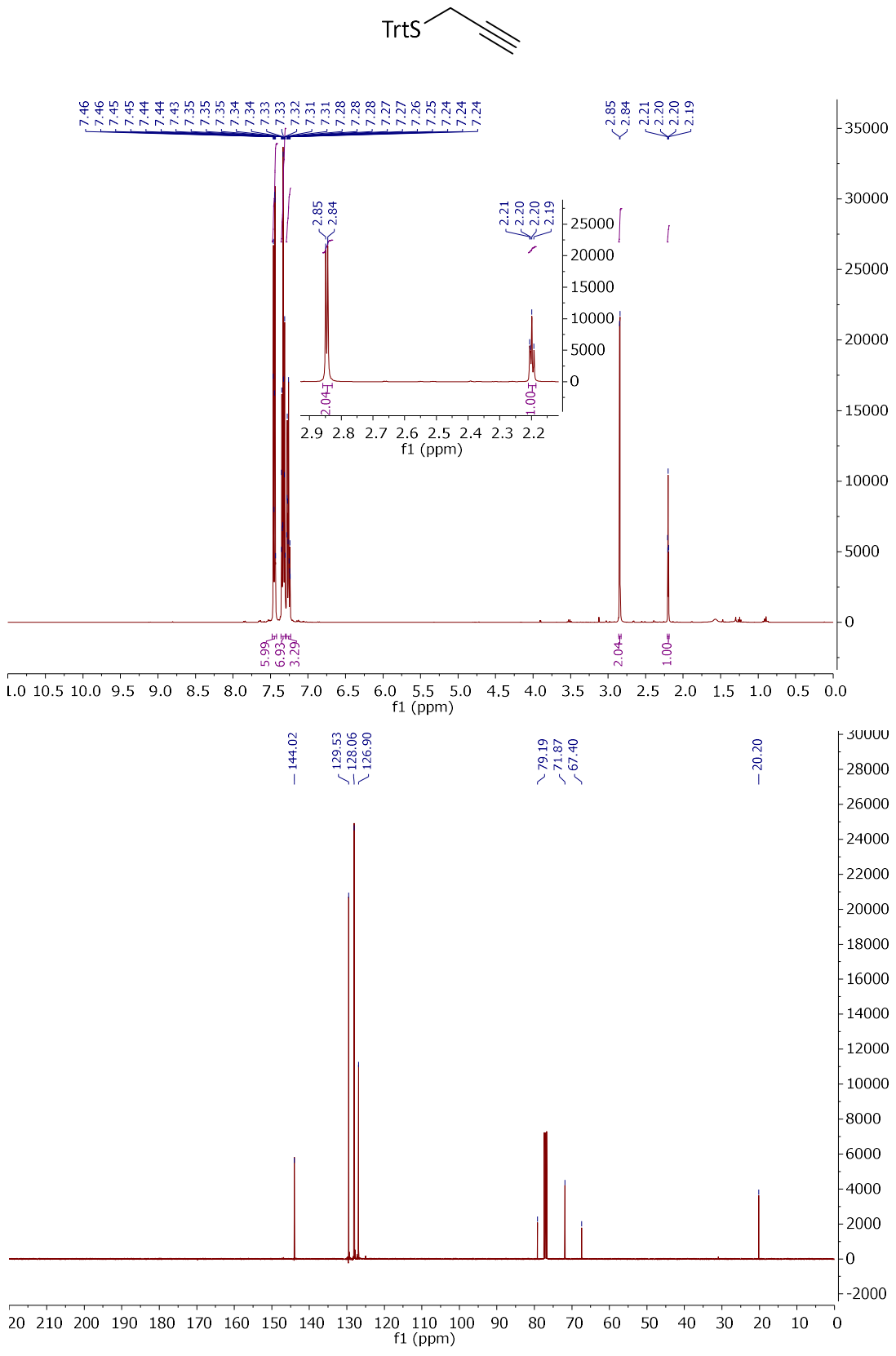

4-(Tritylthio)but-2-yn-1-ol (9b)

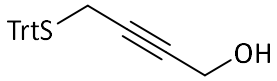

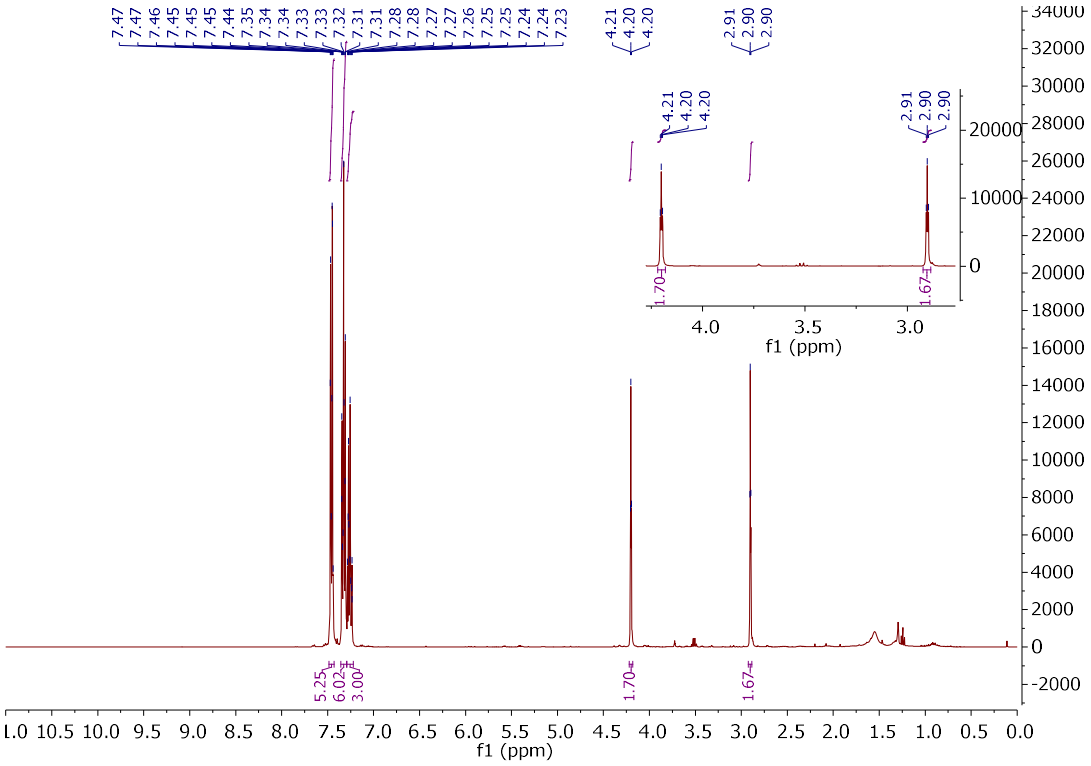

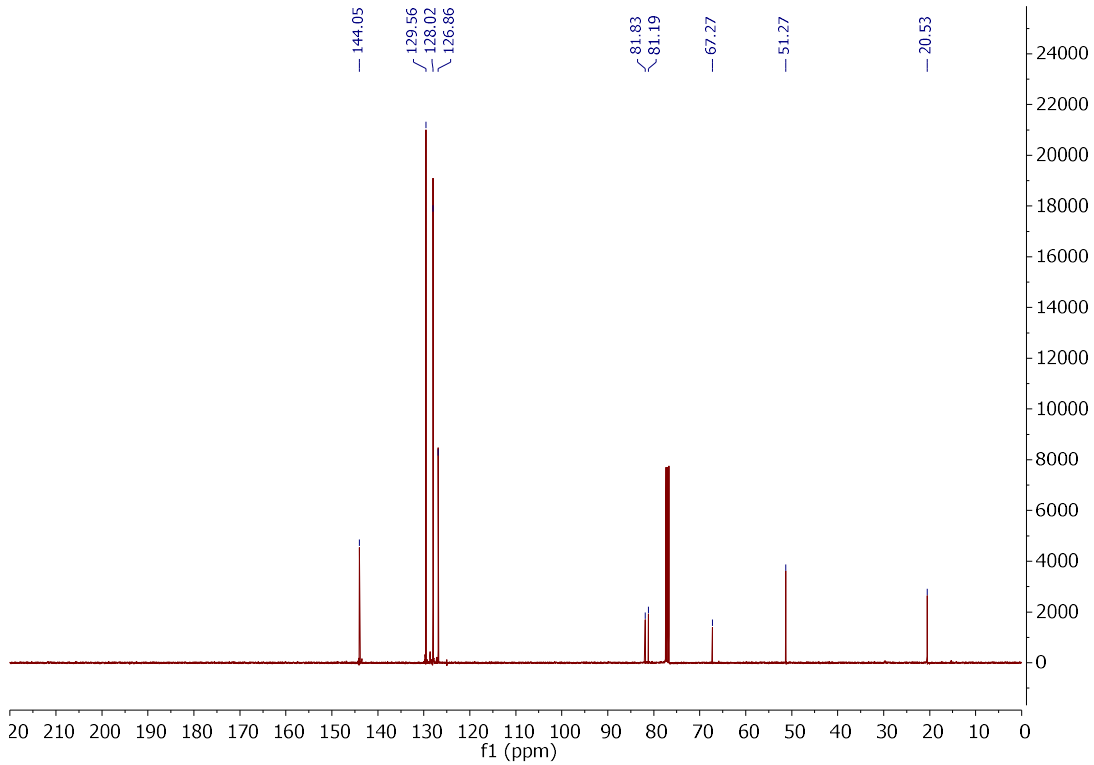

4-(Tritylthio)but-2-ynl (7-amino-4-methylcoumarin)carbamate (9)

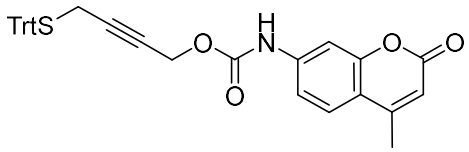

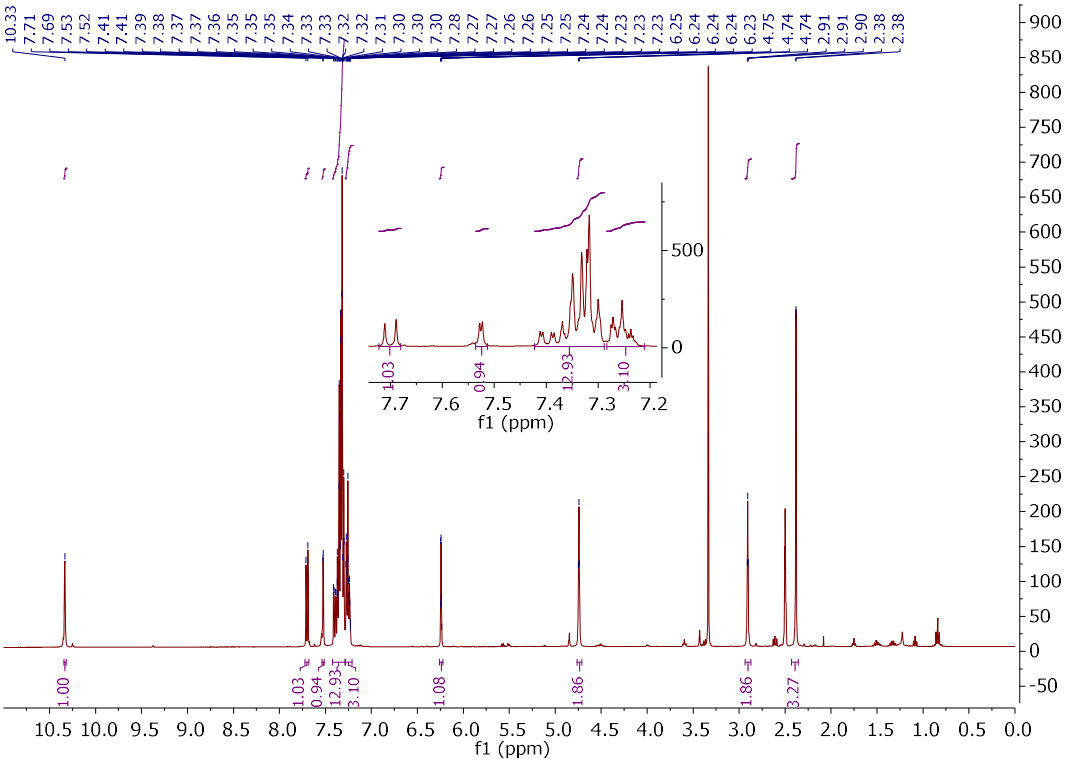

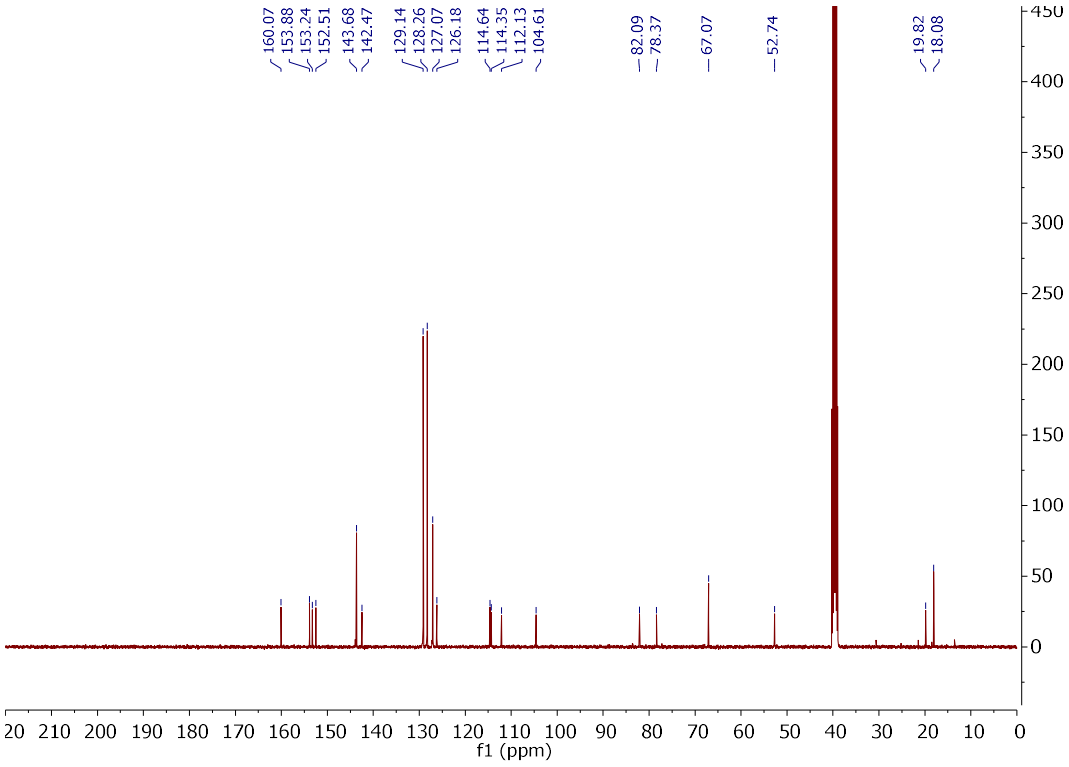

4-(*tert*-Butylthio)but-2-yn-1-yl (7-amino-4-methylcoumarin)carbamate (10)

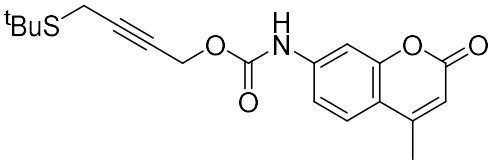

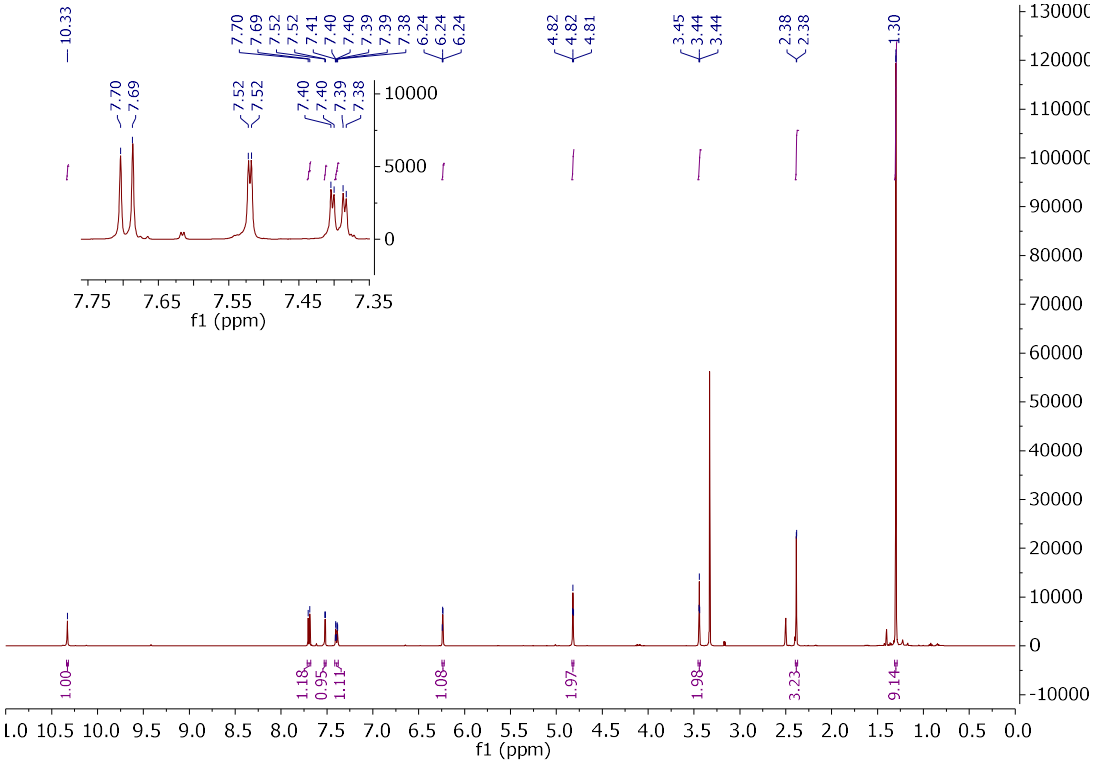

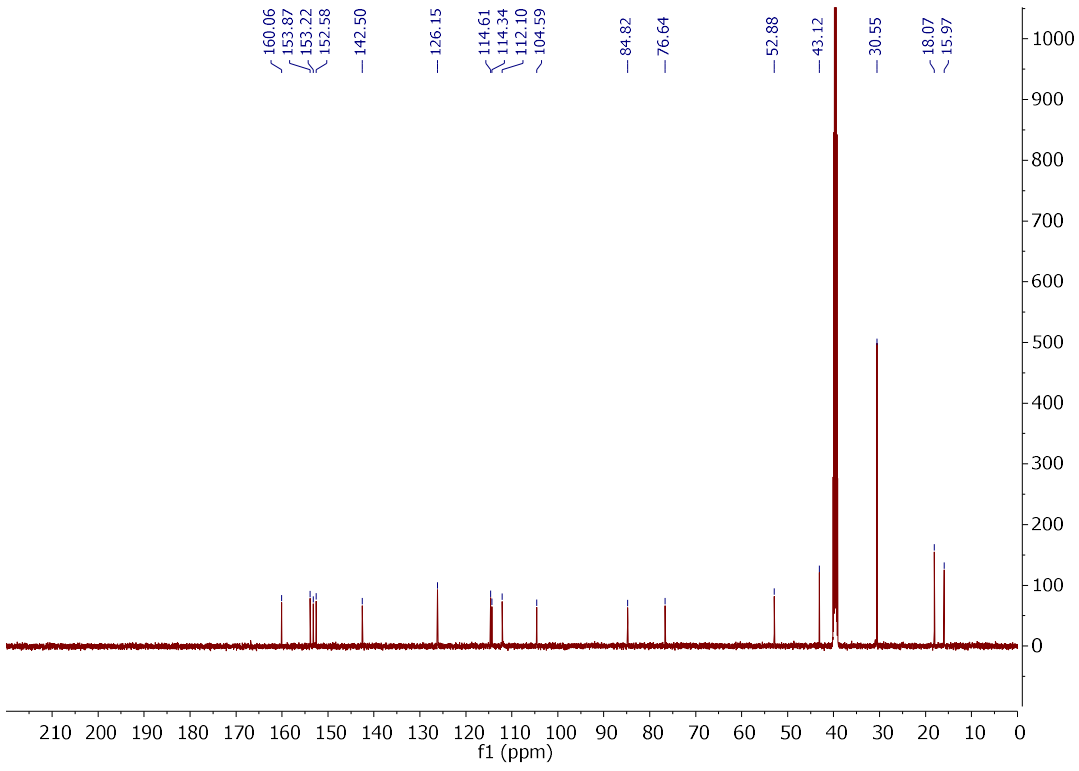

4-(Methylthio)but-2-yn-1-ol (24)

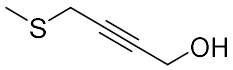

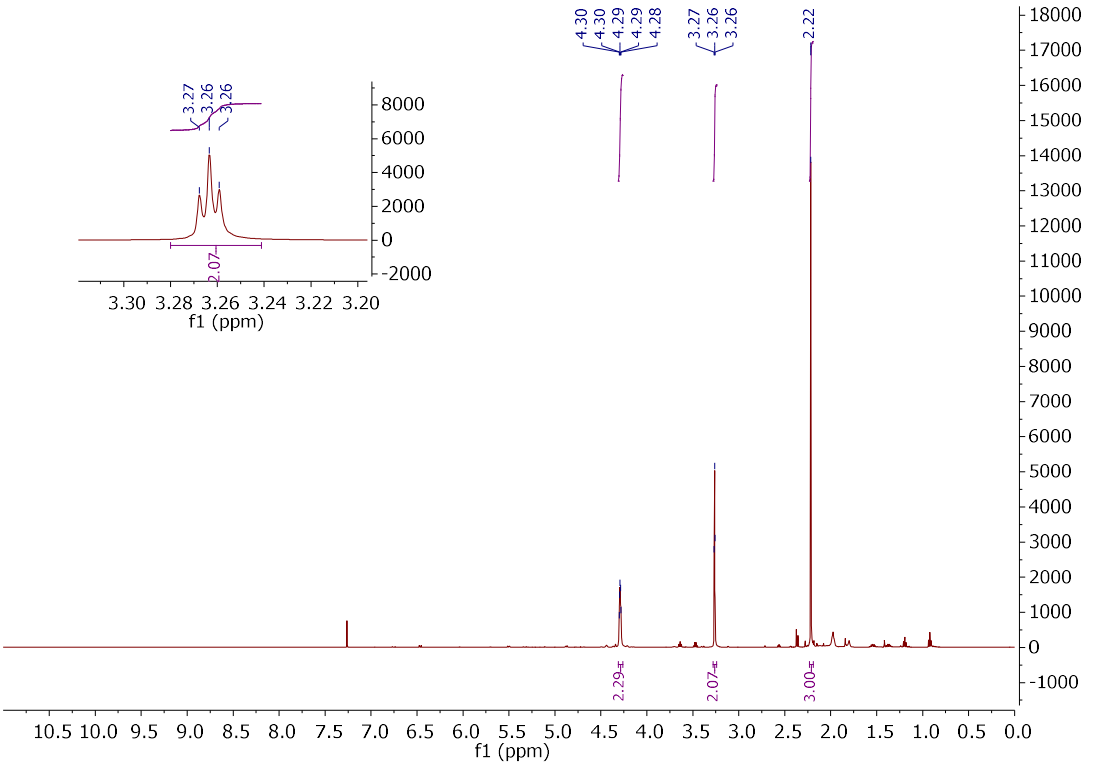

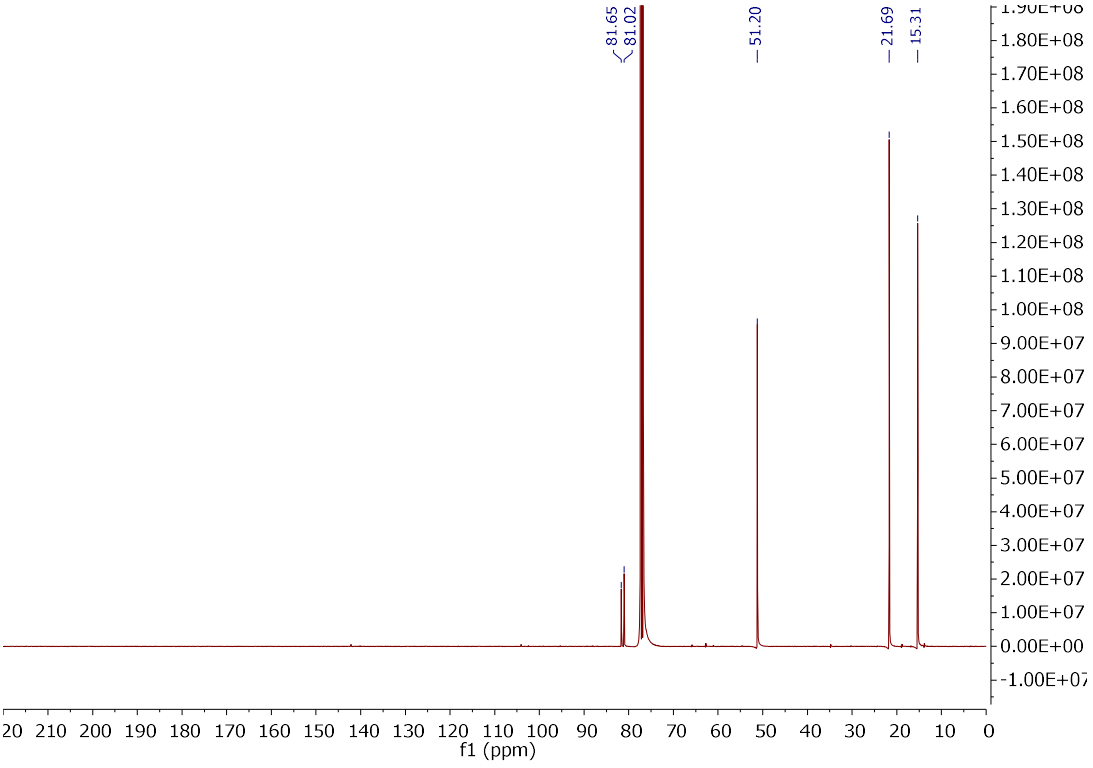

4-(Methylthio)but-2-ynl (7-amino-4-methylcoumarin)carbamate (11)

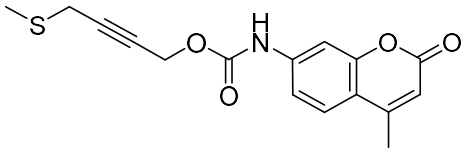

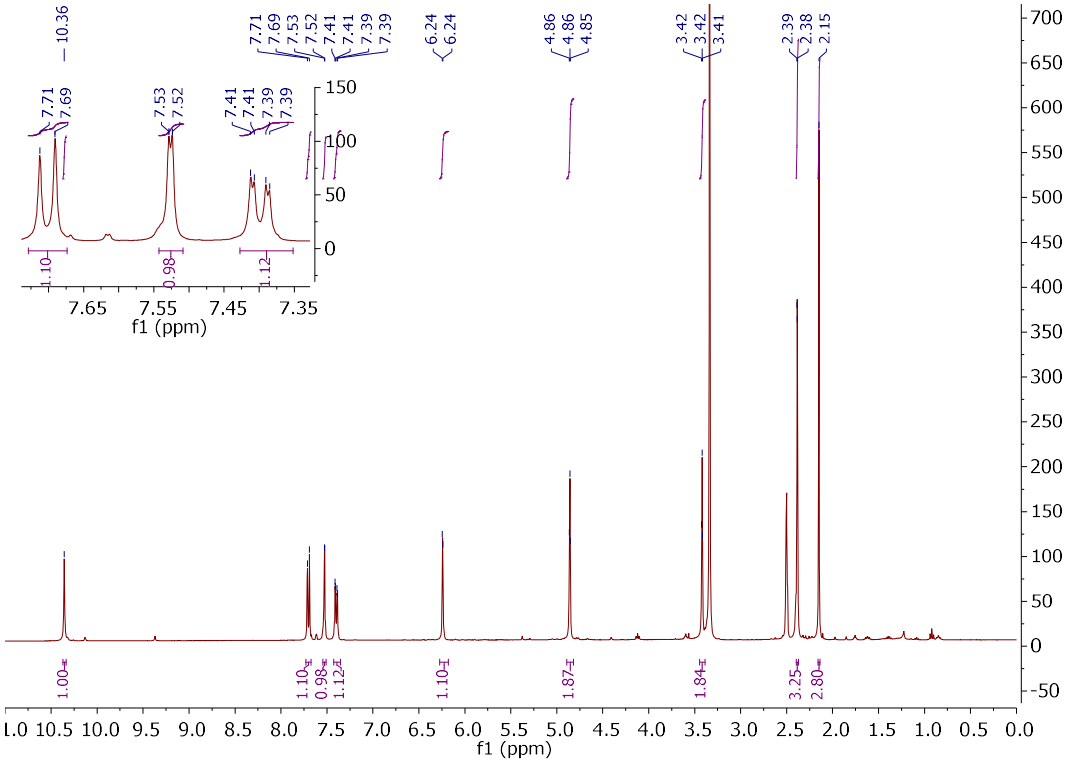

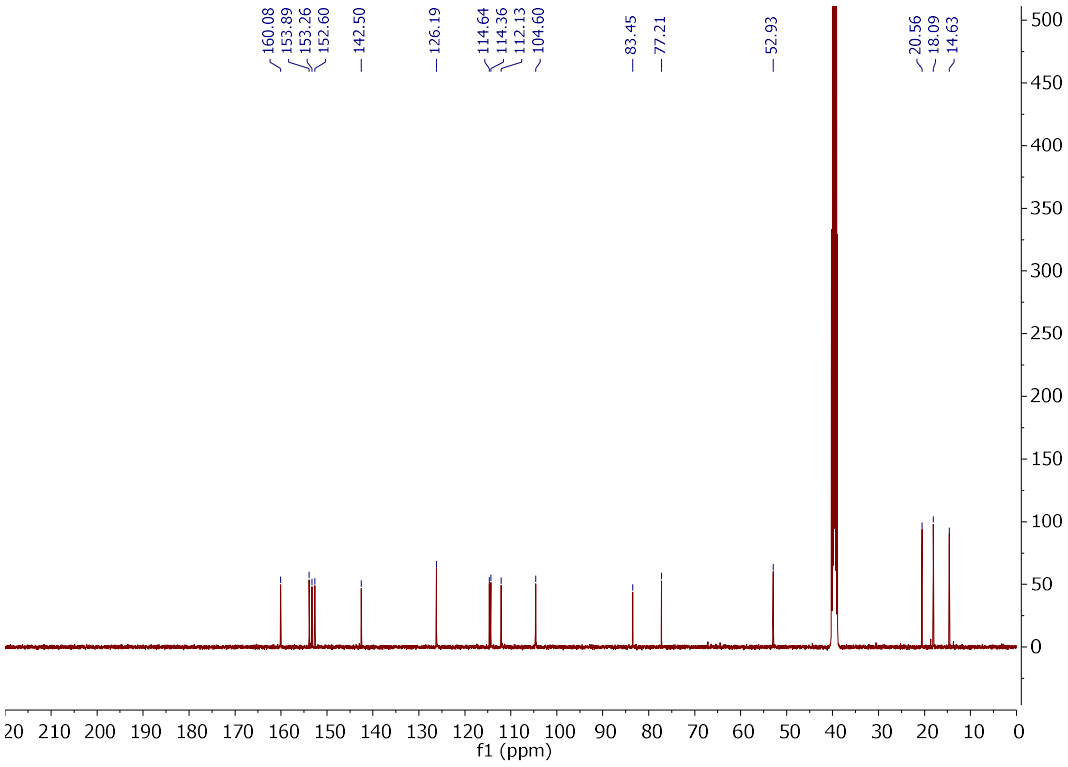

4-(Dimethylamino)but-2-ynl (7-amino-4-methylcoumarin)carbamate (12)

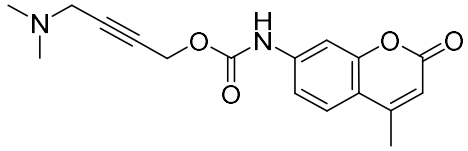

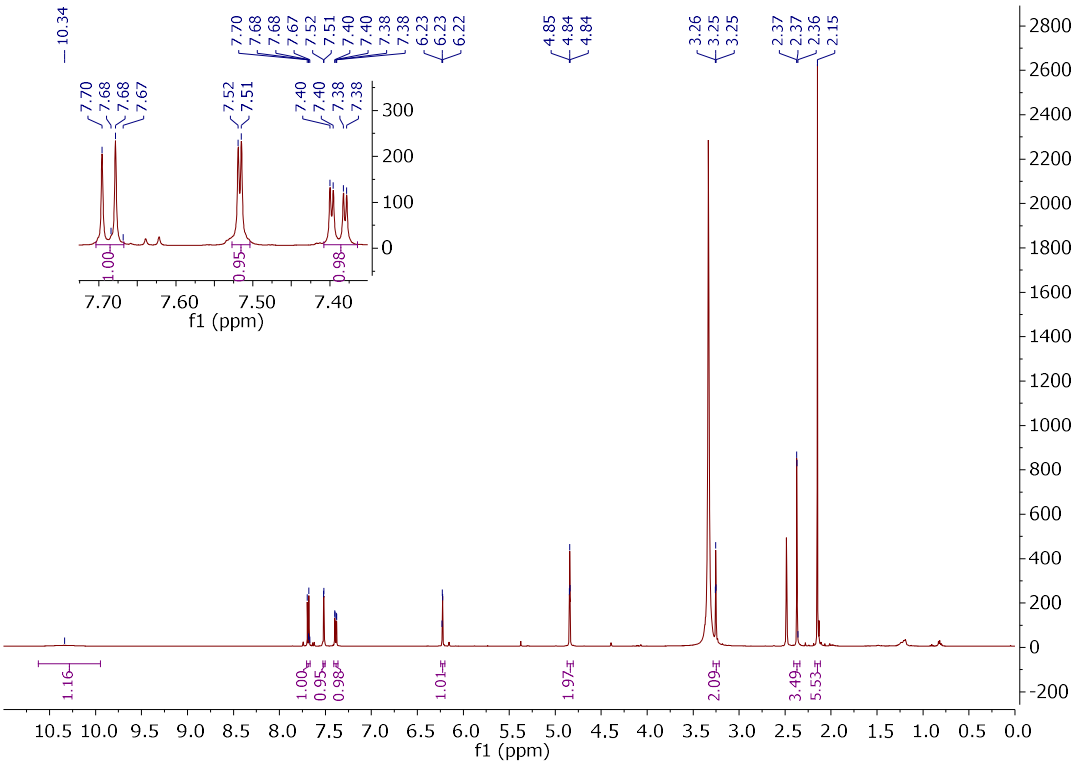

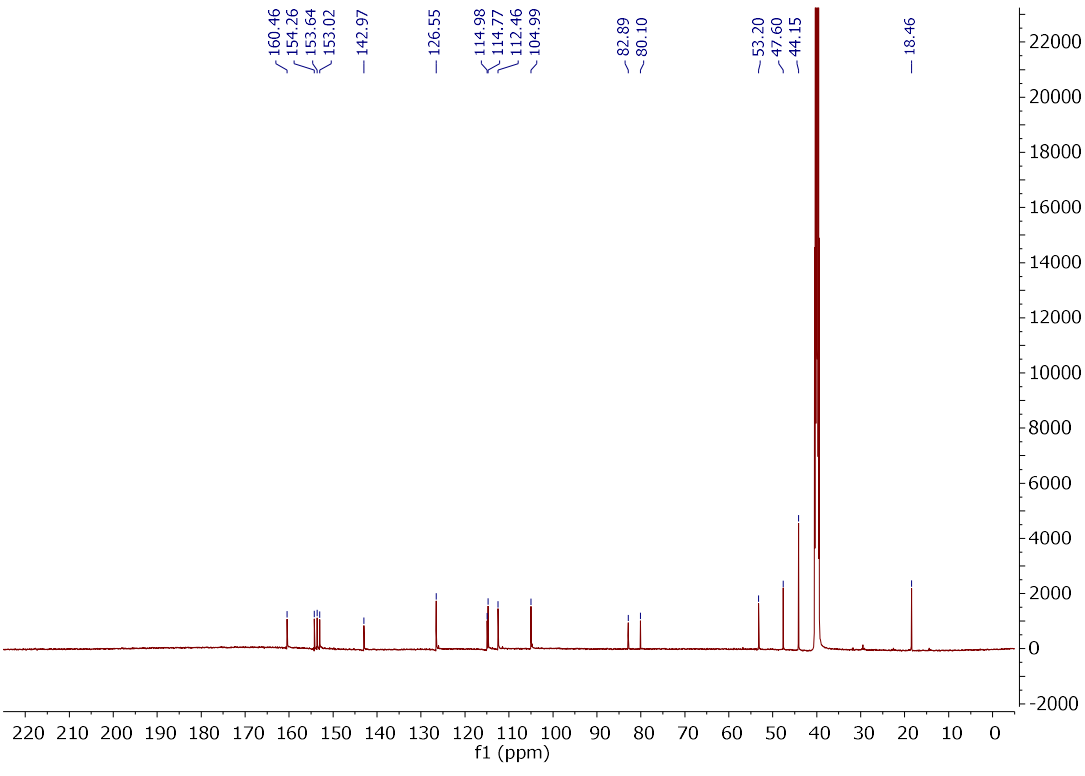

4-(Trityloxy)but-2-ynl (7-amino-4-methylcoumarin)carbamate (13)

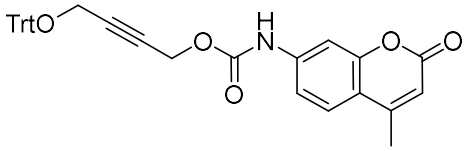

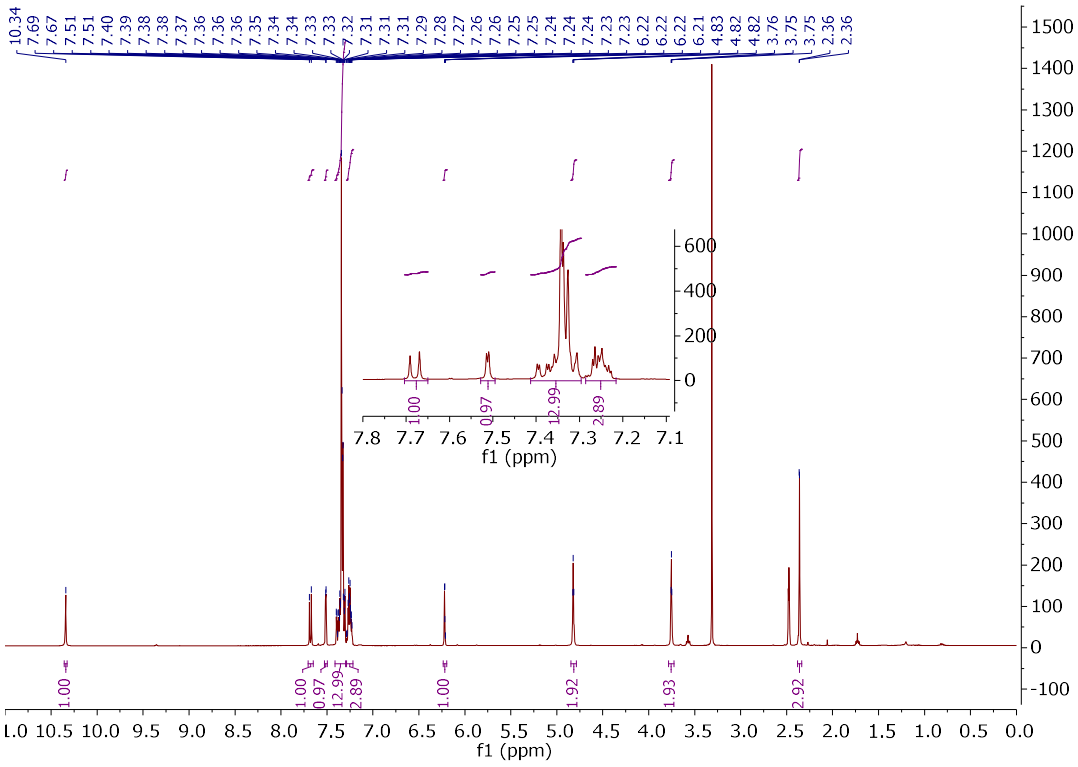

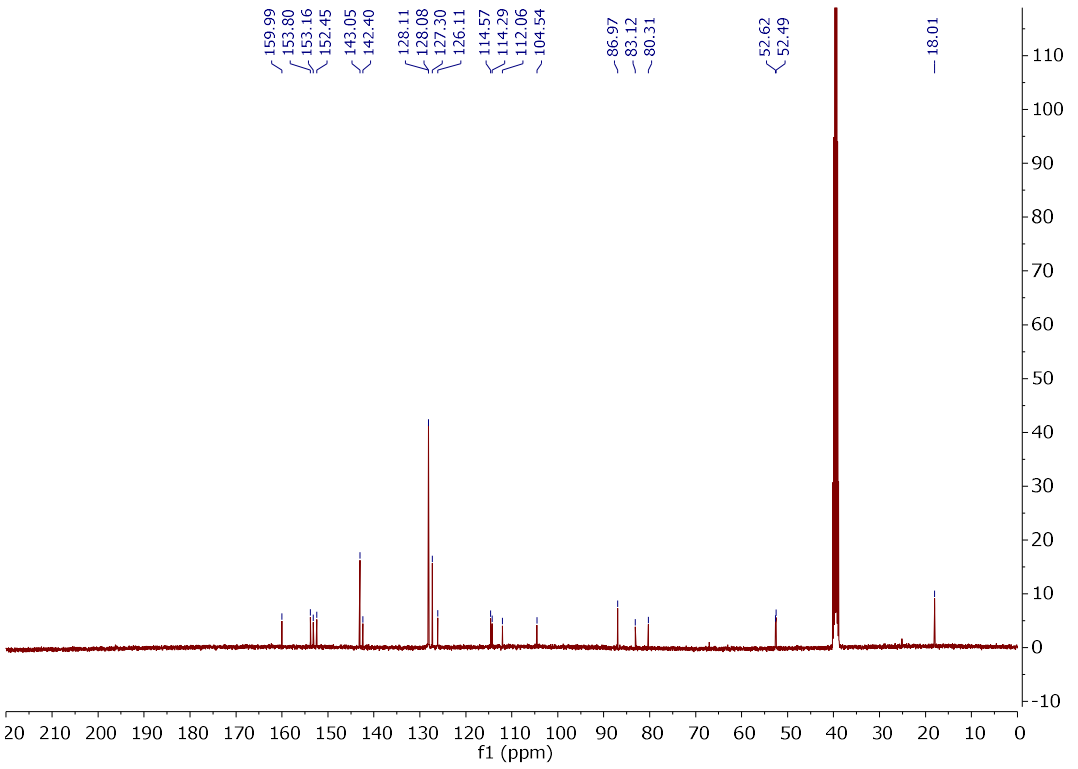

4-Methoxybut-2-ynl (7-amino-4-methylcoumarin)carbamate (14)

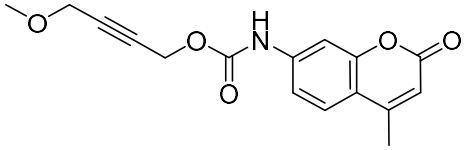

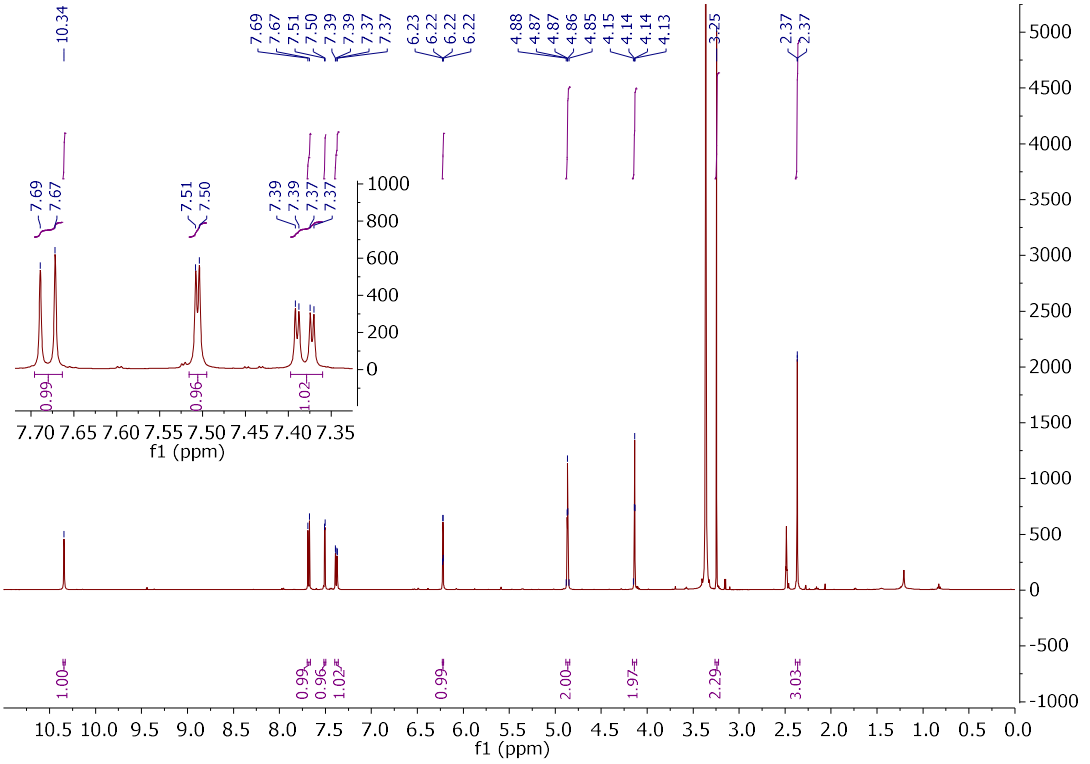

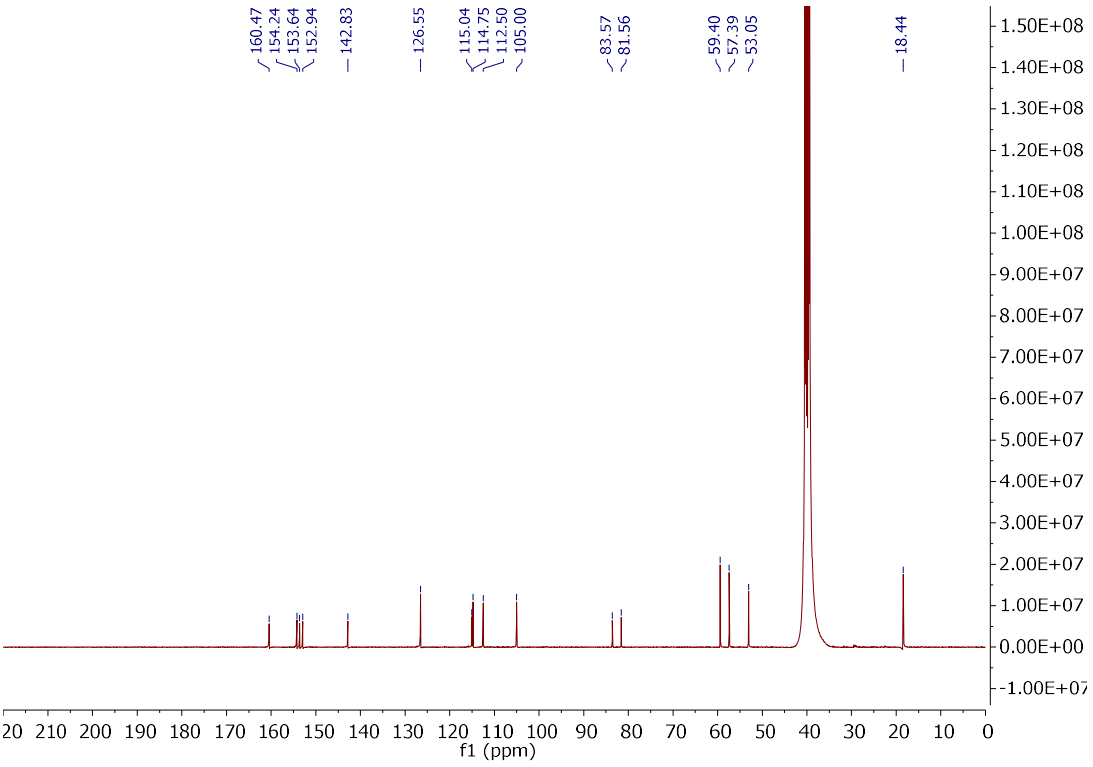

Hex-2-yn-1-yl (7-amino-4-methylcoumarin)carbamate (15)

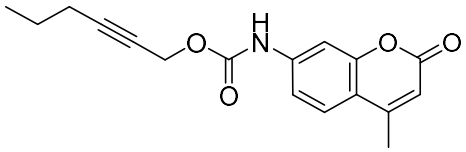

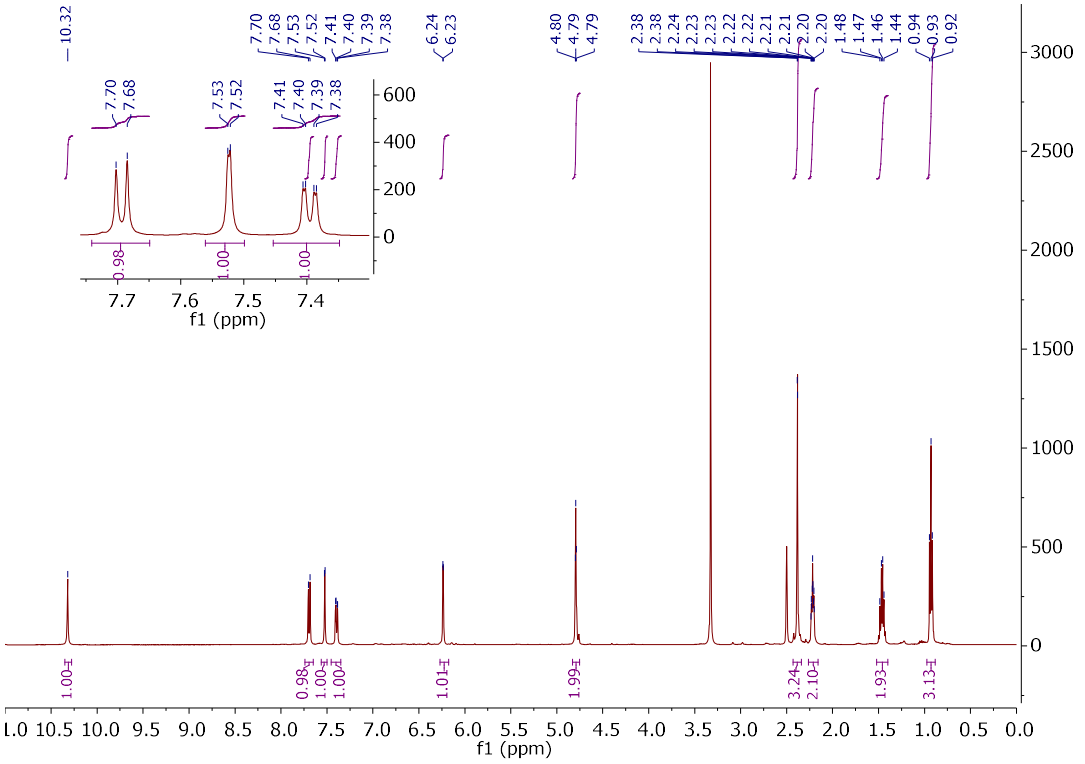

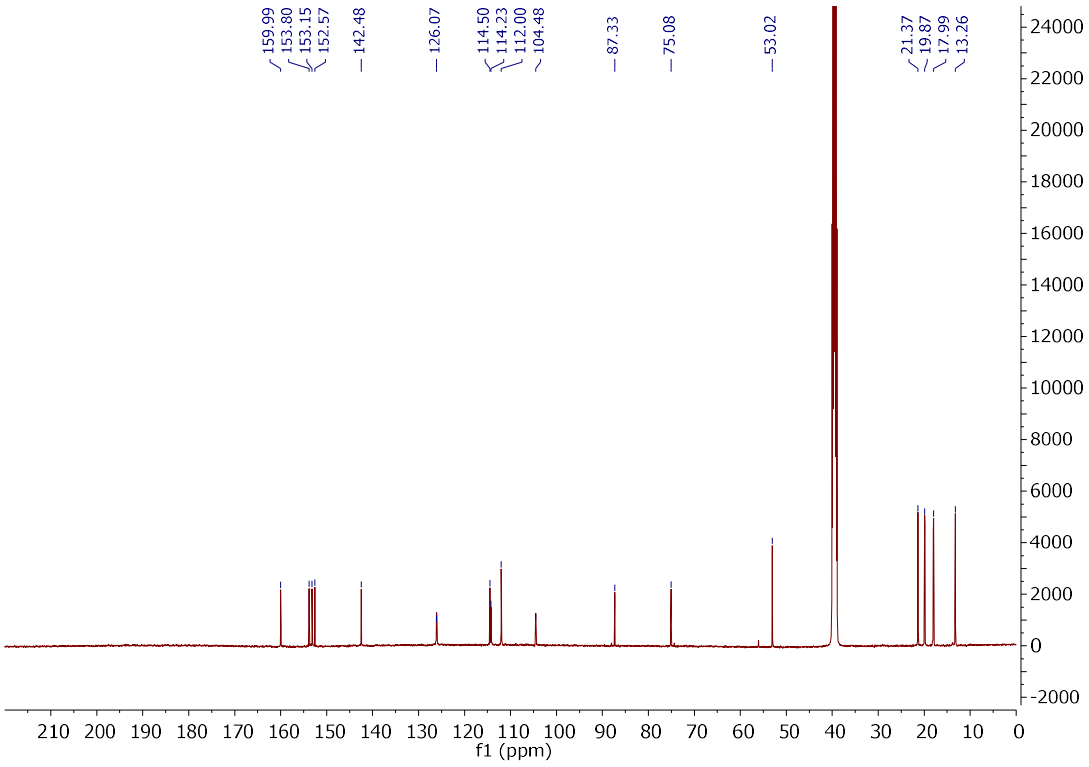

Methyl *N*-(*tert*-butoxycarbonyl)-*S*-(4-hydroxybut-2-yn-1-yl)-*L*-cysteinate (16a)

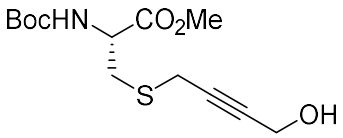

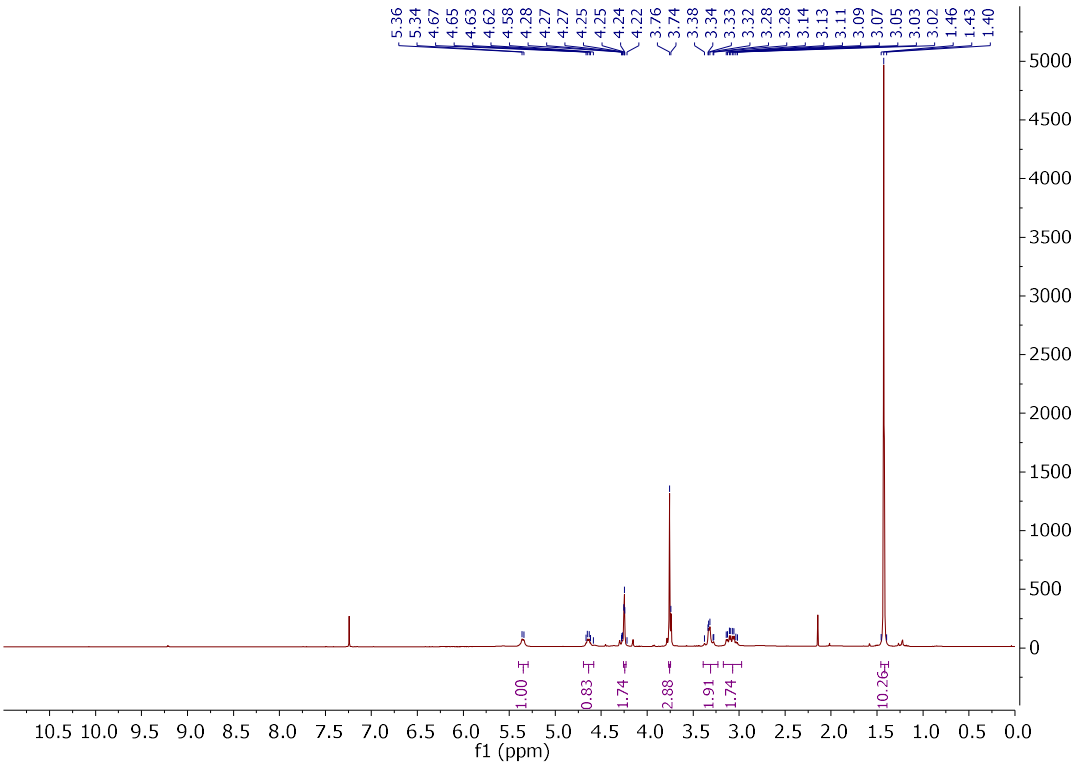

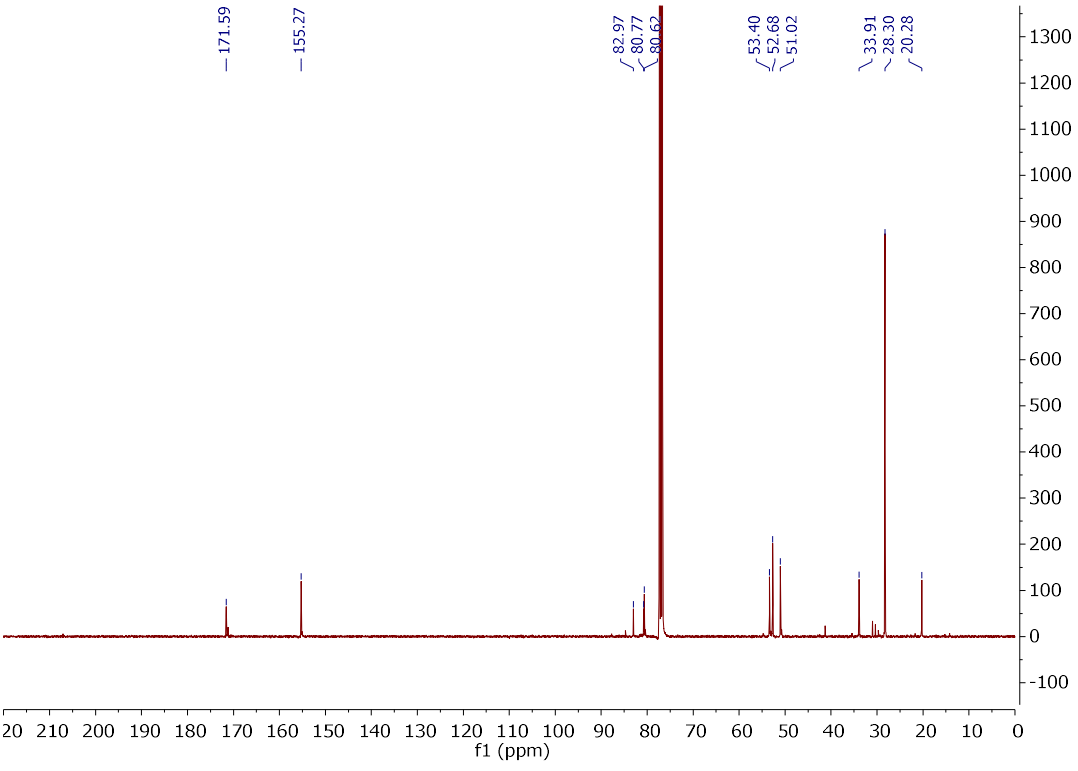

Methyl *N*-(*tert*-butoxycarbonyl)-*S*-(4-(((7-amino-4-methylcoumarin)carbamoyl)oxy)but-2-yn-1-yl)-*L*-cysteinate (16)

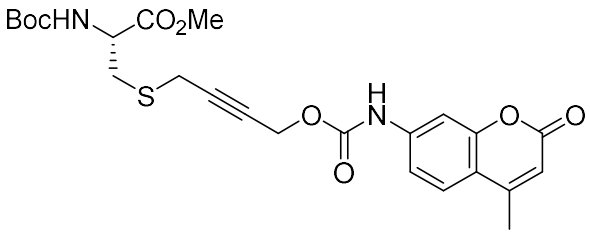

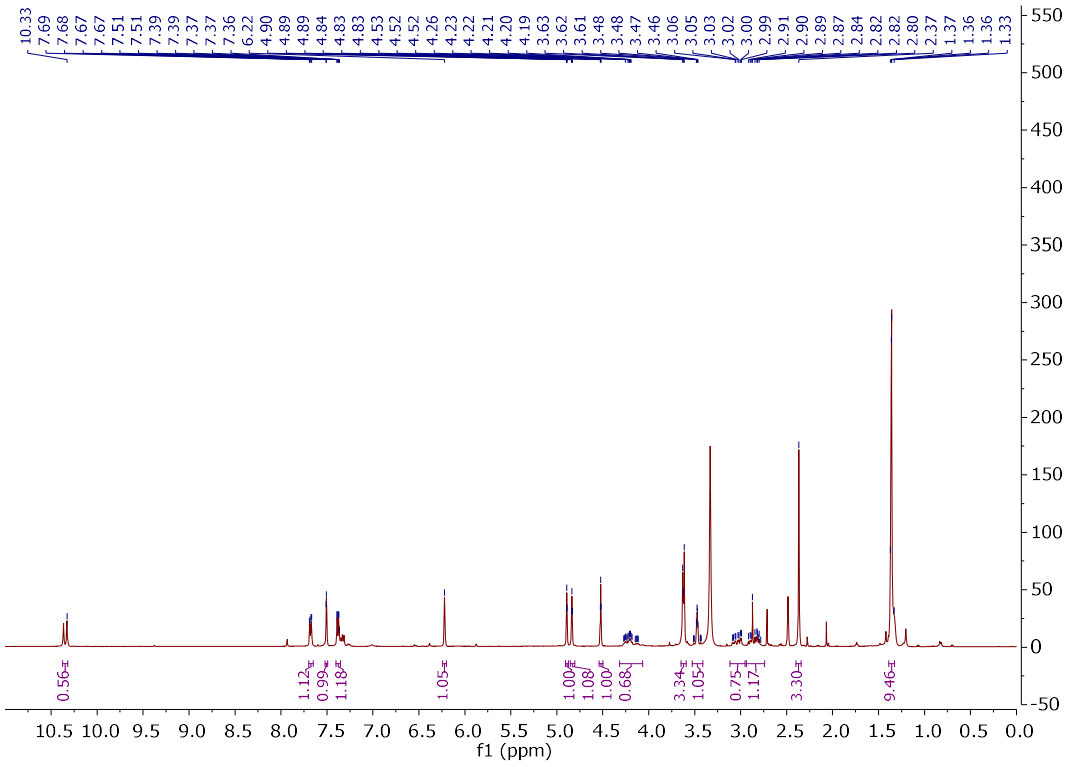

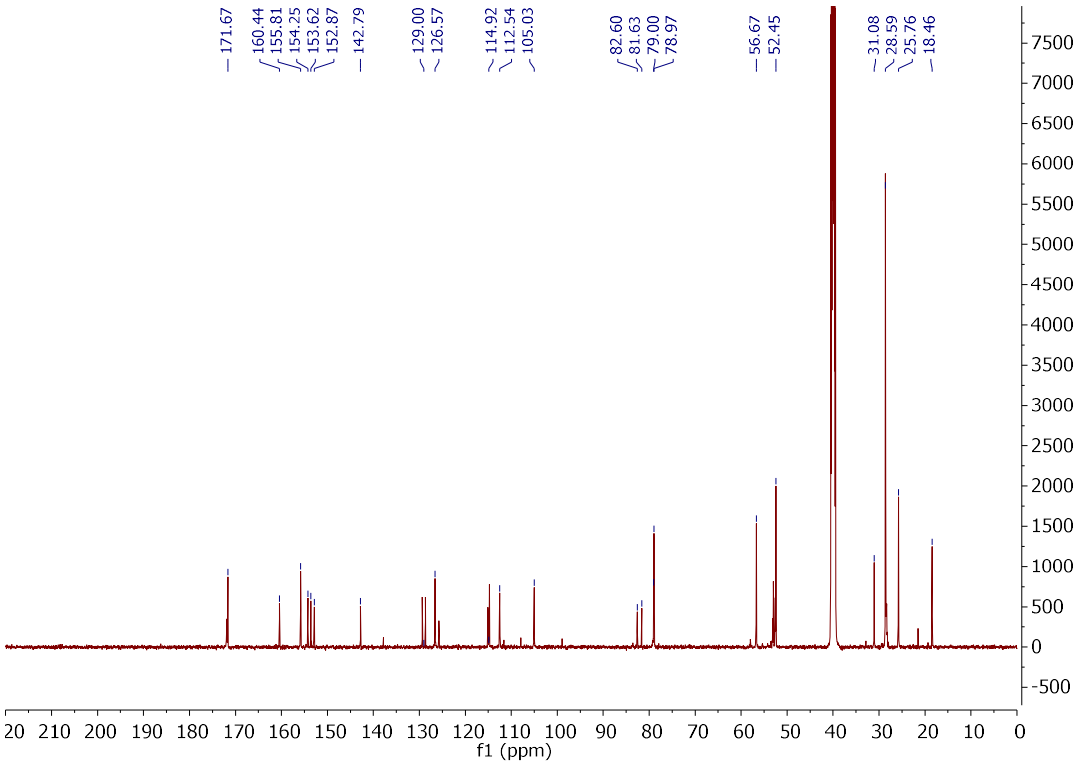
171.67
160.44
155.81
154.25
153.62
152.87
142.79
129.00
126.57
114.92
112.54
105.03
82.60
81.63
79.00
78.97
56.67
52.45
31.08
28.59
25.76
18.46
f1 (ppm)

Methyl *N*-acetyl-*S*-(4-hydroxybut-2-yn-1-yl)-*L*-cysteinate (20b)

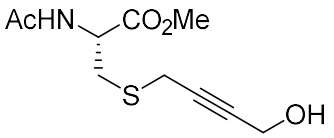

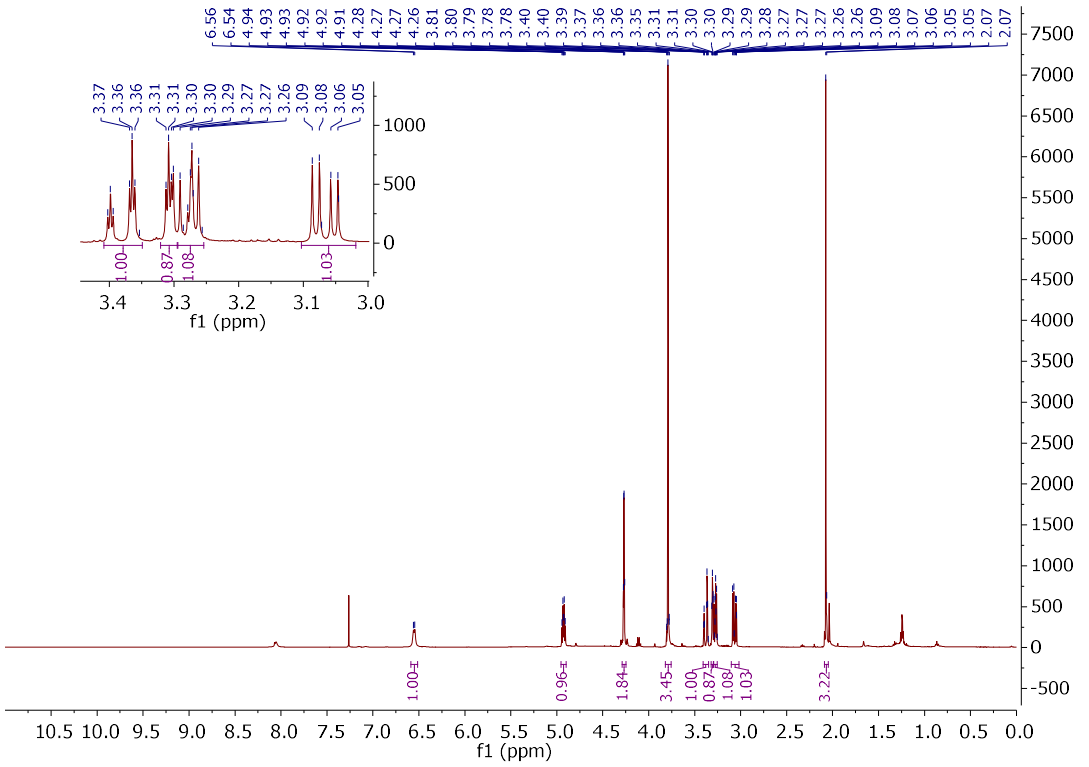

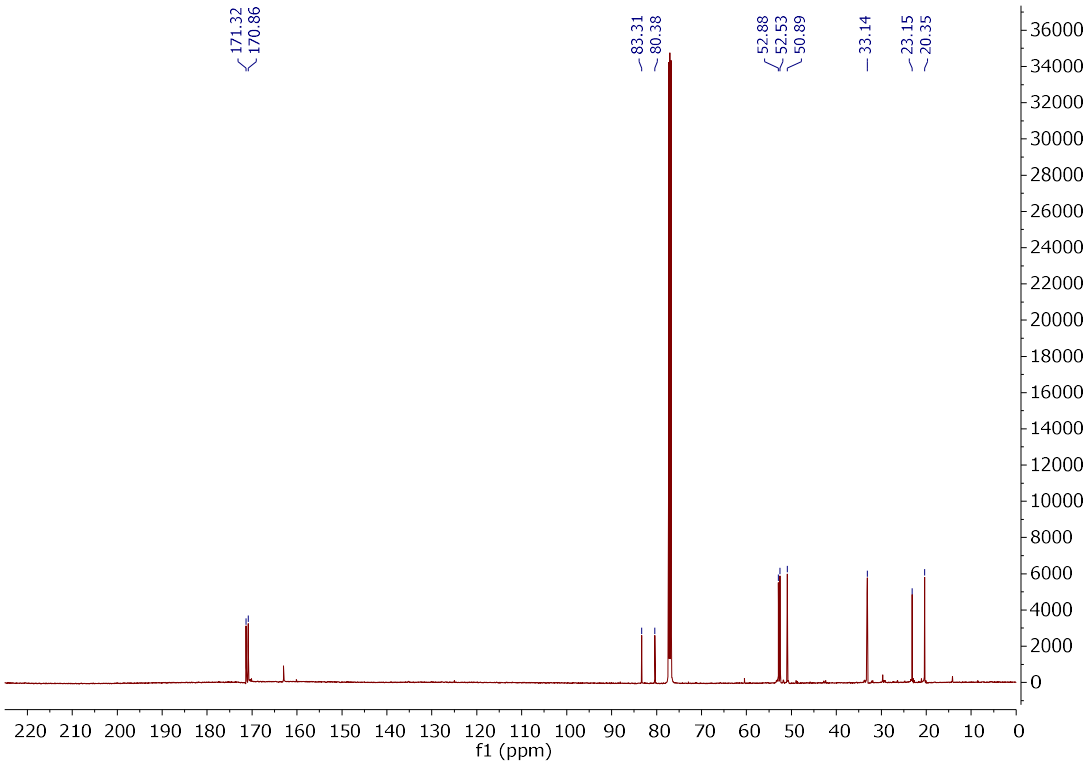

Methyl *N*-acetyl-*S*-(4-(((7-amino-4-methylcoumarin)carbamoyl)oxy)but-2-yn-1-yl)-*L*-cysteinate (20)

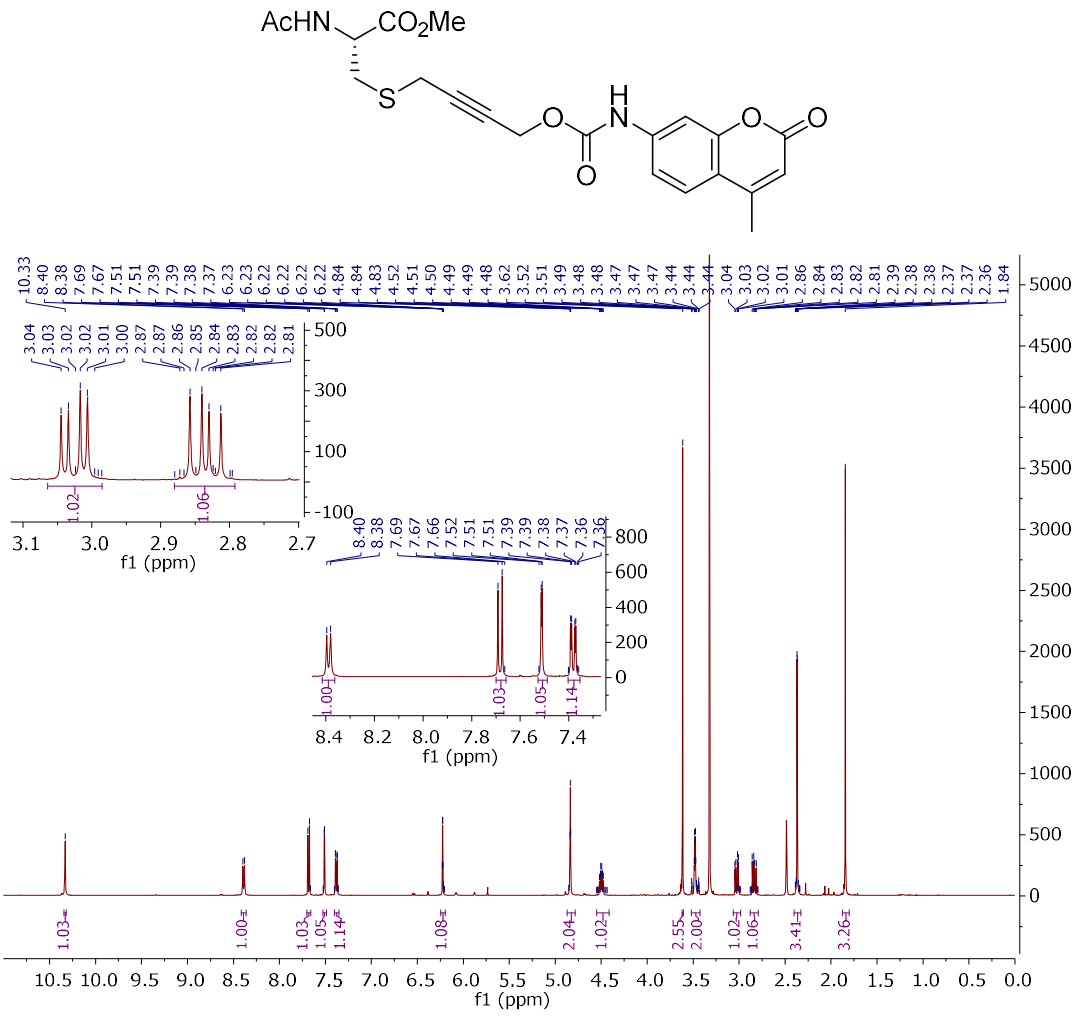

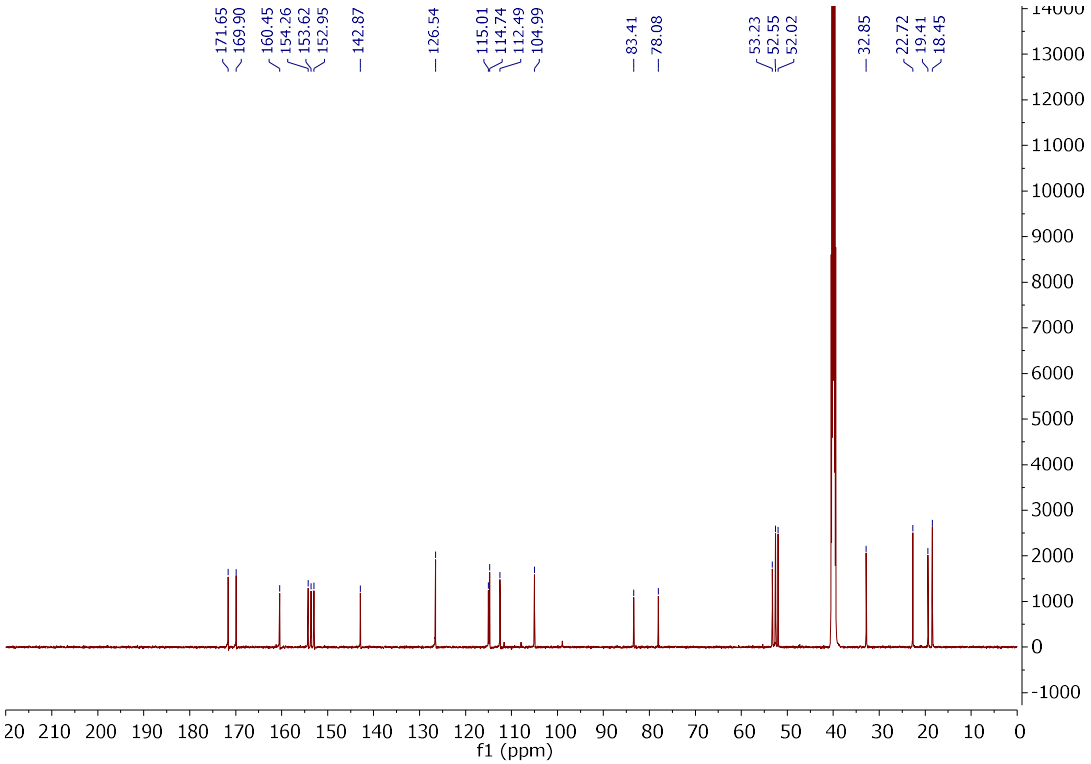
171.65
169.90
160.45
154.26
153.62
152.95
142.87
126.54
115.01
114.74
112.49
104.99
83.41
78.08
53.23
52.55
52.02
32.85
22.72
19.41
18.45
f1 (ppm)

Methyl *S*-(4-(((7-amino-4-methylcoumarin)carbamoyl)oxy)but-2-yn-1-yl)-*L*-cysteinate (21)

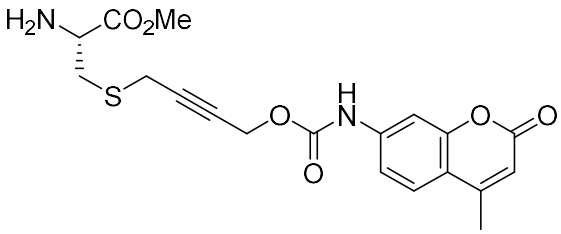

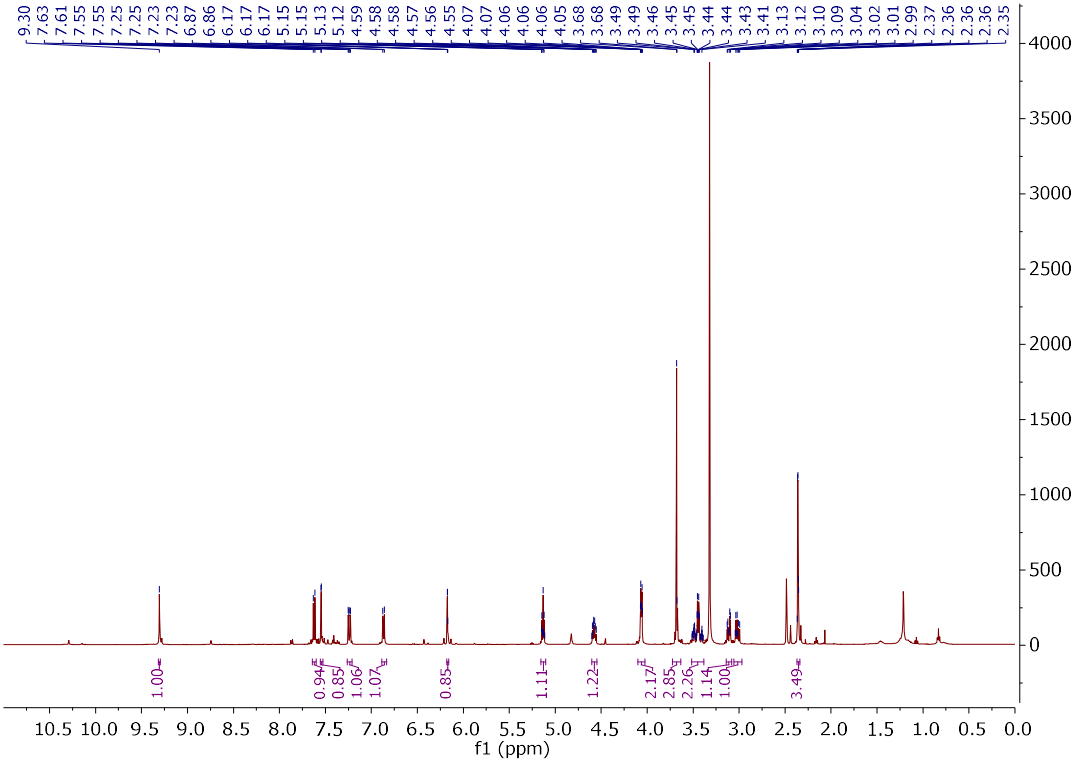

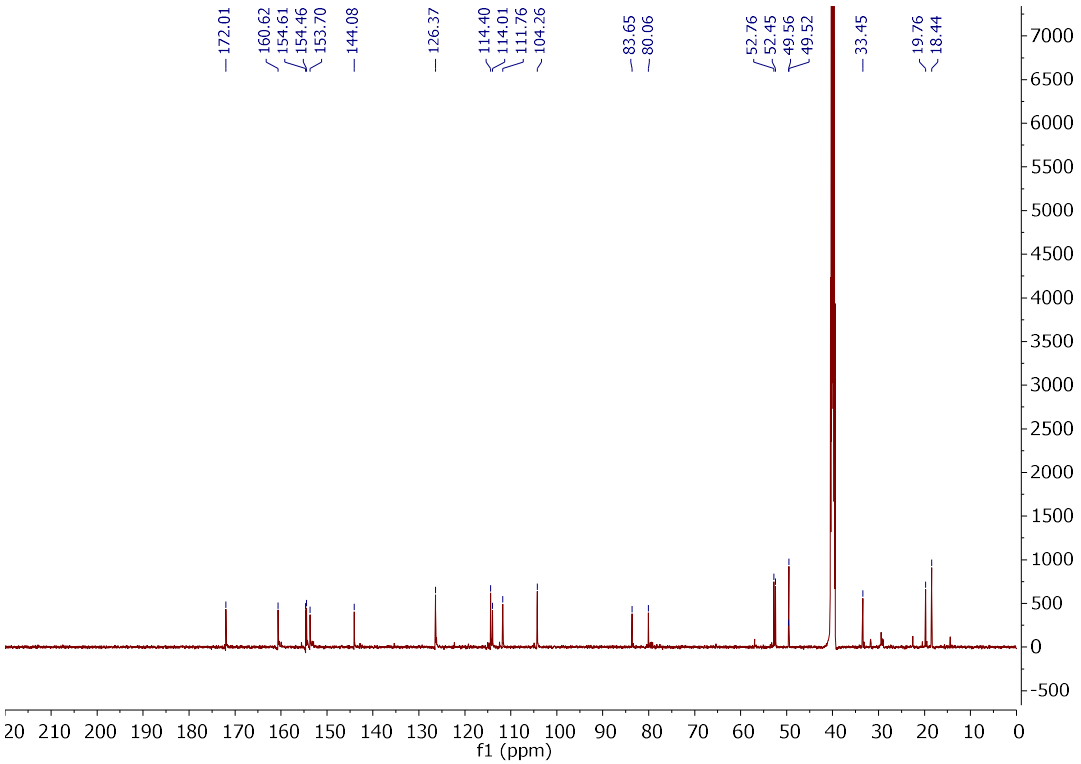
172.01
160.62
154.61
154.46
153.70
144.08
126.37
114.40
114.01
111.76
104.26
83.65
80.06
52.76
52.45
49.56
49.52
33.45
19.76
18.44
f1 (ppm)

But-3-yn-1-yl trityl thioether (22a)

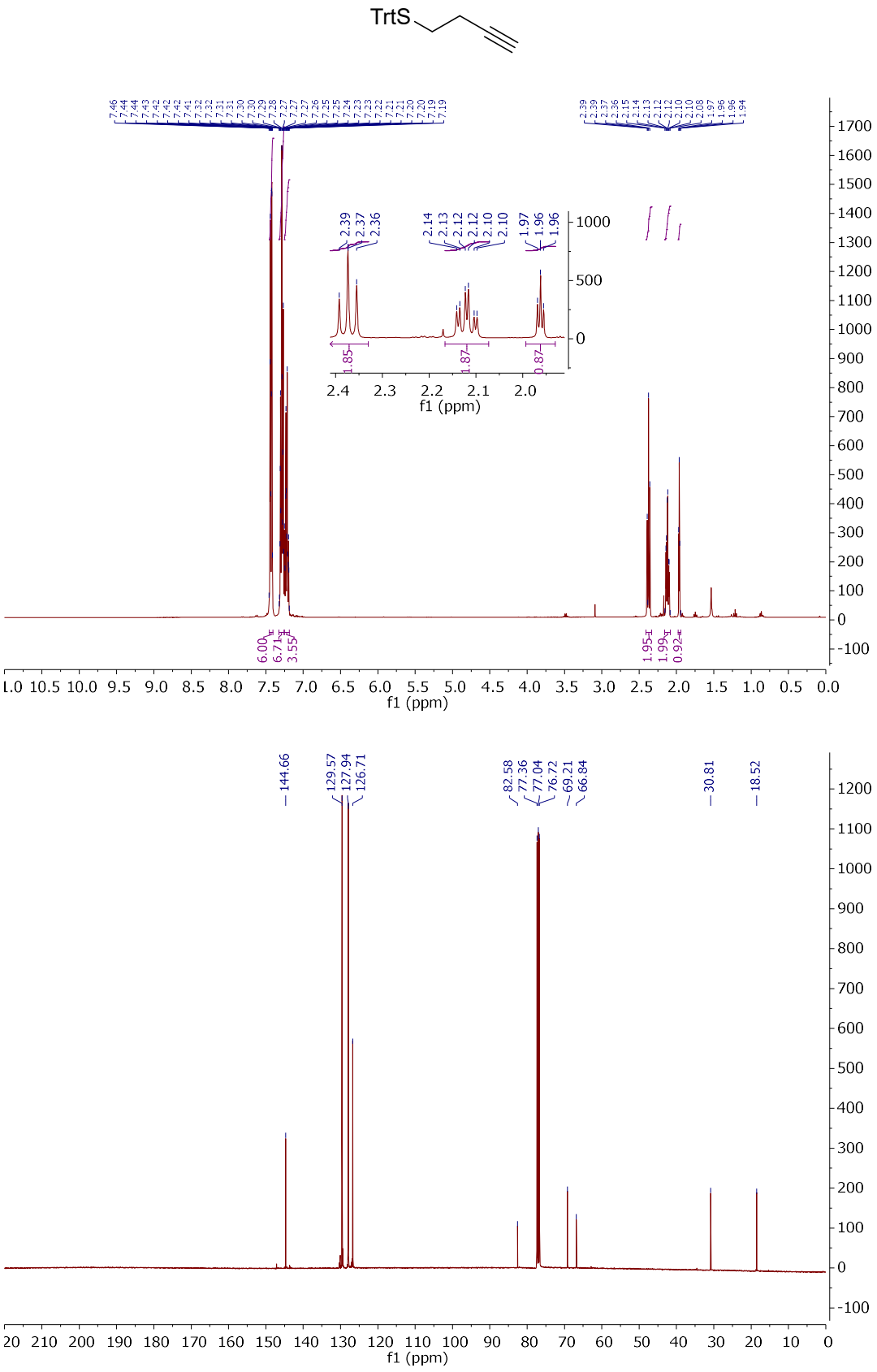

5-(Tritylthio)pent-2-yn-1-ol (22b)

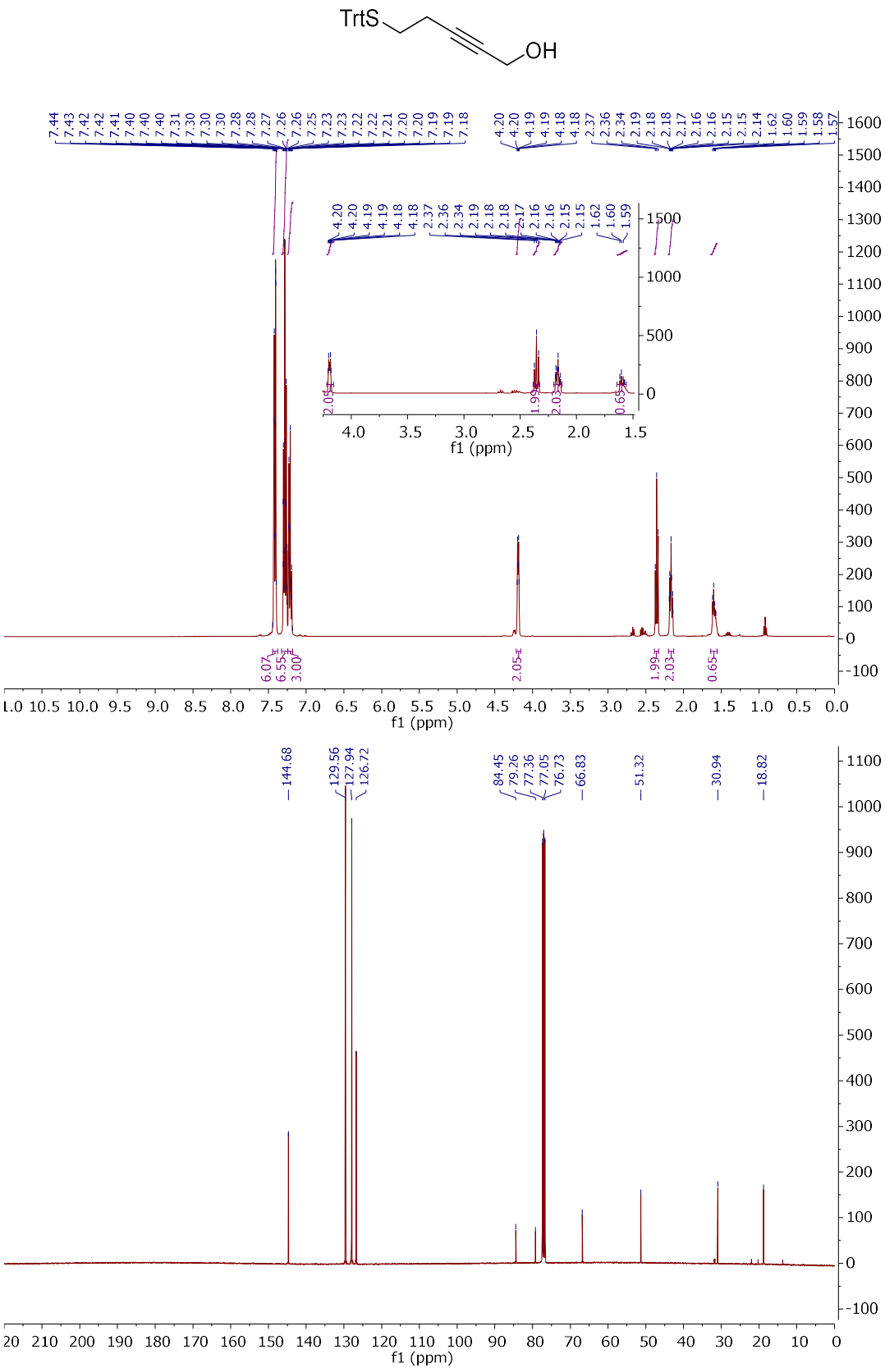

5-(Tritylthio)pent-2-yn-1-yl (7-amino-4-methylcoumarin)carbamate (22)

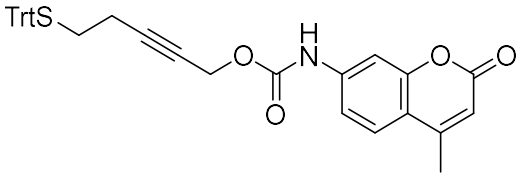

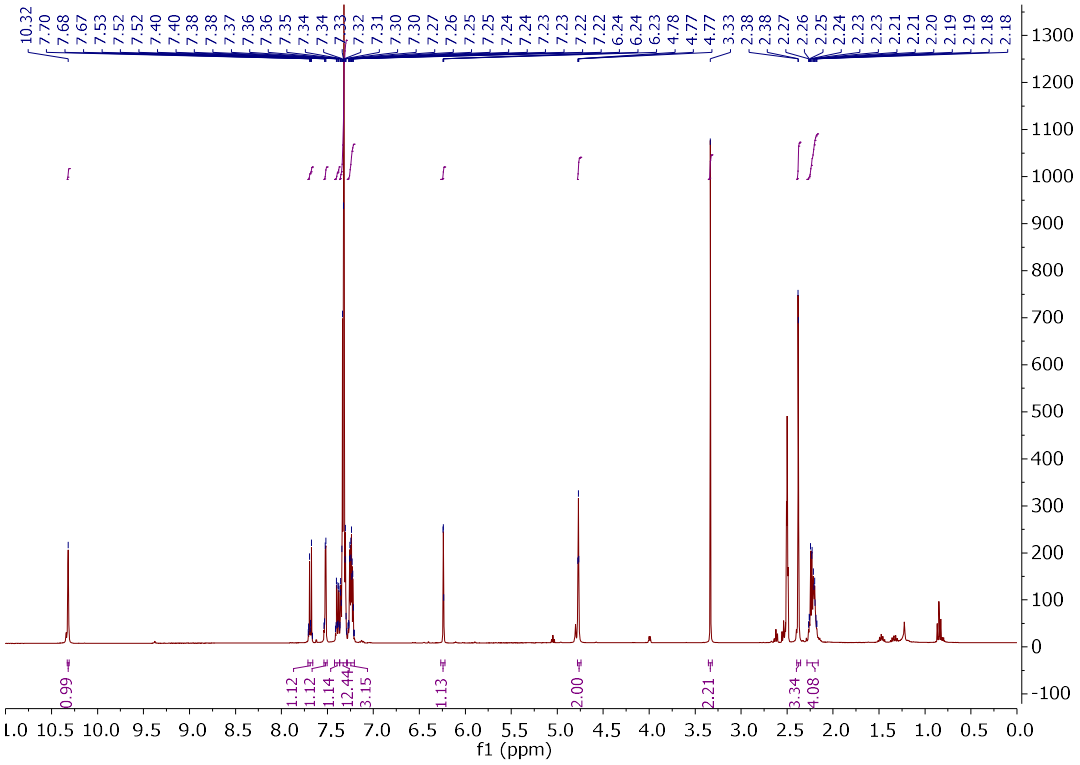

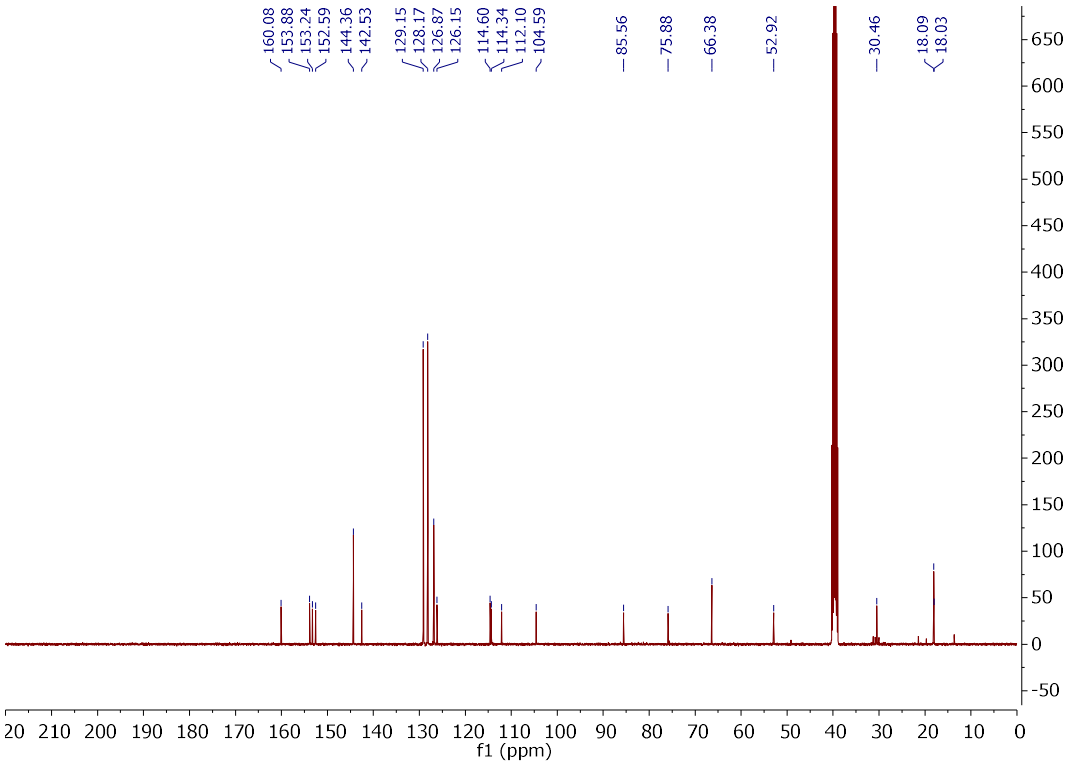

5-(Methylthio)pent-2-yn-1-ol (23a)

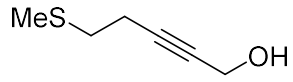

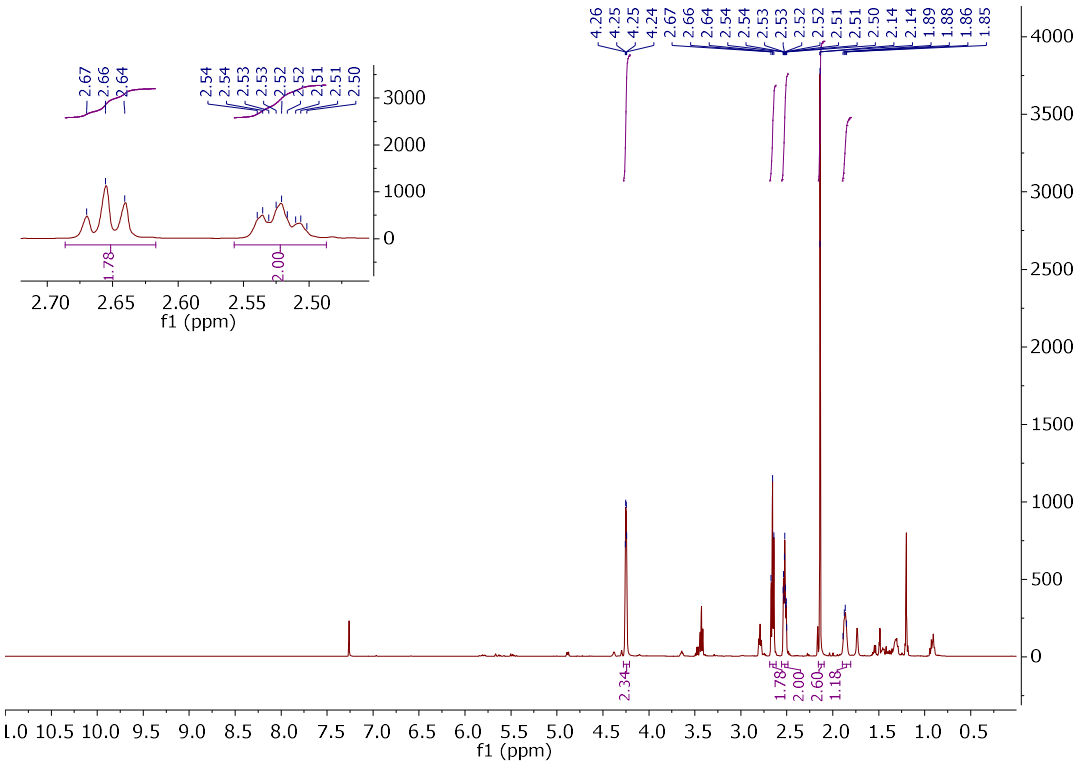

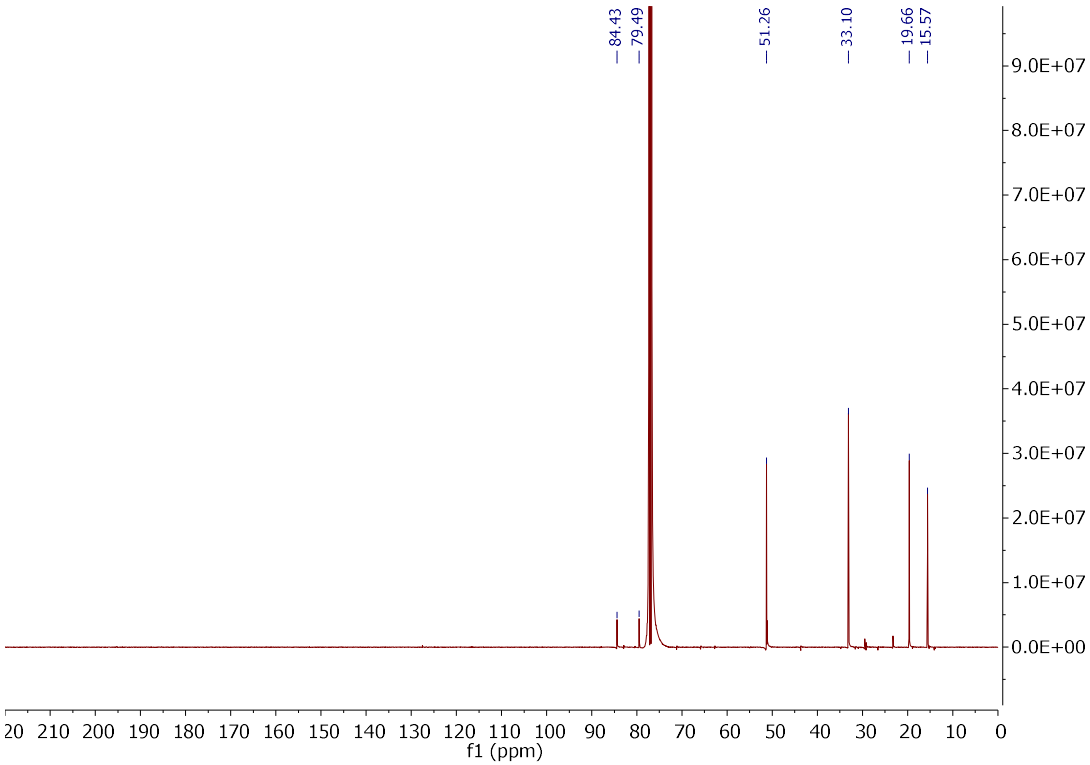

5-(Methylthio)pent-2-yn-1-yl (7-amino-4-methylcoumarin)carbamate (23)

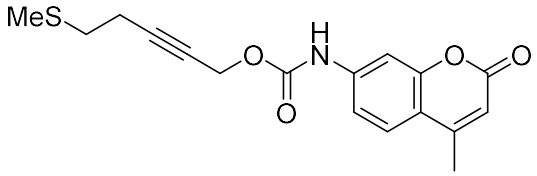

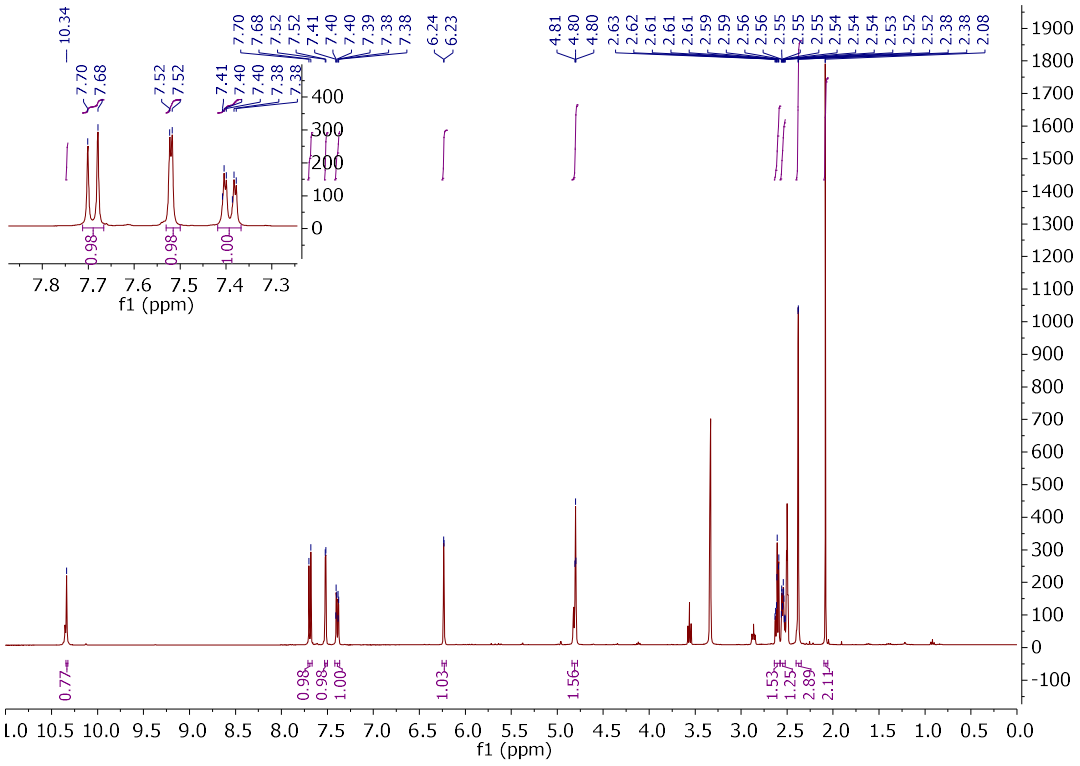

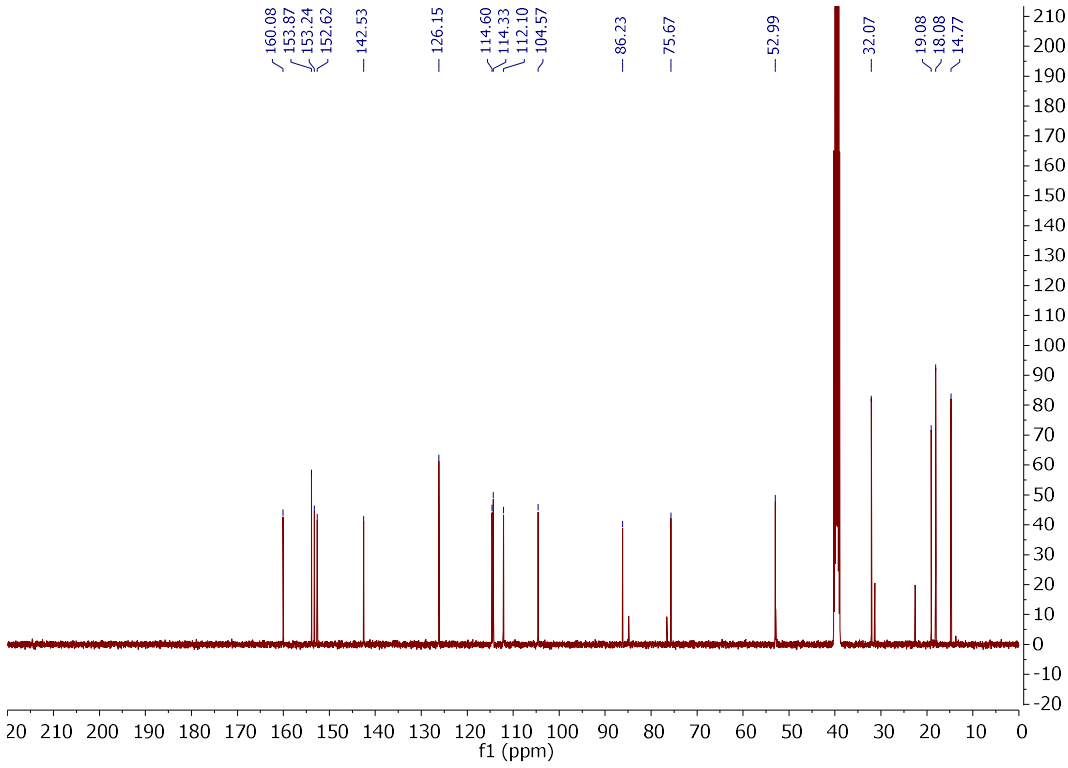

3,6,9-Trioxa-12-thiahexadec-14-yn-16-ol (33)

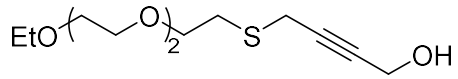

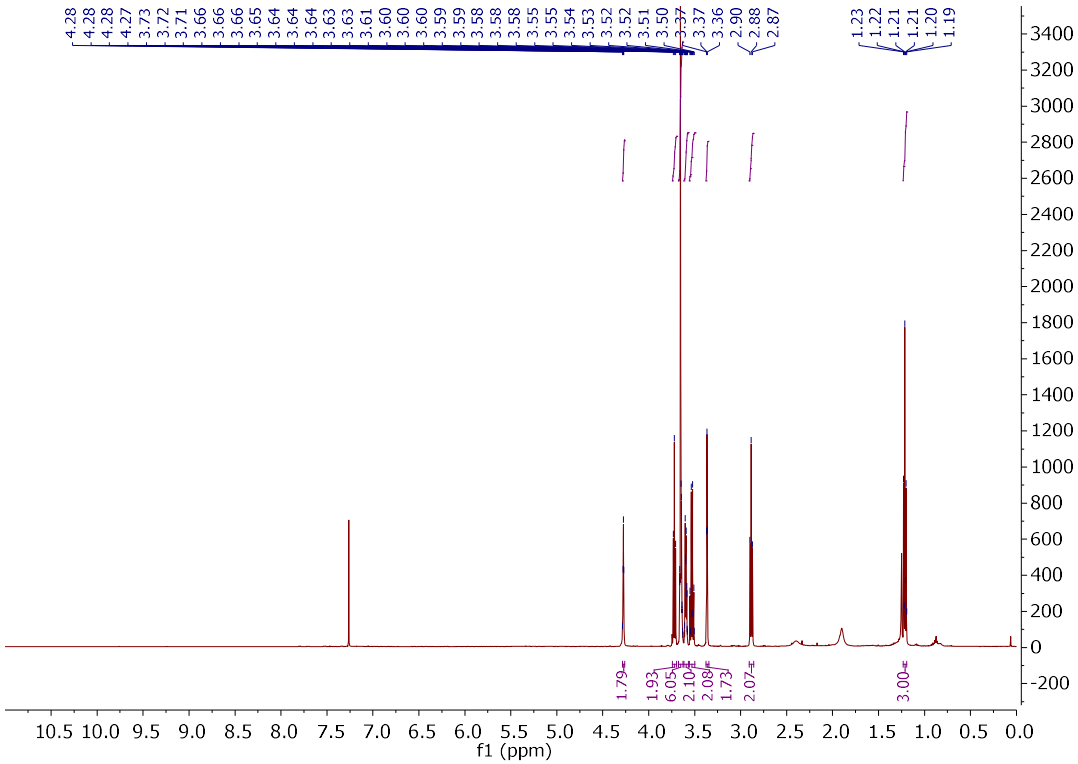

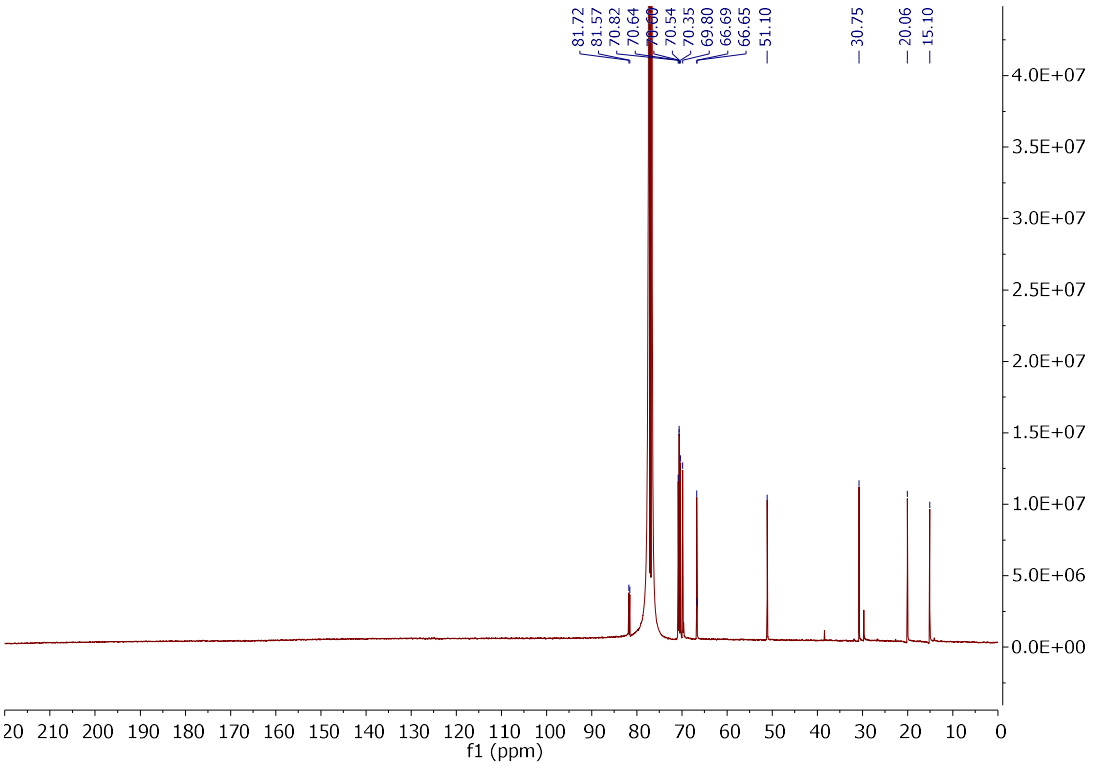

3,6,9-Trioxa-12-thiahexadec-14-yn-16-yl (7-amino-4-methylcoumarin)carbamate (28)

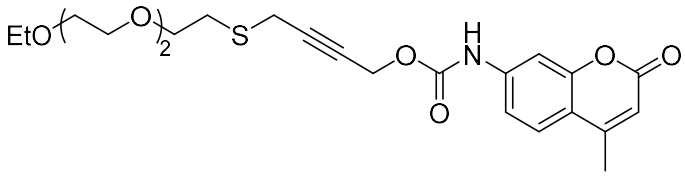

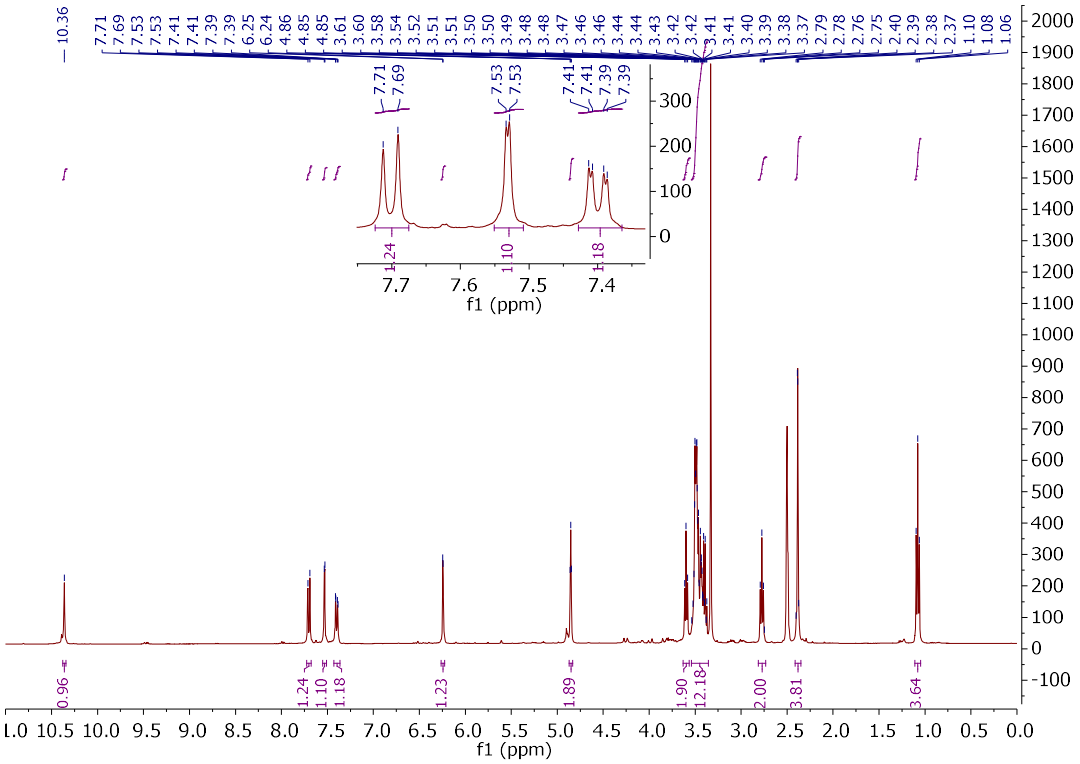

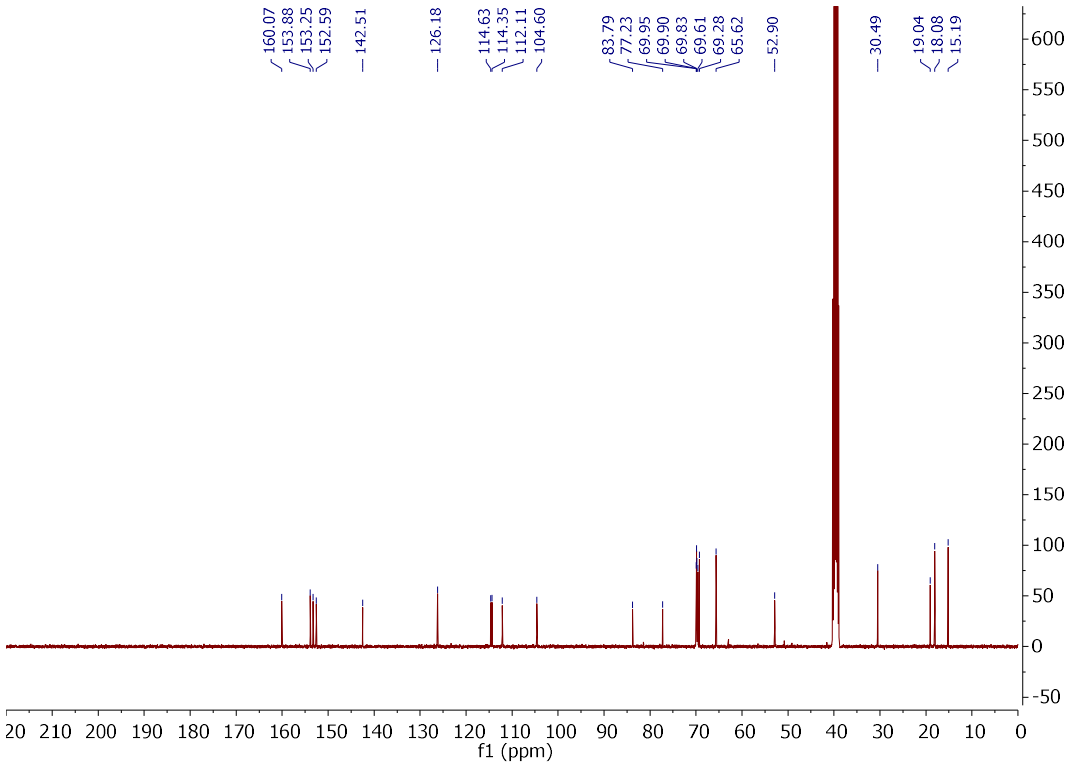

3,6,9-Trioxa-12-thiahexadec-14-yn-16-yl (4-nitrophenyl) carbonate (34)

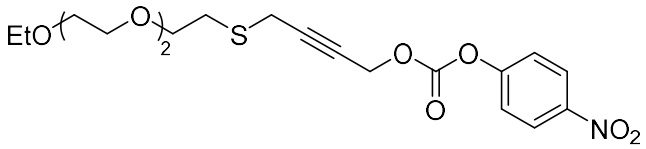

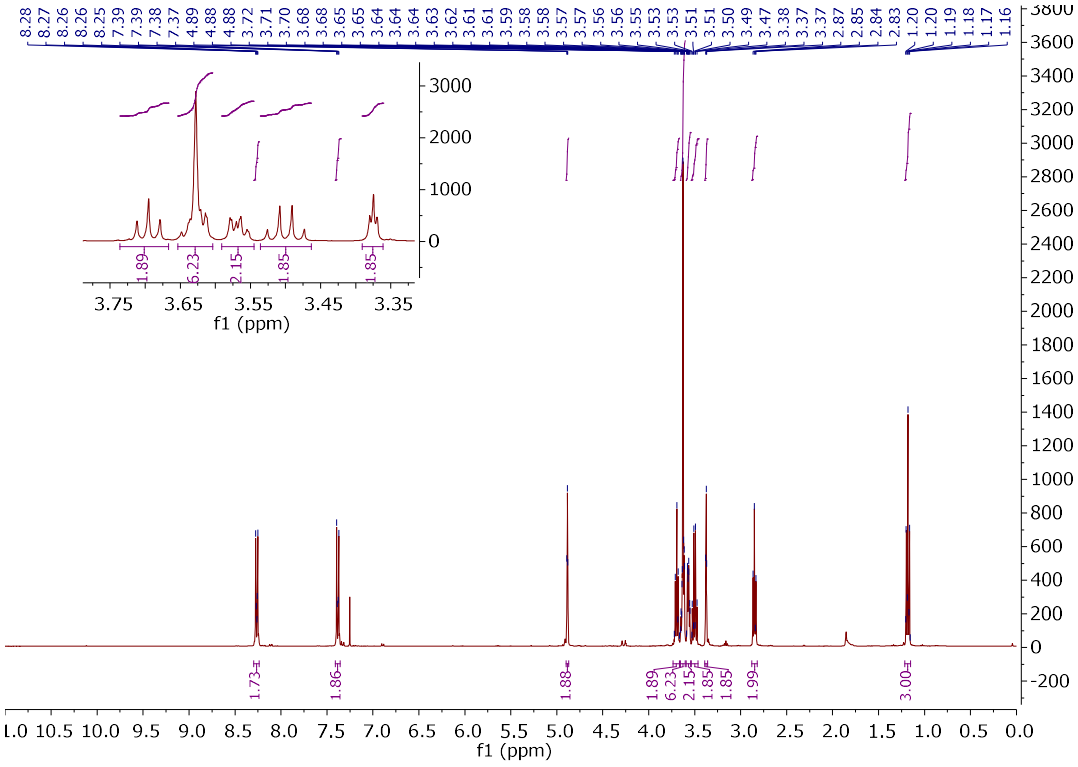

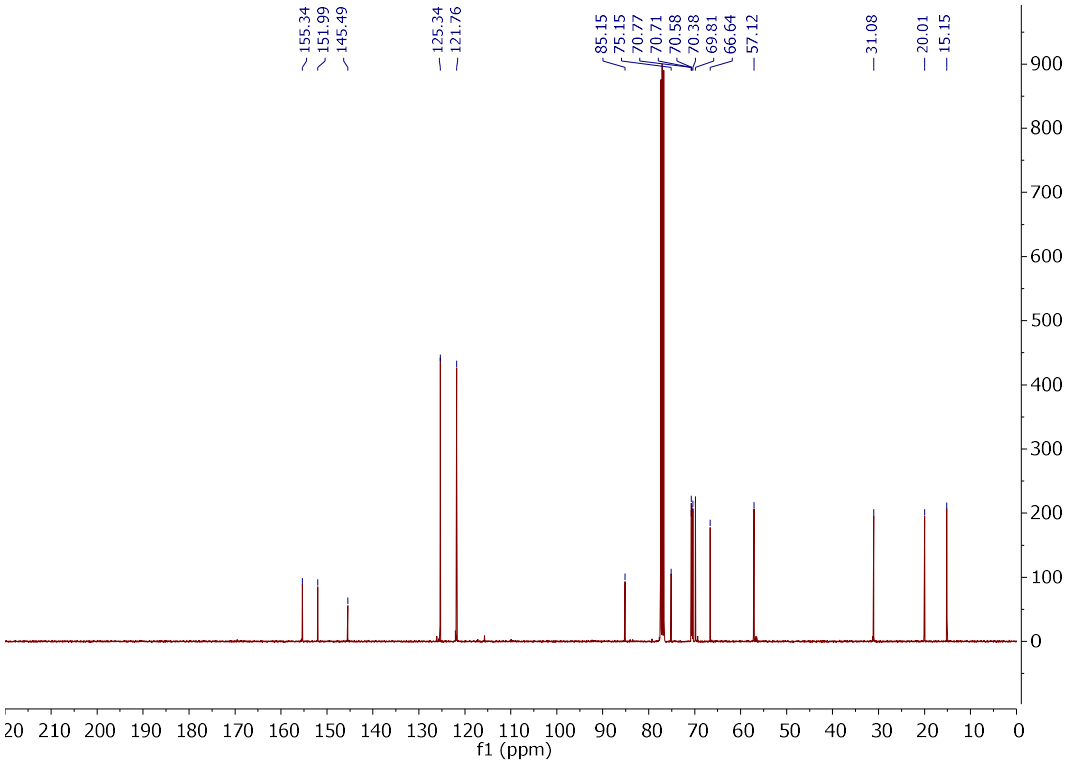

cDox (35)

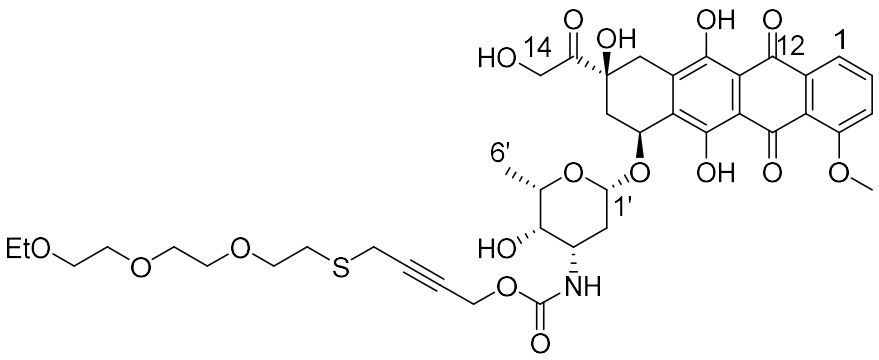
HO
14
O
OH
OH
O
12
1
6'
O
O
1'
OH
O
O
HO
EtO
O
O
S
O
NH
O

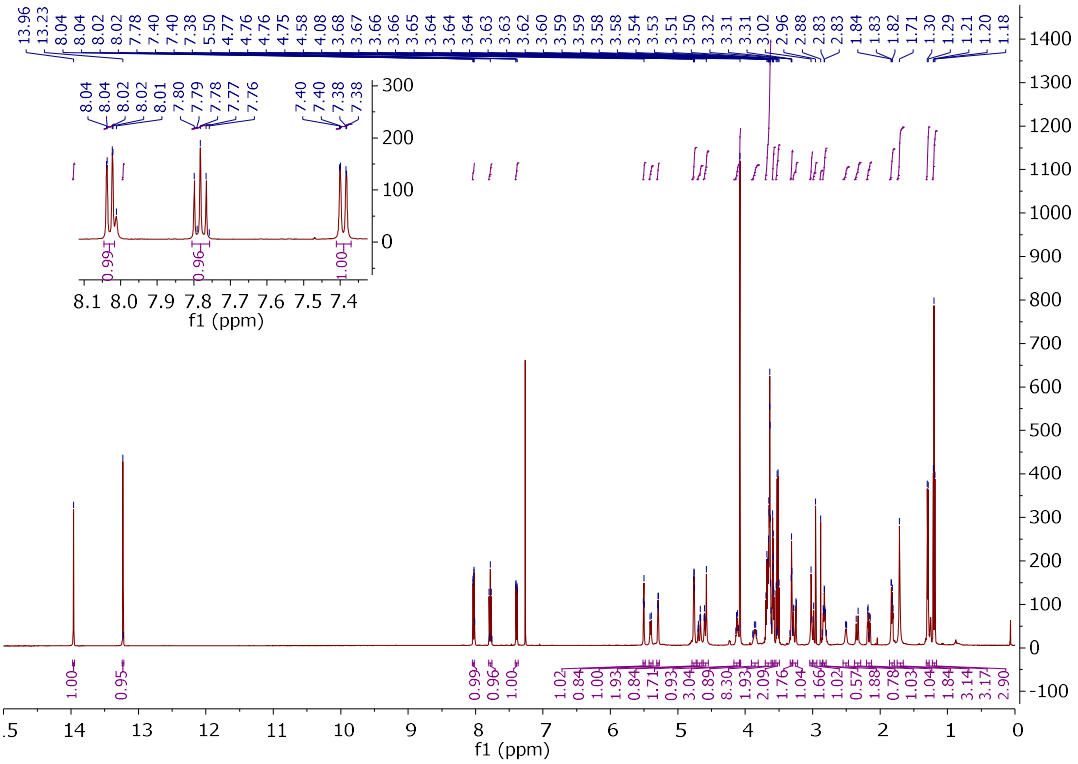
f1 (ppm)
8.1 8.0 7.9 7.8 7.7 7.6 7.5 7.4
f1 (ppm)

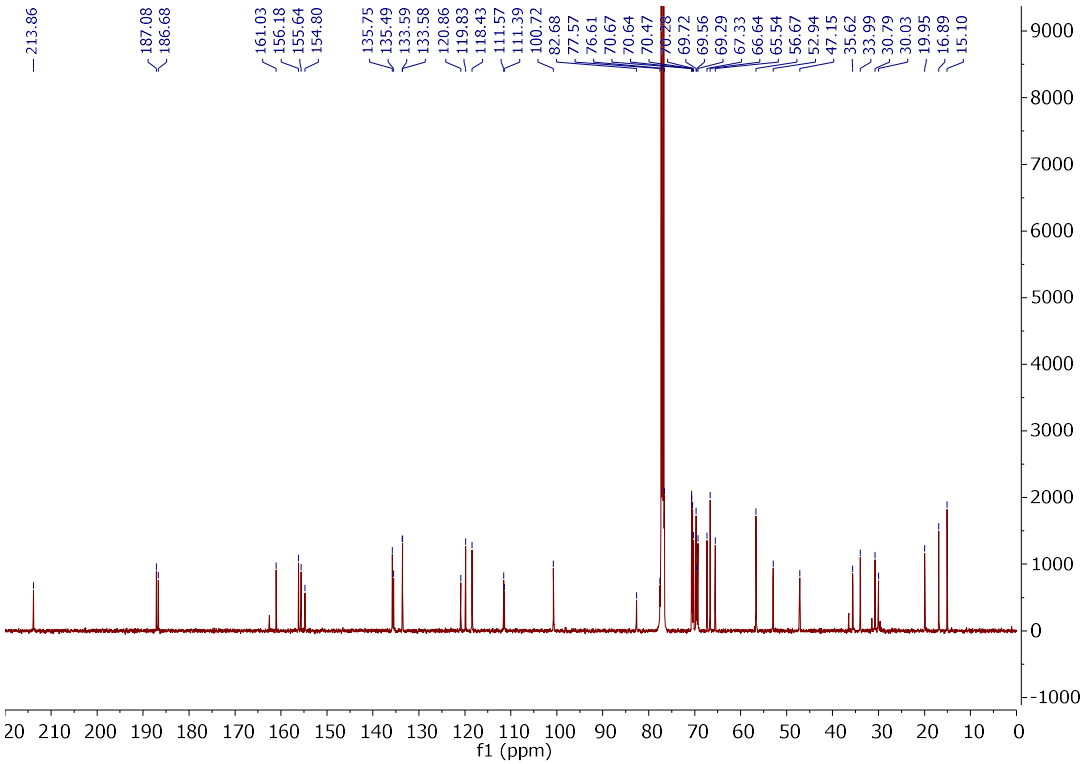
213.86
187.08
186.68
161.03
156.18
155.64
154.80
135.75
135.49
133.59
133.58
120.86
119.83
118.43
111.57
111.39
100.72
82.68
77.57
76.61
70.67
70.64
70.47
70.28
69.72
69.56
69.29
67.33
66.64
65.54
56.67
52.94
47.15
35.62
33.99
30.79
30.03
19.95
16.89
15.10
9000
8000
7000
6000
5000
4000
3000
2000
1000
0
-1000
20 210 200 190 180 170 160 150 140 130 120 110 100 90 80 70 60 50 40 30 20 10 0
f1 (ppm)

tert-Butyl (16-hydroxy-3,6,9-trioxa-12-thiahexadec-14-yn-1-yl)carbamate (36d)

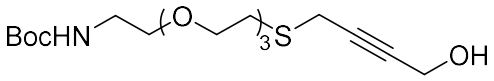

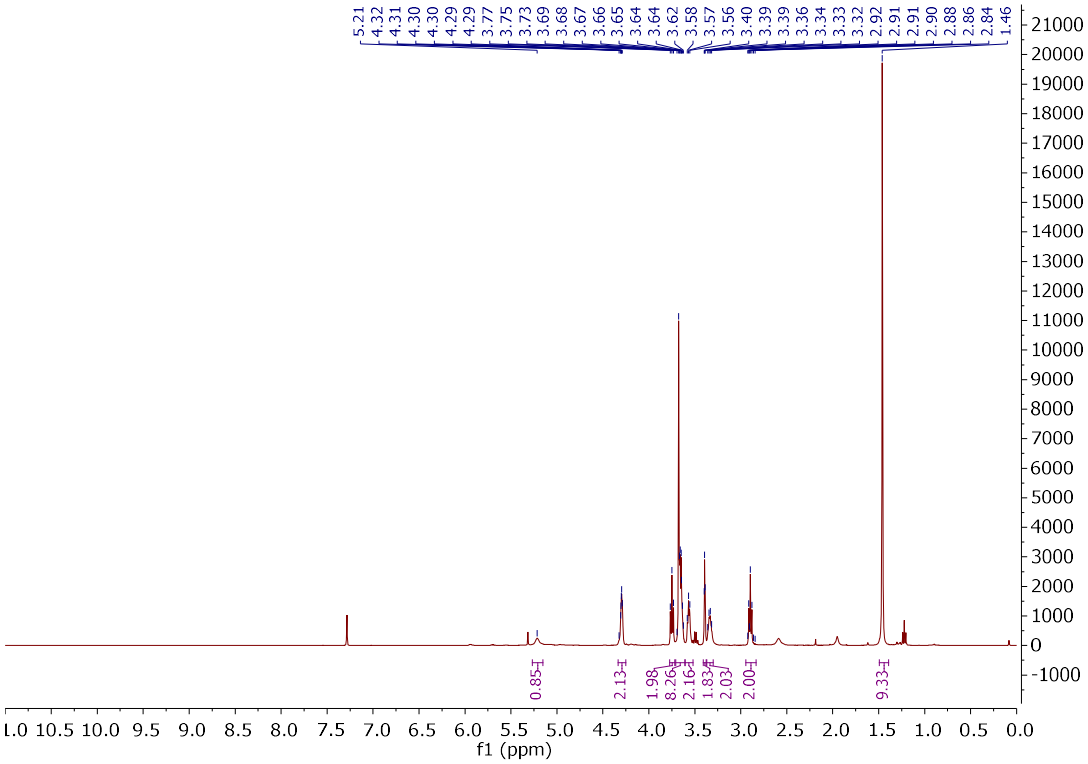

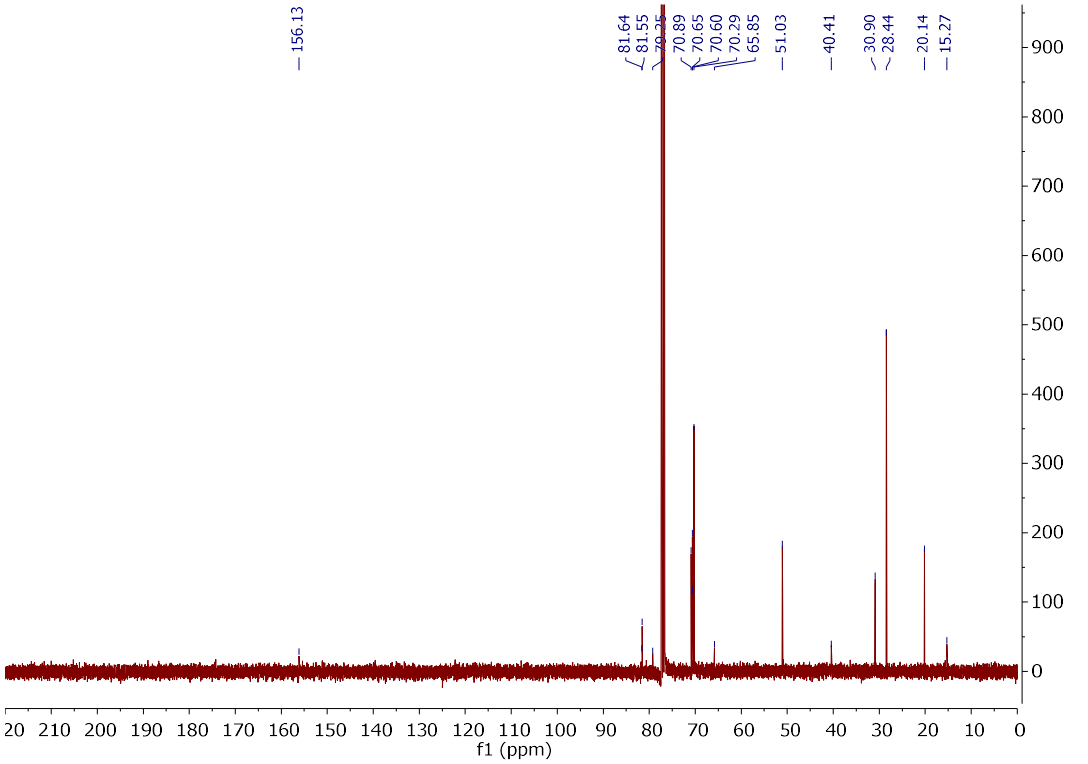

(*E*)-*N*-(16-Hydroxy-3,6,9-trioxa-12-thiahexadec-14-yn-1-yl)-4-oxo-4-phenylbut-2-enamide (36e)

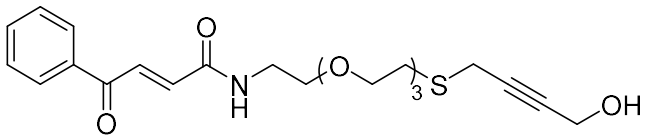

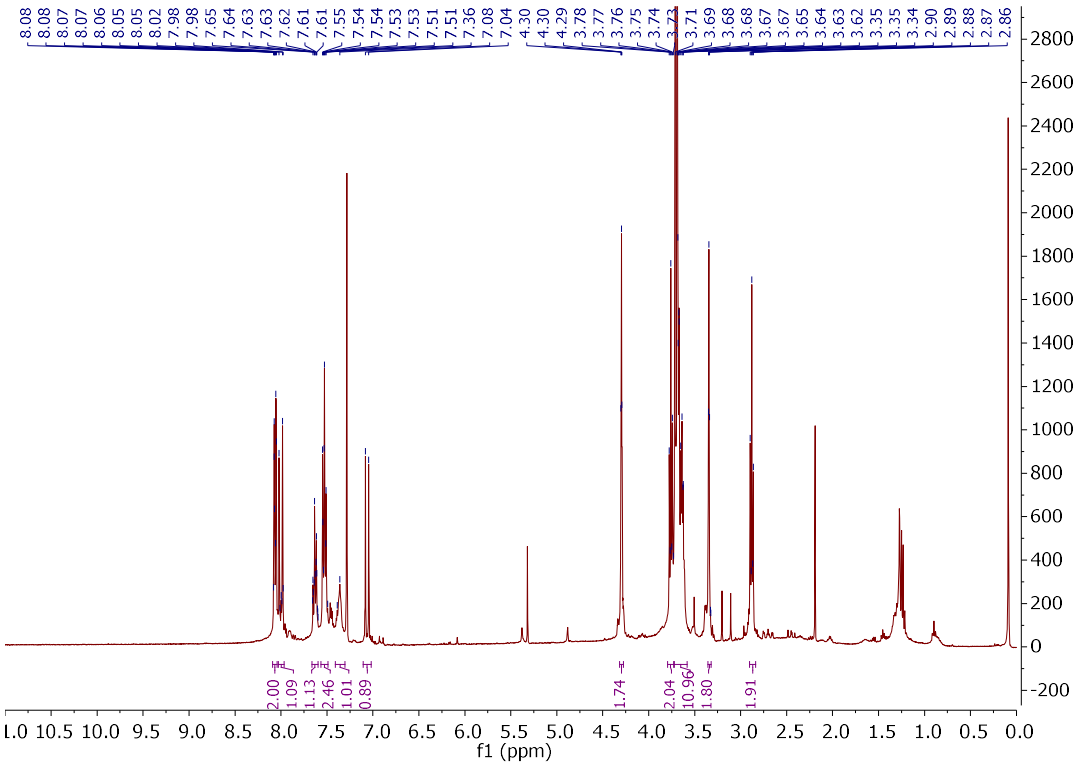

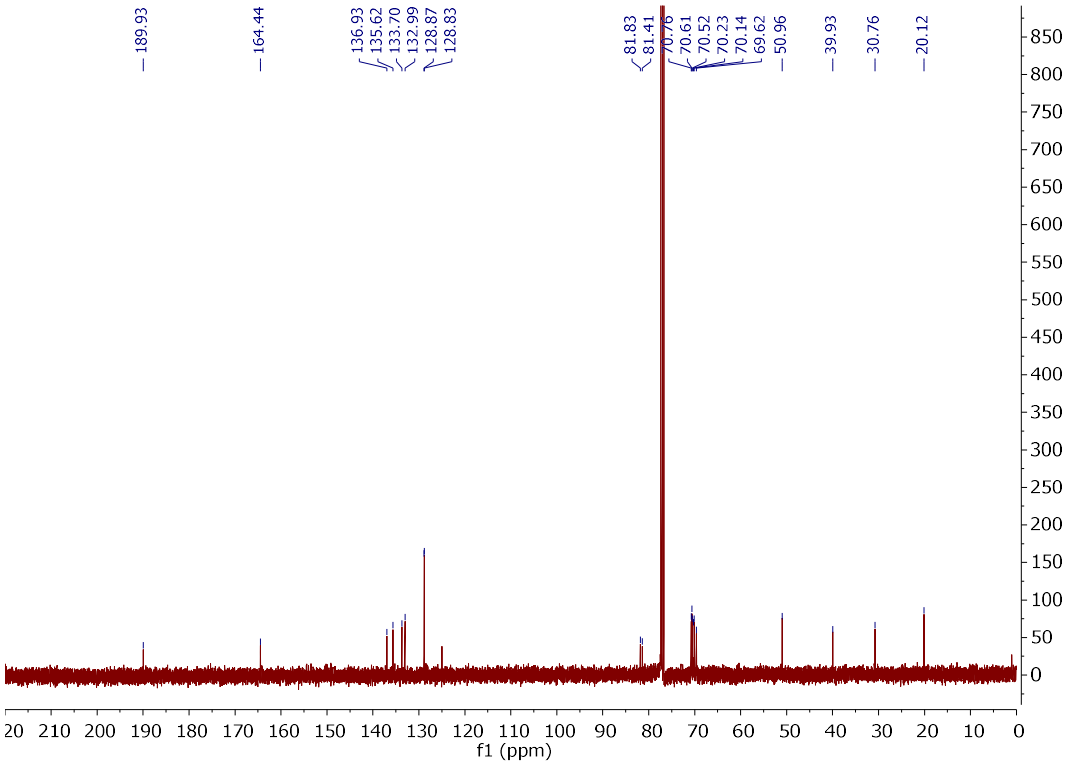

(*E*)-*N*-(16-Hydroxy-3,6,9-trioxa-12-thiahexadec-14-yn-1-yl)-4-oxo-4-phenylbut-2-enamide doxorubicin carbamate (36)

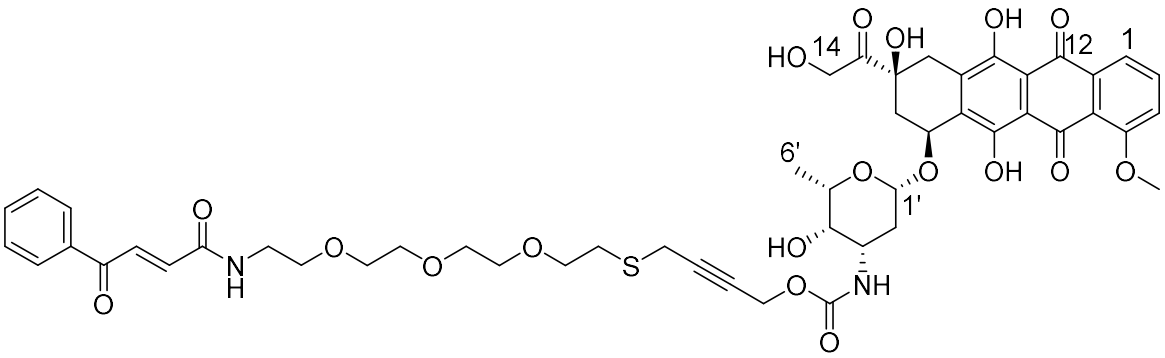

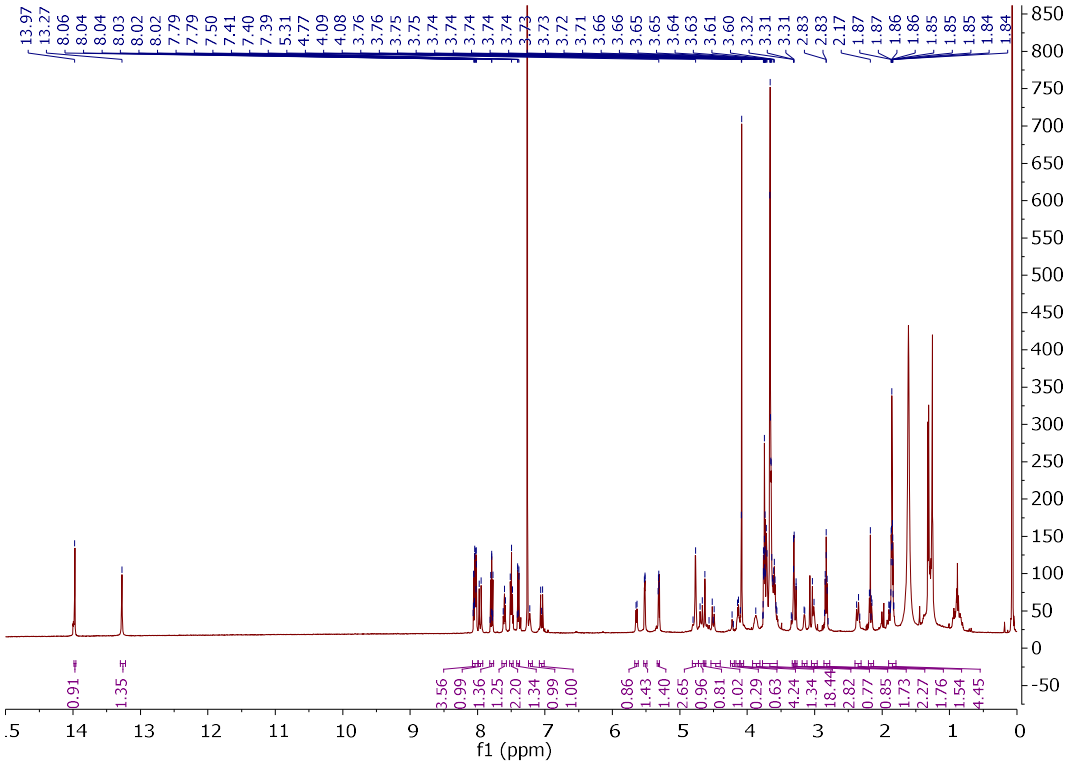

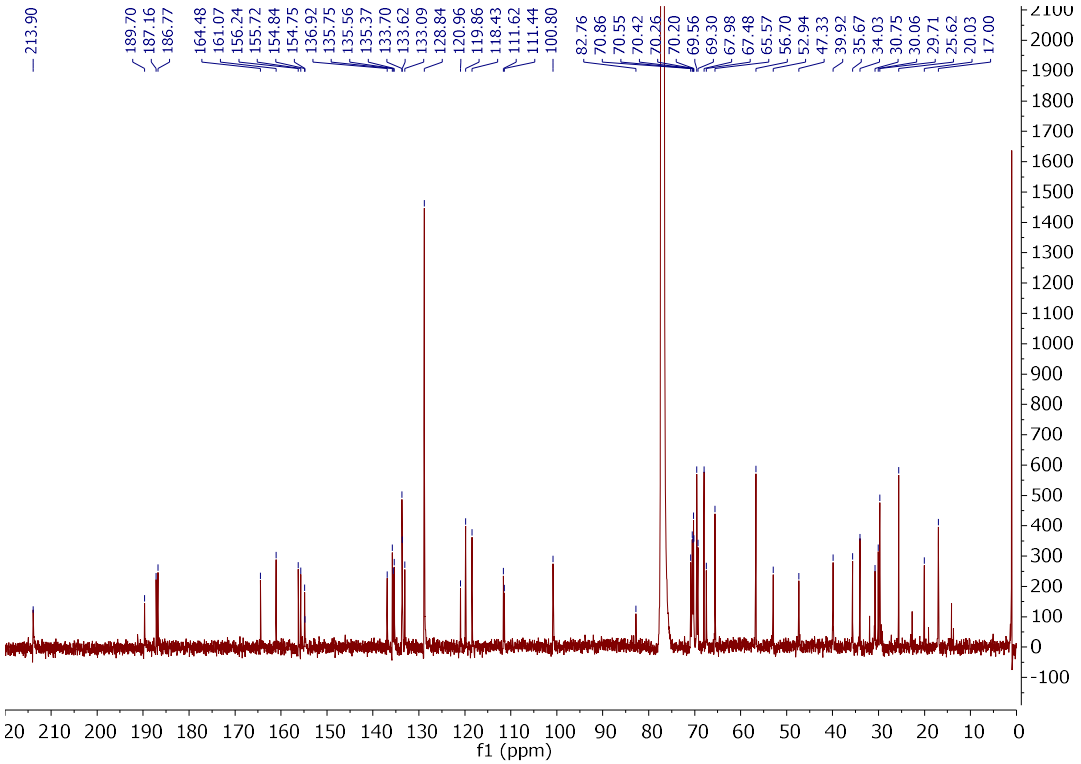
213.90
189.70
187.16
186.77
164.48
161.07
156.24
155.72
154.84
154.75
136.92
135.75
135.56
135.37
133.70
133.62
133.09
128.84
120.96
119.86
118.43
111.62
111.44
100.80
82.76
70.86
70.55
70.42
70.26
70.20
69.56
69.30
67.98
67.48
65.57
56.70
52.94
47.33
39.92
35.67
34.03
30.75
30.06
29.71
25.62
20.03
17.00
f1 (ppm)

5.5 NMR spectra for Chapter 4

6-((*tert*-Butyldimethylsilyl)oxy)hex-2-yn-1-yl dibenzylcarbamate (38c)

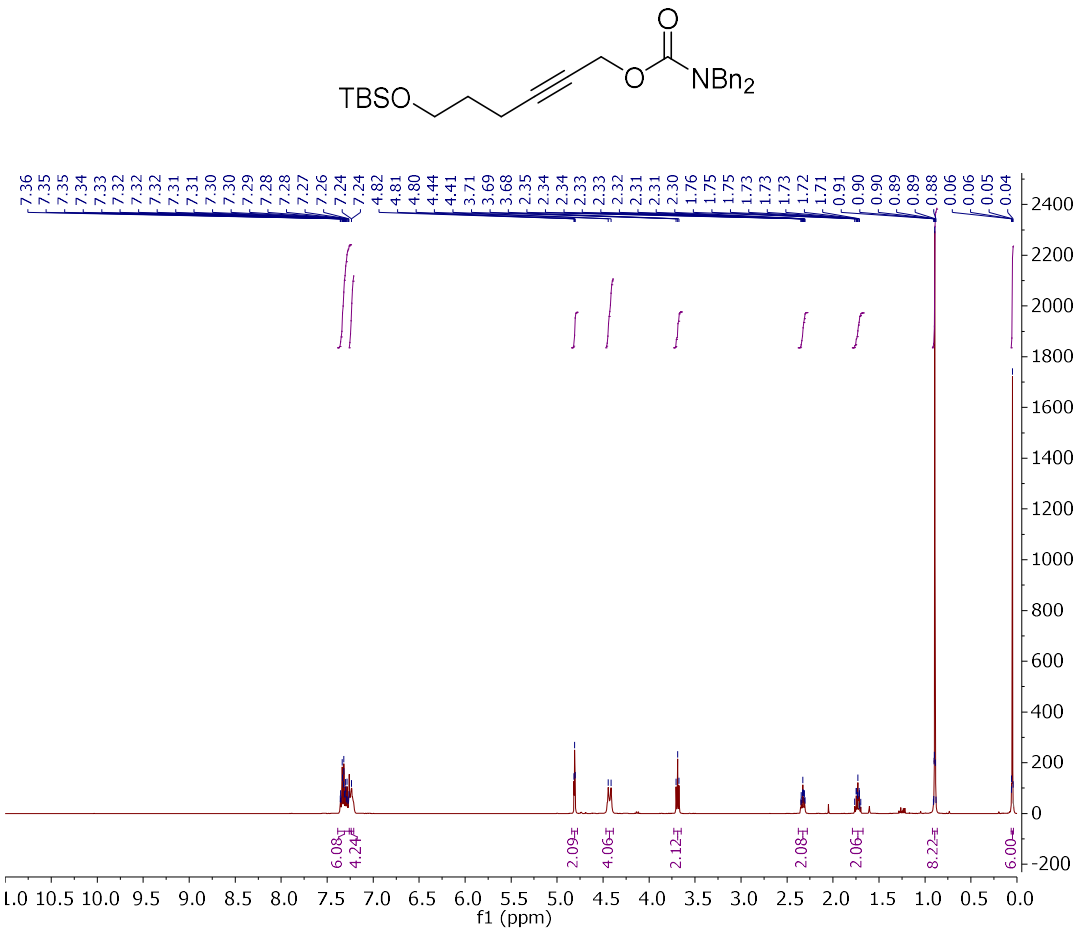

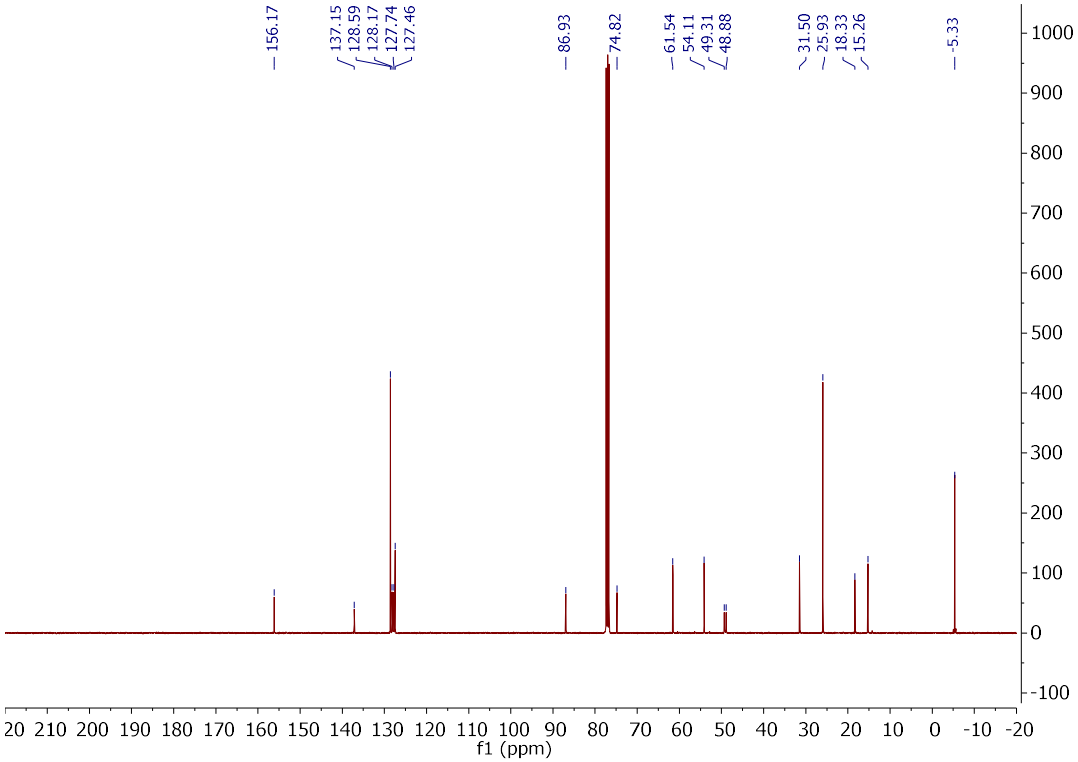
156.17
137.15
128.59
128.17
127.74
127.46
86.93
74.82
61.54
54.11
49.31
48.88
31.50
25.93
18.33
15.26
-5.33
f1 (ppm)

6-Hydroxyhex-2-yn-1-yl dibenzylcarbamate (38d)

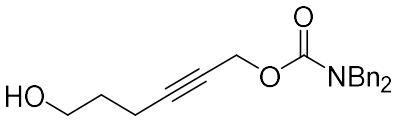

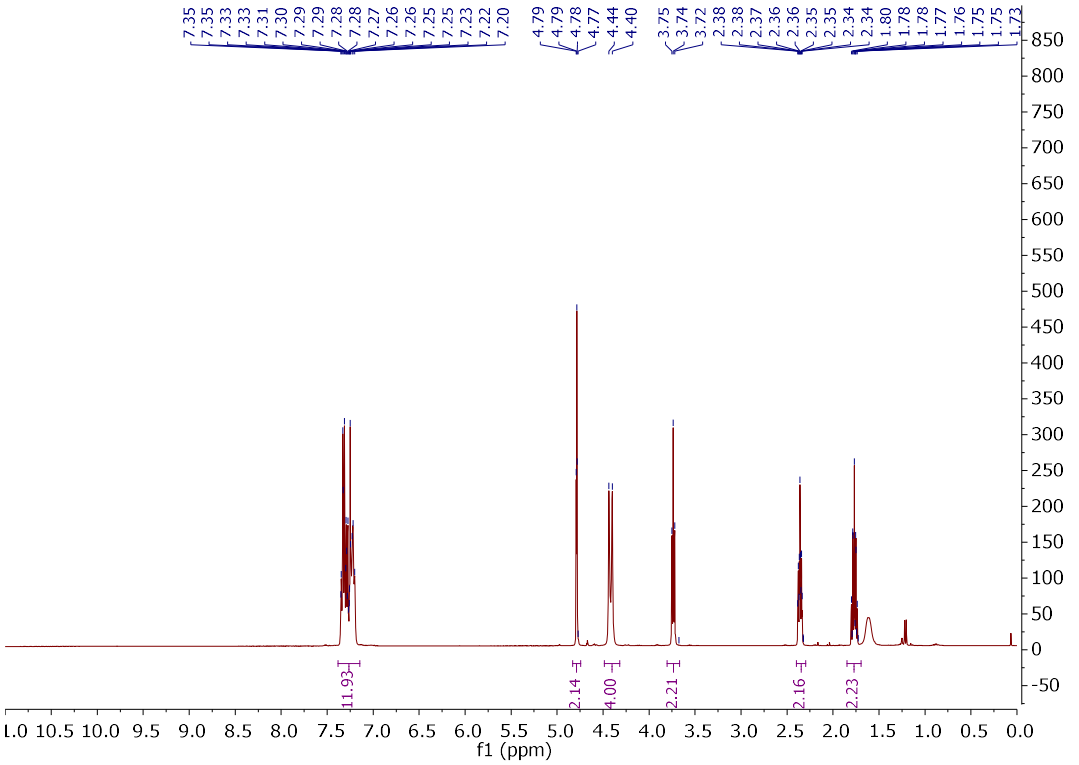

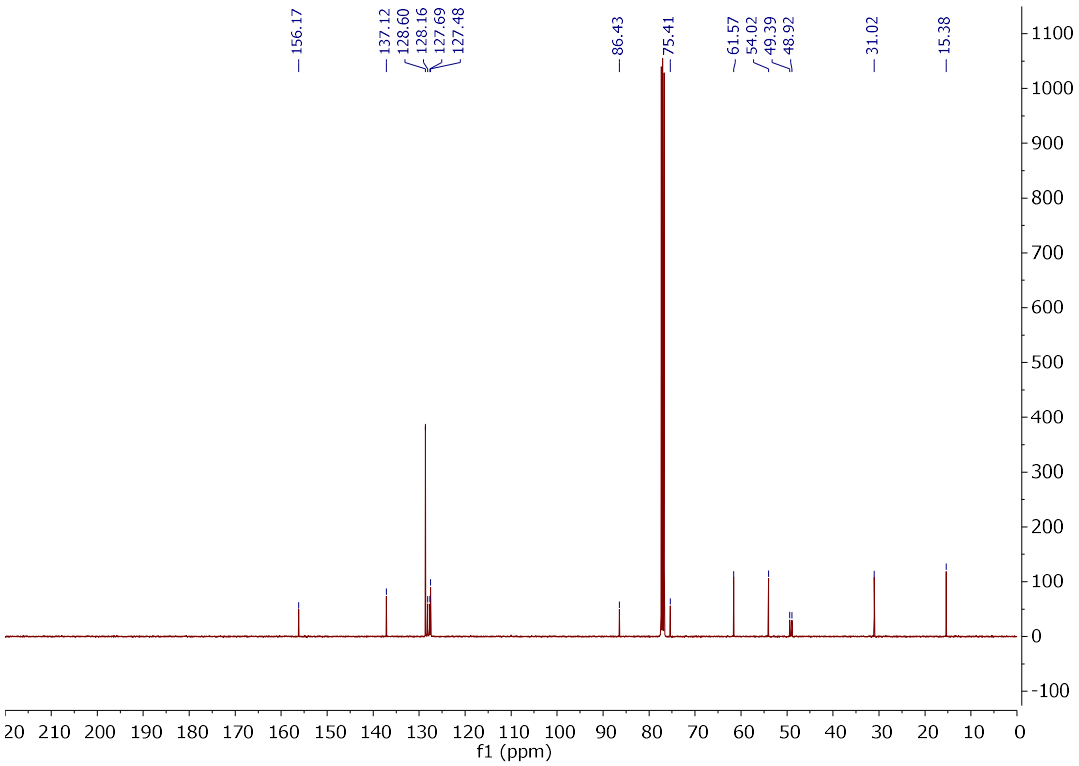

6-((Dibenzylcarbamoyl)oxy)hex-4-ynoic acid (38)

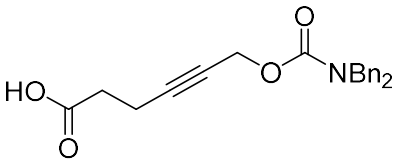

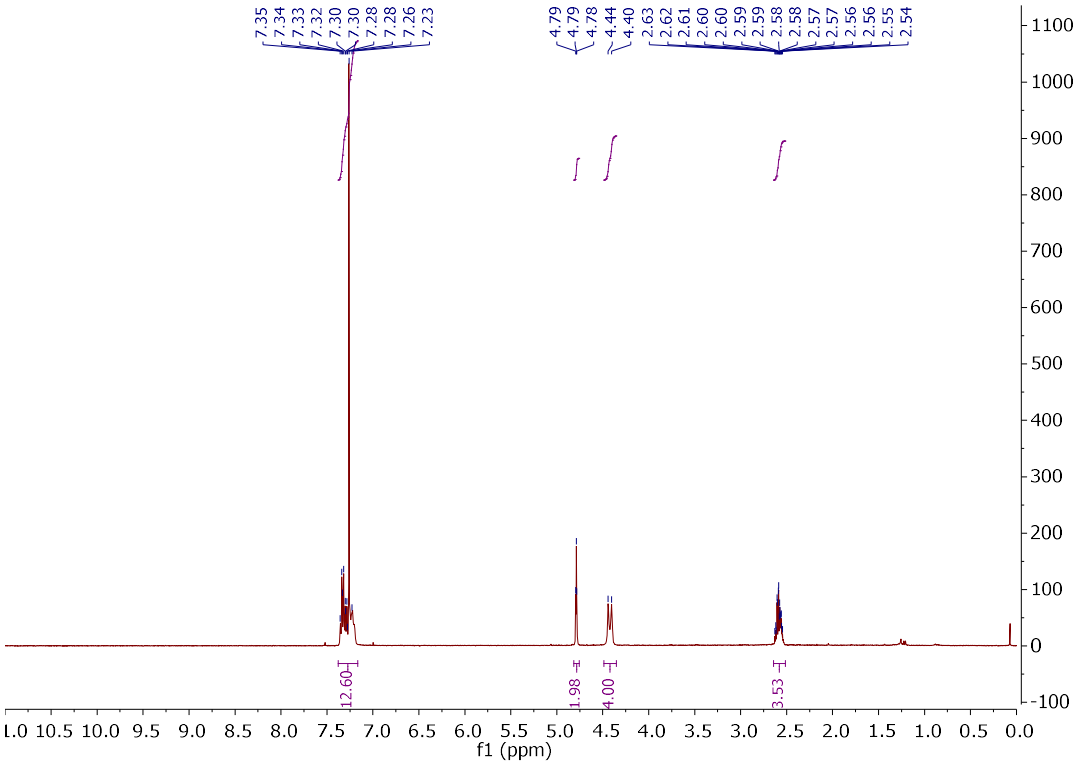

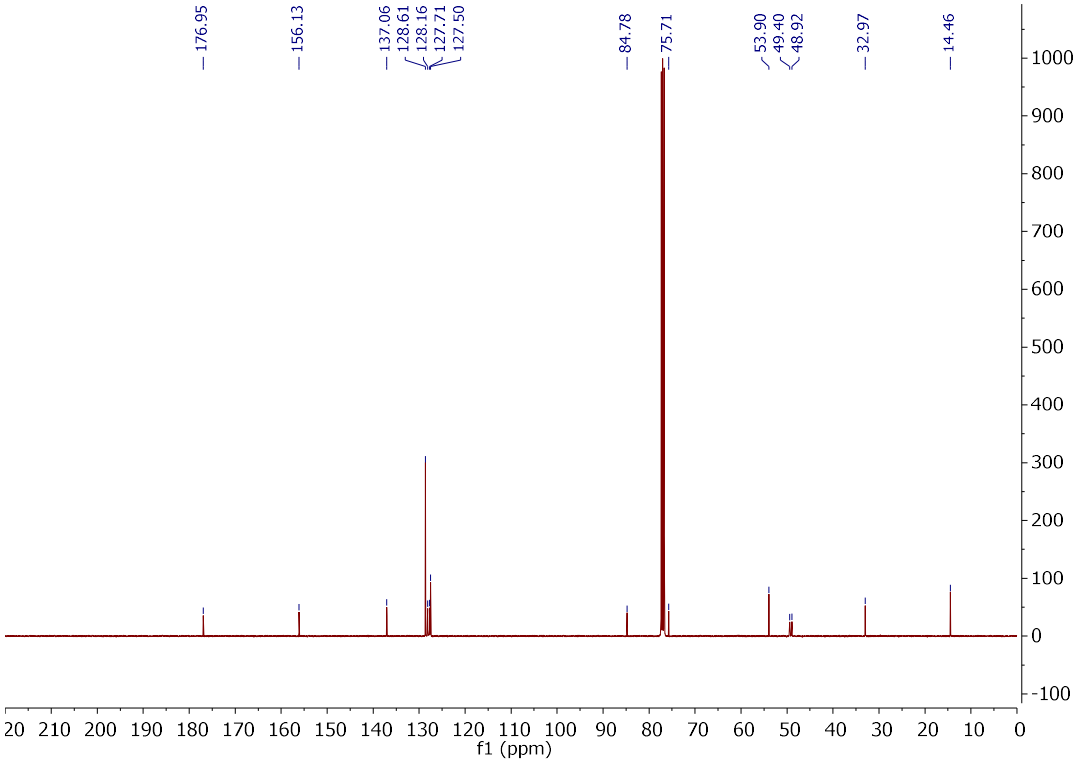

Propargyl morpholine-4-carboxylate (41)

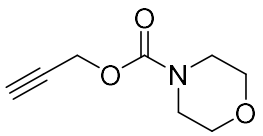

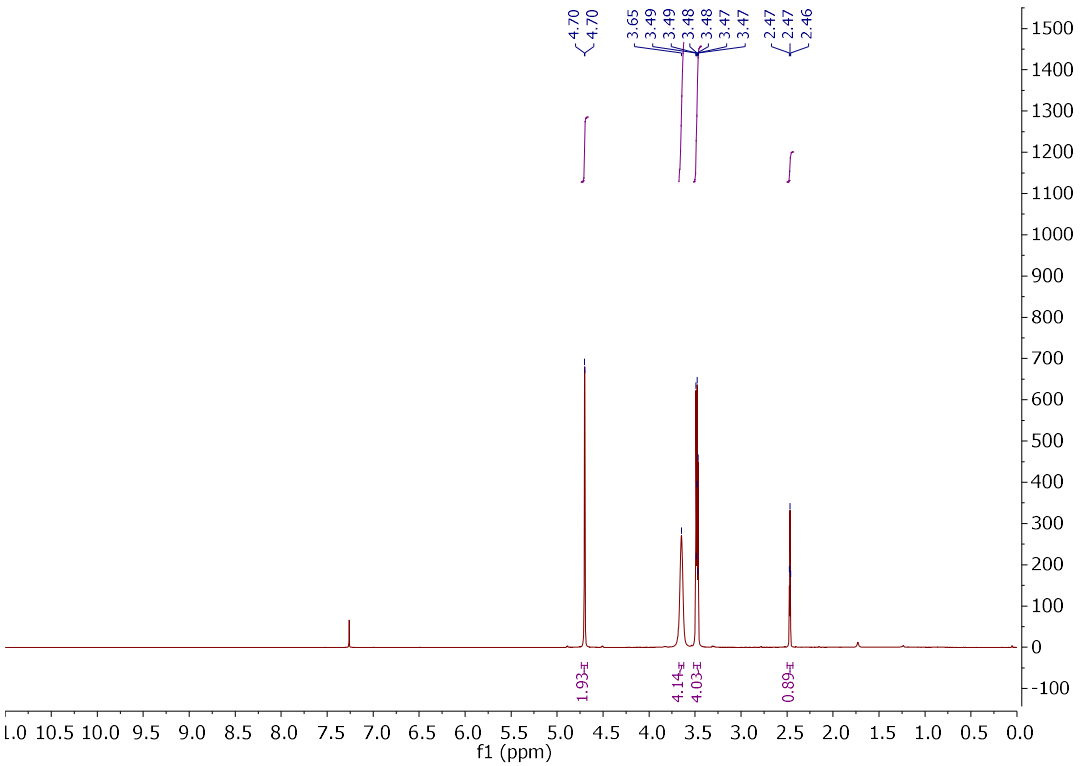

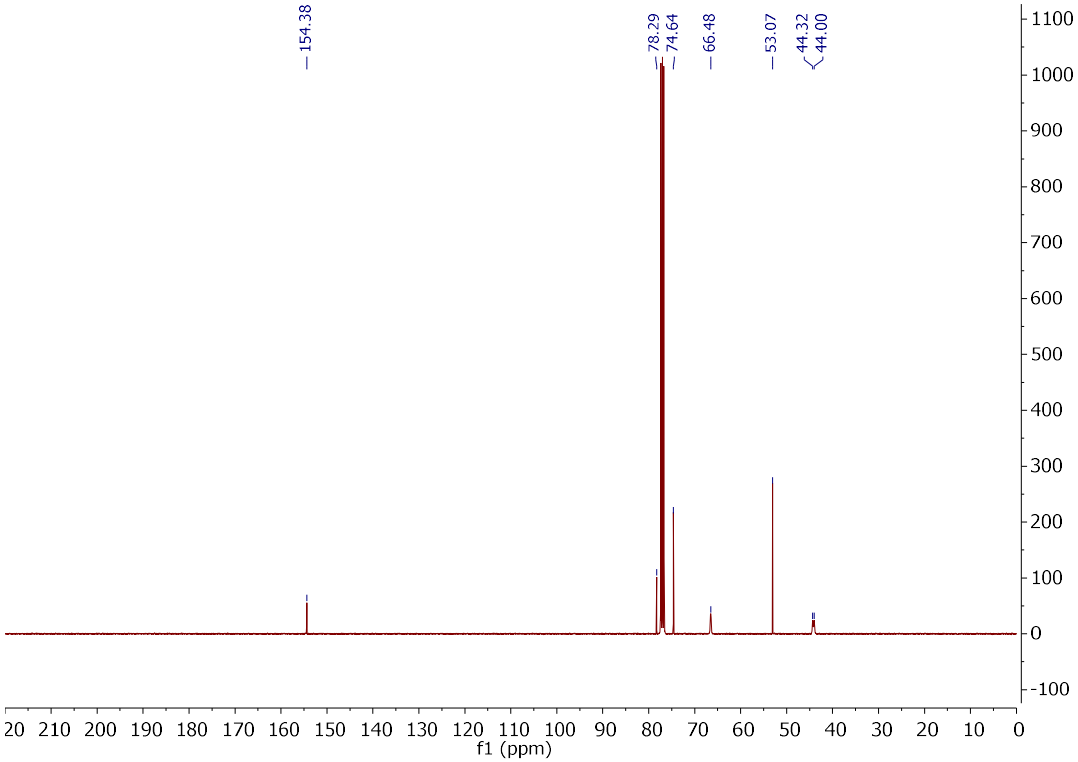

iso-Butyl morpholine-4-carboxylate (42)

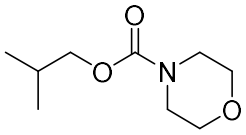

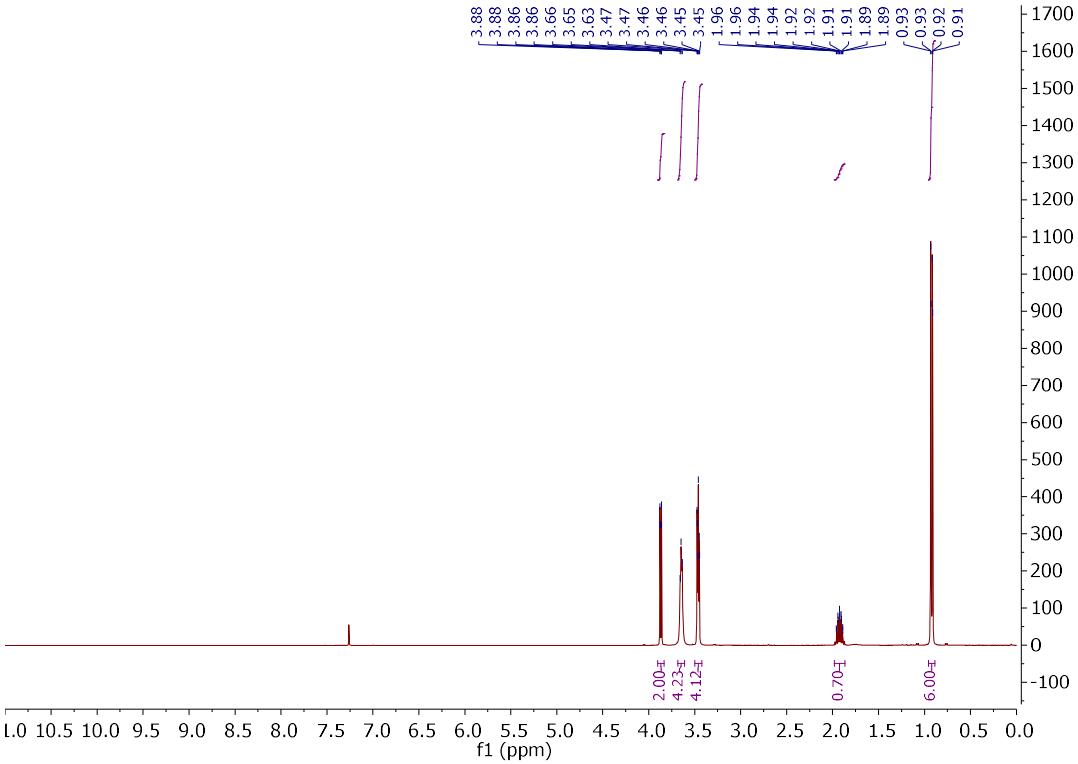

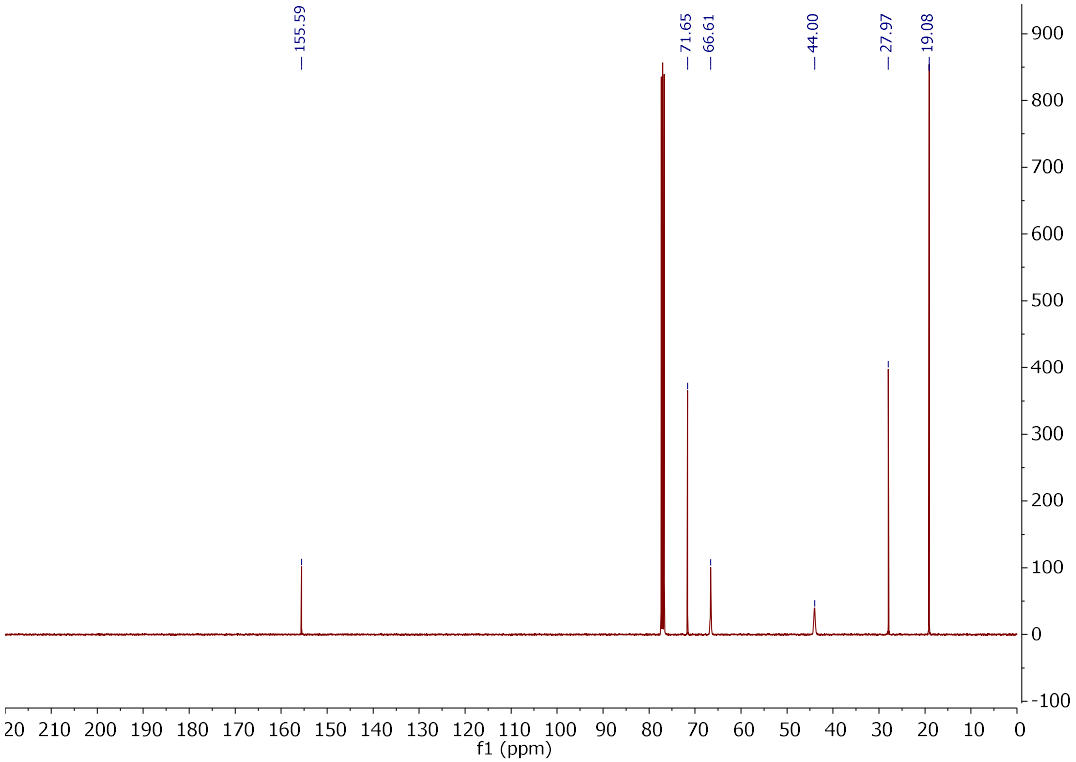

1-Morpholinopent-4-yn-1-one (43)

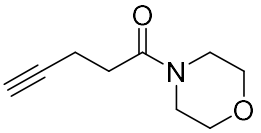

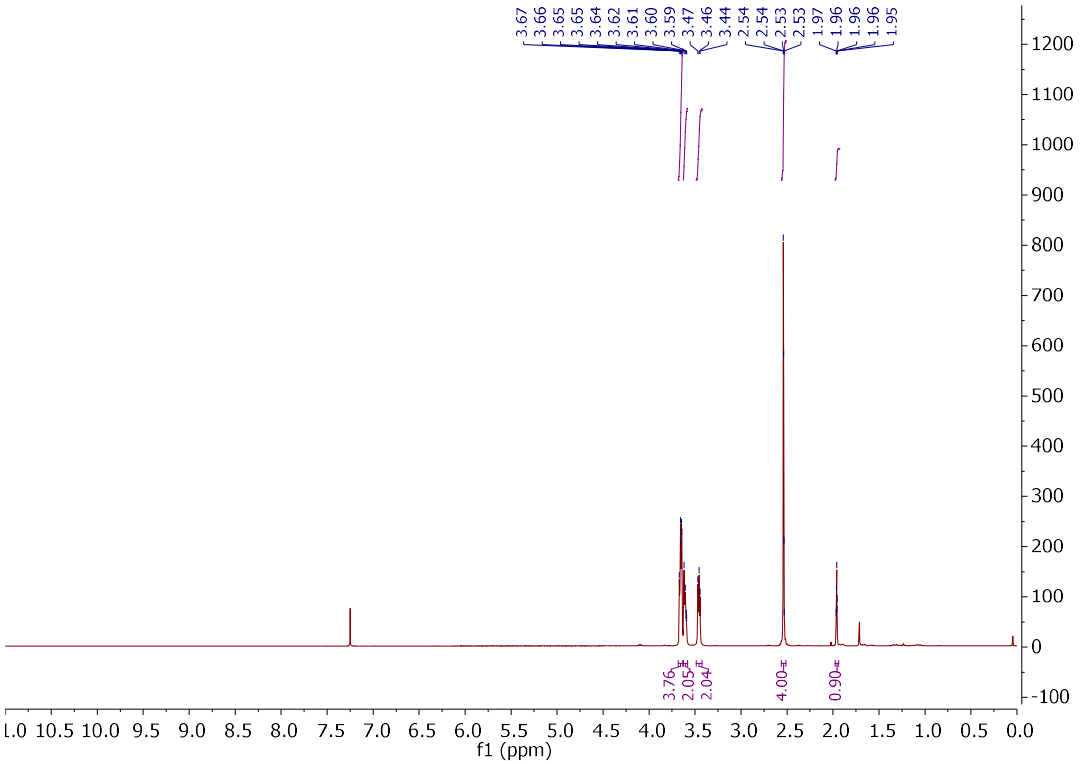

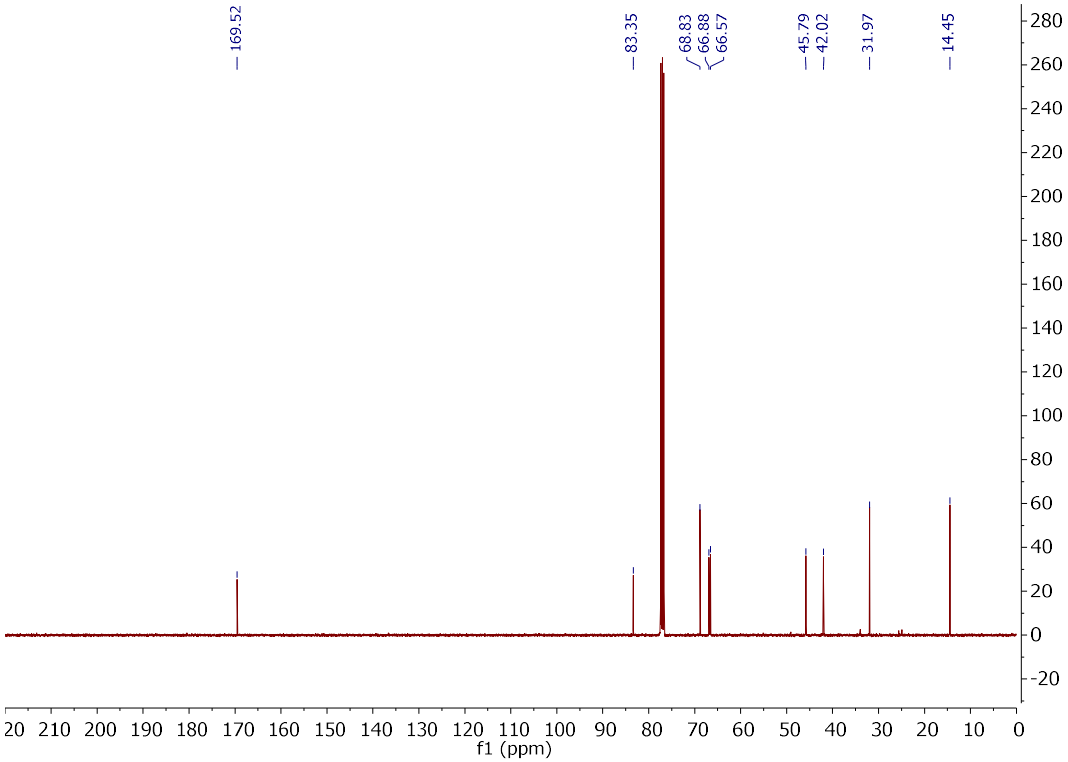

_N_-(2-Methoxyethyl)pent-4-ynamide (44)

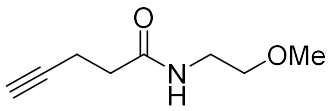

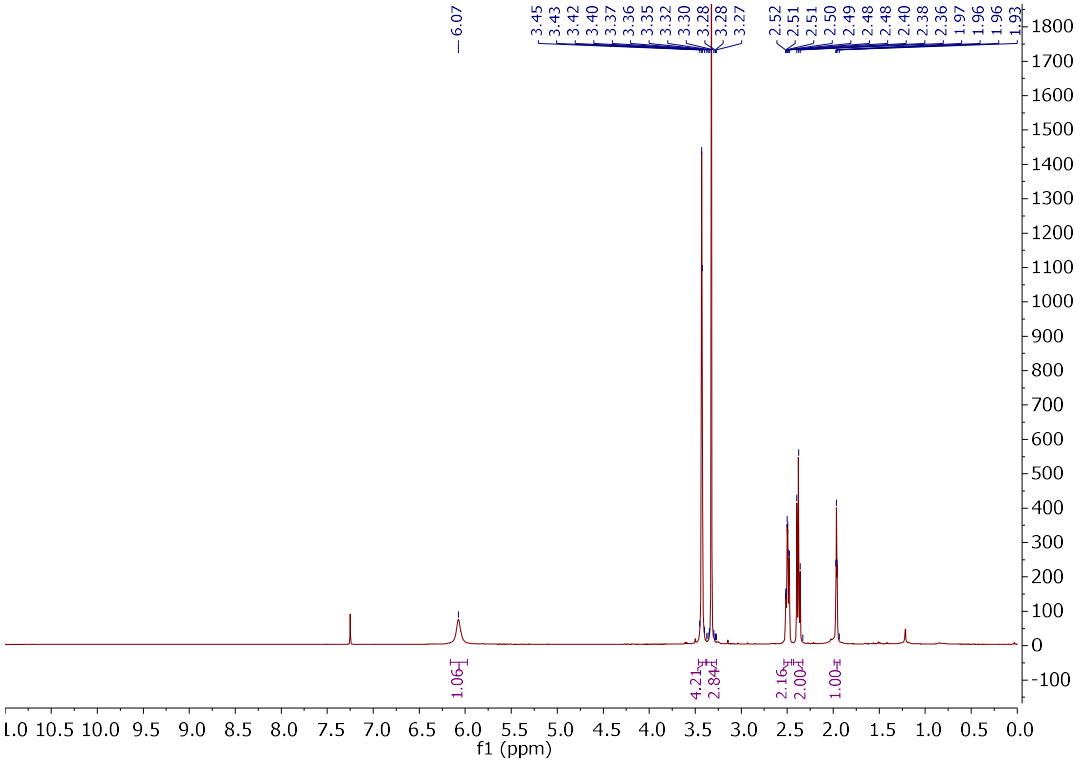
6.07
3.45
3.43
3.42
3.40
3.37
3.36
3.35
3.32
3.30
3.28
3.27
2.52
2.51
2.51
2.50
2.49
2.48
2.48
2.40
2.38
2.36
1.97
1.96
1.96
1.93
1.06
4.21
2.84
2.16
2.00
1.00
f1 (ppm)

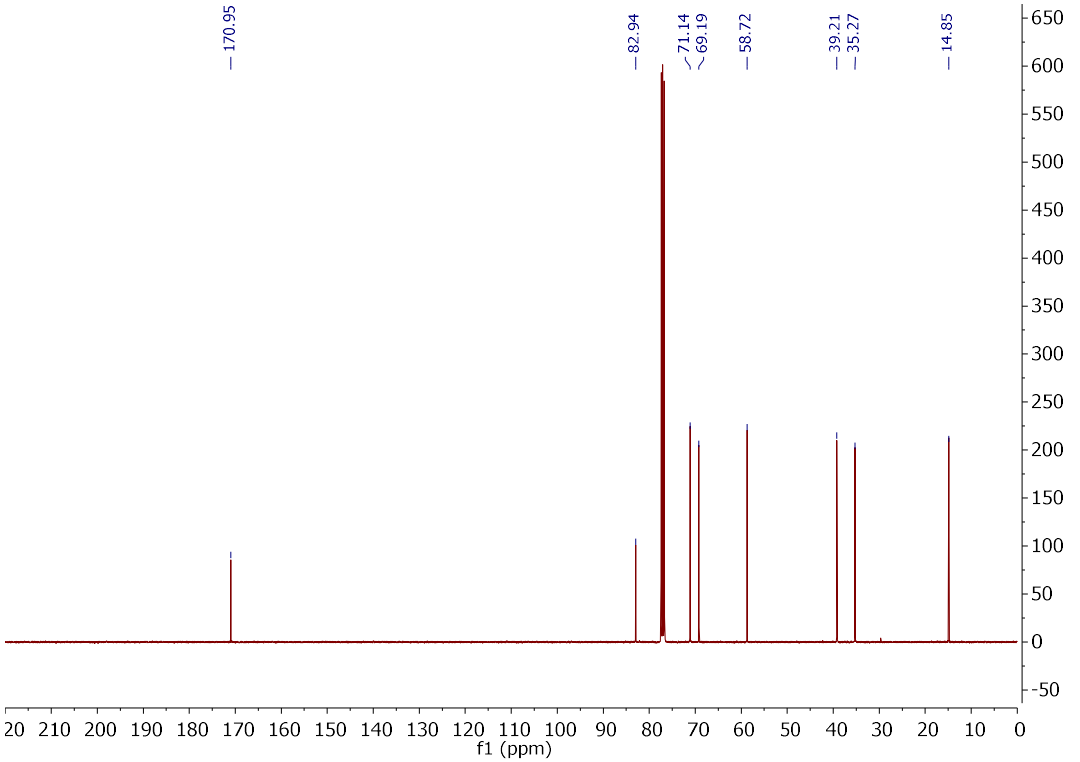
170.95
82.94
71.14
69.19
58.72
39.21
35.27
14.85
f1 (ppm)

pDoxAm (46)

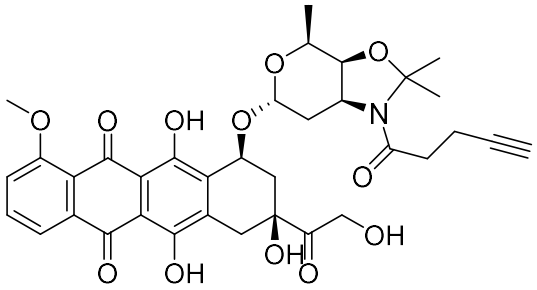
O
O
OH
O
O
N
O
O
OH
OH
O
OH
O

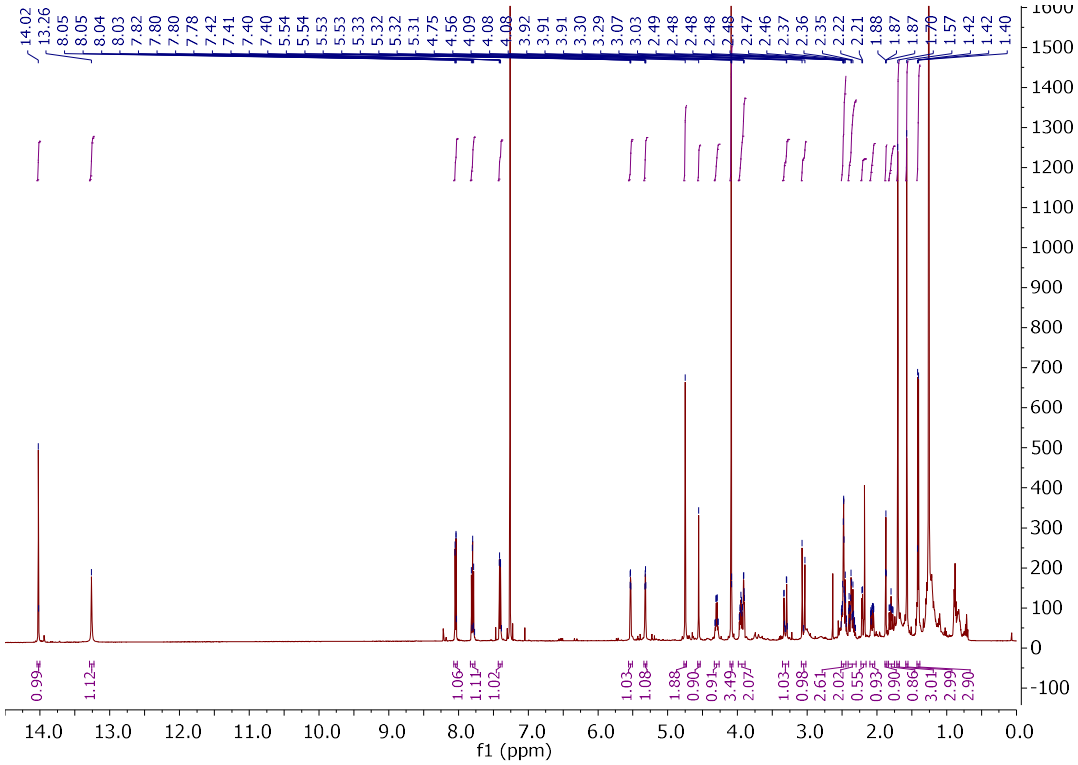
14.02
13.26
8.05
8.05
8.04
8.03
7.82
7.80
7.80
7.78
7.42
7.41
7.40
7.40
5.54
5.54
5.53
5.53
5.33
5.32
5.32
5.31
4.75
4.56
4.09
4.08
4.08
3.92
3.91
3.91
3.30
3.29
3.07
3.03
2.49
2.48
2.48
2.48
2.48
2.47
2.46
2.37
2.36
2.35
2.22
2.21
1.88
1.87
1.87
1.70
1.57
1.42
1.42
1.40
0.99
1.12
1.06
1.11
1.02
1.03
1.08
1.88
0.90
0.91
3.49
2.07
1.03
0.98
2.61
2.02
0.55
0.93
0.90
0.86
3.01
2.99
2.90
14.0
13.0
12.0
11.0
10.0
9.0
8.0
7.0
6.0
5.0
4.0
3.0
2.0
1.0
0.0
f1 (ppm)

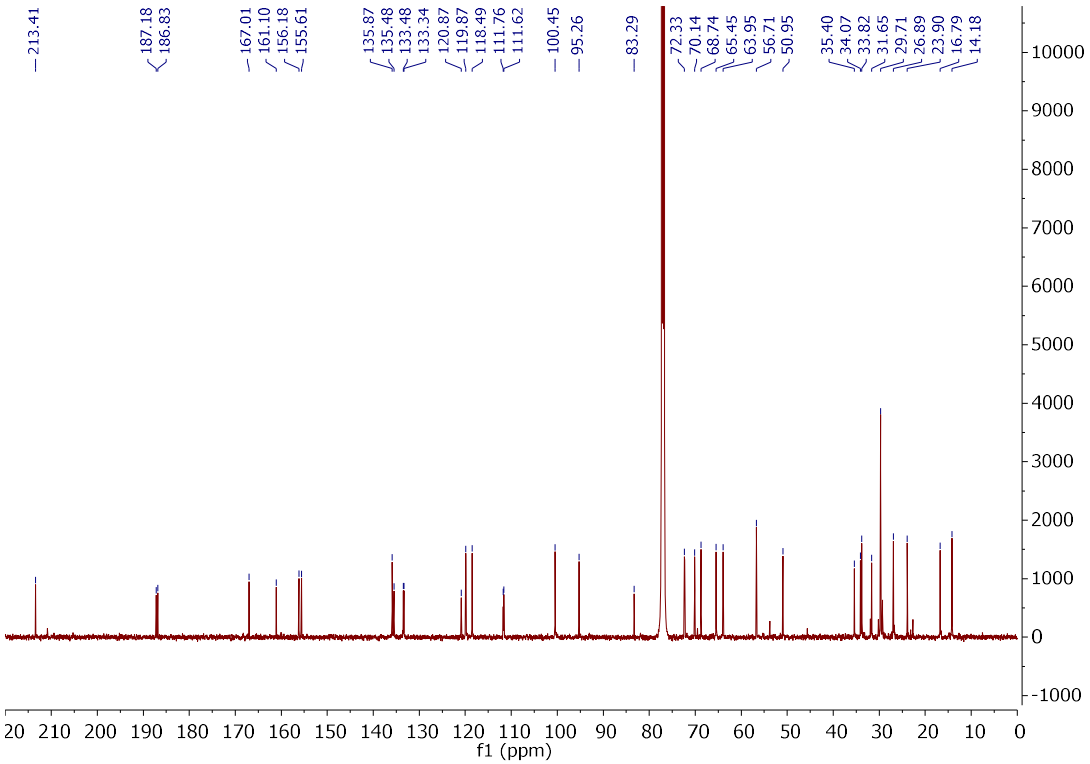
213.41
187.18
186.83
167.01
161.10
156.18
155.61
135.87
135.48
133.48
133.34
120.87
119.87
118.49
111.76
111.62
100.45
95.26
83.29
72.33
70.14
68.74
65.45
63.95
56.71
50.95
35.40
34.07
33.82
31.65
29.71
26.89
23.90
16.79
14.18
10000
9000
8000
7000
6000
5000
4000
3000
2000
1000
0
-1000
20 210 200 190 180 170 160 150 140 130 120 110 100 90 80 70 60 50 40 30 20 10 0
f1 (ppm)

DoxAm (47)

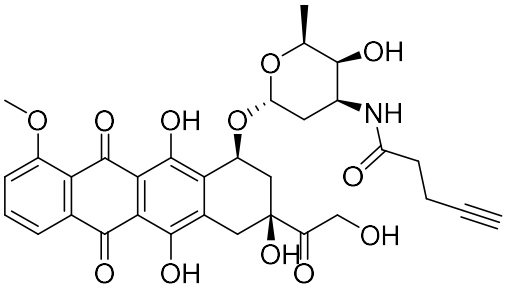

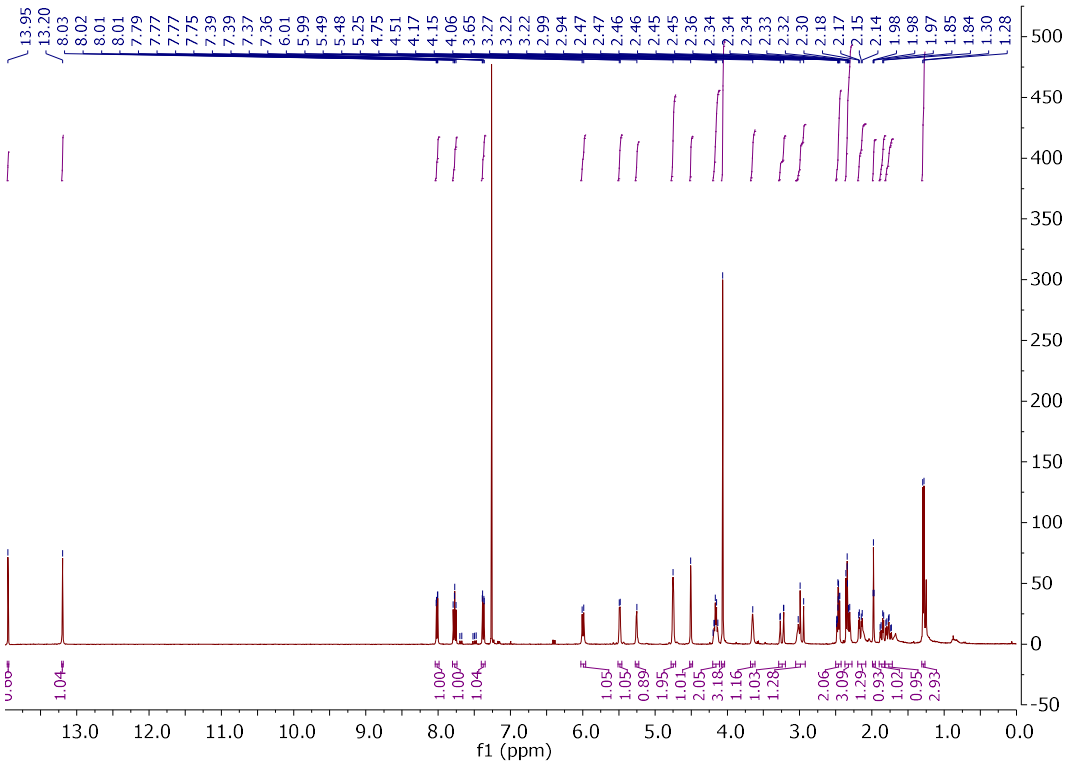

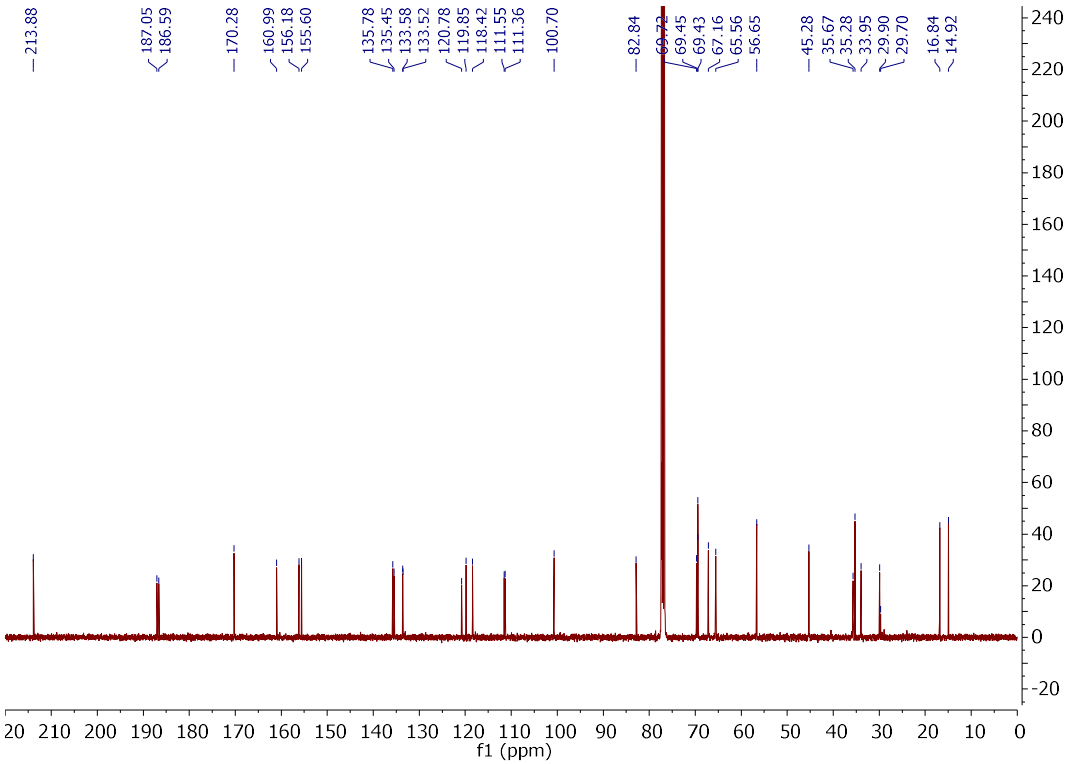
213.88
187.05
186.59
170.28
160.99
156.18
155.60
135.78
135.45
133.58
133.52
120.78
119.85
118.42
111.55
111.36
100.70
82.84
69.72
69.45
69.43
67.16
65.56
56.65
45.28
35.67
35.28
33.95
29.90
29.70
16.84
14.92
f1 (ppm)

pDoxAc (48)

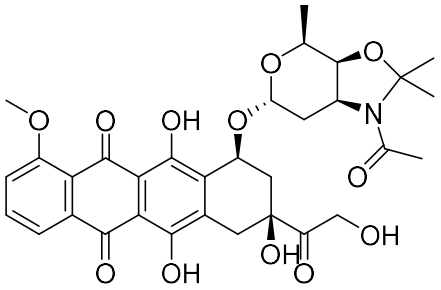

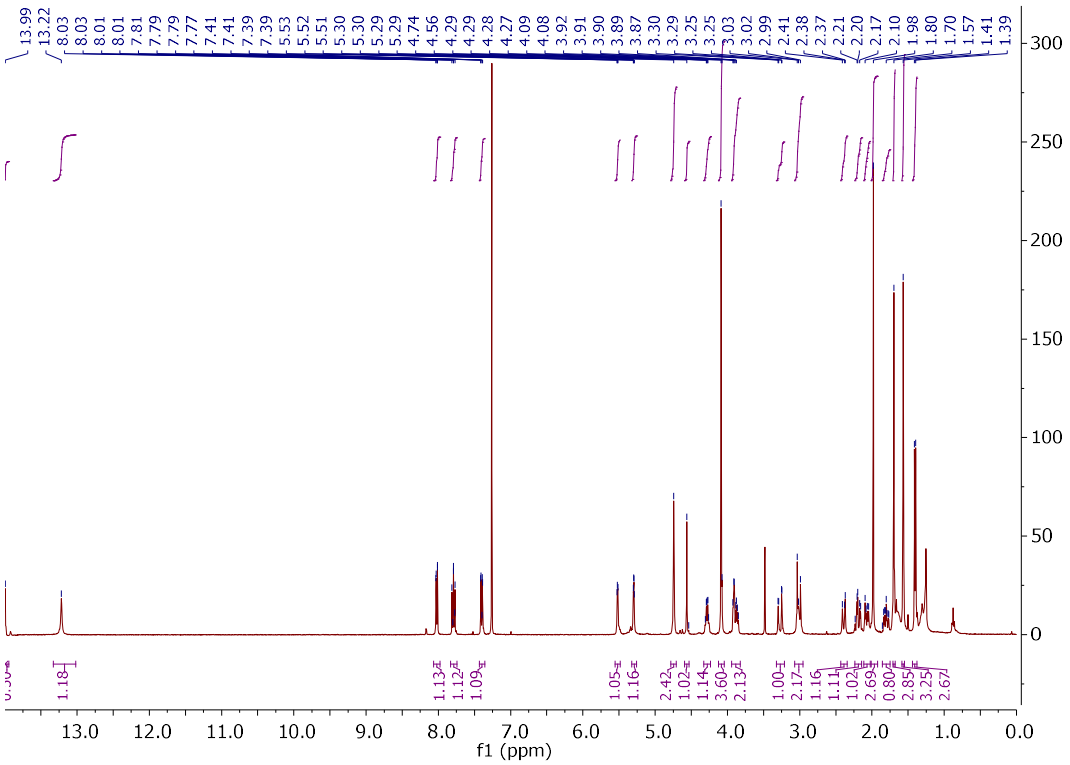
13.99
13.22
8.03
8.03
8.01
8.01
7.81
7.79
7.79
7.77
7.41
7.41
7.39
7.39
5.53
5.52
5.51
5.30
5.30
5.29
5.29
4.74
4.56
4.29
4.29
4.28
4.27
4.09
4.08
3.92
3.91
3.90
3.89
3.87
3.30
3.29
3.25
3.25
3.03
3.02
2.99
2.41
2.38
2.37
2.21
2.20
2.17
2.10
1.98
1.80
1.70
1.57
1.41
1.39
300
250
200
150
100
50
0
1.18
1.13
1.12
1.09
1.05
1.16
2.42
1.02
1.14
3.60
2.13
1.00
2.17
1.16
1.11
1.02
2.69
0.80
2.85
3.25
2.67
13.0
12.0
11.0
10.0
9.0
8.0
7.0
6.0
5.0
4.0
3.0
2.0
1.0
0.0
f1 (ppm)

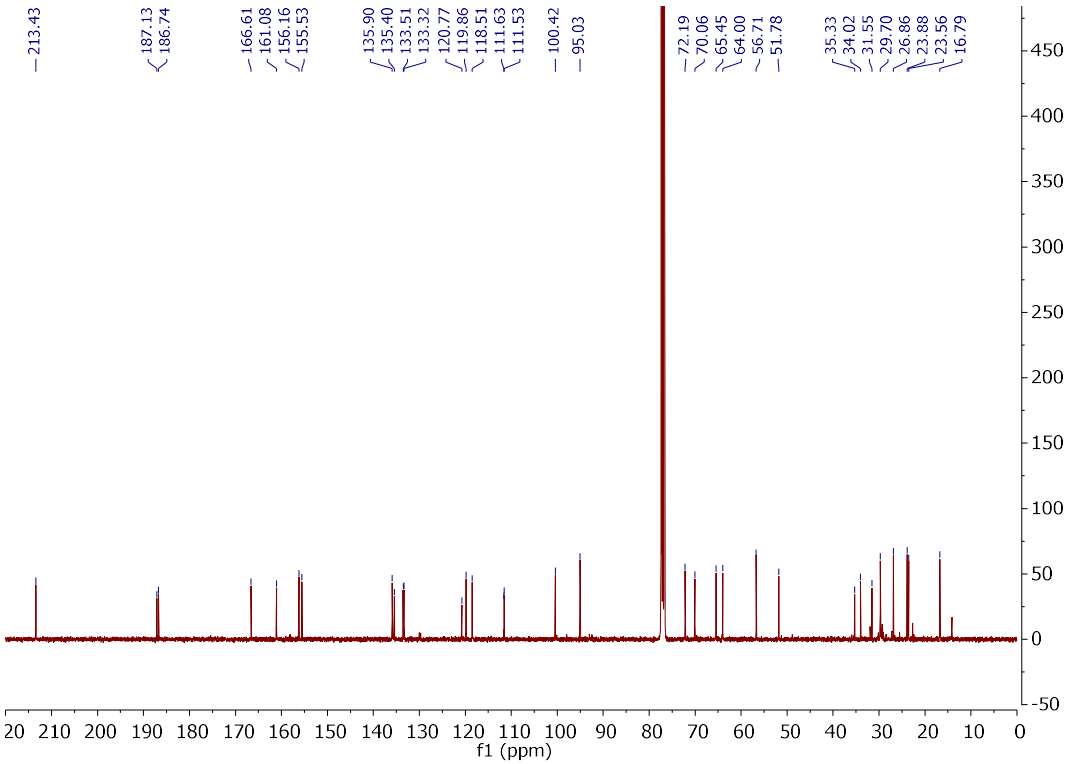
213.43
187.13
186.74
166.61
161.08
156.16
155.53
135.90
135.40
133.51
133.32
120.77
119.86
118.51
111.63
111.53
100.42
95.03
72.19
70.06
65.45
64.00
56.71
51.78
35.33
34.02
31.55
29.70
26.86
23.88
23.56
16.79
f1 (ppm)

FU-am (49)

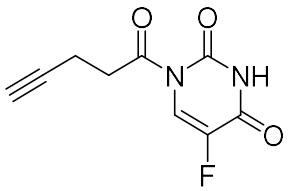
O
O
N
NH
O
F

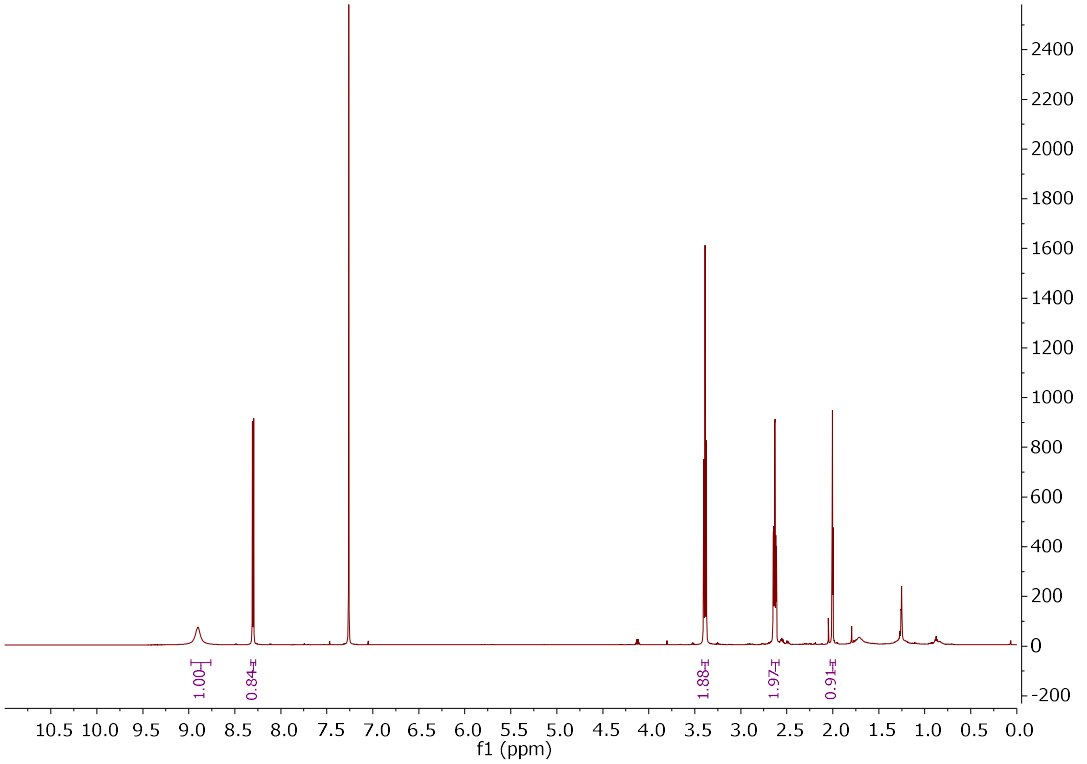
1.00
0.84
1.88
1.97
0.91
f1 (ppm)

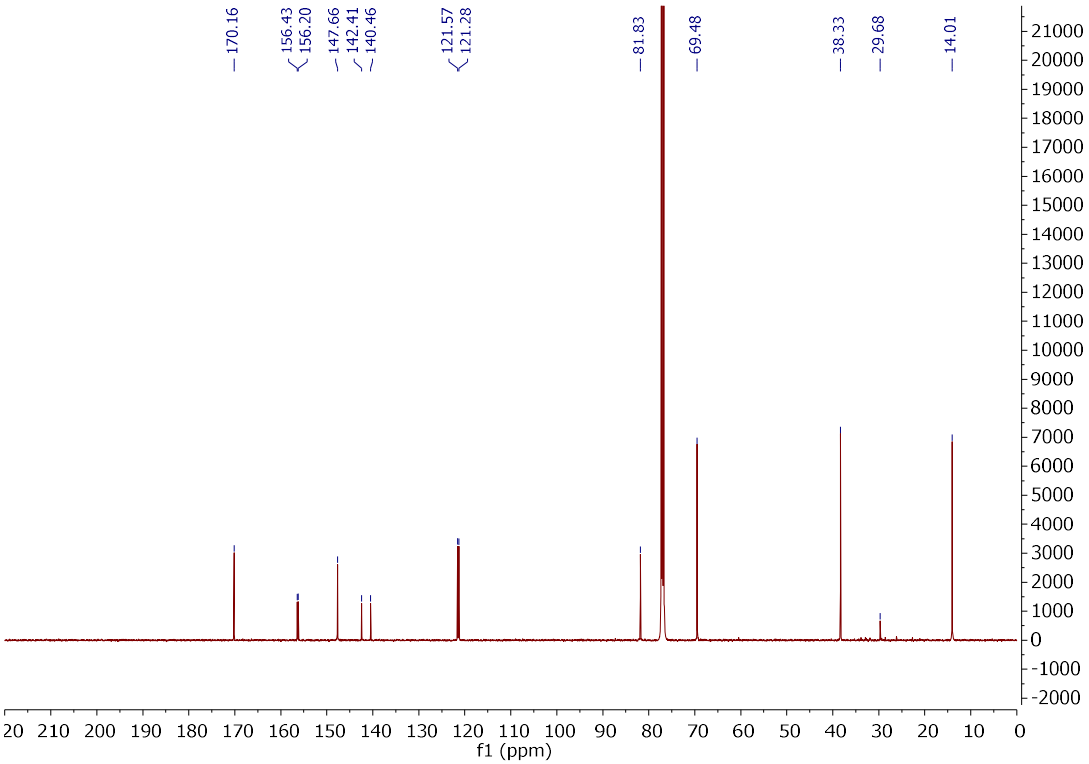
170.16
156.43
156.20
147.66
142.41
140.46
121.57
121.28
81.83
69.48
38.33
29.68
14.01
f1 (ppm)

MMAE-am (50)

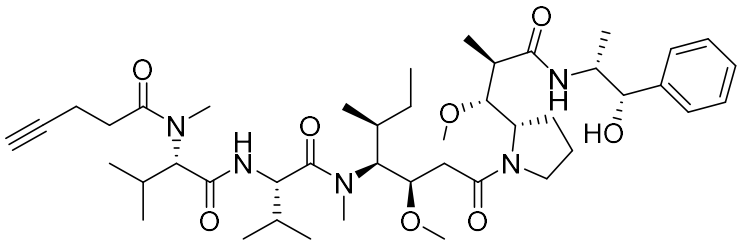
O
N
H
O
HO
O
N
H
O
N
O
O
O
N
O
O

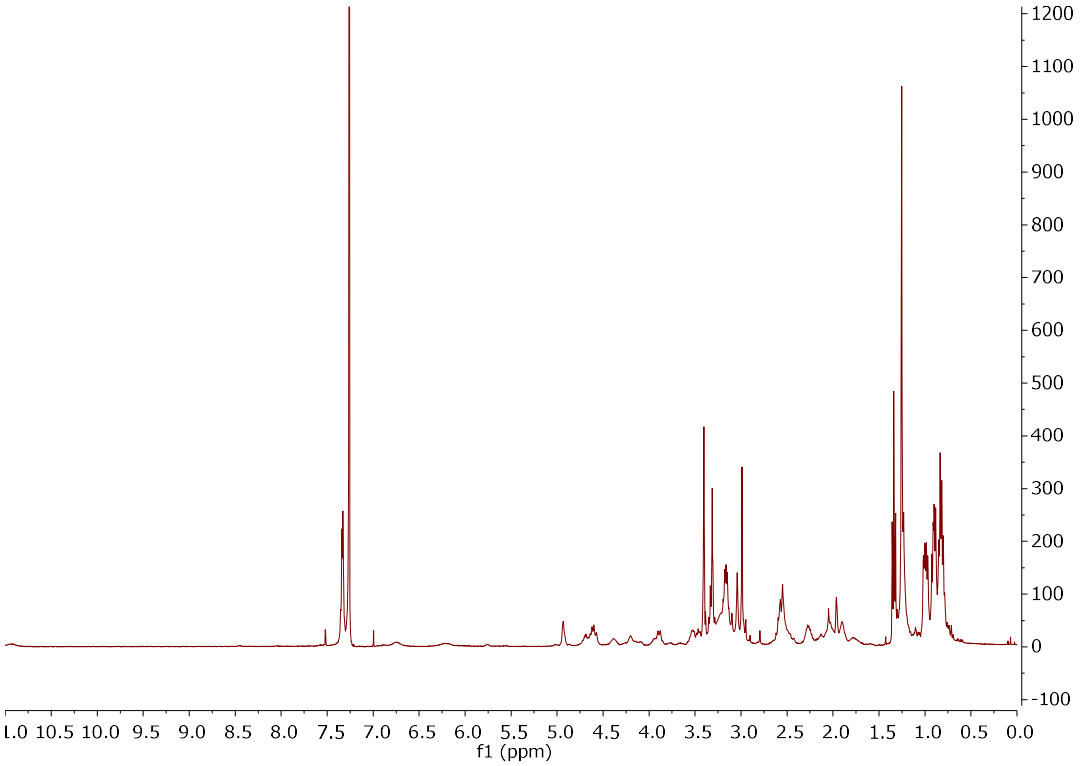
1200
1100
1000
900
800
700
600
500
400
300
200
100
0
-100
1.0 10.5 10.0 9.5 9.0 8.5 8.0 7.5 7.0 6.5 6.0 5.5 5.0 4.5 4.0 3.5 3.0 2.5 2.0 1.5 1.0 0.5 0.0
f1 (ppm)

tert-Butyl (2-(2-((6-hydroxyhex-2-yn-1-yl)oxy)ethoxy)ethyl)-_N_-methylcarbamate (55)

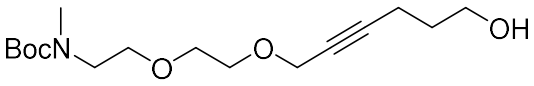

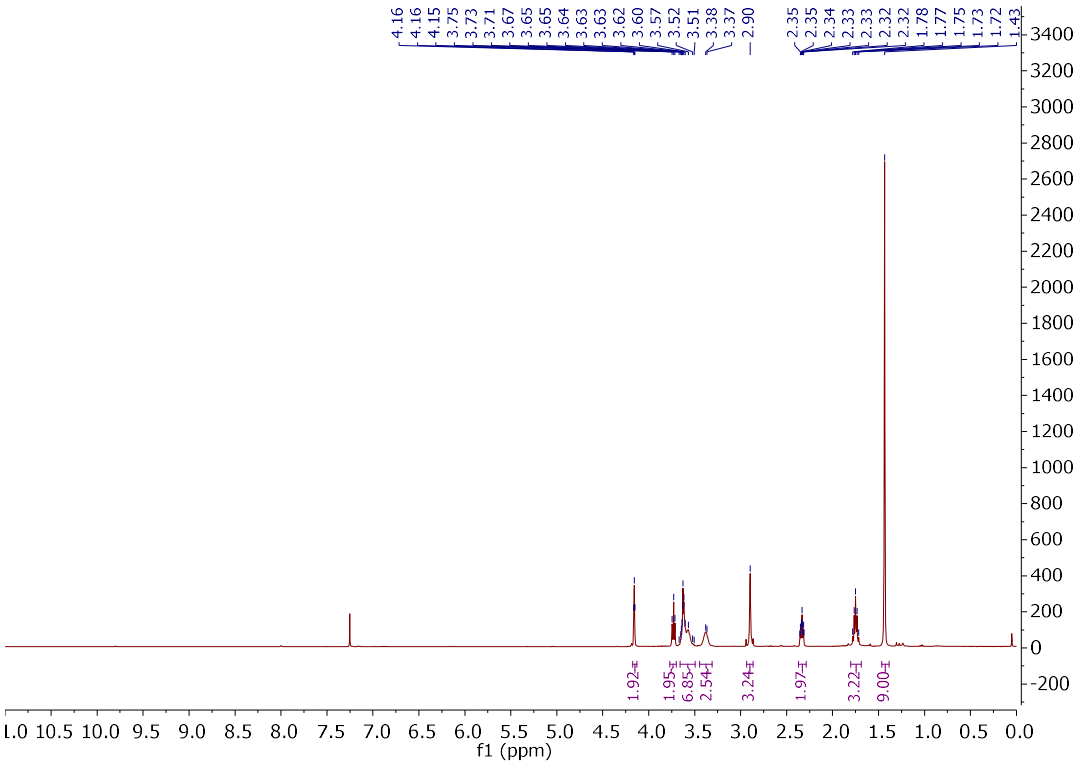

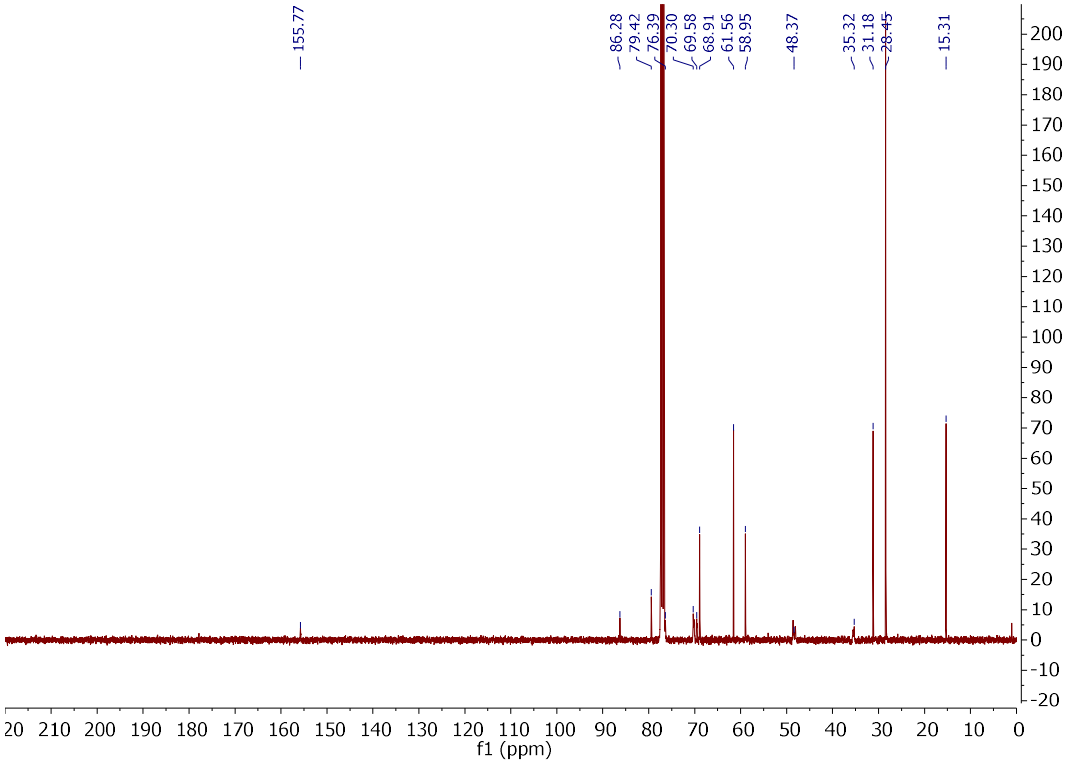

Acrylamide-(platinum cleavable linker)-MMAE (59)

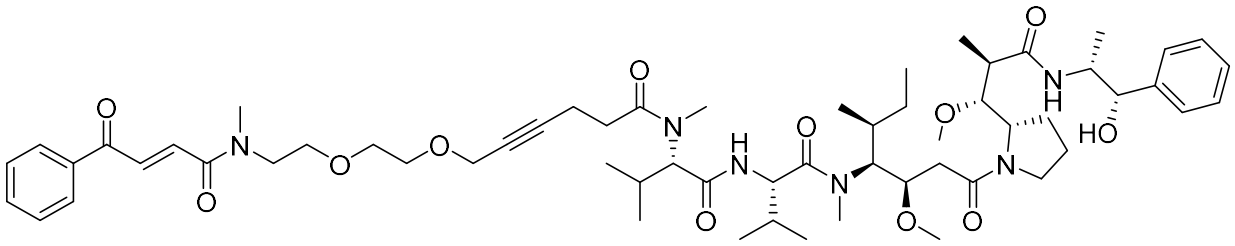

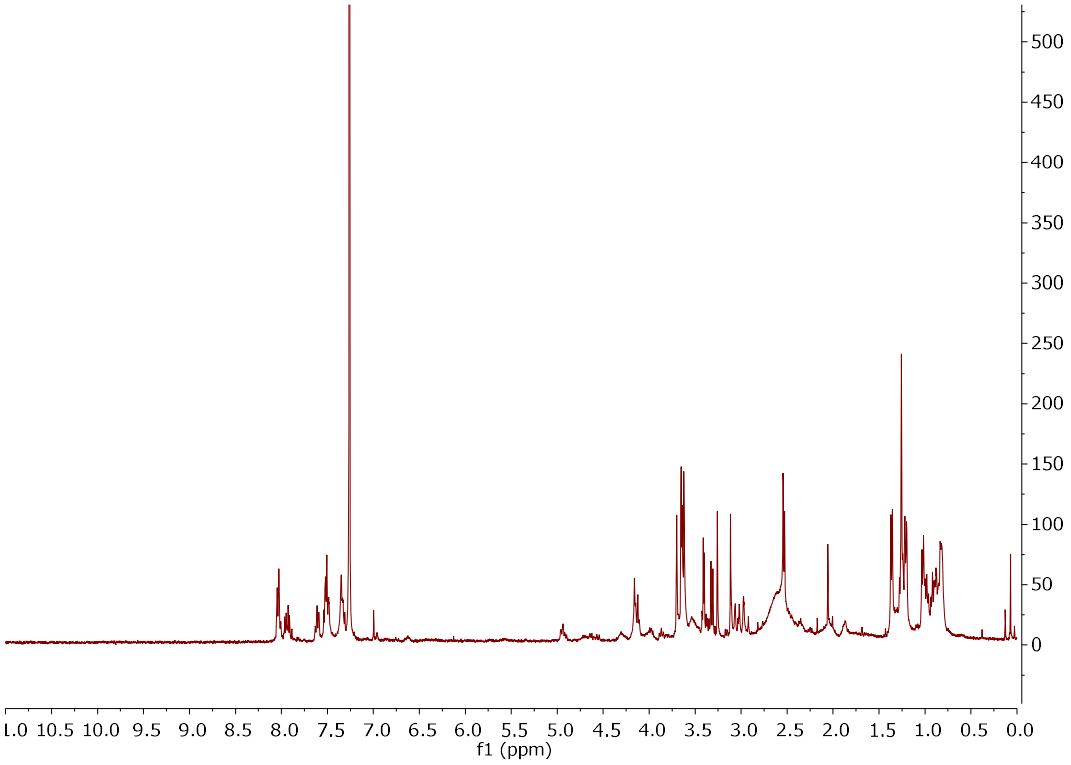

References

1. Stenton, B. J., Oliveira, B. L., Matos, M. J., Sinatra, L. & Bernardes, G. J. L. A thioether-directed palladium-cleavable linker for targeted bioorthogonal drug decaging. *Chem. Sci.* (2018). doi:10.1039/C8SC00256H

2. IARC (WHO). Estimated Cancer Incidence, Mortality and prevalence worldwide (2012). Available at: http://globocan.iarc.fr/Pages/fact_sheets_cancer.aspx?cancer=all. (Accessed: 15th April 2018)

3. S. Staal, K. Daily, C. A. *Colorectal Cancer* (ed. Scholefield, J. H., Eng, C.). (John Wiley & Sons, Ltd, 2014). doi:10.1002/9781118337929

4. Yao, Y., Zhou, Y., Yang, Z., Huang, H. & Shen, H. Adjuvant chemotherapy following surgical resection improves survival in patients with early-stage small cell lung cancer. *Oncol. Res.* **87**, 278–289 (2018).

5. Lennan, E. *Breast Cancer Nursing Care and Management* (ed. Harmer, V.). 149–172 (John Wiley & Sons, Ltd., 2013). doi:10.1002/9781118784921.ch8

6. Mathé, G., Loc, T. B. & Bernard, J. Effet sur la leucémie 1210 de la Souris d'une combinaison par diazotation d'A-méthoptérine et de gamma-globulines de hamsters porteurs de cette leucémie par hététogreffe. *C. R. Hebd. Seances Acad. Sci.* **246,** 1626–1628 (1958).

7. Moolten, F. L. & Cooperband, S. R. Selective destruction of target cells by diphtheria toxin conjugated to antibody directed against antigens on the cells. *Science* **169,** 68–70 (1970).

8. Laguzza, B. C. *et al.* New antitumor monoclonal antibody-vinca conjugates LY203725 and related compounds: design, preparation, and representative in vivo activity. *J. Med. Chem.* **32,** 548–555 (1989).

9. Trail, P. *et al.* Cure of xenografted human carcinomas by BR96-doxorubicin immunoconjugates. *Science* **261,** 212–215 (1993).

10. Schneck, D. *et al.* Disposition of a murine monoclonal antibody vinca conjugate (KS1/4-DAVLB) in patients with adenocarcinomas. *Clin. Pharmacol. Ther.* **47,** 36–41 (1990).

11. Elias, D. J. *et al.* Phase I clinical comparative study of monoclonal antibody KS1/4 and KS1/4-methotrexate immunconjugate in patients with non-small cell lung carcinoma. *Cancer Res.* **50,** 4154–4159 (1990).

12. Odegard, V. H. & Schatz, D. G. Targeting of somatic hypermutation. *Nat. Rev. Immunol.* **6,** 573–583 (2006).

13. Nadler, L. M. *et al.* Serotherapy of a patient with a monoclonal antibody directed against a human lymphoma-associated antigen. *Cancer Res.* **40,** 3147–3154 (1980).

14. Lerch, T. F. *et al.* Infliximab crystal structures reveal insights into self-association. *MAbs* **9,** 874–883 (2017).

15. Liang, S. *et al.* Structural Basis for Treating Tumor Necrosis Factor α (TNFα)-associated diseases with the therapeutic antibody Infliximab. *J. Biol. Chem.* **288,** 13799–13807 (2013).

16. Chari, R. V. J., Miller, M. L. & Widdison, W. C. Antibody-drug conjugates: an emerging concept in cancer therapy. *Angew. Chemie* **53,** 3796–3827 (2014).

17. Guan, M., Zhou, Y.-P., Sun, J.-L. & Chen, S.-C. Adverse events of monoclonal antibodies used for cancer therapy. *Biomed Res. Int.* **2015,** 1–13 (2015).

18. FDA, U. S. Hematology/Oncology (Cancer) Approvals & Safety Notifications. (2018). Available at: www.fda.gov/Drugs/InformationOnDrugs/ApprovedDrugs/ucm279174.htm. (Accessed: 18th February 2018)

19. Mehrling, T. & Soltis, D. Challenges in optimising the successful construction of antibody drug conjugates in cancer therapy. *Antibodies* **7,** 11 (2018).

20. Okeley, N. M. *et al.* Intracellular activation of SGN-35, a potent anti-CD30 antibody-drug conjugate. *Clin. Cancer Res.* **16,** 888–897 (2010).

21. Hamann, P. R. *et al.* Gemtuzumab Ozogamicin, A Potent and Selective Anti-CD33 Antibody−Calicheamicin Conjugate for Treatment of Acute Myeloid Leukemia. *Bioconjug. Chem.* **13,** 47–58 (2002).

22. Erickson, H. K. *et al.* Antibody-maytansinoid conjugates are activated in targeted cancer cells by lysosomal degradation and linker-dependent intracellular processing. *Cancer Res.* **66,** 4426–4433 (2006).

23. Phillips, A. C. *et al.* ABT-414, an Antibody-Drug Conjugate targeting a tumor-selective EGFR epitope. *Mol. Cancer Ther.* **15,** 661–669 (2016).

24. Doronina, S. O. *et al.* Enhanced activity of monomethylauristatin F through monoclonal antibody delivery: effects of linker technology on efficacy and toxicity. *Bioconjug. Chem.* **17,** 114–124 (2006).

25. Doronina, S. O. *et al.* Novel peptide linkers for highly potent antibody−auristatin conjugate. *Bioconjug. Chem.* **19,** 1960–1963 (2008).

26. Ab, O. *et al.* IMGN853, a Folate Receptor- (FR) -targeting antibody-drug conjugate, exhibits potent targeted antitumor activity against FR-expressing tumors. *Mol. Cancer Ther.* **14,** 1605–1613 (2015).

27. Dornan, D. *et al.* Therapeutic potential of an anti-CD79b antibody-drug conjugate, anti-CD79b-vc-MMAE, for the treatment of non-Hodgkin lymphoma. *Blood* **114,** 2721–2729 (2009).

28. Rovalpituzumab Tesirine. *WHO Drug Inf.* **30,** 150 (2016).

29. Cardillo, T. M. *et al.* Sacituzumab Govitecan (IMMU-132), an Anti-Trop-2/SN-38 Antibody–Drug Conjugate: characterization and efficacy in pancreatic, gastric, and other cancers. *Bioconjug. Chem.* **26,** 919–931 (2015).

30. Moon, S.-J. *et al.* Antibody conjugates of 7-Ethyl-10-hydroxycamptothecin (SN-38) for targeted cancer chemotherapy. *J. Med. Chem.* **51,** 6916–6926 (2008).

31. Goldenberg, D. M., Cardillo, T. M., Govindan, S. V., Rossi, E. A. & Sharkey, R. M. Trop-2 is a novel target for solid cancer therapy with sacituzumab govitecan (IMMU-132), an antibody-drug conjugate (ADC). *Oncotarget* **6,** 1169-1173 (2015).

32. Black, J. *et al.* SYD985, a novel duocarmycin-based HER2-targeting antibody-drug conjugate, shows antitumor activity in uterine serous carcinoma with HER2/Neu expression. *Mol. Cancer Ther.* **15,** 1900–1909 (2016).

33. Elgersma, R. C. *et al.* Design, synthesis, and evaluation of linker-duocarmycin payloads: toward selection of HER2-targeting Antibody–Drug Conjugate SYD985. *Mol. Pharm.* **12,** 1813–1835 (2015).

34. van der Lee, M. M. C. *et al.* The preclinical profile of the duocarmycin-based HER2-targeting ADC SYD985 predicts for clinical benefit in low HER2-expressing breast cancers. *Mol. Cancer Ther.* **14,** 692–703 (2015).

35. Kung Sutherland, M. S. *et al.* SGN-CD33A: a novel CD33-targeting antibody-drug conjugate using a pyrrolobenzodiazepine dimer is active in models of drug-resistant AML. *Blood* **122,** 1455–1463 (2013).

36. Jeffrey, S. *et al.* Anti-CD70 antibody-drug conjugates containing pyrrolobenzodiazepine dimers demonstrate robust antitumor activity. *Cancer Research* **72,** 4631–4631 (2012).

37. Donate, F. *et al.* AGS16F Is a Novel Antibody Drug Conjugate directed against ENPP3 for the treatment of renal cell carcinoma. *Clin. Cancer Res.* **22,** 1989–1999 (2016).

38. Golfier, S. *et al.* Anetumab ravtansine: a novel mesothelin-targeting antibody-drug conjugate cures tumors with heterogeneous target expression favored by bystander effect. *Mol. Cancer Ther.* **13,** 1537–48 (2014).

39. Thomas, L. J. *et al.* Development of a novel Antibody–Drug Conjugate for the potential treatment of ovarian, lung, and renal cell carcinoma expressing TIM-1. *Mol. Cancer Ther.* **15,** 2946–2954 (2016).

40. Takegawa, N. *et al.* DS-8201a, a new HER2-targeting antibody-drug conjugate incorporating a novel DNA topoisomerase I inhibitor, overcomes HER2-positive gastric cancer T-DM1 resistance. *Int. J. Cancer* **141,** 1682–1689 (2017).

41. Ogitani, Y. *et al.* DS-8201a, A novel HER2-targeting ADC with a novel DNA topoisomerase I inhibitor, demonstrates

a promising antitumor efficacy with differentiation from T-DM1. *Clin. Cancer Res.* **22,** 5097–5108 (2016).

42. Challita-Eid, P. M. *et al.* Enfortumab vedotin Antibody-Drug Conjugate targeting nectin-4 is a highly potent therapeutic agent in multiple preclinical cancer models. *Cancer Res.* **76,** 3003–3013 (2016).

43. Tse, K. F. CR011, a Fully human monoclonal antibody-auristatin E conjugate, for the treatment of melanoma. *Clin. Cancer Res.* **12,** 1373–1382 (2006).

44. Sapra, P. Anti-CD74 Antibody-doxorubicin conjugate, IMMU-110, in a human multiple myeloma xenograft and in monkeys. *Clin. Cancer Res.* **11,** 5257–5264 (2005).

45. Griffiths, G. L. *et al.* Cure of SCID mice bearing human B-lymphoma xenografts by an anti-CD74 antibody-anthracycline drug conjugate. *Clin. Cancer Res.* **9,** 6567–71 (2003).

46. Dotan, E. *et al.* Labetuzumab govitecan (IMMU-130), an anti-CEACAM5/SN-38 antibody-drug conjugate, is active in patients (pts) with heavily pretreated metastatic colorectal cancer (mCRC): phase II results. *Cancer Res.* **76,** CT065-CT065 (2016).

47. Whiteman, K. R. *et al.* Lorvotuzumab mertansine, a CD56-targeting antibody-drug conjugate with potent antitumor activity against small cell lung cancer in human xenograft models. *MAbs* **6,** 556–566 (2014).

48. Zammarchi, F. *et al.* ADCT-401/MEDI3726, a novel pyrrolobenzodiazepine (PBD)-based antibody-drug conjugate (ADC) targeting PSMA-expressing prostate cancers. in *AACR Annual Meeting* 3111A (2017).

49. Tiberghien, A. C. *et al.* Design and synthesis of tesirine, a clinical Antibody–Drug Conjugate pyrrolobenzodiazepine dimer payload. *ACS Med. Chem. Lett.* **7,** 983–987 (2016).

50. Bardia, A. *et al.* Efficacy and safety of anti-Trop-2 Antibody Drug Conjugate sacituzumab govitecan (IMMU-132) in heavily pretreated patients with metastatic triple-negative breast cancer. *J. Clin. Oncol.* **35,** 2141–2148 (2017).

51. Willner, D. *et al.* (6-Maleimidocaproyl)hydrazone of doxorubicin. A new derivative for the preparation of immunoconjugates of doxorubicin. *Bioconjug. Chem.* **4,** 521–527 (1993).

52. Stein, E. M. *et al.* A phase 1 trial of vadastuximab talirine as monotherapy in patients with CD33-positive acute myeloid leukemia. *Blood* **131,** 387–396 (2018).

53. Yokota, T., Milenic, D. E., Whitlow, M. & Schlom, J. Rapid tumor penetration of a single-chain Fv and comparison with other immunoglobulin forms. *Cancer Res.* **52,** 3402–3408 (1992).

54. Arend, W. P. & Silverblatt, F. J. Serum disappearance and catabolism of homologous immunoglobulin fragments in rats. *Clin. Exp. Immunol.* **22,** 502–513 (1975).

55. Kim, K. M. *et al.* Anti-CD30 diabody-drug conjugates with potent antitumor activity. *Mol. Cancer Ther.* **7,** 2486–2497 (2008).

56. Roopenian, D. C. & Akilesh, S. FcRn: the neonatal Fc receptor comes of age. *Nat. Rev. Immunol.* **7,** 715–725 (2007).

57. Pasche, N. & Neri, D. Immunocytokines: a novel class of potent armed antibodies. *Drug Discov. Today* **17,** 583–590 (2012).

58. Nelson, A. L. & Reichert, J. M. Development trends for therapeutic antibody fragments. *Nat. Biotechnol.* **27,** 331–337 (2009).

59. Strohl, W. R. Current progress in innovative engineered antibodies. *Protein Cell* **9,** 86–120 (2018).

60. Smith, L. M. Potent cytotoxicity of an auristatin-containing antibody-drug conjugate targeting melanoma cells expressing melanotransferrin/p97. *Mol. Cancer Ther.* **5,** 1474–1482 (2006).

61. Berger, C., Madshus, I. H. & Stang, E. Cetuximab in combination with anti-human IgG antibodies efficiently down-regulates the EGF receptor by macropinocytosis. *Exp. Cell Res.* **318,** 2578–2591 (2012).

62. Rudnick, S. I. *et al.* Influence of affinity and antigen internalization on the uptake and penetration of Anti-HER2

antibodies in solid tumors. *Cancer Res.* **71,** 2250–2259 (2011).

63. Burmeister, W. P., Huber, A. H. & Bjorkman, P. J. Crystal structure of the complex of rat neonatal Fc receptor with Fc. *Nature* **372,** 379–383 (1994).

64. Burmeister, W. P., Gastinel, L. N., Simister, N. E., Blum, M. L. & Bjorkman, P. J. Crystal structure at 2.2 A resolution of the MHC-related neonatal Fc receptor. *Nature* **372,** 336–343 (1994).

65. Fujii, H. *et al.* Internalization of antibodies by endothelial cells via fibronectin implicating a novel mechanism in lupus nephritis. *Kidney Int.* **64,** 1662–1670 (2003).

66. Igawa, T. *et al.* Antibody recycling by engineered pH-dependent antigen binding improves the duration of antigen neutralization. *Nat. Biotechnol.* **28,** 1203–1207 (2010).

67. Jain, R. K. Normalization of tumor vasculature: an emerging concept in antiangiogenic therapy. *Science* **307,** 58–62 (2005).

68. Boucher, Y., Baxter, L. T. & Jain, R. K. Interstitial pressure gradients in tissue-isolated and subcutaneous tumors: implications for therapy. *Cancer Res* **50,** 4478–4484 (1990).

69. Frantz, C., Stewart, K. M. & Weaver, V. M. The extracellular matrix at a glance. *J. Cell Sci.* **123,** 4195–4200 (2010).

70. Krol, A., Maresca, J., Dewhirst, M. W. & Yuan, F. Available colume fraction of macromolecules in the extravascular space of a fibrosarcoma: implications for drug delivery. *Cancer Res* **59,** 4136–4141 (1999).

71. Freise, A. C. & Wu, A. M. In vivo imaging with antibodies and engineered fragments. *Mol. Immunol.* **67,** 142–152 (2015).

72. Widdison, W. C. *et al.* Semisynthetic maytansine analogues for the targeted treatment of cancer. *J. Med. Chem.* **49,** 4392–4408 (2006).

73. Nicolaou, K. C. Joys of molecules. 2. Endeavors in chemical biology and medicinal chemistry. *J. Med. Chem.* **48,** 5613–5638 (2005).

74. Hartley, J. A. *et al.* SG2285, a novel C2-aryl-substituted pyrrolobenzodiazepine dimer prodrug that cross-links DNA and exerts highly potent antitumor activity. *Cancer Res.* **70,** 6849–58 (2010).

75. Wolfe, A. L. *et al.* Efficacious cyclic N-acyl O-amino phenol duocarmycin prodrugs. *J. Med. Chem.* **56,** 4104–4115 (2013).

76. Wang, L. *et al.* Suzuki coupling based synthesis and in vitro cytotoxic evaluation of 7-heteroaryl-substituted camptothecin analogs. *Bioorg. Med. Chem. Lett.* **24,** 1597–1599 (2014).

77. Fernandes, C. *et al.* New chiral derivatives of xanthones: synthesis and investigation of enantioselectivity as inhibitors of growth of human tumor cell lines. *Bioorg. Med. Chem.* **22,** 1049–1062 (2014).

78. Shen, B.-Q. *et al.* Conjugation site modulates the in vivo stability and therapeutic activity of antibody-drug conjugates. *Nat. Biotechnol.* **30,** 184–189 (2012).

79. Hamblett, K. J. *et al.* Effects of drug loading on the antitumor activity of a monoclonal antibody drug conjugate. *Clin. Cancer Res.* **10,** 7063–7070 (2004).

80. Ohri, R. *et al.* High-throughput cysteine scanning to identify stable antibody conjugation sites for maleimide- and disulfide-based linkers. *Bioconjug. Chem.* **29,** 473–485 (2018).

81. Dimasi, N. *et al.* Efficient preparation of site-specific Antibody–Drug Conjugates using cysteine insertion. *Mol. Pharm.* **14,** 1501–1516 (2017).

82. Lyon, R. P. *et al.* Self-hydrolyzing maleimides improve the stability and pharmacological properties of antibody-drug conjugates. *Nat. Biotechnol.* **32,** 1059–1062 (2014).

83. Christie, R. J. *et al.* Stabilization of cysteine-linked antibody drug conjugates with N-aryl maleimides. *J. Control.*

Release **220,** 660–670 (2015).

84. Christie, R. *et al.* Pyrrolobenzodiazepine Antibody-Drug Conjugates designed for stable thiol conjugation. *Antibodies* **6,** 20 (2017).

85. Gross, L. *et al.* Immunoconjugates containing novel maytansinoids: promising anticancer drugs. *Cancer Res.* **52,** 127–131 (1992).

86. Wang, L., Amphlett, G., Blättler, W. A., Lambert, J. M. & Zhang, W. Structural characterization of the maytansinoid-monoclonal antibody immunoconjugate, huN901-DM1, by mass spectrometry. *Protein Sci.* **14,** 2436–2446 (2005).

87. Chih, H.-W., Gikanga, B., Yang, Y. & Zhang, B. Identification of amino acid residues responsible for the release of free drug from an antibody-drug conjugate utilizing lysine-succinimidyl ester chemistry. *J. Pharm. Sci.* **100,** 2518–2525 (2011).

88. Doronina, S. O. *et al.* Development of potent monoclonal antibody auristatin conjugates for cancer therapy. *Nat. Biotechnol.* **21,** 778–784 (2003).

89. Lyon, R. P. *et al.* Reducing hydrophobicity of homogeneous antibody-drug conjugates improves pharmacokinetics and therapeutic index. *Nat. Biotechnol.* **33,** 733–735 (2015).

90. Sun, M. M. C. *et al.* Reduction-alkylation strategies for the modification of specific monoclonal antibody disulfides. *Bioconjug. Chem.* **16,** 1282–1290 (2005).

91. McDonagh, C. F. *et al.* Engineered antibody-drug conjugates with defined sites and stoichiometries of drug attachment. *Protein Eng. Des. Sel.* **19,** 299–307 (2006).

92. Junutula, J. R. *et al.* Site-specific conjugation of a cytotoxic drug to an antibody improves the therapeutic index. *Nat. Biotechnol.* **26,** 925–932 (2008).

93. Elias, D. J. *et al.* Monoclonal antibody KS1/4-methotrexate immunoconjugate studies in non-small cell lung carcinoma. *Am. J. Respir. Crit. Care Med.* **150,** 1114–1122 (1994).

94. Wei, B. *et al.* Discovery of Peptidomimetic Antibody–Drug Conjugate Linkers with Enhanced Protease Specificity. *J. Med. Chem.* **61,** 989–1000 (2018).

95. Waight, A. B. *et al.* Structural Basis of Microtubule Destabilization by Potent Auristatin Anti-Mitotics. *PLoS One* **11,** e0160890 (2016).

96. Wang, Y. *et al.* Structural Insights into the Pharmacophore of Vinca Domain Inhibitors of Microtubules. *Mol. Pharmacol.* **89,** 233–242 (2016).

97. Apelgren, L. D., Zimmerman, D. L., Briggs, S. L. & Bumol, T. F. Antitumor activity of the monoclonal antibody-Vinca alkaloid immunoconjugate LY203725 (KS1/4-4-desacetylvinblastine-3-carboxhydrazide) in a nude mouse model of human ovarian cancer. *Cancer Res.* **50,** 3540–3544 (1990).

98. Petersen, B. H., DeHerdt, S. V, Schneck, D. W. & Bumol, T. F. The human immune response to KS1/4-desacetylvinblastine (LY256787) and KS1/4-desacetylvinblastine hydrazide (LY203728) in single and multiple dose clinical studies. *Cancer Res.* **51,** 2286–2290 (1991).

99. Myers, A. G., Cohen, S. B. & Kwon, B. M. A Study of the Reaction of Calicheamicin γ_1 with Glutathione in the Presence of Double-Stranded DNA. *J. Am. Chem. Soc.* **116,** 1255–1271 (1994).

100. Kellogg, B. A. *et al.* Disulfide-linked antibody-maytansinoid conjugates: optimization of in vivo activity by varying the steric hindrance at carbon atoms adjacent to the disulfide linkage. *Bioconjug. Chem.* **22,** 717–727 (2011).

101. Gebleux, R., Wulhfard, S., Casi, G. & Neri, D. Antibody format and drug release rate determine the therapeutic activity of noninternalizing Antibody-Drug Conjugates. *Mol. Cancer Ther.* **14,** 2606–2612 (2015).

102. Cleland, W. W. Dithiothreitol, a new protective reagent for SH groups. *Biochemistry* **3,** 480–482 (1964).

103. Baldwin, A. D. & Kiick, K. L. Tunable degradation of maleimide-thiol adducts in reducing environments. *Bioconjug.*

Chem. **22,** 1946–1953 (2011).

104. Staudinger, H. & Meyer, J. Über neue organische Phosphorverbindungen III. Phosphinmethylenderivate und Phosphinimine. *Helv. Chim. Acta* **2,** 635–646 (1919).

105. Bentley, D. R. *et al.* Accurate whole human genome sequencing using reversible terminator chemistry. *Nature* **456,** 53–59 (2008).

106. Caculitan, N. G. *et al.* Cathepsin B Is Dispensable for cellular processing of Cathepsin B-cleavable Antibody–Drug Conjugates. *Cancer Res.* **77,** 7027–7037 (2017).

107. Sharkey, R. M., Govindan, S. V., Cardillo, T. M. & Goldenberg, D. M. Epratuzumab-SN-38: a new Antibody-Drug Conjugate for the therapy of hematologic malignancies. *Mol. Cancer Ther.* **11,** 224–234 (2012).

108. Cardillo, T. M., Govindan, S. V., Sharkey, R. M., Trisal, P. & Goldenberg, D. M. Humanized anti-Trop-2 IgG-SN-38 conjugate for effective treatment of diverse epithelial cancers: preclinical studies in human cancer xenograft models and monkeys. *Clin. Cancer Res.* **17,** 3157–3169 (2011).

109. Casi, G. & Neri, D. Noninternalizing targeted cytotoxics for cancer therapy. *Mol. Pharm.* **12,** 1880–4 (2015).

110. Kaspar, M., Zardi, L. & Neri, D. Fibronectin as target for tumor therapy. *Int. J. Cancer* **118,** 1331–1339 (2006).

111. Brack, S. S., Silacci, M., Birchler, M. & Neri, D. Tumor-targeting properties of novel antibodies specific to the large isoform of tenascin-C. *Clin. Cancer Res.* **12,** 3200–3208 (2006).

112. Bernardes, G. J. L. *et al.* A traceless vascular-targeting antibody-drug conjugate for cancer therapy. *Angew. Chemie* **51,** 941–944 (2012).

113. Steiner, M. *et al.* Spacer length shapes drug release and therapeutic efficacy of traceless disulfide-linked ADCs targeting the tumor neovasculature. *Chem. Sci.* **4,** 297–302 (2013).

114. Perrino, E. *et al.* Curative properties of noninternalizing antibody-drug conjugates based on maytansinoids. *Cancer Res.* **74,** 2569–2578 (2014).

115. Gébleux, R., Stringhini, M., Casanova, R., Soltermann, A. & Neri, D. Non-internalizing antibody-drug conjugates display potent anti-cancer activity upon proteolytic release of monomethyl auristatin E in the subendothelial extracellular matrix. *Int. J. Cancer* **140,** 1670–1679 (2017).

116. Dal Corso, A., Cazzamalli, S., Gébleux, R., Mattarella, M. & Neri, D. Protease-cleavable linkers modulate the anticancer activity of noninternalizing Antibody–Drug Conjugates. *Bioconjug. Chem.* **28,** 1826–1833 (2017).

117. Heynick, F. The original 'magic bullet' is 100 years old. *Br. J. Psychiatry* **195,** 456 (2009).

118. FDA Approves Gemtuzumab Ozogamicin for CD33-positive AML. Available at: https://www.fda.gov/Drugs/InformationOnDrugs/ApprovedDrugs/ucm574518.htm. (Accessed: 22nd February 2018)

119. FDA Approves Genentech's Kadcyla (Ado-Trastuzumab Emtansine), the First Antibody-Drug Conjugate for Treating Her2-Positive Metastatic Breast Cancer. Available at: https://www.gene.com/media/press-releases/14347/2013-02-22/fda-approves-genentechs-kadcyla-ado-tras. (Accessed: 22nd February 2018)

120. FDA approves Brentuximab vedotin for the treatment of adult patients with primary cutaneous anaplastic large cell lymphoma. Available at: https://www.fda.gov/Drugs/InformationOnDrugs/ApprovedDrugs/ucm584543.htm. (Accessed: 22nd February 2018)

121. FDA approves inotuzumab ozogamicin for relapsed or refractory B-cell precursor ALL. Available at: https://www.fda.gov/Drugs/InformationOnDrugs/ApprovedDrugs/ucm572133.htm. (Accessed: 22nd February 2018)

122. Klán, P. *et al.* Photoremovable protecting groups in chemistry and biology: reaction mechanisms and efficacy. *Chem. Rev.* **113,** 119–191 (2013).

123. Davis, L. & Chin, J. W. Designer proteins: applications of genetic code expansion in cell biology. *Nat. Rev. Mol. Cell Biol.* **13,** 168–182 (2012).

124. Brieke, C., Rohrbach, F., Gottschalk, A., Mayer, G. & Heckel, A. Light-controlled tools. *Angew. Chemie* **51,** 8446–8476 (2012).

125. Neveu, P. *et al.* A caged retinoic acid for one- and two-photon excitation in zebrafish embryos. *Angew. Chemie* **120,** 3804–3806 (2008).

126. Sinha, D. K. *et al.* Photocontrol of protein activity in cultured cells and zebrafish with one- and two-photon illumination. *ChemBioChem* **11,** 653–663 (2010).

127. Il'ichev, Y. V., Schwörer, M. A. & Wirz, J. Photochemical reaction mechanisms of 2-nitrobenzyl compounds: methyl ethers and caged ATP. *J. Am. Chem. Soc.* **126,** 4581–4595 (2004).

128. Kilic, F. *et al.* Caged Progesterone: A new tool for studying rapid nongenomic actions of progesterone. *J. Am. Chem. Soc.* **131,** 4027–4030 (2009).

129. Govan, J. M., Young, D. D., Lively, M. O. & Deiters, A. Optically triggered immune response through photocaged oligonucleotides. *Tetrahedron Lett.* **56,** 3639–3642 (2015).

130. Papageorgiou, G., Ogden, D. & Corrie, J. E. T. An antenna-sensitized nitroindoline precursor to enable photorelease of L-glutamate in high concentrations. *J. Org. Chem.* **69,** 7228–7233 (2004).

131. Veldhuyzen, W. F., Nguyen, Q., McMaster, G. & Lawrence, D. S. A light-activated probe of intracellular protein kinase activity. *J. Am. Chem. Soc.* **125,** 13358–13359 (2003).

132. Griffiths, C. A. *et al.* Chemical intervention in plant sugar signalling increases yield and resilience. *Nature* **540,** 574–578 (2016).

133. Furukawa, K., Abe, H., Tsuneda, S. & Ito, Y. Photoactivatable fluorescein derivatives with azidomethyl caging groups for tracing oligonucleotides in living human cells. *Org. Biomol. Chem.* **8,** 2309 (2010).

134. Lee, H. D. *et al.* Superresolution imaging of targeted proteins in fixed and living cells using photoactivatable organic fluorophores. *J. Am. Chem. Soc.* **132,** 15099–15101 (2010).

135. Gorka, A. P., Nani, R. R., Zhu, J., Mackem, S. & Schnermann, M. J. A near-IR uncaging strategy based on cyanine photochemistry. *J. Am. Chem. Soc.* **136,** 14153–14159 (2014).

136. Anderson, E. D., Gorka, A. P. & Schnermann, M. J. Near-infrared uncaging or photosensitizing dictated by oxygen tension. *Nat. Commun.* **7,** 13378 (2016).

137. Nani, R. R., Gorka, A. P., Nagaya, T., Kobayashi, H. & Schnermann, M. J. Near-IR Light-Mediated Cleavage of Antibody-Drug Conjugates Using Cyanine Photocages. *Angew. Chemie* **54,** 13635–13638 (2015).

138. Wu, N., Deiters, A., Cropp, T. A., King, D. & Schultz, P. G. A genetically encoded photocaged amino acid. *J. Am. Chem. Soc.* **126,** 14306–14307 (2004).

139. Nguyen, D. P. *et al.* Genetic encoding of photocaged cysteine allows photoactivation of TEV protease in live mammalian cells. *J. Am. Chem. Soc.* **136,** 2240–2243 (2014).

140. Uprety, R. *et al.* Genetic encoding of caged cysteine and caged homocysteine in bacterial and mammalian cells. *ChemBioChem* **15,** 1793–1799 (2014).

141. Pan, J. & Carroll, K. S. Light-mediated sulfenic acid generation from photocaged cysteine sulfoxide. *Org. Lett.* **17,** 6014–6017 (2015).

142. Deiters, A., Groff, D., Ryu, Y., Xie, J. & Schultz, P. G. A genetically encoded photocaged tyrosine. *Angew. Chemie* **118,** 2794–2797 (2006).

143. Luo, J., Torres-Kolbus, J., Liu, J. & Deiters, A. genetic encoding of photocaged tyrosines with improved light-activation properties for the optical control of protease function. *ChemBioChem* **18,** 1442–1447 (2017).

144. Arbely, E., Torres-Kolbus, J., Deiters, A. & Chin, J. W. Photocontrol of tyrosine phosphorylation in mammalian cells via genetic encoding of photocaged tyrosine. *J. Am. Chem. Soc.* **134,** 11912–11915 (2012).

145. Lemke, E. A., Summerer, D., Geierstanger, B. H., Brittain, S. M. & Schultz, P. G. Control of protein phosphorylation with a genetically encoded photocaged amino acid. *Nat. Chem. Biol.* **3,** 769–772 (2007).

146. Rakauskaitė, R. *et al.* Biosynthetic selenoproteins with genetically-encoded photocaged selenocysteines. *Chem. Commun.* **51,** 8245–8248 (2015).

147. Gautier, A., Deiters, A. & Chin, J. W. Light-activated kinases enable temporal dissection of signaling networks in living cells. *J. Am. Chem. Soc.* **133,** 2124–2127 (2011).

148. Zou, K., Cheley, S., Givens, R. S. & Bayley, H. Catalytic subunit of protein kinase a caged at the activating phosphothreonine. *J. Am. Chem. Soc.* **124,** 8220–8229 (2002).

149. Matikonda, S. S. *et al.* Bioorthogonal prodrug activation driven by a strain-promoted 1,3-dipolar cycloaddition. *Chem. Sci.* **6,** 1212–1218 (2015).

150. Versteegen, R. M., Rossin, R., ten Hoeve, W., Janssen, H. M. & Robillard, M. S. Click to release: instantaneous doxorubicin elimination upon tetrazine ligation. *Angew. Chemie* **52,** 14112–14116 (2013).

151. Khan, I., Agris, P. F., Yigit, M. V. & Royzen, M. In situ activation of a doxorubicin prodrug using imaging-capable nanoparticles. *Chem. Commun.* **52,** 6174–6177 (2016).

152. Li, J., Jia, S. & Chen, P. R. Diels-Alder reaction-triggered bioorthogonal protein decaging in living cells. *Nat. Chem. Biol.* **10,** 1003–1005 (2014).

153. Rossin, R. *et al.* Triggered Drug release from an Antibody–Drug Conjugate using fast 'click-to-release' chemistry in mice. *Bioconjug. Chem.* **27,** 1697–1706 (2016).

154. Mejia Oneto, J. M., Khan, I., Seebald, L. & Royzen, M. In vivo bioorthogonal chemistry enables local hydrogel and systemic pro-drug to treat soft tissue sarcoma. *ACS Cent. Sci.* **2,** 476–482 (2016).

155. Jiménez-Moreno, E. *et al.* Vinyl ether/tetrazine pair for the traceless release of alcohols in cells. *Angew. Chemie* **56,** 243–247 (2017).

156. Wu, H., Alexander, S. C., Jin, S. & Devaraj, N. K. A bioorthogonal near-infrared fluorogenic probe for mRNA detection. *J. Am. Chem. Soc.* **138,** 11429–11432 (2016).

157. van Brakel, R., Vulders, R. C. M., Bokdam, R. J., Grüll, H. & Robillard, M. S. A doxorubicin prodrug activated by the staudinger reaction. *Bioconjug. Chem.* **19,** 714–8 (2008).

158. Gorska, K., Manicardi, A., Barluenga, S. & Winssinger, N. DNA-templated release of functional molecules with an azide-reduction-triggered immolative linker. *Chem. Commun.* **47,** 4364 (2011).

159. Pawlak, J. B. *et al.* Bioorthogonal deprotection on the dendritic cell surface for chemical control of antigen cross-presentation. *Angew. Chemie* **54,** 5628–5631 (2015).

160. Luo, J., Liu, Q., Morihiro, K. & Deiters, A. Small-molecule control of protein function through Staudinger reduction. *Nat. Chem.* **8,** 1027–1034 (2016).

161. Kim, J. & Bertozzi, C. R. A bioorthogonal reaction of N-oxide and boron reagents. *Angew. Chemie* **54,** 15777–15781 (2015).

162. Xu, M., Tu, J. & Franzini, R. M. Rapid and efficient tetrazine-induced drug release from highly stable benzonorbornadiene derivatives. *Chem. Commun.* **53,** 6271–6274 (2017).

163. Oliveira, B. L., Guo, Z. & Bernardes, G. J. L. Inverse electron demand Diels-Alder reactions in chemical biology. *Chem. Soc. Rev.* **46,** 4895–4950 (2017).

164. Carlson, J. C. T., Mikula, H. & Weissleder, R. Unraveling tetrazine-triggered bioorthogonal elimination enables chemical tools for ultrafast release and universal cleavage. *J. Am. Chem. Soc.* **140,** 3603–3612 (2018).

165. Fan, X. *et al.* Optimized tetrazine derivatives for rapid bioorthogonal decaging in living cells. *Angew. Chemie* **55,** 14046–14050 (2016).

166. Streu, C. & Meggers, E. Ruthenium-induced allylcarbamate cleavage in living cells. *Angew. Chemie* **118,** 5773–5776 (2006).

167. Sasmal, P. K., Carregal-Romero, S., Parak, W. J. & Meggers, E. Light-triggered ruthenium catalyzed allylcarbamate cleavage in biological environments. *Organometallics* **31,** 5968–5970 (2012).

168. Sánchez, M. I., Penas, C., Vázquez, M. E. & Mascareñas, J. L. Metal-catalyzed uncaging of DNA-binding agents in living cells. *Chem. Sci.* **5,** 1901–1907 (2014).

169. Tomás-Gamasa, M., Martínez-Calvo, M., Couceiro, J. R. & Mascareñas, J. L. Transition metal catalysis in the mitochondria of living cells. *Nat. Commun.* **7,** 12538 (2016).

170. Völker, T., Dempwolff, F., Graumann, P. L. & Meggers, E. Progress towards bioorthogonal catalysis with organometallic compounds. *Angew. Chemie* **53,** 10536–10540 (2014).

171. Tonga, G. Y. *et al.* Supramolecular regulation of bioorthogonal catalysis in cells using nanoparticle-embedded transition metal catalysts. *Nat. Chem.* **7,** 597–603 (2015).

172. Sasmal, P. K. *et al.* Catalytic azide reduction in biological environments. *ChemBioChem* **13,** 1116–1120 (2012).

173. Zhu, B. *et al.* A 4-hydroxynaphthalimide-derived ratiometric fluorescent chemodosimeter for imaging palladium in living cells. *Chem. Commun.* **47,** 8656 (2011).

174. Chen, H., Lin, W. & Yuan, L. Construction of a near-infrared fluorescence turn-on and ratiometric probe for imaging palladium in living cells. *Org. Biomol. Chem.* **11,** 1938 (2013).

175. Yusop, R. M., Unciti-Broceta, A., Johansson, E. M. V, Sánchez-Martín, R. M. & Bradley, M. Palladium-mediated intracellular chemistry. *Nat. Chem.* **3,** 239–243 (2011).

176. Santra, M., Ko, S.-K., Shin, I. & Ahn, K. H. Fluorescent detection of palladium species with an O-propargylated fluorescein. *Chem. Commun.* **46,** 3964–3966 (2010).

177. Wang, X., Guo, Z., Zhu, S., Tian, H. & Zhu, W. A naked-eye and ratiometric near-infrared probe for palladium via modulation of a π-conjugated system of cyanines. *Chem. Commun.* **50,** 13525–13528 (2014).

178. Liu, W. *et al.* Water-Soluble colorimetric and ratiometric fluorescent probe for selective imaging of palladium species in living cells. *Inorg. Chem.* **53,** 12590–12594 (2014).

179. Indrigo, E. *et al.* Intracellular delivery of a catalytic organometallic complex. *Chem. Commun.* **53,** 6712–6715 (2017).

180. Li, J. *et al.* Palladium-triggered deprotection chemistry for protein activation in living cells. *Nat. Chem.* **6,** 352–361 (2014).

181. Wang, J. *et al.* Chemical remodeling of cell-surface sialic acids through a palladium-triggered bioorthogonal elimination reaction. *Angew. Chemie* **54,** 5364–5368 (2015).

182. Miller, M. A. *et al.* Nano-palladium is a cellular catalyst for in vivo chemistry. *Nat. Commun.* **8,** 15906 (2017).

183. Pérez-López, A. M. *et al.* Gold-triggered uncaging chemistry in living systems. *Angew. Chemie* **56,** 12548–12552 (2017).

184. Wang, J. *et al.* Palladium-triggered chemical rescue of intracellular proteins via genetically encoded allene-caged tyrosine. *J. Am. Chem. Soc.* **138,** 15118–15121 (2016).

185. Mandai, T. *Handbook of Organopalladium Chemistry for Organic Synthesis* (ed. E. Negishi). 1827–1832 (John Wiley & Sons, Inc.). doi:10.1002/0471212466.ch77

186. Friedman Ohana, R. *et al.* Improved deconvolution of protein targets for bioactive compounds using a palladium

cleavable chloroalkane capture tag. *ACS Chem. Biol.* **11,** 2608–2617 (2016).

187. Weiss, J. T. *et al.* Extracellular palladium-catalysed dealkylation of 5-fluoro-1-propargyl-uracil as a bioorthogonally activated prodrug approach. *Nat. Commun.* **5,** 3277–3286 (2014).

188. Weiss, J. T. *et al.* Development and bioorthogonal activation of palladium-labile prodrugs of gemcitabine. *J. Med. Chem.* **57,** 5395–5404 (2014).

189. Rambabu, D., Bhavani, S., Swamy, N. K., Basaveswara Rao, M. V. & Pal, M. Pd/C-mediated depropargylation of propargyl ethers/amines in water. *Tetrahedron Lett.* **54,** 1169–1173 (2013).

190. Tsuji, J. *Palladium Reagents and Catalysts.* 431–517 (John Wiley & Sons, Ltd, 2005). doi:10.1002/0470021209.ch4

191. Tsuji, J. & Mandai, T. Palladium-catalyzed reactions of propargylic compounds in organic synthesis. *Angew. Chemie* **34,** 2589–2612 (1996).

192. Tsuji, J. *Palladium Reagents and Catalysts.* 453–470 (John Wiley & Sons, Ltd, 1995). doi:10.1002/0470021209

193. Xu, L.-M., Li, B.-J., Yang, Z. & Shi, Z.-J. Organopalladium(IV) chemistry. *Chem. Soc. Rev.* **39,** 712–733 (2010).

194. Rubio-Ruiz, B., Weiss, J. T. & Unciti-Broceta, A. Efficient palladium-triggered release of vorinostat from a bioorthogonal precursor. *J. Med. Chem.* **59,** 9974–9980 (2016).

195. Weiss, J. T., Carragher, N. O. & Unciti-Broceta, A. Palladium-mediated dealkylation of N-propargyl-floxuridine as a bioorthogonal oxygen-independent prodrug strategy. *Sci. Rep.* **5,** 9329 (2015).

196. Goldmacher, V. S., Senter, P. D., Lambert, J. M. & Blattler, W. A. Photoactivation of toxin conjugates. *Bioconjug. Chem.* **3,** 104–107 (1992).

197. Nani, R. R. *et al.* In Vivo Activation of duocarmycin–Antibody Conjugates by near-infrared light. *ACS Cent. Sci.* **3,** 329–337 (2017).

198. Nagaya, T. *et al.* Molecularly targeted cancer combination therapy with near-infrared photoimmunotherapy and near-infrared photorelease with duocarmycin–antibody conjugate. *Mol. Cancer Ther.* **17,** 661–670 (2018).

199. Los, G. V. *et al.* HaloTag: A novel protein labeling technology for cell imaging and protein analysis. *ACS Chem. Biol.* **3,** 373–382 (2008).

200. Senter, P. D., Tansey, M. J., Lambert, J. M. & Blattler, W. A. Novel photocleavable protein crosslinking reagents and their use in the preparation of antibody-toxin conjugates. *Photochem. Photobiol.* **42,** 231–237 (1985).

201. Li, H., Grasa, G. & Colacot, T. J. A highly efficient, practical, and general route for the synthesis of $(R_3P)_2Pd(0)$: structural evidence on the reduction mechanism of Pd(II) to Pd(0). *Org. Lett.* **12,** 3332–3335 (2010).

202. Colacot, T. J., Grasa, G. A. & Li, H. (Johnson Matthey Ltd.) Preparation of a metal complex. WO2010128316 A1 (2010).

203. Frederick, C. A. *et al.* Structural comparison of anticancer drug-DNA complexes: adriamycin and daunomycin. *Biochemistry* **29,** 2538–2549 (1990).

204. Bernardim, B. *et al.* Stoichiometric and irreversible cysteine-selective protein modification using carbonylacrylic reagents. *Nat. Commun.* **7,** 13128 (2016).

205. Vaneycken, I. *et al.* Preclinical screening of anti-HER2 nanobodies for molecular imaging of breast cancer. *FASEB J.* **25,** 2433–2446 (2011).

206. Valabrega, G., Montemurro, F. & Aglietta, M. Trastuzumab: mechanism of action, resistance and future perspectives in HER2-overexpressing breast cancer. *Ann. Oncol.* **18,** 977–84 (2007).

207. Lewis Phillips, G. D. *et al.* Targeting HER2-positive breast cancer with trastuzumab-DM1, an antibody-cytotoxic drug conjugate. *Cancer Res.* **68,** 9280–90 (2008).

208. Spicer, C. D. & Davis, B. G. Palladium-mediated site-selective Suzuki-Miyaura protein modification at genetically

encoded aryl halides. *Chem. Commun.* **47,** 1698–1700 (2011).

209. Vinogradova, E. V., Zhang, C., Spokoyny, A. M., Pentelute, B. L. & Buchwald, S. L. Organometallic palladium reagents for cysteine bioconjugation. *Nature* **526,** 687–691 (2015).

210. Willwacher, J., Raj, R., Mohammed, S. & Davis, B. G. Selective metal-site-guided arylation of proteins. *J. Am. Chem. Soc.* **138,** 8678–8681 (2016).

211. Cycloocten-5-oic acid, Aldrich CPR. Available at: https://www.sigmaaldrich.com/catalog/product/aldrich/t179795?lang=en&region=GB. (Accessed: 12th January 2018)

212. Ziegler, K. & Wilms, H. Uber vielgliedrige Ringsysteme XIII: Ungesättigte Kohlenwasserstoff-8-Ringe. *Justus Liebigs Ann. Chem.* **567,** 1–43 (1950).

213. Bloodworth, A. J., Melvin, T. & Mitchell, J. C. Mechanistic aspects of oxygen transfer by gem-dialkylperoxonium ions. *J. Org. Chem.* **53,** 1078–1082 (1988).

214. Tetraethylene glycol monoamine, Carbosynth. Available at: https://www.carbosynth.com/carbosynth/website.nsf/(w-productdisplay)/EB5EA781A9D2834E802579A5003F5368. (Accessed: 12th January 2018)

215. Acker, G., Palumbo, A., Neri, D., Vajkoczy, P. & Czabanka, M. F8-SIP mediated targeted photodynamic therapy leads to microvascular dysfunction and reduced glioma growth. *J. Neurooncol.* **129,** 33–38 (2016).

216. Corrie, P. G. Cytotoxic chemotherapy: clinical aspects. *Medicine (Baltimore).* **36,** 24–28 (2008).

217. FDA, U. S. Cisplatin Description. Available at: https://www.accessdata.fda.gov/drugsatfda_docs/label/2010/018057s079lbl.pdf.

218. P. T. Daley-Yates & McBrien, D. C. Cisplatin metabolites in plasma, a study of their pharmacokinetics and importance in the nephrotoxic and antitumour activity of cisplatin. *Biochem Pharmacol.* **33,** 3063–3070 (1984).

219. WC, Z. *et al.* Inter- and intratumoral disposition of platinum in solid tumors after administration of cisplatin. *Clin Cancer Res.* **8,** 2992–2999 (2002).

220. Dedon, P. C. & Borch, R. F. Characterization of the reactions of platinum antitumor agents with biologic and nonbiologic sulfur-containing nucleophiles. *Biochem. Pharmacol.* **36,** 1955–1964 (1987).

221. Ivanov, A. I. *et al.* Cisplatin Binding Sites on Human Albumin. *J. Biol. Chem.* **273,** 14721–14730 (1998).

222. Cisplatin as Chemotherapeutic Prevalence. Available at: www.cancer.gov/research/progress/discovery/cisplatin. (Accessed: 15th January 2018)

223. Farris, F. F., King, F. G., Dedrick, R. L. & Litterst, C. L. Physiological model for the pharmacokinetics of cis-dichlorodiammineplatinum(II) (DDP) in the tumored rat. *J. Pharmacokinet. Biopharm.* **13,** 13–39 (1985).

224. Stewart, D. J. *et al.* Factors affecting platinum concentrations in human surgical tumour specimens after cisplatin. *Br. J. Cancer* **71,** 598–604 (1995).

225. Abu Sohel, S. M. & Liu, R.-S. Carbocyclisation of alkynes with external nucleophiles catalysed by gold, platinum and other electrophilic metals. *Chem. Soc. Rev.* **38,** 2269 (2009).

226. Mauleon, P. & Toste, F. D. *Modern Gold Catalyzed Synthesis* (ed. Hashmi, K. A. S., Toste, F. D.). 75–134 (Wiley-VCH Verlag GmbH & Co. KGaA, 2012). doi:10.1002/9783527646869.ch4

227. Belger, K. & Krause, N. Smaller, faster, better: modular synthesis of unsymmetrical ammonium salt-tagged NHC–gold(I) complexes and their application as recyclable catalysts in water. *Org. Biomol. Chem.* **13,** 8556–8560 (2015).

228. Harkat, H., Dembelé, A. Y., Weibel, J.-M., Blanc, A. & Pale, P. Cyclization of alkynoic acids with gold catalysts: a surprising dichotomy between AuI and AuIII. *Tetrahedron* **65,** 1871–1879 (2009).

229. Tomás-Mendivil, E. *et al.* Cycloisomerization versus hydration reactions in aqueous media: a Au(III)-NHC catalyst that makes the difference. *Org. Lett.* **14,** 2520–2523 (2012).

230. Alemán, J., del Solar, V. & Navarro-Ranninger, C. Anticancer platinum complexes as non-innocent compounds for catalysis in aqueous media. *Chem. Commun.* **46,** 454–456 (2010).

231. Wang, W., Xu, B. & Hammond, G. B. Efficient synthesis of γ-keto esters through neighboring carbonyl group-assisted regioselective hydration of 3-alkynoates. *J. Org. Chem.* **74,** 1640–1643 (2009).

232. Ebule, R., Liang, S., Hammond, G. B. & Xu, B. Chloride-tolerant gold(I)-catalyzed regioselective hydrochlorination of alkynes. *ACS Catal.* **7,** 6798–6801 (2017).

233. Dorel, R. & Echavarren, A. M. Gold(I)-catalyzed activation of alkynes for the construction of molecular complexity. *Chem. Rev.* **115,** 9028–9072 (2015).

234. Mondelli & Vigevani. N, O-isopropylidene derivatives of the antitumour antibiotics daunorubicin and doxorubicin. *J. Chem. Res. - Miniprint* **6,** 1717–37 (1984).

235. Alonso-de Castro, S., Cortajarena, A. L., López-Gallego, F. & Salassa, L. Bioorthogonal catalytic activation of platinum and ruthenium anticancer complexes by FAD and flavoproteins. *Angew. Chemie* **57,** 3143–3147 (2018).

236. Chalker, J. M., Wood, C. S. C. & Davis, B. G. A convenient catalyst for aqueous and protein Suzuki-Miyaura cross-coupling. *J. Am. Chem. Soc.* **131,** 16346–16347 (2009).

237. Rojas, A. J., Pentelute, B. L. & Buchwald, S. L. Water-soluble palladium reagents for cysteine S-arylation under ambient aqueous conditions. *Org. Lett.* **19,** 4263–4266 (2017).

238. Dupuy, S., Crawford, L., Bühl, M. & Nolan, S. P. The gold(I)-catalysed protodecarboxylation mechanism. *Chem. - A Eur. J.* **21,** 3399–3408 (2015).

239. Dupuy, S., Lazreg, F., Slawin, A. M. Z., Cazin, C. S. J. & Nolan, S. P. Decarboxylation of aromatic carboxylic acids by gold(I)-N-heterocyclic carbene (NHC) complexes. *Chem. Commun.* **47,** 5455 (2011).

240. Fackler, J. P., Khan, M. N. I., King, C., Staples, R. J. & Winpenny, R. E. P. Decarboxylation of (triphenylphosphine)gold(I) carboxylates. *Organometallics* **10,** 2178–2183 (1991).

241. Dal Corso, A., Gébleux, R., Murer, P., Soltermann, A. & Neri, D. A non-internalizing antibody-drug conjugate based on an anthracycline payload displays potent therapeutic activity in vivo. *J. Control. Release* **264,** 211–218 (2017).

242. Fior, R. *et al.* Single-cell functional and chemosensitive profiling of combinatorial colorectal therapy in zebrafish xenografts. *Proc. Natl. Acad. Sci.* **114,** E8234–E8243 (2017).

243. Kaschula, C. H. *et al.* Structure–activity studies on the anti-proliferation activity of ajoene analogues in WHCO1 oesophageal cancer cells. *Eur. J. Med. Chem.* **50,** 236–254 (2012).

244. Jones, S. B., Simmons, B. & MacMillan, D. W. C. Nine-step enantioselective total synthesis of (+)-minfiensine. *J. Am. Chem. Soc.* **131,** 13606–13607 (2009).

245. Calogeropoulou, T., Angelou, P., Detsi, A., Fragiadaki, I. & Scoulica, E. Design and synthesis of potent antileishmanial cycloalkylidene-substituted ether phospholipid derivatives. *J. Med. Chem.* **51,** 897–908 (2008).

246. Druais, V. *et al.* A convergent approach toward the C1-C11 subunit of phoslactomycins and formal synthesis of phoslactomycin B. *Org. Lett.* **11,** 935–938 (2009).

247. Hernández, A.-I., Balzarini, J., Karlsson, A., Camarasa, M.-J. & Pérez-Pérez, M.-J. Acyclic nucleoside analogues as novel inhibitors of human mitochondrial thymidine kinase. *J. Med. Chem.* **45,** 4254–4263 (2002).

248. Padwa, A., Meske, M. & Ni, Z. Synthesis of novel bicyclic nitrogen heterocycles by the intramolecular dipolar cycloaddition reaction of nitrones with allenes and alkynes. *Tetrahedron* **51,** 89–106 (1995).

249. Streit, U., Birbaum, F., Quattropani, A. & Bochet, C. G. Photocycloaddition of arenes and allenes. *J. Org. Chem.* **78,** 6890–6910 (2013).

250. Rettig, M. F., Wing, R. M. & Wiger. X-ray crystallographic, chemical, and spectroscopic studies of the palladium dichloride complexes of cyclonona-1,5-diene, cycloocta-1,5-diene, cycloocta-1,4-diene, and cyclohepta-1,4-diene. *J. Am. Chem. Soc.* **103,** 2980–2986 (1981).

251. Drew, D., Doyle, J. R. & Shaver, A. G. Cyclic diolefin complexes of platinum and palladium. *Inorg. Synth.* **28,** 346–9 (1990).

252. Madan, R., Anand, R. C. & Varma, I. K. Thermal behaviour of polymers based on nadimides. *J. Therm. Anal. Calorim.* **59,** 531–9 (2000).

253. von Delius, M., Hauke, F. & Hirsch, A. Evaluation of an intramolecular approach for the synthesis of the elusive $C_{58}N_2$ heterofullerene family. *European J. Org. Chem.* 4109–4119 (2008).

254. Kleinbeck, F. & Toste, F. D. Gold(I)-catalyzed enantioselective ring expansion of allenylcyclopropanols. *J. Am. Chem. Soc.* **131,** 9178–9179 (2009).

255. Singh, V., Wang, S. & Kool, E. T. Genetically encoded multispectral labeling of proteins with polyfluorophores on a DNA backbone. *J. Am. Chem. Soc.* **135,** 6184–6191 (2013).

256. Lercher, L., McGouran, J. F., Kessler, B. M., Schofield, C. J. & Davis, B. G. DNA modification under mild conditions by Suzuki-Miyaura cross-coupling for the generation of functional probes. *Angew. Chemie* **52,** 10553–10558 (2013).